UNIVERSITY OF OKLAHOMA

GRADUATE COLLEGE

CHEMICAL GENETICS AND MOLECULAR PHARMACOLOGY OF THE OXYSTEROL-BINDING PROTEINS

A DISSERTATION

SUBMITTED TO THE GRADUATE FACULTY

in partial fulfillment of the requirements for the

Degree of

DOCTOR OF PHILOSOPHY

By

ZACHARY C. SEVERANCE
Norman, Oklahoma
2020

Downloaded from SHAREOK. Persistent Handle URL: https://hdl.handle.net/11244/325259

CHEMICAL GENETICS AND MOLECULAR PHARMACOLOGY OF THE

OXYSTEROL-BINDING PROTEINS

A DISSERTATION APPROVED FOR THE
DEPARTMENT OF CHEMISTRY AND BIOCHEMISTRY

BY THE COMMITTEE CONSISTING OF

Dr. Anthony W.G. Burgett, Chair

Dr. Shanteri Singh

Dr. Ann H. West

Dr. Indrajeet Sharma

Dr. Brian M. Kemp

© Copyright by ZACHARY C. SEVERANCE 2020
All Rights Reserved.

This is dedicated to my family and my girlfriend. To my mother and father, you are my heroes and always will be. You inspire me every day and I did this for you. To my brother, I offer this as evidence that you can do anything you put your mind to. To Melanie, you are my rock. Thank you for believing in me when no one else did. I love you all.

Acknowledgements

This dissertation would not be possible without the help of many important people in my life. First and foremost, I would like to thank my family, to whom this dissertation is dedicated, for their unwavering support throughout my entire life. It goes without saying that I wouldn't be the person or scientist I am today without you. Thank you, Melanie, for putting up with the long hours and late nights (and me in general) and for creating a distraction-free environment so I could focus on my science. I know it wasn't easy and I couldn't have done it without you.

I would also like to thank my science family. Thank you, Dr. Anthony Burgett, for always trusting and believing in me as a scientist. You were the first person in academia to believe in me and give me an opportunity to be a research scientist, and I will forever be grateful for that. Thank you, Dr. Naga Rama Kothapalli, for being a great mentor and for your invaluable training and general insight for the last four years. You are a great friend and colleague. I would also like to thank all the members of the Burgett Research Group that I have worked and grown with: Dr. Juan Nuñez, Dr. Brett Roberts, Dr. Anh Le-McClain, Dr. Ryan Bensen, Dr. Cori Malinky, Mr. Robert Fogel, Mr. Matthew Finneran, Ms. Ines Forrest, and Mr. Jorge Luis Berrios Rivera.

Science and the general pursuit of objective truth is always a collaborative effort, so I would like to I would like to thank Dr. Brett Roberts and Dr. Ryan Bensen for their contributions to Chapter 2 and 3, and Dr. Juan Nuñez for his contributions to Chapter 4. I would also like to thanks Dr. Anh Le-McClain and Dr. Cori Malinky for creating many of the small molecules used in Chapters 2, 3, and 4. I would like to thank, Dr. Robert H. Cichewicz, Dr. Ann H. West, Dr. Adam S. Duerfeldt, Dr. Christina R. Bourne, Dr. Si Wu,

and Dr. Helen I. Zgurskaya for use of their lab equipment through the years. Additionally, thank you to the Wu Research Group at the University of Oklahoma, particularly Dr. Zhe Wang and Ms. Hongyan Ma, for your collaboration and contributions to the proteomic mass spectrometry experiments. I would also like to thanks Dr. Fares Najar for his collaboration and help with the RNA Seq bioinformatics.

Last but not least, I would also like to a give a special thank you to my committee members, Dr. Shanteri Singh, Dr. Ann H. West, Dr. Robert H. Cichewicz, Dr. Brian M. Kemp, and Dr. Indrajeet Sharma, who were an invaluable part of my growth as a scientist. Thank you very much for your wisdom, guidance, and support during the last four years.

Table of Contents

Acknowledgements iv

List of Tables xiii

List of Figures xiv

Abstract xx

Chapter 1. Introduction 1

1.1 Overview of the OSBP/ORP family of proteins 1

1.2 Overview of OSBP/ORP ligand binding 3

1.3 Lipids in biology 7

1.3.1 Sterols 7

1.3.2 Phospholipids 8

1.4 OSBP biology 9

1.4.1 Overview of OSBP 9

1.4.2 Cholesterol Trafficking 11

1.4.3 Lipid Metabolism 12

1.4.4 Cell Signaling 13

1.5 ORP4 biology 16

1.5.1 Overview of ORP4 16

1.5.2 Localization and vimentin regulation 17

1.5.3 Cell survival and proliferation 20

1.6 OSBP and ORP4 in human disease biology 22

1.6.1 OSBP as a broad-spectrum antiviral target 22

1.6.1.2 Positive-sense single-stranded RNA viruses 23

1.6.1.3 Role of OSBP in hepatitis C virus (HCV) biology 25
1.6.1.4 Role of OSBP in Enterovirus biology 29
1.6.1.5 Other OSBP requiring viruses 33
1.6.1.6 OSBP as a component of cellular innate antiviral response 37
1.6.2 ORP4 as a precision anticancer target 40
1.7 Small-molecule targeting of OSBP and ORP4 42
1.7.1 ORPphilins 43
1.7.2 Minor enviroxime-like compounds 44
1.8 The chemical genetics approach to biology 48
Chapter 2. Transient OSW-1-compound treatment induces a unique, persistent multigenerational decrease in oxysterol-binding protein (OSBP) levels and antiviral prophylaxis 51
Abstract 51
Allocation of Contribution 52
2.1 Introduction 53
2.2 Methods and Materials 57
2.2.1 Plasmids and Cloning 57
2.2.2 Cell Lines and Viruses 58
2.2.3 General Cell Culture 59
2.2.4 Cell Lysis Method 1 (AC Lysis Buffer Freeze/Thaw) 60
2.2.5 Cell Lysis Method 2 (MPER Lysis) 61
2.2.6 Western Blotting 62
2.2.7 Washout Experiment 63

2.2.8 Cycloheximide Chase Experiment 63
2.2.9 Cytotoxic Assay Protocol 63
2.2.10 Antiviral Experiments 64
2.2.11 Immunofluorescent Microscopy 66
2.2.12 iTRAQ Proteomic Mass Spectrometry 67
2.2.13 LC-MS/MS Analysis of iTRAQ Labeled Peptides 68
2.2.14 Mass Spectrometry Label-Free 2D OSBP Quantification 69
2.2.15 [^{3}H]25-OHC Competitive Binding Assay Procedure 70
2.2.16 OSW-1-Compound Generation and Preparation 70
2.2.17 Statistical Analysis 70
2.3 Results 71
2.3.1 Continual OSW-1-compound treatment results in time and proteasome-dependent loss of OSBP and ORP4 in the cell 71
2.3.2 Transient exposure to non-toxic, low nanomolar concentrations of the OSW-1-compound (i.e., “the washout experiment”) induces a specific, persistent and multigenerational decrease in cellular OSBP levels 74
2.3.3 Transient treatment with the OSW-1-compound induces antiviral prophylaxis against clinically isolated Enteroviruses 84
2.3.4 The loss and long-term repression of OSBP is unique to the OSW-1-compound and not other OSBP-targeting antiviral compounds 86
2.3.5 The OSW-1-compound is the only OSBP-targeting antiviral compound capable of inducing prophylactic antiviral activity in cells 87

2.3.6 The OSW-1-compound and the other OSBP-targeting antiviral compounds interact with OSBP through multiple modes of binding and have distinct effects on OSBP activity in the cell 90
2.4 Discussion 97
2.5 Conclusions 100
Chapter 3: Mechanistic studies on the cellular responses triggered by the OSW-1-compound 102
Abstract 102
Allocation of Contribution 103
3.1 Introduction 104
3.2 Methods and Materials 107
3.2.1 Cell Lines and Viruses 107
3.2.2 General Cell Culture 107
3.2.3 Cell Lysis Method 1 (AC Lysis Buffer Freeze/Thaw) 107
3.2.4 Cell Lysis Method 2 (MPER Lysis) 107
3.2.5 Western Blots 107
3.2.6 Washout Experiment 108
3.2.7 Cycloheximide Chase Experiment 108
3.2.8 iTRAQ Proteomic Mass Spectrometry 108
3.2.9 LC-MS/MS Analysis of iTRAQ Labeled Peptides 108
3.2.10 OSW-1-Compound Generation and Preparation 108
3.2.11 Synthesis of Deuterated OSW-1 Standard 108

3.2.12 Intracellular OSW-1 Quantification using LC-MS and Single-Cell MS Methods 109
3.2.13 Single-Cell MS Analysis 109
3.2.14 Proteasome Inhibitor Experiment 110
3.2.15 Calpain Inhibitor Experiment 111
3.2.16 Autophagy Experiment 111
3.2.17 RT-PCR Analysis 112
3.2.18 RNA Seq Analysis 113
3.2.19 Cell Media Analysis for OSBP Levels 114
3.2.20 Cell Pellet Analysis for OSBP Levels 115
3.2.21 Statistical Analysis 115
3.3 Results 116
3.3.1 Persistent intracellular OSW-1-compound is not responsible for long-term OSBP repression 116
3.3.2 Verification of long-term OSBP repression results 118
3.3.3 Long-term OSBP repression does not occur through canonical mechanisms and is mediated through RNA regulation 120
3.3.4 OSW-1-compound treatment induces cellular autophagy through mTORc1 inhibition 125
3.3.5 Global transcriptomic and proteomic analysis reveal significant changes to RNA regulation after OSW-1-compound treatment 131
3.4 Discussion 135
3.5 Conclusions 141

Chapter 4: Ligand binding profiling and structure-activity relationship (SAR) of ORP subfamily 1: OSBP and ORP4 143
Abstract 143
Allocation of Contribution 143
4.1 Introduction 144
4.2 Materials and Methods 148
4.2.1 Plasmids and Cloning 148
4.2.2 General Cell Culture and Cell Lines 148
4.2.3 Transfection Procedure 149
4.2.4 MPER Cell Lysis for Binding Assay Procedure 150
4.2.5 [^{3}H]25-OHC Competitive Binding Assay Procedure 150
4.2.6 Western Blot 151
4.2.7 OSBP/ORP4 Homology Modeling and Docking Studies 152
4.3 Results 153
4.3.1 OSBP and ORP4 do not bind non-cholesterol oxysterols 153
4.3.2 OSBP and ORP4 bind a variety of cholesterol oxysterols with varying oxidation position and stereochemistry 155
4.3.3 Structure-activity relationship (SAR) studies against oxysterol side chain analogs 159
4.3.4 THEV SAR studies against OSBP and ORP4 165
4.4 Discussion 168
4.5 Conclusions 170
Chapter 5: Conclusions and Future Directions 172

References 179

Appendix 1: Chapter 2 Supplemental..... 206

Appendix 2: Chapter 3 Supplemental..... 225

Appendix 3: Chapter 4 Supplemental..... 232

List of Tables

Table 1. K_i binding values (nM) of non-cholesterol oxysterol compounds..... 155
Table 2. K_i binding values (nM) of cholesterol oxysterols..... 159
Table 3. K_i binding values (nM) of oxysterol side chain analogs (SA) 162

List of Figures

Figure 1: Cholesterol and 25-hydroxycholesterol structure and numbering. 3

Figure 2: Human OSBP/ORP subfamilies and protein domains. 5

Figure 3: ORP-ORD (human) and Osh-ORD (yeast) protein crystal structures with cholesterol or oxysterol bound. 6

Figure 4: OSBP and ORP4 targeting small molecules. 47

Figure 5: 25-Hydroxycholesterol and OSBP Interacting Small-Molecule Antiviral Compounds. 57

Figure 6: Cellular OSBP and ORP4 levels decrease after OSW-1-compound treatment. 71

Figure 7: OSBP and ORP4 loss is proteasome-dependent. 72

Figure 8: OSBP levels are more substantially decreased than ORP4 levels after OSW-1-compound treatment. 74

Figure 9: Experimental workflow for “the washout experiment”. 75

Figure 10: Low dose (1 nM), transient treatment (6-hour) with the OSW-1-compound results in a persistent, multigenerational decrease in OSBP levels. 76

Figure 11: Mass spectrometry confirms OSBP loss in cells after OSW-1-compound treatment. 77

Figure 12: OSBP loss occurs in all cell lines tested under WO conditions and OSW-1-compound treatment with concentrations less than 1 nM and exposure times less than 1-hour result in significant OSBP loss. 78

Figure 13: OSBP and ORP4 levels are regulated differently after OSW-1-compound treatment despite the same mechanism of loss and similar half-lives. 81

Figure 14: iTRAQ proteomic mass spectrometry reveals OSW-1-compound treatment does not broadly alter the cellular proteome. 82
Figure 15: OSW-1-compound treatment induces prophylactic antiviral activity against clinically isolated *Enteroviruses*..... 85
Figure 16: The OSW-1-compound is the only OSBP-targeting antiviral compound that decreases cellular OSBP levels. 87
Figure 17: The OSW-1-compound is the only OSBP-targeting compound that induces prophylactic antiviral activity. 89
Figure 18: The OSBP-targeting antiviral compounds interact with OSBP through different modes of binding. 92
Figure 19: THEV co-incubation with the OSW-1-compound rescues OSW-1-compound induced OSBP loss and ORP4-targeting associated cytotoxicity. 94
Figure 20: The OSBP-interacting antiviral compounds have distinct effects on OSBP localization in cells. 97
Figure 21: Intracellular OSW-1-compound levels are undetectable 24 hours post-washout (pWO). 117
Figure 22: OSBP is not trapped in the cell pellet, or released into the cell media after OSW-1-compound treatment..... 119
Figure 23: Long-term OSBP repression is not regulated on a transcriptional or post-translational level. 122
Figure 24: Exogenous OSBP-Myc-His is not regulated in the same manner as endogenous OSBP. 124
Figure 25: OSW-1-compound treatment induces cellular autophagy. 126

Figure 26: OSW-1-compound treatment inhibits mTORc1. 128
Figure 27: OSW-1-compound treatment decreases ribosomal subunit production on both a transcript and protein level. 130
Figure 28: Proteomic and transcriptomic analysis after OSW-1-compound washout treatment. 131
Figure 29: Gene ontology analysis of iTRAQ and RNA Seq datasets. 134
Figure 30: OSBP transcript variants. 135
Figure 31: Non-cholesterol oxysterol compounds do not competitively inhibit [^{3}H]25-OHC binding to OSBP or ORP4. 154
Figure 32: Library of cholesterol oxysterols with varying hydroxylation positions and stereochemistry tested in the [^{3}H]25-OHC competitive binding assay. 157
Figure 33: OSBP and ORP4 require the sterol isohexyl side chain for binding. 161
Figure 34: Any modification of the isohexyl sterol side chain length significantly impairs binding to OSBP and ORP4. 164
Figure 35: OSBP-THEV homology modeling and docking. 165
Figure 36: The THEV THP group approximates the sterol side chain in the sterol binding pocket. 166
Figure 37: The C-3 THP group of THEV is required for binding to OSBP and ORP4. 167
Figure 38: Proposed innate antiviral response model. 179
Figure 39: Full Western blots of Figure 6. 206
Figure 40: Full Western blots of Figure 7. 207
Figure 41: Full OSBP Western blots of Figure 8A. 208

Figure 42: Full ORP4 Western blots of Figure 8B. 209
Figure 43: Full Western blots of Figure 10A. 210
Figure 44: Full Western blots of Figure 10B. 211
Figure 45: Full Western blots of Figure 12A. 212
Figure 46: Full Western blots of Figure 12B. 213
Figure 47: Full Western blots of Figure 12C. 214
Figure 48: Full Western blots of Figure 12D. 215
Figure 49: Full Western blots of Figure 13A. 216
Figure 50: Full Western blots of Figure 13B. 217
Figure 51: Full Western blot of lysate for iTRAQ proteomic mass spectrometry analysis in Figure 14. 218
Figure 52: Full Western blot of HeLa cell washout experiment for Figure 15. 219
Figure 53: Full Western blots of Figure 16. 220
Figure 54: Full Western blots of Figure 17C. 221
Figure 55: Full OSBP binding curves for Figure 18. 222
Figure 56: Full ORP4 binding curves for Figure 18. 223
Figure 57: Full Western blot of Figure 19A. 224
Figure 58: Full Western blots of Figure 23A. 225
Figure 59: Full Western blots of Figure 23B and Figure 25A. 226
Figure 60: Full Western blots of an RNA Seq sample for Figure 23D (top) and Figure 23E (bottom). 227
Figure 61: Full Western blots of Figure 24. 228
Figure 62: Full Western blots of Figure 25B (left) and Figure 25C (right). 229

Figure 63: Full Western blots of Figure 26B (top) and Figure 26C (bottom). 230

Figure 64: RNA Seq bioinformatics analysis outline for Figure 28B. 231

Figure 65: Full Western blots of OSBP and ORP4 binding lysates. 232

Figure 66: OSBP and ORP4 binding curves for 25-OHC. 233

Figure 67: OSBP and ORP4 binding curves for UDCA. 234

Figure 68: OSBP and ORP4 binding curves for TUDCA. 235

Figure 69: OSBP and ORP4 binding curves for Serofendic Acid 236

Figure 70: OSBP and ORP4 binding curves for U-18666A. 237

Figure 71: OSBP and ORP4 binding curves for Diosgenin. 238

Figure 72: OSBP binding curves for Digitoxigenin 239

Figure 73: OSBP and ORP4 binding curves for Paxilline. 240

Figure 74: OSBP binding curves for 22-azacholesterol. 241

Figure 75: OSBP and ORP4 binding curves for 21-acetoxypregnenolone. 242

Figure 76: OSBP and ORP4 binding curves for 25-hydroxycholestanol. 243

Figure 77: OSBP and ORP4 binding curves for 7α-25-diOHC. 244

Figure 78: OSBP binding curves for 5α-OHC-6-ketocholesterol. 245

Figure 79: OSBP and ORP4 binding curves for 25(*R*),27-diOHC 246

Figure 80: OSBP and ORP4 binding curves for 25(*S*), 27-diOHC. 247

Figure 81: OSBP and ORP4 binding curves for 24(*R*)-OHC. 248

Figure 82: OSBP and ORP4 binding curves for 24(*S*)-OHC. 249

Figure 83: OSBP and ORP4 binding curves for 22(*R*)-OHC. 250

Figure 84: OSBP and ORP4 binding curves to 22(*S*)-OHC. 251

Figure 85: OSBP and ORP4 binding curves for 20(*R*), 22(*S*)-OHC. 252

Figure 86: OSBP and ORP4 binding curves for 20-OHC. 253
Figure 87: OSBP and ORP4 binding curves for SA-1. 254
Figure 88: OSBP and ORP4 binding curves for SA-2. 255
Figure 89: OSBP and ORP4 binding curves for SA-3. 256
Figure 90: OSBP and ORP4 binding curves for SA-4. 257
Figure 91: OSBP and ORP4 binding curves for SA-5. 258
Figure 92: OSBP and ORP4 binding curves for SA-6. 259
Figure 93: OSBP and ORP4 binding curves for SA-7. 260
Figure 94: OSBP and ORP4 binding curves for SA-8. 261
Figure 95: OSBP and ORP4 binding curves for SA-9. 262
Figure 96: OSBP and ORP4 binding curves for SA-10. 263
Figure 97: OSBP and ORP4 binding curves for SA-11. 264
Figure 98: OSBP and ORP4 binding curves for SA-12 265

Abstract

The overall aim of my work was to better understand the cellular biology, biochemistry, and molecular pharmacology of oxysterol-binding protein (OSBP) and OSBP-related protein 4 (ORP4). More specifically, my research uses standard cellular biology and protein biochemistry approaches, coupled with a chemical genetics approach, to probe the function, regulation, and disease contributions of OSBP and ORP4 to develop these proteins as viable drug targets; with particular emphasis on studying OSBP as a broad-spectrum antiviral target.

OSBP and the ORPs comprise a family of lipid-binding proteins organized into 6 subfamilies. ORP subfamily 1 consists of OSBP and its closest homolog, ORP4. OSBP is required for the proliferation of a wide array of human pathogenic RNA viruses, while ORP4 is required for the survival and proliferation of cancer cells, making OSBP and ORP4 attractive broad-spectrum antiviral and precision anticancer targets, respectively. The naturally occurring small molecule OSW-1 selectively targets OSBP and ORP4 with high affinity and is used as a chemical probe in this dissertation, along with various other small molecules, to study OSBP and ORP4.

Chapter 1 introduces the OSBP/ORP protein family and discusses the previously established biology and disease contributions of OSBP and ORP4, while also introducing the research approach used to study these proteins in this dissertation.

Chapter 2 outlines the discovery of a unique OSBP regulatory response in cells, triggered by the OSW-1-compound, that results in the long-term repression of cellular OSBP levels. In human cells, transient, non-toxic treatment of the OSW-1-compound resulted in ~90% multigenerational decrease in cellular OSBP levels that persists for over 72 hours after the compound has been removed. We were able leverage the discovery of this response to induce *prophylactic* antiviral activity in cells (i.e., the cells retain antiviral activity in the absence of the OSW-1-compound). The long-term repression of OSBP and the prophylactic antiviral activity are unique to the OSW-1-compound and not generally OSBP-targeting small molecules. These results establish the OSW-1-compound as the first identified antiviral prophylactic small molecule that exerts activity through modulating a host protein (i.e., OSBP). We also reveal that OSBP can be targeted in multiple, distinct ways for antiviral development.

Chapter 3 investigates the mechanism of OSBP regulation responsible for long-term OSBP repression, and other responses triggered by the OSW-1-compound. We show that OSBP levels are not repressed by canonical mechanisms of protein regulation. Instead, the OSW-1-compound triggers OSBP regulation on an RNA level, and also causes significant changes to an RNA regulatory pathway and antiviral host defense mechanism called nonsense-mediated decay (NMD). Additionally, we determined that OSW-1-compound treatment induces cellular autophagy through mTORc1 inhibition. Collectively, our results indicate the responses triggered by the OSW-1-compound create a multifaceted innate antiviral environment in cells. We hypothesize that this multifaceted response comprises an unidentified arm of innate antiviral response in cells that could harnessed by small molecules and exploited to create a new class of broad-spectrum preventative antiviral compounds.

Chapter 4 reports the first comprehensive structure-activity relationship (SAR) study of oxysterol binding to human OSBP and ORP4. OSBP and ORP4 are attractive antiviral and precision anticancer drug targets, respectively; however, drug development

against these proteins is limited by the lack of defined SAR between OSBP and ORP4 and their oxysterol ligands. The characterization of oxysterol ligand binding to OSBP and ORP4 performed in this chapter provides critical information necessary to guide the development of novel small-molecule antiviral and anticancer therapeutics.

Chapter 5 summarizes and outlines the implications of the findings in this dissertation, and introduces our current overall model of our innate antiviral response hypothesis.

In total, the work presented in **Chapters 2-5** outlines the discovery and elucidation of novel OSBP cellular biology that can be triggered by exogenous small molecules and exploited as a novel OSBP-centered preventative broad-spectrum antiviral therapeutic approach. We also comprehensively investigate small molecule binding to OSBP and ORP4 and reveal that OSBP can be targeted for antiviral development in multiple, distinct ways.

Chapter 1. Introduction

1.1 Overview of the OSBP/ORP family of proteins

Oxysterol-binding protein (OSBP) and the OSBP-related proteins (ORPs) constitute a conserved family of lipid-binding proteins found in eukaryotes [1,2]. The founding member of this family, OSBP, was discovered in the 1980s by its ability to bind 25-hydroxycholesterol (25-OHC) and other oxysterols (**Figure 1**) [3,4]. OSBP was first successfully cloned from cells in 1989, and by 2001, human genome sequencing revealed 11 OSBP-related protein in humans (ORPs 1-11), organized into six subfamilies (**Figure 2**) [2,5–8]. The research in this dissertation primarily pertains to ORP subfamily 1 members, OSBP and ORP4; however, the sequence similarity and potential redundancy in function of the ORP protein family suggests that the findings in this dissertation may also be relevant to the other ORP subfamilies (**Figure 2**). The OSBP/ORPs have a wide range of reported functions in lipid trafficking and cellular regulation that are incompletely understood [1,2]. Importantly, the OSBP/ORPs have also been implicated in various human disease states [9,10].

Despite these diverse reported cellular activities, the individual OSBP/ORPs all share the ability to bind lipids using an ~50kDa C-terminal OSBP-related ligand-binding domain (ORD) (**Figure 2**) [1,2]. ORDs present in individual OSBP/ORPs are reported to bind different lipids including cholesterol (**1**), oxysterols (**2**), and phospholipids (**Figure 1**) [1,2]. The ORDs of all OSBP/ORPs contain a conserved fingerprint region, with the amino acid sequence 'EQVSHHPP' (**Figure 2**) [8,11]. The ability to bind lipids allow many OSBP/ORPs to commonly function in non-vesicular lipid transport , a poorly understood, yet critical process in cells [12–14]. More specifically, OSBP/ORPs frequently act as lipid

transfer proteins (LTPs), transporting lipid monomers between targeted organelles [1,2,15]. The hydrophobic nature of lipids does not permit their unaided movement through the aqueous cytosol to the various organelles that require them [12–14]. The OSBP/ORPs engaged in the inter-organelle transport of lipids interact with organelles at locations in the cell that are extremely close in space (e.g. ER and Golgi membranes, 10-20 nm apart), known as membrane contact sites (MCSs), which allows the protein to contact the two organelles simultaneously and form a protein bridge between them [12,15]. Consequently, the OSBP/OPRs possess various protein domains that allow for the targeting of different organelle membranes, facilitating lipid transfer between the contacted organelles (**Figure 2**) [1,2]. Many OSBP/ORPs, including OSBP and ORP4, possess a PH domain, which can anchor the protein to membranes containing phosphatidylinositol 4-phosphate (PI4P) (e.g. the Golgi, lysosomes etc.) (**Figure 2**) [1,2]. Additionally, OSBP, ORP4, and many other ORPs possess an FFAT domain, which interacts with the endoplasmic reticulum (ER)-resident protein VAP, effectively anchoring the protein to the ER (**Figure 2**) [1,2]. A combination of PH and FFAT domains therefore allow for OSBP/ORPs to simultaneously anchor to the ER and another organelle membrane, such as the Golgi, and traffic cholesterol from the ER, where it is synthesized, to the Golgi [1,2,15]. Cholesterol trafficking from the ER to the Golgi in this manner is one of the better elucidated activities of OSBP in the cell (see **Section 1.4: OSBP biology** for more information) [15].

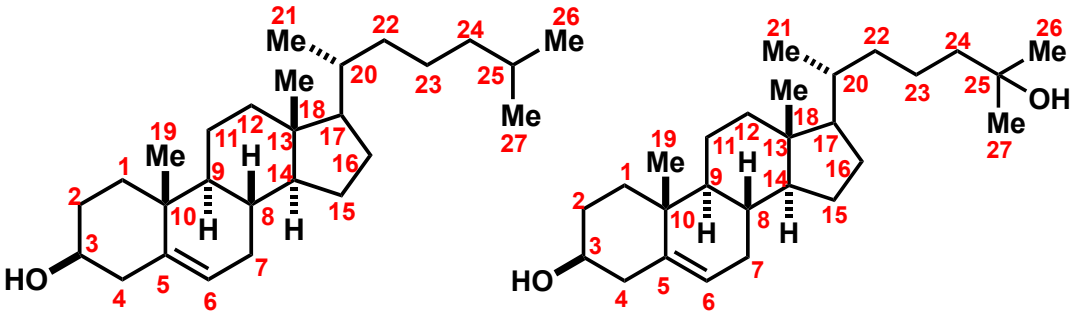

Figure 1: Cholesterol and 25-hydroxycholesterol structure and numbering. Cholesterol (**1**) is an abundant and essential 27-carbon biomolecule, consisting of a sterol core (rings A-D), and a sterol side chain. Oxidation of the sterol core or sterol side chain, introducing a carbonyl, hydroxyl, or epoxide functional group creates a cholesterol derivative with increased polarity known as an oxysterol (**2**). For example, when cholesterol is hydroxylated at C25, the resultant oxysterol is named 25-hydroxycholesterol (**2**) [290].

1.2 Overview of OSBP/ORP ligand binding

Despite recent advancements, information pertaining to how these proteins precisely interact with sterols, oxysterols and phospholipids in the ORD is limited, and minimal structural data exists for this family of proteins. The majority of the scarce structural information is derived from crystal structures of the ORD of certain ORP homologs in yeast, known as Osh proteins, from *S. cerevisiae* (Osh3, Osh4, and Osh6), and *K. Lactis* (Osh1) (**Figure 3C, D**) [16–19]. More recently, crystal structures were determined for human ORP subfamily 2 members, ORP1-ORD and ORP2-ORD, complexed with cholesterol and PI(4,5)P_2, respectively (**Figure 3A, B**) [11,20]. Despite large differences in overall sequence identity between yeast Osh and human ORP proteins, the core of the ORP1-ORD, where sterols (i.e., cholesterol and oxysterols) bind, is highly

conserved and exhibits a similar arrangement of ligand interacting hydrophobic residues in the binding tunnel between the two species [20].

The ORD structure consists of a hydrophobic 19-strand β-barrel, flanked by two central helices, and capped with a flexible N-terminal α-helical lid (**Figure 3**) [2,21]. Collectively, these structures revealed that sterols enter a linear, hydrophobic binding pocket in the ORD, in a conserved "head-down" sterol binding orientation, with the 3-hydroxyl of the sterol A-ring at the bottom of the binding pocket (**Figure 3**) [1,2,9,16–19,20]. The sterol core interacts with a number of hydrophobic residues as it extends up the interior of the hydrophobic binding tunnel, with the sterol side chain extending up toward the N-terminal lid, interacting with hydrophobic residues in the lid (**Figure 3**) [1,2,9,16–19,20]. Sterols and phospholipids bind competitively in the ORD, with the phospholipid headgroup interacting with the histidine residues in the fingerprint region at the entrance of the ORD binding pocket, orienting phospholipids in a conserved "tail-first" manner, with the phospholipid acyl chains extending into the hydrophobic binding pocket [2,22]. The two histidine in the fingerprint region are required for phospholipid binding to the ORPs (**Figure 2**) [11,15,23,24]. More details on ligand binding to the OSBP/ORP ORD can be found in **Chapter 4**.

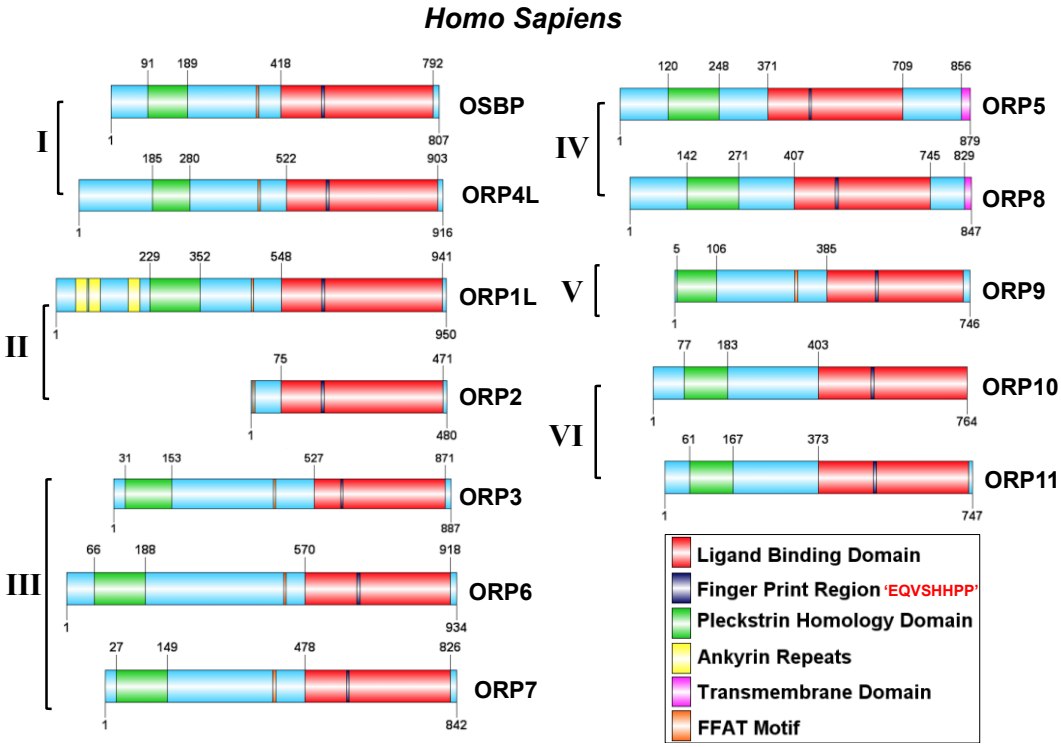

Figure 2: Human OSBP/ORP subfamilies and protein domains.
The OSBP/ORPs found in humans can be organized into six subfamilies. All ORPs share an OSBP-related ligand-binding domain (ORD) (red) that binds sterols and phospholipids. Within the ORD resides a conserved fingerprint region (purple) that all ORPs share, with the consensus sequence 'EQVSHHPP'. OSBP and ORP4 comprise subfamily 1.

The OSBP/ORPs have been shown to bind and transport a broad array of sterols and phospholipids, and have been observed executing various activities in the cell [2,25,26]. Originally implicated as merely oxysterol binding proteins, the OSBP/ORPs have more recently emerged as critical mediators of many lipid-related biological processes, with important contributions to human disease biology [2,9,10].

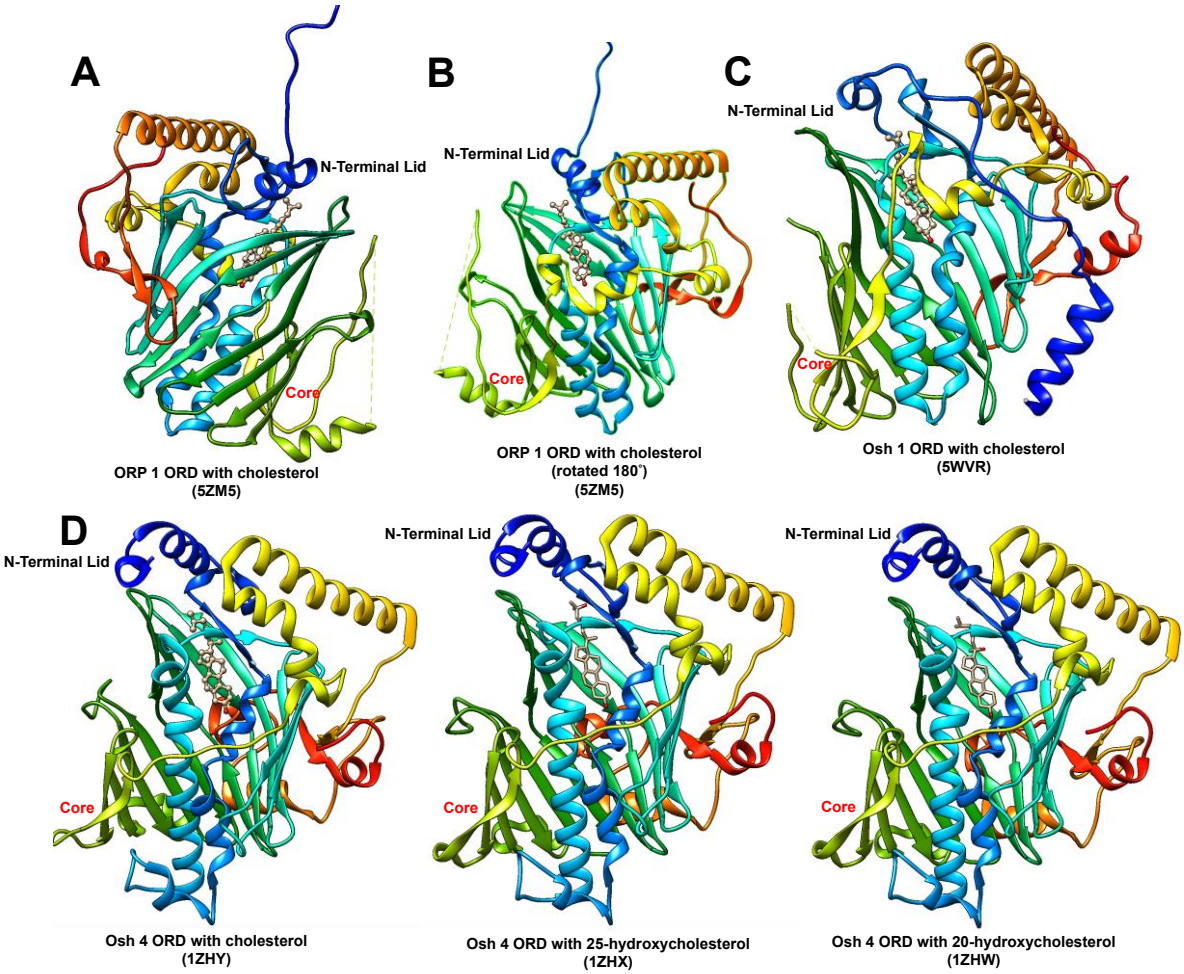

Figure 3: ORP-ORD (human) and Osh-ORD (yeast) protein crystal structures with cholesterol or oxysterol bound.

A) Human ORP1-ORD β-barrel (green) with cholesterol bound in the ORD sterol binding pocket, showing the sterol head (A-ring) oriented at the bottom of the hydrophobic tunnel, and the sterol side chain extending toward the top of the tunnel, interacting with the N-terminal lid region of the protein (blue). **B)** ORP1-ORD with cholesterol bound rotated 180º with β-barrel rotated to the back and the two central helices (blue) rotated to the front to better visualize the cholesterol ligand. **C)** *K. Lactis* (yeast) Osh1 with cholesterol bound. **D)** *S. cerevisiae* (yeast) Osh4 with cholesterol, 25-OHC, and 20-OHC bound. Collectively, these structures reveal that both cholesterol and oxysterols bind in a conserved "head-down" binding orientation in the ORP and Osh-ORD sterol binding pocket. Images were generated using UCSF Chimera. Protein colored rainbow (blue for N-terminus, red for C-terminus).

1.3 Lipids in biology

1.3.1 Sterols

The OSBP/ORPs cellular function centers on the capability to bind and transport lipids, particularly sterols and phospholipids [2,9,10]. Cholesterol (**Figure 1** (**1**)) is a lipophilic biomolecule that is commonly found as a structural component in various cellular membranes, mediating membrane fluidity and rigidity [27,28]. In addition to being a critical structural component of cell membranes, cholesterol and cholesterol derivatives, called oxysterols, are the precursors of many other critical biomolecules such as bile acids, vitamin D, and steroid hormones [28]. Oxysterols, such as 25-OHC, are cholesterol derivatives that are oxidized on the sterol core or sterol side chain resulting in the introduction of oxygen containing functional groups like hydroxyls, carbonyls, or epoxides (**Figure 1** (**2**)) [29,30]. This oxidation can occur enzymatically, primarily by cytochrome P450 enzymes, or non-enzymatically through autoxidation processes [29].

In addition to being important biosynthetic intermediates of bile acids, steroid hormones and vitamin D, oxysterols have more recently been recognized as bioactive molecules, involved in various cellular phenomena such as liver X receptors (LXRs), sterol regulatory-element binding proteins (SREBPs), certain G protein-coupled receptors (GPCRs), and the Hedgehog signaling pathway [30]. LXRs are nuclear receptors involved in the transcriptional regulation of lipid metabolism and are activated by oxysterols [31,32]. Transcription factors, known as SREBPs, are the master regulators of cholesterol synthesis and are regulated by oxysterols [33]. Additionally, oxysterols are also important regulators of cholesterol homeostasis on a non-transcriptional level [33]. The Hedgehog signaling pathway is a cellular pathway activated by oxysterols that is critical

for embryonic development, adult stem cell maintenance, and is also involved in cancer biology [34]. Oxysterols are also ligands for certain GPCRs [30,35]. GPCR183 binds 7α, 27-OHC and mediates cellular immune processes [35]. In summary, oxysterols are not just oxidized cholesterol by-products and metabolic intermediates, but rather, possess a pervasive role in many distinct areas of biology.

1.3.2 Phospholipids

Phospholipids are also important lipids in biology, and ligands for the OSBP/ORPs. Phospholipids are amphipathic molecules, and are the primary component of the phospholipid bilayers that compartmentalize cells and organelles; consequently, phospholipids are frequently found in various cellular membranes [36]. Aside from their obvious structural role comprising all cellular membranes, phospholipids have various other roles in the cell, including as second messengers in cell signaling transduction [36,37].

Phospholipid based second messengers can be activated in various ways, including GPCR activation [37]. Activated GPCR receptors use phospholipases to cleave certain membrane phospholipids resulting in the generation of inositol 1,4,5-triphosphate (IP_3) and diacylglycerol (DAG) [37,38]. The cleaved IP_3 functions as a second messenger, binding to IP_3 receptors and inducing Ca^{2+} release from the ER to regulate various cellular activities (e.g. oxidative phosphorylation) [37,38].

Phospholipids can also be utilized as fuel sources for lipid transport in the cell [39]. Generally speaking, the OSBP/ORPs appear to bind phospholipids in the ORD for two reasons: facilitate phospholipid transport between membranes, and counter-transporting phospholipids as an energy source to transport other lipids against a concentration

gradient [2,15,40]. Phospholipids can be utilized as an energy source to transport lipids against their concentration gradient similar to how ATP is utilized as an energy source for ion pumps to transport ions across their concentration gradient [39]. Cholesterol transfer from the ER to the Golgi by OSBP requires the subsequent counter-transport of PI4P from the Golgi to the ER, where the PI4P phosphate group is cleaved by the enzyme, Sac1, to provide energy for the cholesterol trafficking (see **Section 1.4.2: OSBP biology: Cholesterol Trafficking** for more information on how OSBP/ORPs use phospholipids for lipid transport) [15,39].

1.4 OSBP biology

1.4.1 Overview of OSBP

OSBP was originally investigated in the 1980s as the potential missing link in the end-product regulatory feedback mechanism of cholesterol biosynthesis in cells [4,5,41,42]. End-product regulated cholesterol biosynthesis in cells (i.e., the rate of cholesterol biosynthesis is decreased in an organism if cholesterol is provided in the diet) was first discovered in the early 1930s [43], but the precise mechanisms mediating this regulation remained unclear until the 1990s [44,45]. Early reports observed that various oxysterols potently repressed both cellular cholesterol biosynthesis and uptake [46]. Additionally, multiple sterol-repressed genes were discovered to contain a common nucleotide sequence named the sterol regulatory element (SRE) [47–49]. Together, these observations implied the existence of an endogenous oxysterol-binding protein that was capable of integrating oxysterol levels and cholesterol homeostasis through interaction with SREs [42]. The discovery and elucidation of OSBP was pursued as the potential SRE regulator of cholesterol biosynthesis in the cell [42]. Despite initially encouraging results after the

discovery of OSBP, further investigation determined that although OSBP specifically binds oxysterols with high affinity, it had no apparent role in regulating cholesterol biosynthesis or acting through SREs. A new protein class, sterol regulatory element-binding proteins (SREBPs), were later found responsible for the oxysterol-mediated regulation of cholesterol biosynthesis in 1993 [44,45]. Despite this early misdirection, OSBP has since been implicated in a number of other critical lipid-related biological processes; however, many of OSBP's cellular activities remain poorly understood.

OSBP is an 807 amino acid, ~89 kDa protein ubiquitously expressed in all human tissues [50,51]. OSBP has been reported to be involved in various cellular activities including non-vesicular lipid transport, regulation of lipid metabolism, and cell signaling [9]. The OSBP-ORD has been reported to bind 25-OHC with a K_D of 8-32 nM and cholesterol with a K_D of 173 nM , as well as phosphatidylinositols with undetermined binding values [2,5,9,15,42,52–55] (**Figure 4A**). As previously mentioned, no structural data of OSBP currently exists, but mutational studies have shown that the OSBP fingerprint region in the ORD is required for phosphatidylinositol binding, while the 'ELSK' motif in the OSBP-ORD is required for sterol binding (**Figure 2, 3**) [11]. In addition to an ORD, OSBP possesses an FFAT domain used to interact with the ER-resident protein, VAP, and an N-Terminal PH domain that interacts with Arf1 and PI4P, which are commonly in the Golgi membrane [9,26,56]. This domain architecture allows OSBP to function at MCSs between various cellular organelles (e.g. the ER and the Golgi) and transfer lipids between the contacted organelles [2].

1.4.2 Cholesterol Trafficking

One of the better understood activities of OSBP in the cell is the ability to transfer cholesterol between membranes [2,15]. OSBP has been shown to localize to the ER-Golgi interface under certain stimuli [15,51,57]. Increases in cellular 25-OHC levels or decreases in cellular cholesterol levels, results in localization of OSBP from the cytosol to the ER-Golgi to mediate the transport of cholesterol from the ER, where it is synthesized, to the Golgi [15,57]. This transfer occurs at MCSs between the ER and Golgi and is accomplished through various localization domains [2,15]. An FFAT domain interacts with the ER-resident protein, VAPA; while the PH domain interacts with PI4P and Arf1 in the Golgi membrane, effectively anchoring OSBP between the two organelles [15]. The cholesterol transfer activity also requires the subsequent counter-transport of PI4P by OSBP from the Golgi to the ER, where it is hydrolyzed by the ER enzyme, Sac1; sustaining the PI4P gradient and providing the energy necessary for OSBP to transport cholesterol from the ER to the Golgi against its concentration gradient [15,51]. PI4P counter-transport and subsequent hydrolysis by Sac1 provides the fuel for the trafficking of cholesterol and is analogous to the use of ATP by ion pumps [39,58]. The cholesterol trafficking of OSBP is believed to "burn" approximately 50% of cellular PI4P [39,58]. The immense amount of PI4P required to sustain this process may be regulated in part by OSBP interaction with PI4KB, a kinase that catalyzes the production of PI4P [39,58]. OSBP and PI4KB co-localize and both interact with Arf1 in the Golgi membrane, which may be a mechanism to locally supply OSBP with PI4P as it burns through a considerable amount of the cellular PI4P stores [39,58]. OSBP has been shown to transport cholesterol between other organelles as

well, including between the ER and lysosome, using the OSBP PH domain to interact with PI4P in the lysosomal membrane [59].

1.4.3 Lipid Metabolism

OSBP has been reported to regulate sphingomyelin (SM) biosynthesis through indirect regulation of the ceramide transfer protein, CERT; therefore, OSBP effectively integrates sterol regulation and SM biosynthesis in the cell [60–62]. The biosynthesis of SM occurs in the Golgi through the metabolism of ceramide, which is transported from the ER to the Golgi by CERT [60–62]. SM biosynthesis can be stimulated in cells by increasing cellular 25-OHC levels, or decreasing cellular cholesterol, suggesting a connection between OSBP localization stimuli and stimulation of SM biosynthesis [60–62].

The transport of ceramide by CERT was found to be dependent on both OSBP and VAPA [60–62]. RNAi of either OSBP or VAPA, in multiple cell lines, inhibited CERT-dependent ceramide transport to the Golgi, while overexpression of OSBP enhanced 25-OHC stimulated SM biosynthesis [60–62]. OSBP interaction with VAPA via the OSBP FFAT domain, and PI4P/Arf interaction via the OSBP PH domain were also shown to be required for CERT recruitment to the Golgi and subsequent SM biosynthesis [60–62]. Curiously, OSBP and CERT only displayed weak interactions with each other, implying that OSBP-CERT interaction is not driving OSBP-dependent CERT localization to the Golgi [60–62]. Instead, it is proposed that OSBP ER-Golgi localization, resulting in OSBP PH domain-Arf1 interaction at the Golgi, may stimulate the co-localized PI4KB enzyme. PI4KB stimulation would locally increase PI4P levels at the Golgi and subsequently recruit CERT, which also localizes to the Golgi through a PI4P-interacting PH domain

[60–62]. This model is supported by OSBP FFAT mutants that cannot bind VAPA, but still stimulate recruitment of CERT to the Golgi; however, these mutants did not restore SM biosynthesis [60–62]. These results suggest that the OSBP PH domain interactions with the Golgi are stimulating CERT localization, but both OSBP ER and Golgi interaction are required to restore SM biosynthesis [60–62].

1.4.4 Cell Signaling

OSBP has been reported to be phosphorylated at Ser240 by Protein Kinase D (PKD), a Golgi-localized kinase that also activates PI4KB and inhibits CERT function via phosphorylation [63]. PKD is localized and activated at the Golgi by interacting with diacylglycerol (DAG) that accumulates as a product of SM biosynthesis [63]. OSBP is phosphorylated by PKD at the Golgi, which leads to impairment of OSBP Golgi localization through masking of the OSBP PH domain, potentially via phosphorylation-induced interaction with another protein [63]. OSBP phosphorylation by PKD at Ser240 also impairs CERT Golgi localization and induces Golgi fragmentation [63]. The SM product-mediated Golgi localization of PKD, in combination with its role in OSBP, PI4KB, and CERT regulation via phosphorylation, indicates that PKD phosphorylation is part of a SM biosynthesis regulatory feedback loop [63]. Consistent with this model, depletion of SM or cholesterol causes the dephosphorylation of OSBP and reestablishes Golgi localization for cholesterol trafficking and SM biosynthesis [63,64]. Further studies have revealed that OSBP is also phosphorylated at Ser381-391 and Ser195 and 200, and this phosphorylation regulates OSBP ER activity [64].

OSBP is also reported to be involved in various lipid-related cell signaling responses, functioning commonly as a sterol-dependent scaffold protein for signaling complexes. OSBP is reported to function as a cytoplasmic sterol sensor that regulates ERK 1/2 signaling [53,65]. OSBP was observed in a ~440 kDa oligomeric complex with the serine/threonine phosphatase PP2A, the tyrosine phosphatase PTPPBS, and cholesterol [53,65]. This complex has dual phosphatase activity against phosphorylated ERK 1/2 (pERK 1/2) and thus negatively regulates ERK 1/2 phosphorylation and activation [53,65]. The OSBP PH domain was required to form the oligomeric complex with cholesterol, PP2A, and PTPPBS [53,65]. When cellular cholesterol is lowered or cellular oxysterols are increased, the oligomeric OSBP-dual phosphatase complex disassembles in manner believed to unmask the OSBP PH domain, resulting in ablation of the negative ERK 1/2 regulation and therefore activation of ERK 1/2 signaling [65]. Complex disassembly and PH domain unmasking results in OSBP localization to the ER-Golgi to transport and resupply the cell with cholesterol [53,65]. A subsequent study confirmed the role of OSBP in ERK 1/2 regulation, showing that OSBP overexpression reduces pERK levels in hepatocytes [66]. Although ERK 1/2 signaling can mediate a myriad of cellular responses, the study did not directly show the downstream effect of ERK 1/2 activation on cellular cholesterol; however, ERK signaling is intimately involved in cholesterol homeostasis, and depletion of membrane cholesterol has previously been shown to significantly increase pERK levels in cells [53,65,67]. It is hypothesized that the OSBP-dual phosphatase complex functions as a cytoplasmic sterol sensor [53,65]. OSBP has a higher affinity for 25-OHC than cholesterol (**Figure 4A**), thus as cellular cholesterol is depleted and oxidized into oxysterols, these oxysterols may displace cholesterol from the OSBP-ORD [53,65].

Competitive displacement of cholesterol from the OSBP-ORD results in disassembly of the oligomeric complex, ERK 1/2 activation, and OSBP ER-Golgi localization to facilitate replenishment of cellular cholesterol and mediate its transport throughout the cell [53,65].

The results of another study looking at the role of OSBP in hepatocytes suggests that OSBP may also have a role in insulin signaling [66]. This study found that OSBP silencing in hepatocytes inhibited insulin-mediated induction of SREBP-1c. Additionally, overexpression of OSBP has similar effects on SREBP-1c, Insig-1 and Insig-2a responses as insulin [66]. Due to the role of ERKs in insulin signaling, the authors hypothesize that OSBP's role in ERK signaling may have implications on insulin signaling as well [66].

OSBP is also implicated as an essential mediator of STAT3 activation [68]. 7-ketocholesterol has been shown to increase profilin-1 expression, an actin binding protein that has a role in endothelial dysfunction [68,69]. Further studies revealed that when stimulated with 7-ketocholesterol, OSBP forms an oligomeric complex that regulates STAT3 activation and leads to profilin-1 expression [68]. In unstimulated conditions, the OSBP PH domain is masked, however, upon binding of oxysterol in the OSBP-ORD, a conformational change occurs in OSBP that unmasks the PH domain and facilitates an interaction with JAK2 [68]. Upon interaction with OSBP, JAK2 subsequently phosphorylates the OSBP-ORD at Tyr394 [68]. OSBP Tyr394 phosphorylation creates a site for STAT3 docking to OSBP, resulting in an OSBP-JAK2-STAT3 complex [68]. After STAT3 docks to OSBP, STAT3 is phosphorylated by JAK2, after which STAT3 localizes to the nucleus where it is recruited to the profilin-1 promotor to activate profilin-1 transcription [68].

A recent report also found that OSBP is required for mTORc1 activation [59]. The protein complex, mTORc1, is a main cellular signaling hub responsible for integrating various cellular inputs, such as nutrient levels and growth factors, to regulate downstream cell signaling responses [70]. mTORc1 activation occurs at the lysosome, and this study found that cholesterol trafficked from the ER to the lysosomal membrane by OSBP was required for mTORc1 localization and subsequent activation [59]. Consequently, the chemical or genetic knockdown of OSBP was found to cause mTORc1 inhibition and induce cellular autophagy [59]. This is an important finding, as it indicates that OSBP is required for mTORc1 activation, effectively coupling sterol regulation to mTORc1 signaling [59].

1.5 ORP4 biology

1.5.1 Overview of ORP4

In 1999, ORP4 was the second oxysterol-binding protein discovered, after the founding member, OSBP, and prior to the identification of the rest of the ORP family members [8,71,72]. ORP4 was discovered based on its selective expression in tumor cells and expression correlation with metastasis (see **Section 1.6.2**: **ORP4 as a precision anticancer target** for more information about the role of ORP4 in cancer biology) [72]. ORP4 shares ~64% overall sequence identity and ~67% ORD sequence identity with OSBP and possesses the same protein domains as OSBP, such as the FFAT, PH, and ORD domains [10,56,8,71] . However, despite similar sequence identities and protein domain architecture, OSBP and ORP4 appear to be involved in vastly different cellular activities [9,73].

In contrast to the universal expression of OSBP, ORP4 is only expressed in select human tissues such as the brain, retina, testis, and heart [8,71]. Additionally, ORP4 possesses three N-terminally truncated transcript variants, ORP4L (~108 kDa), ORP4M (~85 kDa), and ORP4S (~50 kDa and 60 kDa) [74–76]. It is important to note that although the ORP4L variant possesses the same domains as OSBP, ORP4M is N-terminally truncated in a manner that also truncates the PH domain, and therefore is not believed to target PI4P like ORP4L. ORP4S is further lacking in domains and possesses only an FFAT domain and a partially truncated ORD [74,76]. Similar to OSBP, the ORP4-ORD can bind 25-OHC with a K_D of 10-54 nM, cholesterol with a K_D of 68 nM, and phosphatidylinositols with undetermined binding values [9,21,52,74,76] (**Figure 4A**). ORP4S is reported to display similar binding values (25-OHC K_D = 23 nM and cholesterol K_D = 60 nM), however, one of the earliest ORP4S publications reported that ORP4S does not bind 25-OHC [74,76]. Relative to OSBP, the function of ORP4 in cells is more unclear. The best elucidated role of ORP4 in the cell is as a G protein-coupled receptor (GPCR) scaffold protein for cell signaling processes involved in cell proliferation and bioenergetics in T-cell Acute Lymphoblastic Leukemia (T-ALL) cell models [38,76,77]. ORP4 also has a role in regulating the vimentin network and is required for the survival and proliferation of immortalized and cancer cell lines [74,76].

1.5.2 Localization and vimentin regulation

Although ORP4L possesses domains for targeting the ER and Golgi, ORP4L appears primarily localized to the plasma membrane (PM) in T-cell Acute Lymphoblastic Leukemia (T-ALL) cells and other cell models [38,76,77]. More recently, and in contrast to

previous reports, ORP4L was also shown to localize to the ER-Golgi upon 25-OHC treatment (or cholesterol depletion) in HeLa cells in an OSBP, VAPA, and PI4P-interaction dependent manner [78]. ORP4L knockout studies revealed that in this context, ORP4L is required for TGN and Golgi organization and PI4P content [78]. Previous studies utilized an ORP4L antibody with an internal epitope which is possibly masked upon Golgi localization; however the use of a new, C-terminal V5 epitope-tagged ORP4L and V5 monoclonal antibody revealed the nuanced localization patterns of ORP4L, clearly showing both Golgi/TGN and PM localization patterns [78]. Although the ER-Golgi localization of ORP4L was dependent on sterol, OSBP, VAPA, and PI4P interaction, ORP4L PM localization was not, suggesting the execution of different cellular activities based on localization [78]. ER-Golgi localized ORP4L appears to be involved in lipid transport and Golgi organization, while PM localized ORP4L appears to be involved in cell signaling processes [38,76,77,78]. The OSBP-interaction dependent ER-Golgi localization of ORP4L implies that OSBP and ORP4L are endogenous interacting partners, and ORP4L is recruited to the ER-Golgi through OSBP interaction [78]. Consistent with this model, previous reports suggest that OSBP and ORP4L may interact endogenously to form heterodimers that require the dimerization domain (OSBP A.A. 261-288, ORP4 A.A. 316-343) [21]. Alternatively, OSBP-dependent ORP4L ER-Golgi localization could be mediated in a manner similar to OSBP-dependent CERT Golgi localization, where OSBP localization stimulates PI4P production at the Golgi that subsequently recruits ORP4L [78].

Additionally, in Chinese Hamster Ovary (CHO) and HeLa cells, ORP4S localized with the structural protein vimentin, resulting in vimentin aggregation (i.e., remodeling)

while ORP4L did not cause aggregation or alter vimentin organization, but weakly associated with peripheral vimentin [21,74]. Vimentin is an intermediate filament (IF), and critical part of the cytoskeleton, with a well-known role in sterol transport and regulation [21,79,80].

In contrast to OSBP, the PH domain of ORP4 does not appear to regulate Golgi localization, but rather regulates ORP4 vimentin network interaction [76]. It is hypothesized that the PH domain of ORP4L may interfere with vimentin localization and aggregation, as ORP4L only weakly associates with peripheral vimentin [74]. Consistent with this hypothesis, both ORP4S and ORP4M were found to localize with vimentin and cause aggregation, which possess no PH domain and an N-terminally truncated, predicted non-functional PH domain, respectively [74,76]. Additionally, ORP4L PH domain mutants that cannot bind PI4P caused vimentin localization and aggregation [74,76].

The weak association of ORP4L with vimentin is sterol independent and is believed to occur as a consequence of the ORP4L leucine repeat motif; vimentin polymerizes using leucine repeats, suggesting vimentin may also form contacts with the ORP4L leucine repeat motif [21]. ORP4S localizes and remodels vimentin through interaction with the ORD in a sterol-independent manner, which may displace ORP4L leucine repeat-mediated interaction with vimentin, consequently aggregating and collapsing the vimentin network [21]. This mechanism may contribute to vimentin's well-known role in sterol regulation and transport, having been implicated in contributing to lipid trafficking between the endosome/lysosome and ER and endosome/lysosome and Golgi, among involvement in other sterol-related processes [21,80]. ORP4L therefore may use vimentin intermediate filaments as a "scaffold or track" to move between organelles

and facilitate lipid transfer, with ORP4S or ORP4M being able to collapse the vimentin filaments and regulate this transfer [21].

1.5.3 Cell survival and proliferation

The most established activity of ORP4 in cells is its role in cell proliferation and survival [38,76,77]. Silencing of all ORP4 variants was found to significantly decrease cellular proliferation leading to growth arrest in HeLa and HEK293 cells, but was not cytotoxic [76]. In contrast, ORP4 silencing induced apoptosis in non-malignant, non-transformed IEC-18 cells [76]. Additionally, the expression of any single ORP4 variant (i.e., ORP4L, ORP4M, or ORPS) was able to rescue the growth arrest in HeLa and HEK293 cells, suggesting these variants may be redundant in terms of their role in cell proliferation [76]. This result also indicates that the FFAT and ORD domains are required for ORP4's role in cell survival and proliferation, but not the PH domain, since only ORP4L possesses a functional PH domain [76]. The ORP4 silencing-induced apoptosis in IEC-18 cells was rescued after the cells were transformed with the oncogenic protein, H-Ras; presumably due to activation of proliferation pathways and inhibition of apoptosis, which are common physiological changes seen after IEC H-Ras transformation [76]. Interestingly, H-Ras transformation increased ORP4L and ORP4S expression as much as 7-fold, suggesting that ORP4 plays a role in the cellular transformation/immortalization process [76]. Overall, these results indicate that ORP4 is involved in the proliferation and survival of rapidly dividing cells, particularly cancer and immortalized cells, and ORP4 may also play a role in the transformation process of immortalized cell lines and oncogenesis [76].

Mechanistic insight was provided for the role of ORP4 in cell survival and proliferation when it was discovered that ORP4 functions as an essential GPCR scaffold protein that drives cellular bioenergetics in T-cell Acute Lymphoblastic Leukemia (T-ALL) cell models [38,77,81]. ORP4L was found to interact with GPCR components, phospholipase C β3 (PLCβ3), CD3ε, and $G\alpha_{q/11}$ at the PM in T-ALL cells [59]. This GPCR complex requires ORP4L to recruit and scaffold the individual components to mediate cell signaling [59]. The Yan group from Jinan University in Guangzhou, China were the first to make this discovery and subsequently published multiple papers on the topic, collectively building a detailed model of ORP4 function in T-ALL cells [38,77,81].

They found that upon stimulus, ORP4L recruits this PLCβ3, CD3ε, and $G\alpha_{q/11}$ GPCR signaling complex at the PM, effectively coupling the T-cell surface glycoprotein CD3ε, to the GTPase $G\alpha_{q/11}$, and the phospholipase PLCβ3 [38,77,81,82]. ORP4L then extracts PIP_2 from the PM and presents it to PLCβ3, allowing for PLCβ3 to cleave the PIP_2 into DAG and IP_3 [38,77,81]. IP_3 then binds to IP_3 receptor type 1 (ITPR1) on the ER, a process tightly regulated by ORP4L through the ORP4L-ER-targeting FFAT domain, and ORP4L interaction with the ITPR1 C-terminal tail. These interactions facilitate IP_3 binding to ITPR1 which stimulates Ca^{2+} release from the ER [38,77,81]. The resultant release of the second messenger, Ca^{2+}, drives downstream Ca^{2+}-dependent bioenergetic events such as Ca^{2+}-dependent dephosphorylation of pyruvate dehydrogenase (PDH) to increase PDH activity and drive oxidative phosphorylation [38,77,81].

ORP4L was also shown to have a role in Ca^{2+} regulation and signaling in cervical cancer cells, although the exact mechanism of regulation was not elucidated, preliminary results suggest this process is mechanistically similar to T-ALL cells [83]. Overall, it

appears that ORP4L regulates many steps of GPCR induced Ca^{2+} release to sustain bioenergetics in T-ALL cells, and most likely other cells as well, providing context for its role in cell proliferation and survival. This mechanistic model is believed to contribute to the role of ORP4 as a precision anticancer target (see **Section 1.6.2: ORP4 as an anticancer target** for more information).

1.6 OSBP and ORP4 in human disease biology

Due to the pervasive role of the OSBP/ORPs in lipid-related biology, several OSBP/ORPs have been implicated in contributing to a number of human disease states [2,9,10]. OSBP is a druggable broad-spectrum antiviral target required for the proliferation of a wide array of human RNA viral pathogens including: hepatitis C virus (HCV), encephalomyocarditis virus (EMCV), the entire *Enterovirus* genus, *Flaviviruses* such as dengue virus (DENV), and Zika virus (ZIKV), and possibly *Coronaviruses* [84–89,90]. Many of these viruses are established public health menaces, and none have any current treatments [84–89,90]. Additionally, ORP4L is a precision anticancer target selectively overexpressed in many cancers, both solid tumors and leukemias [72,77,91]. ORP4 appears to have a critical role in cancer cell proliferation, survival, and oncogenesis, through its role as a regulator of cellular Ca^{2+} homeostasis [38,76,77].

1.6.1 OSBP as a broad-spectrum antiviral target

OSBP is reported to play a role as a host factor during viral infections through its cholesterol trafficking ability and regulation of lipid metabolism in the cell [2,9]. To date, all viruses found to require OSBP for replication and/or other stages of the viral life cycle are positive-sense single-stranded RNA ((+)ssRNA) viruses. Although much progress has

been made in the last decade in our understanding of OSBP as a host factor for these viruses, further research is required to better understand the precise contributions of OSBP to RNA viral infection and develop it as a viable antiviral target. In the current model, OSBP is exploited by virally infected cells to transport cholesterol to the viral replication compartment (VRC); the VRC is a remodeled host membrane used as the site of viral replication [84,92]. Consequently, OSBP silencing or pharmacological inhibition significantly inhibits viral replication and other lipid-related processes required for various stages of the viral life cycle, making OSBP an attractive antiviral target for antiviral drug development [84,93].

1.6.1.2 Positive-sense single-stranded RNA viruses

Positive-sense single-stranded RNA ((+)ssRNA) viruses are the most abundant genetic class of virus [94]. (+)ssRNA viruses are also pathogenic in humans, animals and plants [94]. (+)ssRNA viruses have the advantage of possessing positive-sense single-stranded RNA genomes, which are mRNA-like (i.e., mRNA is positive-sense single-stranded RNA) [95]. Therefore, even the pure RNA of (+)ssRNA viruses is infectious, as it can be directly translated by host ribosomes and does not need to be transcribed or otherwise converted prior to translation [95]. This incredibly voluminous and diverse genetic class of virus encompasses eight viral families that infect vertebrates, including four enveloped virus families: *Picornaviridae, Astroviridae, Caliciviridae, Hepeviridae*, and four non-enveloped virus families: *Flaviviridae, Togaviridae, Arteriviridae, and Coronaviridae* [96]. Enveloped viruses are those that, in addition to possessing genetic material (e.g. ssRNA) and a viral capsid, also possess a lipid bilayer envelope [97]. The

envelope is derived from host cell membrane budding and surrounds the virus [97,98]. The viral envelope functions to protect the viral genetic material, promote viral entry into cells, and aid in host immune system evasion [97,98].

A hallmark of all (+)ssRNA viruses is the ability to remodel host membranes and alter host lipid metabolism to aid in the viral replication, maturation, and egress processes [94,99]. This host membrane remodeling results in the formation of mini-organelles, or viral replication compartments (VRCs) [99]. VRCs are remodeled host organelle membranes, commonly derived from host membranes like the ER or mitochondria, that function as sites for viral replication complexes and viral replication [94,99,100]. *Picornaviridae*, *Flaviviridae* and *Coronaviridae* family VRCs originate particularly from the host ER [101,102]. These VRCs are closely associated with lipid droplets (LDs), which aid in viral assembly and morphogenesis [103,104]. VRCs go by a variety of names (e.g. membranous web, replication organelle, vesicle packets etc.) depending on the type of (+)ssRNA virus [94,105]. VRCs differ in certain characteristics between (+)ssRNA viruses [94,99]. VRC morphology can be broadly categorized as either protrusive or invagination-type, characterized by whether the remodeled host membrane protrudes out into the cytoplasm, or invaginates in, away from the cytoplasm; additionally, VRCs can be single or doubled membraned [93,94,100,106]. Despite morphological differences in VRCs between (+)ssRNA viruses, these mini-organelles serve a common function: provide a scaffold for the formation of viral replication complexes, insulate replication complexes from host defense factors, and limit diffusion to concentrate viral replication components to increase the efficiency of replication and aid in viral packing [94,107,108].

1.6.1.3 Role of OSBP in hepatitis C virus (HCV) biology

Hepatitis C virus (HCV) is a (+)ssRNA virus of the *Flaviviridae* family in the genus *Hepacivirus* [109]. HCV infection has no current prophylactic treatment and often causes chronic liver diseases such as liver cirrhosis, fibrosis, and hepatocellular carcinoma [110]. Studies estimate that 3% of people in the world are infected with HCV, with as many as 3.9 million people chronically infected in the US alone [111,112]. The HCV RNA is translated into a single polyprotein that is cleaved by proteases into three structural proteins (core, E1, E2) and seven nonstructural proteins (p7, NS2, NS3, NS4A, NS4B, NS5A, NS5B) [110]. HCV infection results in the formation of an ER-derived, protrusion-type VRC called a "membranous web" for viral replication complex formation [99,105,113].

The first report that implicated OSBP in viral infection was published by the Siddiqui group from UC San Diego in 2009 after a proteomic analysis of HCV ribonucleoprotein (RNP) complex revealed that OSBP is one of a few of host proteins associated with the HCV RNP complex in HCV infected cells [2,114]. The HCV RNP complex is the site of viral RNA replication, and these RNP complexes are associated with the VRC [114,115]. This study found that OSBP is recruited to the viral RNP complex through interaction with the N-terminal domain 1 of the HCV NS5A protein [114]. NS5A is a critical nonstructural HCV protein that has the ability to anchor to the ER, and has been shown to also interact with VAPA, the same ER-resident protein OSBP targets to anchor to the ER [114,116]. NS5A association with the ER and VAPA have been shown to be essential for viral replication [114,117–119]. Subsequent RNAi investigations revealed that OSBP knockout decreased HCV gene expression, replication, and secretion [114]. Together,

these results implicate OSBP as a host factor involved in HCV maturation and establish OSBP as a putative antiviral target.

Further research by the same group in 2011 determined that host protein kinase D (PKD) negatively regulates HCV secretion through phosphorylation-mediated inhibition of OSBP and CERT [104]. CERT is another lipid transfer protein that transports ceramide from the ER to the Golgi for sphingomyelin (SM) biosynthesis [104]. Activated PKD phosphorylates CERT and OSBP at Ser132 and Ser240, respectively, resulting in inhibition of their lipid transfer ability, and diminishment of OSBP Golgi localization [104] (see **Section 1.4.4: Cell signaling** for more information on PKD regulation of OSBP and CERT). As previously mentioned, OSBP regulates CERT function, effectively integrating sterol regulation and SM biosynthesis [61] (see **Section 1.4.3: Lipid metabolism** for more information on OSBP regulation of CERT). PKD-induced attenuation of OSBP and CERT function therefore simultaneously impairs both cellular cholesterol trafficking and SM biosynthesis [61,104]. Impairment of OSBP and CERT activity in this manner was found to inhibit secretion of HCV virions [104]. Inhibitors of SM biosynthesis have previously been show to decrease HCV replication [120], and HCV virions are enriched in both cholesterol and SM, indicating a critical role for these lipids in the HCV life cycle [121,122]. During HCV infection, an unknown cellular mechanism is reported to decrease PKD activity [104]. The PKD inactivation stops impairment of OSBP and CERT function, restoring the trafficking of cholesterol and SM biosynthesis required for TGN-mediated HCV virus secretion [104]. This study not only provides additional information about the role of OSBP in HCV secretion, but also highlights the necessity

of Golgi proteins (PKD) and lipids (cholesterol and SM) in HCV maturation and secretion [104].

Additional research further indicated that OSBP is essential for HCV replication, this time implicating OSBP as critical for the integrity of the HCV membranous web [107]. Previously reports showed that phosphatidylinositol 4-kinases (PI4Ks), and their enzymatic product, PI4P, were required for HCV replication and the integrity and morphology of the cholesterol-enriched membranous web [123–129]. Additionally, cholesterol depletion had been reported to have similar effects on membranous web integrity [130–132]. However, the role of PI4Ks and PI4P in the HCV membranous web, including how the web becomes enriched in PI4P and cholesterol, remained unknown [107].

A subsequent 2011 report revealed that HCV protein, NS5A, also recruits and activates host protein, PI4KA, to the membranous web resulting in PI4P production and a PI4P-enriched membranous web; silencing of PI4KA alters membranous web morphology and inhibits PI4P enrichment at the membranous web [125,133,134]. The PI4P-rich membranous web subsequently recruits OSBP in a PI4P-dependent manner using the OSBP PI4P-interacting PH domain [107]. OSBP recruitment facilitates the transport of cholesterol by OSBP from the ER to the membranous web, while counter-transporting PI4P [107]. This process required the OSBP ORD, FFAT, and PH domains [107]. The lipid transport process at the HCV membranous web is comparable to the OSBP mediated cholesterol-PI4P exchange between the ER and the Golgi in non-infected cells (see **Section 1.4.2: Cholesterol trafficking** for more information) and illustrates that OSBP is a PI4K effector during HCV infection [107]. Knockdown of OSBP, or deletion of the aforementioned OSBP domains, also would result in inhibition of cellular SM

biosynthesis [61,135], possibly contributing to the decrease in HCV replication as inhibitors of SM synthesis have previously been show to decrease HCV replication [120]. Although OSBP recruitment and subsequent lipid trafficking abilities were required for HCV replication and membranous web integrity, it is unknown exactly why HCV replication requires cholesterol and/or SM at the membranous web. Various theories include regulation of membranous web fluidity, lipid-mediated stimulation of viral enzymes, or recruitment of other viral or host factors to the membranous web [107,136]. More recently, it was shown that cholesterol homeostasis has a critical role in poliovirus (PV) polyprotein processing, indicating that cholesterol may play a role in the cleavage of viral polyprotein into discrete, mature viral proteins [137,138].

Importantly, many RNA viruses require various host PI4Ks, including PI4KA (HCV) and PI4KB (*Picornaviruses*), indicating that PI4P and effector proteins like OSBP may be broadly required for many RNA viruses [101,139,140]. Subsequent antiviral experiments using the *Picornavirus* family member in the *Enterovirus* genus, poliovirus (PV), which requires PI4KB, but not PI4KA, showed that OSBP knockout inhibits PV replication as well. This supports the hypothesis that OSBP may be a broadly used PI4K effector required for many different RNA viruses, and establishes the PI4K-PI4P-OSBP axis as a widely used viral hijacking mechanism to alter host lipid homeostasis [107]. In 2013, it was determined that minor enviroxime-like compounds, which are distinguished from major enviroxime-like compound by their ability to inhibit HCV infection, exerted their biological activity through targeting OSBP, further supporting the role of OSBP in HCV infection [85] (see **Section 1.7.2: Minor enviroxime-like compounds** for more information).

In addition to the role of OSBP in HCV replication and secretion, OSBP may also affect HCV viral entry and secretion through an alternate mechanism. HCV has been connected to very low density lipoprotein (VLDL)-related uptake and egress, hijacking host lipoproteins for egress, and overexpressing VLDL receptors for viral entry by HCV-mediated activation of sterol regulatory element binding proteins (SREBPs) [104,141,142]. The overexpression of OSBP in hepatocytes has been shown to upregulate SREBP-1c, resulting in a significant increase in VLDL triglycerides, suggesting the role of OSBP in HCV infection may be more pervasive and nuanced than originally believed [66].

Collectively, these results indicate that OSBP is required for multiple critical processes in the HCV life cycle (i.e., viral replication, secretion, and possibly uptake as well) through its role as a cholesterol transfer protein, regulator of SM biosynthesis, and involvement in VLDL related lipogenesis. Additionally, these results imply that OSBP may be an essential host factor for other RNA viruses that depend on the PI4K-PI4P-OSBP axis for cholesterol recruitment to the VRC.

1.6.1.4 Role of OSBP in Enterovirus biology

Since the discovery that OSBP was a required host factor for HCV infection, OSBP has been implicated as also being required for the replication of *Enterovirus* genus viruses [84]. *Enteroviruses* contain ~7.5 kb (+)ssRNA genomes that are translated into a polyprotein that is then cleaved by proteases to give rise to structural proteins (VP1-VP4) and nonstructural proteins (2A-2C and 3A-3D) [84]. *Enteroviruses* are non-enveloped viruses that create a protrusion-type VRC, known as a replication organelle (RO) [99,143]. The genus *Enterovirus* resides within the *Picornaviridae* family and comprises 81 non-

polio and 3 polio *Enteroviruses* consisting of diverse viruses including: rhinoviruses, enterovirus (species), echovirus, coxsackievirus, and poliovirus [144–146]. These viruses cause many common human diseases, ranging from life threatening, to more benign, including: the common cold, hand-foot-and-mouth disease (HFMD), polio, myocarditis, acute respiratory infections, viral pneumonia, encephalitis, meningitis, acute flaccid myelitis, and many more [144–149]. *Enteroviruses* are incredibly voluminous, with >150 different types of human rhinovirus (HRV) alone, which are responsible for approximately half of all common colds and cost the economy billions each year in lost work and medical costs [150,151]. In addition to this diversity and volume, like many RNA viruses, *Enteroviruses* have a high rate of mutation resulting in >250 distinct serotypes, making vaccine development against individual *Enteroviruses* and serotypes an unrealistic therapeutic approach [152,153]. Because these viruses comprise everything from the common cold to PV, *Enterovirus* infections are very common and potentially severe; however, there are no current approved treatments or prophylactics against these viruses, with only PV possessing a vaccine [84,89,154].

The role of OSBP in *Enterovirus* replication was first inferred based on OSBP knockout studies that showed that in addition to HCV, PV replication (an *Enterovirus*) was also inhibited [107]. As previously mentioned, HCV and *Enteroviruses,* like PV, require different host PI4Ks (PI4KA and PI4KB, respectively), suggesting the PI4K-PI4P-OSBP axis may be effectively targeted for antiviral activity against many different RNA viruses [101,139,140]. Further studies revealed that minor enviroxime-like compounds (i.e., T-00127-HEV2 (THEV), AN-15-H5, and 25-OHC), a class of antiviral compounds found to exert antiviral activity through targeting OSBP, significantly inhibit PV replication, confirming

the role of OSBP as a host factor in RNA viruses other than HCV [85]. Shortly after, the anti-*Enteroviral* compounds OSW-1, itraconazole (ITZ), and TTP-8307 (TTP) were also found to exert their antiviral activity through targeting OSBP [84,87,89].

Subsequent studies by a number of other researchers revealed that OSBP is required for all *Enterovirus* genus virus replication, but does not appear to be required for vesicle stomatitis virus (VSV, a (-)ssRNA virus) and human parechovirus 1 (HEeV1, a *Picornavirus* family member in the *Parechovirus* genus) [58,61,62,64,116]. Collectively, these results indicate that despite being required for the replication of all *Enteroviruses*, OSBP may not be required by other *Picornavirus* family members and (-)ssRNA viruses [84,89]. The reported necessity of OSBP as a host factor for all *Enterovirus* replication involves an evolutionarily conserved mechanism for PI4K/PI4P-mediated cholesterol recruitment at the *Enterovirus* ROs, similar to HCV.

The *Enterovirus* 3A protein is a critical viral replication protein that imbeds into host membranes and is important for RO formation [101]. During infection, the viral 3A protein forms a complex with host factors GBF1 and Arf1 and modulates their activity to recruit the PI4K, PI4KB to the viral RO; PI4KB subsequently catalyzes the production of PI4P, resulting in a PI4P-rich viral RO [86,101]. There is evidence suggesting that the viral 2BC protein may also participate in this process [86]. OSBP is then recruited to the viral RO through interaction with the OSBP PH domain with Arf1 and PI4P in the RO, where OSBP transports cholesterol from the ER to the RO while counter transporting PI4P from the viral RO to the ER [84,86,89,151]. Therefore, *Enteroviruses* also utilize the PI4K-PI4P-OSBP axis to hijack the cholesterol trafficking ability of OSBP to fortify the viral RO with cholesterol. The viral RNA polymerase ($3D^{pol}$) was shown to interact with PI4P *in*

vitro, suggesting PI4P accumulation at the viral RO may additionally support viral replication as a scaffold for viral replication elements [101].

OSBP knockdown, pharmacological inhibition, or alteration of the PH, FFAT, or ORD domains inhibits *Enterovirus* replication [58,61,62,64,116]. Small molecules that target OSBP to exert antiviral activity (i.e., OSW-1 and 25-OHC) were only effective in inhibiting viral replication prior to the existence of viral ROs in host cells, but were still effective hours after the initiation of viral infection [86,89]. This indicates that OSBP is required for the development of the viral RO, and OSBP targeting specifically inhibits viral replication and not entry during *Enterovirus* infections, although a role for OSBP in viral entry cannot be ruled out in this context [86,89]. Additionally, antiviral targeting of OSBP by OSW-1 was shown to be effective in numerous cell lines and animal species, highlighting the ubiquitous necessity of OSBP in *Enterovirus* infections [89]. *Enterovirus* ROs can also usurp cholesterol from various other cellular compartments other than the ER, including lipid droplets and endosomes [125]. Additionally, disruption of cholesterol homeostasis inhibits many steps of *Enterovirus* infection, highlighting the cholesterol dependence of these, and likely other viruses, establishing OSBP as an attractive target for novel antiviral therapies [151,155]. The broad dependence of cholesterol in various steps of *Enterovirus* infection also suggests that OSBP may provide additional, more nuanced contributions to *Enterovirus* infection.

Interestingly, single-point mutations in the *Enterovirus* 3A protein (V45A, I54F, H57Y for Coxsackievirus B3 (CVB3), and A70T for PV) rescued replication inhibition in the presence of PI4KB inhibitors (>50-fold increase in PV replication) and to a lesser extent OSBP inhibitors (~5-fold increase in PV replication) [85,92,137,156,157]. These results

indicate that viable viral mutants can be generated that decouple *Enterovirus* dependence on OSBP and PI4KB.

Overall, the contributions of OSBP as a host factor for *Enteroviruses* is similar to its contributions for HCV, utilizing a viral protein (NS5A and 3A for HCV and *Enteroviruses*, respectively) to exploit the PI4K-PI4P-OSBP axis to recruit OSBP and mobilize cholesterol to VRCs.

1.6.1.5 Other OSBP requiring viruses

In addition to the entire *Enterovirus* genus and HCV, there is also direct evidence that OSBP is required for encephalomyocarditis virus (EMCV) [87,92,137] and *Flavivirus* replication [88], and indirect evidence OSBP is required for *Coronaviruses* as well [90].

Similar to *Enteroviruses*, EMCV is a non-enveloped member of the *Picornaviridae* family that forms a protrusion-type VRC; however, EMCV is a member of the *Cardiovirus* genus [99,158,159]. ECMV infection can occur in a broad array of animals, including humans, and infection typically occurs from ingesting ECMV-containing water or food. ECMV infection has been shown to cause pathologies such as myocarditis, diabetes, and disorders of the reproductive and nervous systems [158]. There are no current treatments for EMCV infection [159]. Similar to HCV and *Enteroviruses*, EMCV RNA is translated into a polyprotein that is subsequently cut into approximately 13 mature viral proteins (L-1ABCD-2ABC-3ABCD) [158].

In 2015, EMCV replication was reported to exploit the same replication pathway as HCV and therefore required OSBP for replication (see **Section 1.6.1.3: Role of OSBP in HCV biology** for more information) [137]. The EMCV viral protein 3A interacts and

hijacks host PI4KA to the VRC, resulting in a PI4P-rich VRC [137]. VRC PI4P-enrichment subsequently recruits OSBP to facilitate cholesterol transport to the VRC, thus exploiting OSBP function in the same manner as both HCV and *Enteroviruses* (i.e., the PI4K/PI4P/OSBP axis) [137]. As would be expected, EMCV replication was also dependent on PI4KA, PI4P and OSBP [137]. Additionally, TTP-8307, a small molecule which exerts its antiviral activity through targeting OSBP, significantly inhibits EMCV replication after treatment [87]. Interestingly, EMCV utilizes its viral 3A protein for PI4K recruitment, like *Enteroviruses*, but the EMCV 3A protein recruits PI4KA instead of PI4KB, like HCV, despite EMCV being only distantly related to HCV [137].

The evolutionary convergence of replication pathways between the distantly related, evolutionarily divergent, *Picornaviridae* member EMCV and *Flaviviridae* member HCV, suggests that there may be limited host pathways that can be effectively usurped to facilitate host lipid remodeling for replication during viral infection [137]. This observation implies that OSBP may be exploited by many more viruses than originally believed, thus confirming OSBP as an attractive broad-spectrum antiviral target.

In contrast to *Enteroviruses*, EMCV replication does not require GBF1, and the EMCV 3A protein does not interact with GBF1, indicating the EMCV 3A-mediated PI4K recruitment complex does not involve the 3A-GBF1-ARF1 complex used by *Enteroviruses* [137,160,161]. It is important to note that there is very little sequence similarity between the EMCV 3A and *Enterovirus* 3A proteins, with the only commonality being a C-terminal hydrophobic region believed to be used for membrane targeting that is required for viral replication [92,137,162]. Interestingly, single-point mutations of the EMCV 3A protein (A32V and A34V) rescued viral replication after PI4KA knockdown or

inhibition, but the virus did not compensate by using other cellular PI4Ks and did not accumulate PI4P and OSBP, or cholesterol at the VRCs [92]. However, the 3A mutants remained sensitive to OSBP knockdown or inhibition, indicating a decoupling of PI4KA and OSBP dependence in these EMCV 3A mutants, and highlighting the critical requirement of OSBP as a host factor for these viruses, even in viral mutants [92]. This result indicates that exploiting OSBP as an antiviral target against these viruses may be a therapeutic strategy that would be difficult to gain viral mutational resistance against. Curiously, single-point mutations in *Enterovirus* 3A protein also causes resistance to PI4KB inhibitors, and to a lesser extent, OSBP inhibitors, thus also uncoupling resistance in the viral mutants [92,137,162] (see **Section 1.6.1.4: Role of OSBP in *Enterovirus* biology** for more information).

Flaviviruses are a genus of enveloped virus that belong to the *Flaviviridae* family and include important human viral pathogens such as dengue virus (DENV), Zika virus (ZIKV), and West Nile virus (WNV) [163]. Dengue virus gives rise to dengue fever and infects ~390 million people annually spanning over 100 countries [88]. There are no current treatments for *Flaviviruses*, with only dengue virus possessing a developed vaccine [88,163]. However, the dengue virus vaccine is minimally effective in children under 9, can only be administered to children ages 9-16 who have previously had dengue fever, and increases the likelihood of severe dengue fever in unexposed populations, severely limiting its efficacy and applicability [88,163,164]. These viruses produce an invagination-type VRC known as “vesicle packets” that are derived from the host ER [105,99,163]. *Flavivirus* RNA is translated into a single polyprotein that is cleaved into three structural proteins

(envelope protein, membrane precursor protein, and capsid protein), as well as seven nonstructural proteins (NS1, NS2a, NS2b, NS3, NS4a, NS4b, and NS5) [165].

In 2018, a high throughput screen (HTS) for DENV inhibitors revealed that the small molecules, itraconazole (ITZ) and posaconazole (POS) inhibit replication of multiple DENV serotypes and ZIKV through targeting OSBP [88]. Further pharmacological inhibition (i.e., OSW-1 treatment) and OSBP knockdown studies confirmed that OSBP is required for the replication of both DENV and ZIKV, but OSBP inhibition does not inhibit translation of the viral genome [88]. However, this result is inconsistent with a previous report a decade earlier that showed OSBP silencing did not significantly inhibit DENV replication, and OSW-1 treatment displayed only minor DENV inhibition [107].

Interestingly, DENV replication is independent of both PI4KA and PI4KB, and DENV infection does not recruit OSBP to the DENV VRC, indicating that OSBP may be contributing to *Flavivirus* infections in a different manner than both HCV and the *Enteroviruses* [88,107,166]. However, *Flaviviruses* still require alteration of normal cellular lipid homoeostasis. Particularly, alteration of cholesterol homeostasis has been shown to inhibit DENV replication, suggesting DENV requires the cholesterol trafficking ability of OSBP for replication [88,167,168]. Importantly, these results indicate that OSBP targeting may be a viable antiviral approach against viruses that do not exploit the PI4K-PI4P-OSBP axis for cholesterol accumulation at the VRC.

There is also indirect evidence that OSBP is required for the replication of feline coronavirus (FCoV) [90]. *Coronaviruses* are a family of enveloped viruses with protrusion-type VRCs that can infect a range of animals; with human coronaviruses (HCoV) like SARS-CoV, SARS-CoV-2 (virus causing COVID-19), and MERS-CoV, commonly

causing respiratory diseases and other pathologies in humans with currently no approved treatments [99,90,169,170]. In 2019, it was reported that ITZ treatment significantly inhibits FCoV replication [90]. Although mechanistic studies were not conducted to empirically determine the anti-FCoV target, the anti-*Enterovirus* and anti-*Flavivirus* activities of ITZ are exerted by targeting OSBP, suggesting ITZ-mediated FCoV inhibition works through targeting OSBP as well [84,88]. Additionally, FCoV is reported to be closely associated with cholesterol through the entire viral life cycle [90,171]. SARS-CoV replication has previously been shown to be dependent on PI4KB and PI4P for replication, indicating *Coronavirus* replication may require the PI4K-PI4P-OSBP axis, like HCV, *Enteroviruses*, and EMCV [172]. Overall, these results indirectly point to OSBP as being a druggable *Coronavirus* antiviral target required for *Coronavirus* replication.

1.6.1.6 OSBP as a component of cellular innate antiviral response

As previously described, OSBP is hijacked by many different (+)ssRNA viruses to facilitate a myriad of essential lipid-related remodeling activities critical for multiple stages of the viral life cycle. Therefore, it is not surprising that cells have developed an innate antiviral response to counteract this hijacking [155]. Innate antiviral responses are host cells first line of immune defense triggered upon viral entry, many of which are associated with interferon (IFN)-stimulated genes (ISG) [155,173]. Interferon (IFN)-inducible transmembrane proteins (IFITMs) were recently identified as being involved in antiviral processes against a wide array of viruses including SARS-CoV, Ebola, dengue, and West Nile virus, among others; however, the precise mechanism of these IFITM-mediated antiviral responses remained enigmatic [155,174,175].

In 2013, an innate IFN-inducible antiviral response mechanism involving OSBP, VAPA, and IFN-inducible transmembrane protein 3 (IFITM3) was elucidated [155]. The study found that IFITM3 interacts with VAPA using VAPA's coiled coiled domain (CCD) and transmembrane domain (TMD), inhibiting the ability of OSBP to interact with VAPA and subsequently traffic cellular cholesterol [155]. Interestingly, the IFITM3-VAPA interaction abolished OSBP-VAPA interaction, despite OSBP interacting with the VAPA major sperm protein domain (MSP), which does not overlap with the IFITM3-VAPA interaction site, suggesting IFITM3 interaction may cause structural or localization changes to VAPA [116,155].

In order to enter cells, viruses commonly use multivesicular bodies (MVBs) to traverse endosomal compartments, which facilitates the delivery of the virus from the outside of the cell to the cytosol [155,176,177]. Normally, esterified cholesterol is delivered to these endosomal compartments, hydrolyzed to liberate cholesterol, and delivered to the cytosol; however, impairment of the OSBP-VAPA interaction inhibits cholesterol egress from the endosome and MVBs and alters cellular cholesterol homeostasis [155,178]. The accumulation of cholesterol in the endosome and MVBs as a result of IFITM3 blocking the OSBP-VAPA interaction inhibits fusion of the virion containing endosomal compartment with the MVBs, and thus inhibits the release of virion particles and interferes with the delivery of virus to the cell [155,176,177]. This process has been referred to as the "greasy response", due to the disruption of cholesterol homeostasis and accumulation of cholesterol that occurs in this innate antiviral response [155,179].

As was previously mentioned the HCV viral protein, NS5A, has been shown to interact with both OSBP and VAPA, and this interaction is critical for viral replication

and egress [114,155,118]. These interactions therefore may not only be essential for HCV biology, but also may be an evolved mechanism to evade IFITM-mediated antiviral activity, essentially tethering OSBP and VAPA together to promote cholesterol trafficking [155].

OSBP may also be involved in the innate antiviral activity of 25-OHC [180–182]. The enzyme that produces 25-OHC, cholesterol-25-hydroxylase (CH25H), is an IFN-stimulated gene (ISG) and is expressed during innate antiviral response in cells [180–184]. This results in an increase in 25-OHC levels during viral infection that inhibits the replication of a broad array of enveloped and non-enveloped viruses including: Ebola virus (EBOV), Zika virus (ZIKV), hepatitis C virus (HCV), human rhinovirus (HRhV) and many other viruses [180–184]. Subsequent studies revealed that 27-OHC also possesses antiviral activity, although higher concentrations of 27-OHC are required than 25-OHC to induce antiviral activity [182]. Importantly, both of these oxysterols are high-affinity ligands of OSBP (see **Chapter 4**); additionally, 22-OHC was shown not to possess antiviral activity and does not bind OSBP (see **Chapter 4**), indicating a correlation between OSBP ligand binding and the antiviral activity of oxysterols [184,185].

Although the antiviral mechanism behind IFN-induced 25-OHC production remains incompletely understood, it is hypothesized that 25-OHC binding to OSBP contributes to the antiviral activity of 25-OHC through multiple possible mechanisms [180–184]. One model suggests that increased 25-OHC production results in increased OSBP binding of 25-OHC in the cell, which inhibits OSBP binding of cholesterol and subsequent cholesterol trafficking to the VRC, resulting in a decrease in viral proliferation [180]. Another model suggests that IFN-induced 25-OHC production inhibits viral entry to

the cell in a manner very similar to the "greasy response" observed in the IFITM3-mediated innate antiviral response [155,182,179]. This study found that 25-OHC and 27-OHC treatment inhibits OSBP-VAPA interaction leading to the disruption of cholesterol homeostasis and inhibition of viral entry; effectively recapitulating the IFITM3-mediated antiviral response described previously using only oxysterol ligands of OSBP [182]. IFN-induced CH25H expression and the subsequent increase in 25-OHC levels may also have a role in antiviral mechanisms independent of OSBP including: regulating the production of enzymes involved in cholesterol synthesis via oxysterol interaction with liver X and estrogen receptor α, NF-kB-mediated increases in the abundance of inflammatory cytokines such as IL-6, or oxysterol membrane interaction [186]. IFN-induced CH25H expression may also have 25-OHC-independent roles in innate antiviral response as well, as a CH25H mutant lacking enzymatic activity still displayed antiviral activity against HCV, but lost antiviral activity against murine gammaherpesvirus 68 (MHV-68); suggesting a complex role for CH25H and 25-OHC in innate antiviral response [187].

These studies collectively highlight not only the pervasive, nuanced role OSBP may play in broad-spectrum viral infection, but also its pervasive role in distinct innate antiviral responses.

1.6.2 ORP4 as a precision anticancer target

OSBP and ORP4 were originally implicated as anticancer targets involved in cancer cell survival when it was discovered that the potent anti-proliferative class of natural products, called ORPphilins (see **Section 1.7.1: ORPphilins** for more information), exert anti-proliferative activity through targeting OSBP and ORP4 [52]. Subsequent studies have revealed that ORP4 is required for the proliferation and/or

survival of cancer cells and immortalized cells [38,76,77,81]. Additionally, our group and other research groups have determined that chemical or genetic knockdown of OSBP in cell culture is not cytotoxic, nor antiproliferative [61,135,188,189,190]. Together, these results provide strong evidence that ORP4 is the antiproliferative target of OSW-1.

ORP4 is overexpressed in many cancers such as ovarian cancer, colorectal cancer, and certain leukemias (The Human Protein Atlas). For example, leukocytes from chronic myeloid leukemia (CML) patients contain ORP4L, whereas leukocytes from healthy individuals do not [72,75,91]. Additionally, ORP4L is overexpressed in leukemia stem cells (LSCs), and chemical or genetic knockdown of ORP4L kills LSCs via autophagic cell death, both in cell culture and mice models, while healthy hematopoietic stems cells (HSCs), not expressing ORP4L, are unaffected [77]. ORP4 is also recognized as a potential biomarker for solid tumors such as breast and lung cancer, and may be an indicator of poor prognosis, as ORP4 overexpression was significantly correlated with metastasis [72].

ORP4 overexpression has been shown to increase cervical cancer cell proliferation (i.e., HeLa, C33A, and CaSki cells) and ORP4 overexpression in IEC-18 cells transformed with oncogenic H-Ras promotes cell transformation into tumors [22,75,83]. Additionally, transformation of human foreskin keratinoctyes (HFKs) with human papilloma virus (HPV) oncoproteins, E6 and E7, a process which immortalizes cell lines, increased ORP4 mRNA expression >10-fold further confirming the role of ORP4 in oncogenesis and immortalization of cells [72].

Mechanistically, ORP4 appears to be contributing to cancer cell survival and proliferation through its role in regulating Ca^{2+}-dependent bioenergetics as a GPCR scaffolding protein, and regulator of IP_3 interaction with the IP_3 receptor to facilitate Ca^{2+}

release from the ER [38,76,77,81]. However, this model has only been shown in T-ALL cell models, and inferred for cervical cancer cell models, but mechanistic information in other cancer cell models is limited [38,77,81,83] (see **Section 1.5.3: Cell survival and proliferation** for more information on this ORP4 model). One additional report indicates that the OSW-1-compound kills leukemia cells by disrupting Ca^{2+} homeostasis, but implicated sodium-calcium exchanger 1 (NXC1) and mitochondrial calcium overload as the mechanism of cytotoxicity, indicating ORP4 may have additional roles in Ca^{2+} regulation that are not included in the current T-ALL model [191]. However, this result may also represent an off-target effect of the OSW-1-compound and may not be directly connected to ORP4 function as a Ca^{2+} regulator. At the moment, further research is required to more completely determine the contributions of ORP4 to cancer biology.

The necessity of ORP4 in cancer cells and its apparent role in oncogenesis, combined with ORP4 overexpression in many cancers and selective tissue expression in healthy individuals, provides a context to selectively target and eradicate cancer cells. These characteristics indicate that ORP4 is an attractive precision anticancer target.

1.7 Small-molecule targeting of OSBP and ORP4

OSBP and ORP4 have previously been reported to be targeted by various structurally-diverse small molecules [52,85,87]. OSBP and ORP4 are targeted by a class of naturally occurring anti-proliferative small molecules known as ORPphilins (**Figure 4B**) [52]. Additionally, OSBP is also targeted by a class of antiviral compounds known as minor enviroxime-like compounds (**Figure 4C**) [85,87]. Although these structurally diverse small molecules have been shown to exert their biological activity by targeting OSBP and/or

ORP4, many of the precise biological effects of these small molecules in cells remain to be characterized.

1.7.1 ORPphilins

Starting in the 1990s, a structurally-diverse group of naturally occurring, potent anti-proliferative small molecules consisting of OSW-1 (**3**), cephalostatin 1 (**4**), schweinfurthin A (**5**), and ritterazine B (**6**) (**Figure 4B**) were shown to display a similar pattern of sensitivity against the NCI-60 that was indicative of a shared and novel cellular target [52]. The NCI-60 is the National Cancer Institute panel of 60 different cancer cell lines that can be used to test a compound's anticancer efficacy. The pattern of sensitivity of a set of compounds against the various cancer cell lines can also be used to determine if the compounds exert anti-proliferative activity through similar mechanisms [192,193]. A 2011 report revealed that these compounds exert bioactivity through targeting OSBP and ORP4 and were aptly named ORPphilins [52].

The ORPphilins all target OSBP and ORP4 through binding in the ORD sterol binding pocket and display inhibition binding values (K_i) in the low to high nanomolar range (**Figure 4B**) [52]. The K_i binding values were determined based on the compounds ability to inhibit [^{3}H]25-OHC binding to OSBP and ORP4 using a radioligand competitive binding assay [52] (see **Chapter 4** for more information on this binding assay). Additionally, the ORPphilins all target both OSBP and ORP4; however, schweinfurthin A targets OSBP with ~30-fold higher affinity than ORP4 (i.e., OSBP K_i 68 ± 23 nM compared to ORP4 K_i 2600 ± 570 nM), suggesting small molecules could be developed with the ability to target OSBP or ORP4 specifically [52]. Despite the ORPphilins all targeting OSBP and ORP4 through binding in the ORD sterol binding pocket, these

compounds appear to have different effects on OSBP/ORP4. Cephalostatin 1 and OSW-1 treatment leads to the proteasome-dependent decrease of OSBP levels in the cell, but ritterazine B and schweinfurthin A do not have an effect on cellular OSBP levels [52]. Additionally, despite sharing potent anti-proliferative capabilities and a similar pattern of sensitivity against the NCI-60, these compounds appear to have distinct anti-proliferative/cytotoxic effects in cells. OSW-1 has an NCI-60 GI_{50} of 0.78 nM and is 30 to 150-fold more cytotoxic against glioblastoma and leukemia cells relative to non-transformed astrocytes and lymphocytes, indicating a selective cytotoxicity toward cancer cells [52,194]. Cephalostatin 1 has an NCI-60 GI_{50} of 2.2 nM and treatment results in induction of apoptosis through an unusual cellular mechanism [52,195,196]. Schweinfurthin A has an NCI-60 GI_{50} of 360 nM and displayed selective anti-proliferative abilities against cancer cells lacking NF-1 [52,197]. Ritterazine B possesses an NCI-60 GI_{50} of 3.2 nM [198].

OSW-1 has also been reported to induce broad-spectrum anti-*Enterovirus*, anti-HCV, and anti-*Flavivirus* activity in cells through targeting OSBP, and therefore can be classified as both an ORPphilin and minor enviroxime-like compound [88,89,107].

1.7.2 Minor enviroxime-like compounds

Minor enviroxime-like compounds are a class of antiviral compounds that exert antiviral activity through targeting OSBP (**Figure 4C**) [85,87]. Prior to the identification of OSBP as the cellular target of this class of compounds in 2013, minor enviroxime-like compounds were categorized based on inducing similar cellular responses as the enviroxime-like compounds, hence the name [85]. Enviroxime is an antiviral compound that exerts antiviral activity through targeting PI4KB [85,157]. Enviroxime antiviral activity is

abrogated by the introduction of an A70T mutation in the PV viral 3A protein, despite enviroxime not directly interacting with the viral 3A protein [85,199,200]. Enviroxime-like compounds are therefore compounds that possess minimal structural similarity to enviroxime, but also target PI4KB and have their antiviral activity attenuated by the same viral 3A A70T resistant mutant (>50-fold increase in resistance) [85].

Minor enviroxime-like compounds are antiviral compounds that do not target PI4KB, and instead target OSBP, but also share resistance to the viral 3A A70T mutant (although to a much lesser extent than the enviroxime-like compounds, with only ~5-fold increase in resistance), and possess anti-HCV activity [85]. Minor enviroxime-like compounds all cause the same phenotypic response in cells as 25-OHC, resulting in localization of OSBP to the ER-Golgi upon treatment. In addition to phenotype, 25-OHC (**1**) also shares the other minor enviroxime-like compound characteristics and therefore is considered a part of this compound class (**Figure 4A**) [85]. Itraconazole (ITZ) (**7**), T00127-HEV2 (THEV) (**8**), and TTP-8307 (TTP) (**9**) can be classified as minor enviroxime-like compounds (**Figure 4C**) [85,87].

The only minor enviroxime-like compound with a reported OSBP binding value is ITZ, the FDA approved antifungal compound, which interacts with OSBP with a K_D of ~430 nM as measured by microscale thermophoresis [84]. However, the location of ITZ binding to OSBP remains unknown [84]. This report is limited as it does not appear to use any known OSBP ligands with established binding values as a control (i.e., 25-OHC) to verify the accuracy of the obtained ITZ binding value [84]. ITZ (**7**), THEV (**8**), and TTP (**9**) all inhibit the lipid transfer ability of OSBP, and knockdown of OSBP increases their antiviral activity, indicating OSBP is the cellular antiviral target of these compounds

[84,85,87] (**Figure 4C**). Curiously, overexpression of OSBP attenuated the antiviral activity of THEV and ITZ, but overexpression of OSBP did not attenuate the antiviral activity of TTP, indicating that TTP may target other cellular components in addition to OSBP to induce antiviral activity in cells [84,85,87]. Further research is required to determine how these compounds target OSBP to induce antiviral activity.

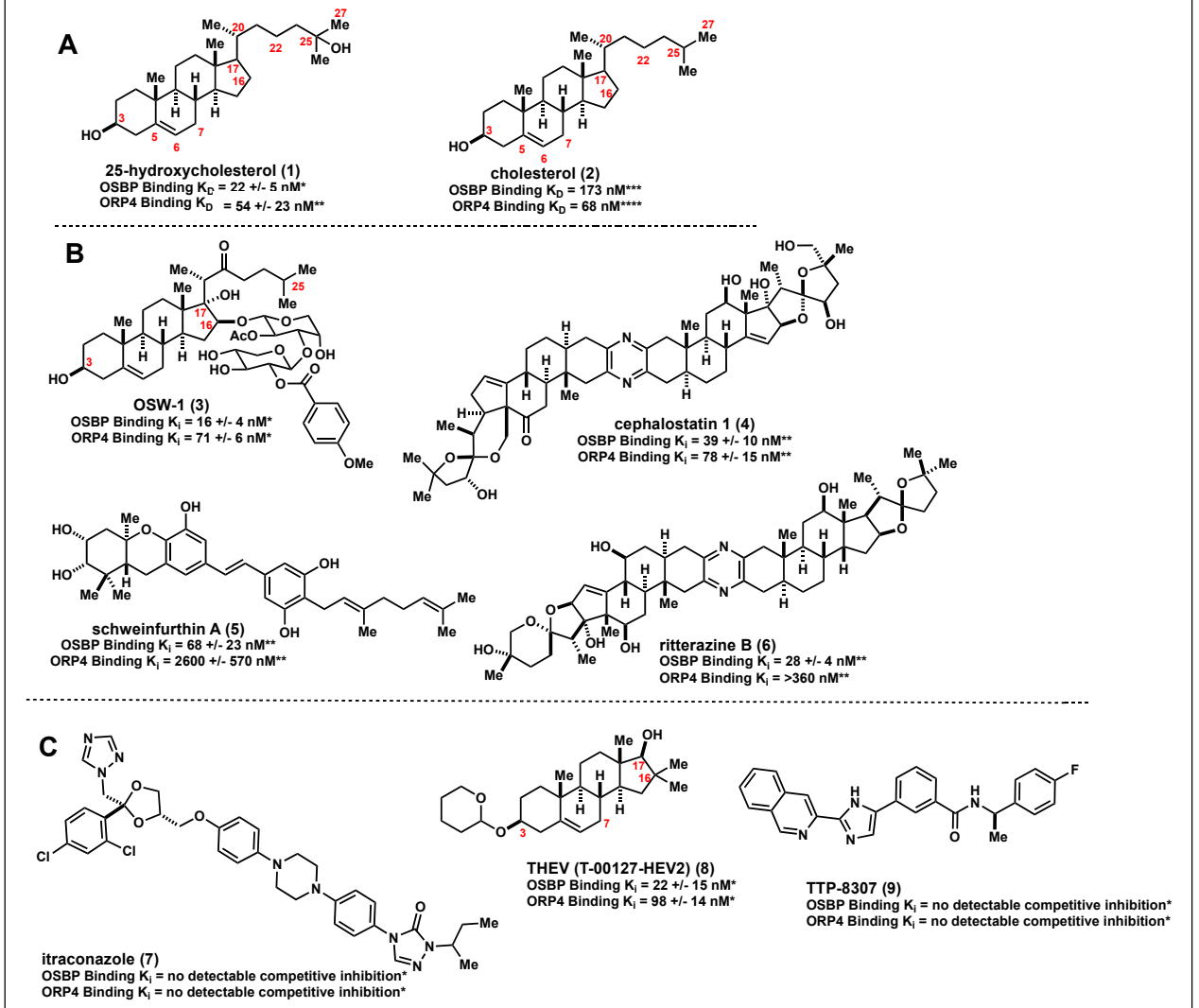

Figure 4: OSBP and ORP4 targeting small molecules.

A) OSBP and ORP4 K_i values are determined through measuring the inhibition of binding of [^{3}H]25-hydroxycholesterol ([^{3}H]25-OHC) (**1**) to human OSBP or ORP4 protein overexpressed in HEK293T lysate. We have determined the K_D of 25-OHC to human OSBP as 22 ± 5 nM. Literature report of the K_D for 25-OHC to human ORP4 is 54 ± 23 nM [52]. **B)** Natural product compound ORPphilins: OSW-1 (**3**), cephalostatin 1 (**4**) schweinfurthin A (**5**) and ritterazine B (**6**) were compounds identified to induce their biological activity through binding to OSBP and ORP4. **C)** Minor enviroxime-like antiviral compounds itraconazole (**7**), THEV (**8**), and TTP-8307 (**9**) are compounds previously shown to target OSBP [84,85,87,89,190] (*published results from Roberts et al. 2019 [190] ; ** published results from Burgett et al. 2011) [52]; *** published results from Wang et al. 2008 [53]; **** published results from Charman et al. 2014 [76]).

1.8 The chemical genetics approach to biology

The scientific term "chemical genetics" describes the use of small molecules, often times naturally occurring, to discover novel insights into cellular biology [201,202]. The name "chemical genetics" comes from this approach's similarities to traditional genetic screens [201,202]. In genetic screens, random mutations producing phenotypes allow for the identification of the biological role of a specific gene [201,202]. Similarly, in chemical genetics living systems are subject to random perturbations by exogenous small molecules and the resultant phenotype of the perturbed system is analyzed [201,202]. This allows researcher to trace the phenotype back to specific perturbations caused by the small molecule to obtain functional information about the small molecule target [201,202]. Chemical genetics approaches have been used to make tremendous breakthroughs in biology and medicine including the discovery of the protein, tubulin, and tubulin inhibitors, as well as mTORc1, and mTORc1 inhibitors [203,204]. Although chemical genetics has been used ad hoc for many decades, only in the last 15-20 years has this approach been used to systematically probe living systems and tease apart increasingly complex questions in cellular biology [202].

The various exogenous small molecules previously reported to target OSBP and ORP4 (see **Section 1.7: Small-molecule targeting of OSBP and ORP4** for more information) allowed us to apply a chemical genetics approach to study OSBP and ORP4. More specifically, we utilized the OSW-1-compound and several other small molecules as chemical tools to probe the cellular function(s), regulation, and disease contributions of OSBP and ORP4. This chemical genetics approach has led to the discovery of new insights into the role of OSBP in cellular biology and viral infection as well as ORP4 in

cancer biology. These new insights are critical for the development of viable clinical antiviral and precision anticancer therapies targeting OSBP and ORP4, respectively.

The structural complexity inherent to many natural products like the OSW-1-compound (**3**) (**Figure 4B**), often confers high specificity interaction with a cellular target (i.e, OSBP or ORP4) and minimizes the promiscuous, off-target interactions of less complex, synthetically-derived small molecules [205,206]. The ability to selectively target particular proteins with high specificity allows us to probe the biological function(s) of the individual target protein by precise perturbation of the target in an endogenous context, circumventing the messiness and lack of flexibility that is often associated with studying proteins using traditional genetics approaches [207]. The power to precisely target and perturb specific cellular components of a living system not only provides information on the targeted component, but can also provide information on the relationships between individual components of a system that give rise to complex biology like cell signaling pathways. Genetic approaches of investigation, for example, deleting or overexpressing genes to knockout or overexpress particular proteins, involves altering the native state of the cell by manipulating genomics elements [207]. This can lead to a myriad of non-specific global cellular changes, artifacts, and confounding results that make it difficult to tease apart the noise introduced by altering the native system, from the actual function(s) of the protein [207]. Further, many genetic approaches lack reversibility and are not able to be modulated in the cell (i.e., there is no quantifiable dose-response), resulting in an irreversible change to the cell's native/endogenous state [207].

The small-molecule, or chemical genetics approach, circumvents these issues and allows for the reversible, dose and time-dependent study of biological systems in the

native state, without manipulating endogenous elements like the genome or gene products [207]. The combination of chemical genetics and traditional genetics approaches, therefore, provides a foundation to comprehensively study a component of a living system (i.e., OSBP). This dissertation uses a combination of traditional genetics, chemical genetics, and other approaches to better understand the cellular biology, biochemistry, and molecular pharmacology of ORP subfamily 1: OSBP and ORP4, with particular emphasis on OSBP as an antiviral target.

Chapter 2. Transient OSW-1-compound treatment induces a unique, persistent multigenerational decrease in oxysterol-binding protein (OSBP) levels and antiviral prophylaxis

Abstract

OSBP and ORP4 comprise ORP subfamily 1 and are reported to be involved in diverse cellular activities including lipid transport, metabolism, and signaling; however, many of their cellular function(s) remain unclear. OSBP and ORP4 have been implicated in RNA viral infection and cancer cell survival and proliferation, making them attractive broad-spectrum antiviral and precision anticancer targets, respectively. OSBP is an essential host factor required by many human pathogenic RNA viruses to facilitate the host lipid remodeling process that is vital for many stages of the viral life cycle, including viral proliferation. OSW-1 is a naturally occurring small molecule known to selectively target OSBP and ORP4 with high affinity. We discovered a unique OSBP regulatory process in cells that is triggered by the OSW-1-compound, and leads to the long-term repression of cellular OSBP levels. In human cell lines, low dose (1 nM), transient (6h), non-toxic treatment of the OSW-1-compound resulted in ~90% multigenerational decrease in cellular OSBP levels that persists for over 72 hours after the compound has been removed from the cells. We were able leverage the discovery of this response to induce *prophylactic* antiviral activity in cells (i.e., the cells retain antiviral activity in the absence of the OSW-1-compound). Using three other previously reported OSBP-targeting antiviral small molecules, T00127-HEV2 (THEV), TTP-8307 (TTP), and itraconazole (ITZ), we show that the long-term repression of OSBP and the prophylactic antiviral activity are unique to the OSW-1-compound, and not all OSBP-targeting antiviral compounds. These results establish OSW-1 as the first identified antiviral prophylactic small molecule that exerts activity through modulating a host protein. We also determined that OSW-1, THEV, TTP, and ITZ target OSBP through multiple modes of binding that result in distinct effects on OSBP activity in the cell, suggesting OSBP can be targeted for antiviral development in multiple, distinct ways. We hypothesize that the unique long-term repression of OSBP triggered by the OSW-1-compound, may be part of a larger, unidentified arm of innate antiviral response in cells that could be harnessed by small molecules and exploited to create a new class of broad-spectrum preventative antiviral treatments against many viruses that currently have no treatment.

Allocation of Contribution

The following chapter (Chapter 2) is reproduced with permission in part from (i) "Transient Compound Treatment Induces a Multigenerational Reduction of Oxysterol-Binding Protein (OSBP) Levels and Prophylactic Antiviral Activity," Roberts, B. L.; **Severance, Z. C.**; Bensen, R. C.; Le, A. T.; Kothapalli, N. R.; Nunez, J. I.; Ma, H.; Wu, S.; Standke, S. J.; Yang, Z.; Reddig, W. J.; Blewett, E. L.; Burgett, A. W. G. *ACS Chem. Biol.* **2019**, 14 (2), 276–287: DOI: 10.1021/acschembio.8b00984, https://pubs.acs.org/doi/full/10.1021/acschembio.8b00984 [189]. (ii) "Differing Activities of Oxysterol-Binding Protein (OSBP) Targeting Anti-Viral Compounds," **Severance, Z. C.**; Roberts, B. L.; Bensen, R. C.; Le-McClain, A. T.; Malinky, C. A.; Mettenbrink, E. M.; Nunez, J. I.; Reddig, W. J.; Blewett, E. L.; Burgett, A. W. G. *Antiviral Res.* **2019**, 170, 104548: DOI: 10.1016/j.antiviral.2019.104548 [190]. Further permissions related to the material excerpted in this chapter should be directed to the American Chemical Society (ACS) and Elsevier.

I produced the results presented in this chapter with the following exceptions. Dr. Brett Roberts and Dr. Ryan Bensen conducted the experiments for the K562 and HCT-116 cell lines, respectively, for **Figure 6, 8, 10, and 12**. Dr. Ryan Bensen also performed the HEK293 cytotoxic assay in **Figure 19B** and assisted with the compound serial dilutions for some of the binding assay experiments in **Figure 18**. Additionally, Dr. Brett Roberts conducted the experiments in **Figure 10B, 13A,** and **20**, as well as performed the HCT-116 experiments in **Figure 16**, and some of the HCT-116 experiments in **Figure 19A**. Prof. Earl Blewett from Oklahoma State University Center of Health Sciences performed the antiviral experiments in **Figure 15** and **17**. Ms. Hongyan Ma from the Wu Research Group at the University of Oklahoma performed the mass spectrometry analysis for **Figures 11** and **14**. Dr. Anh Le-McClain and Dr. Cori Malinky synthesized the small molecules, THEV and TTP, respectively.

2.1 Introduction

ORP subfamily 1 consists of OSBP and the ORP family member most closely related to OSBP, ORP4 (~64% overall amino acid sequence identity, ~67% ORD amino acid sequence identity) [208] (see **Section 1.1: Overview of the OSBP/ORP family of proteins** for more information). OSBP is ubiquitously expressed in all human tissues and has been shown to localize to the ER-Golgi interface under certain stimuli (e.g. increases in cellular 25-OHC, or decreases in cellular cholesterol), anchoring at MCSs between the two organelles and mediating cholesterol trafficking from the ER to the Golgi [15,51] (see **Section 1.4: OSBP biology** for more information). ORP4 is expressed in select human tissues and appears to function, in part, as a G protein-coupled receptor (GPCR) scaffold protein at the plasma membrane (PM) that is involved in cellular Ca^{2+} regulation, mediating cell proliferation and bioenergetics in T-cell Acute Lymphoblastic Leukemia (T-ALL) cell models and likely other cells as well [38,76,77]. ORP4 is also required for the survival and proliferation of cancer and immortalized cells [76] (see **Section 1.5: ORP4 biology** for more information).

More recently, the function of several OSBP/ORPs have been implicated in a number of human disease states [2,9]. The role of ORP4 in cancer cell proliferation, survival and bioenergetics makes it a precision anticancer target involved in cancer biology, driving cancer cell proliferation and survival in certain leukemias and possibly other cancers [11-13] (see **Section 1.6.2: ORP4 as a precision anticancer target** for more information). Additionally, OSBP is a broad-spectrum antiviral target required for the proliferation of a wide array of (+)ssRNA human viral pathogens including the entire *Enterovirus* genus, which gives rise to diseases such as the common cold, hand, foot, and

mouth disease (HFMD), respiratory infections and pneumonia, acute hemorrhagic conjunctivitis, and the polio-like paralytic disease, acute flaccid myelitis [146,154]. OSBP is also required for the proliferation of other significant human RNA viruses like the hepatitis C virus (HCV), dengue virus (DENV), Zika virus (ZIKV), encephalomyocarditis virus (EMCV), and likely many more RNA viruses [84–89,92]. OSBP is exploited by virally infected cells to transport cholesterol from the host ER to the viral replication compartment (VRC) [84–89,92]. The VRC is a remodeled host membrane, commonly derived from the host ER, which protects the virus from host defense elements and is required for viral replication; therefore, without OSBP present in the cell, the ability for the virus to replicate is significantly inhibited [84–89,92,93]. Pervasive host lipid remodeling, a hallmark of all (+)ssRNA and other viruses, suggests that OSBP may also provide additional, more nuanced, lipid-related contributions to RNA viral infection that have not yet been elucidated [94] (see **Section 1.6.1: OSBP as a broad-spectrum antiviral target** for more information).

The simplicity and rapid mutability of these viruses has limited the development of both antiviral treatments and vaccines, consequently, these pathogens currently lack effective therapeutics [209]. Developing targeted antiviral therapies against OSBP would be an ideal antiviral approach. Targeting a host protein such as OSBP could circumvent the high mutability associated with targeting elements of the RNA virus itself, thus greatly decreasing the probability of a virus gaining mutational resistance to an antiviral treatment. Additionally, targeting a host protein that is an evolutionarily conserved requirement for many RNA viruses, not just specific, individual RNA viruses, allows for a broad-spectrum antiviral approach that may be effective against many different RNA

viruses, including newly emergent viruses (e.g. SARS-CoV-2) and future viruses that have not yet emerged.

The naturally occurring anti-proliferative small molecule, OSW-1 (**2**) (**Figure 5**), has previously been shown to target OSBP and ORP4 in cells with high affinity and specificity [52] (see **Section 1.7.1: ORPphilins** for more information on the OSW-1-compound). The OSW-1-compound has also previously been shown to induce apoptosis [210,211], mitochondrial dysfunction [191], and intracellular calcium release [191], all of which are now associated with altering ORP4 function in cells [38,76]. Further studies have shown that silencing of ORP4 leads to negative effects on growth and viability in cancer cells [76,77]. Additionally, our group and other researchers have determined that chemical or genetic knockdown of OSBP in cell culture is not cytotoxic, nor antiproliferative [61,135,188,189,190]. Therefore, the antiproliferative/cytotoxic activity that the OSW-1-compound was originally investigated for, is likely caused by targeting ORP4 and not OSBP. Building off this information, we utilized the OSW-1-compound (**2**) and other small molecules (**Figure 5**) as tools to probe and better understand the cellular function(s), regulation, and disease contributions of OSBP and ORP4, necessary information for their development into viable antiviral and precision anticancer targets, respectively .

Utilizing the OSW-1-compound as a small-molecule biological probe and employing a chemical genetics approach, we discovered an OSBP regulatory response in cells, triggered by the OSW-1-compound, that results in the long-term repression of cellular OSBP levels. In human cell lines, low dose (1 nM), transient treatment (6-hour) of the OSW-1-compound triggers an ~90% *multigenerational* decrease in cellular OSBP

levels that persists for over 72 hours after the OSW-1-compound has been removed from cell culture, with no change in cellular viability or proliferation rate. We were able to leverage the discovery of this unique cellular OSBP regulatory response to induce *prophylactic* antiviral activity in cells. Several other structurally-diverse OSBP-targeting antiviral small molecules including T-00127-HEV2 (THEV) [85] (**3**), itraconazole (ITZ) [84] (**4**), and TTP-8307 (TTP) [87] (**5**) were also investigated (**Figure 5**) (see **section 1.7.2: Minor enviroxime-like compounds** for more information on these compounds). The OSW-1-compound is the only OSBP-targeting antiviral compound that caused reduction or long-term repression of OSBP levels, and the only compound capable of inducing antiviral prophylaxis in cells. Additionally, we determined that the OSBP-targeting antiviral compounds target OSBP through multiple modes of binding that result in distinct effects on OSBP cellular activity. These results highlight not only the unique effect of the OSW-1-compound on cellular OSBP levels and regulation, but also the potential for OSBP to be targeted for antiviral development in multiple, distinct ways.

We report the OSW-1-compound as the first identified small-molecule antiviral *prophylactic* whose activity is mediated through modulation of a host protein (i.e., OSBP). Exploiting this unique, unrecognized OSBP regulatory process in the cell as a novel prophylactic antiviral approach could lead to a new paradigm in antiviral therapeutics and pioneer a new class of *preventative* broad-spectrum antiviral treatments against many significant human viral RNA pathogens with no current treatment.

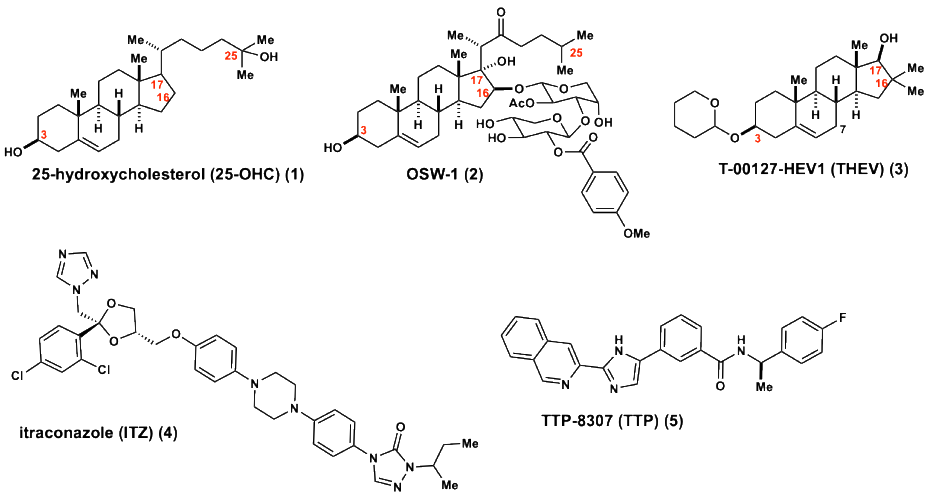

Figure 5: 25-Hydroxycholesterol and OSBP Interacting Small-Molecule Antiviral Compounds.

2.2 Methods and Materials

2.2.1 Plasmids and Cloning

Human OSBP cDNA was obtained in a pOTB7 vector from the Mammalian Gene Collection (Thermo). OSBP was PCR amplified to possess 5' NheI and 3' HindIII cut sites. The cDNA construct was then cloned into the pcDNA 3.1/myc-His (-) C mammalian expression vector (Sigma). OSBP was cloned in a manner where OSBP expresses without the myc-His tag. The ORP4L construct containing 5' NheI and 3' HindIII cut sites was PCR amplified from HCT-116 cDNA. The LacZ construct containing 5' NotI and 3' BamHI cut sites was PCR amplified from K-12 *E. coli* genomic DNA. The completed plasmids were propagated in DH5α *E. coli* and isolated through miniprep and maxiprep kits (Thermo). Gene sequences were verified through Oklahoma Medical Research Foundation (OMRF) [212].

2.2.2 Cell Lines and Viruses

HEK293 (ATCC CRL-3249) and HeLa (ATCC CCL-2) were cultured in DMEM (Thermo 11995073) supplemented with 10% Hyclone (Fisher Sci SH3006603) and 1% penicillin-streptomycin (Thermo 15140122). HCT-116 (ATCC CCL-247) was cultured in McCoy 5A media (Thermo 16600108) supplemented with 10% Hyclone and 1% penicillin streptomycin. HCT-116 p21-/- cells were a gift from the Vogelstein Laboratory (Johns Hopkins University) and cultured in McCoy 5A media (Thermo 16600108) supplemented with 10% Hyclone and 1% penicillin streptomycin. K562 (ATCC CCL-243) was cultured in RPMI 1640 (Thermo 22400105) media supplemented with 10% Hyclone and 1% penicillin streptomycin. MCF-7 cells were a gift from R. Cichewicz (University of Oklahoma, Norman) and cultured in MEM (Thermo 11095114) media 10% Hyclone, 1% penicillin streptomycin and 0.2 mg/mL insulin (Thermo A11382II). MRC-5 cells were a gift from E. Blewett (Oklahoma State University Center for Health Sciences, Tulsa) and cultured in MEM media supplemented with 10% Hyclone and 1% penicillin streptomycin. RD (rhabdomyosarcoma) cells (ATCC CCL-136) were cultured in DMEM (Fisher Sci SH30081.0) with 10% FBS (Atlanta Biological S11550) and 1% penicillin-streptomycin (Gibco 15140-122). Coxsackievirus A9 (strain CoxA9-01) and Echovirus 2 (strain Echo2-01) were obtained from the Oklahoma State Department of Health Laboratory. They are clinical isolates, obtained from Oklahoma residents and typed by the Oklahoma State Department of Health and/or the Center for Disease Control and Prevention. All other identifiers have been stripped off. These viruses were passaged twice in RD cells, aliquoted in 1.0 mL amounts and stored in complete medium at -80 ºC.

Each virus was titered on RD cells using a TCID-50 assay [213]. To allow M.O.I. to be determined, a conversion factor of 0.7 was used to change TCID-50 to pfu/ml.

2.2.3 General Cell Culture

All mammalian cell lines were cultured at 37 ºC in 5% CO_2. All handling of the mammalian cell culture was performed in a standard tissue culture hood using standard aseptic technique. Cell lines were cultured in the complete media described above. Cell culture stocks were aliquoted in 2 mL cryogenic vials (Corning 430659) in complete media with a DMSO concentration (5-11%) as specified by ATCC for each cell line and stored in liquid nitrogen vapor phase. Before beginning a new culture, the freezer stocks were thawed, diluted in 9 mL complete media and plated in Nunclon Delta 10 cm^2 dishes (VWR 10171744). After allowing ~16 hours for the revived cells to attach, the DMSO containing media was replaced with DMSO-free complete media. All revived cultures were split at least twice prior to use in an experiment. Cell cultures were restarted approximately every 3-4 weeks. All cell based experimental results reported used multiple restarted cell culture stocks in the independent experiments that make up the replicate results to ensure reproducibility between cell culture stocks. For experiments, cell cultures were used with a confluency of ~70%. The cell cultures were not allowed to become superconfluent, and the cellular morphology and proliferation rate of the cell culture was carefully tracked to identify any abnormalities; any cell culture showing the slightest abnormalities were discarded and the cell line restarted from frozen stocks. For experiments, cells were allowed to recover from seeding a minimum of 16 hours prior to the start of an experiment.

The adherent mammalian cell lines are split every ~2-3 days with the following general procedure: the complete media is removed via aspiration and the cells are gently washed with 5 mL of 1X PBS. TrypLE™ Express (Gibco 12605- 010) trypsin reagent (2.5 mL for 10 cm^2 plate) is added and incubated for ~5-10 min at 37 ºC. After ~5-10 minutes, 7.5 mL of the complete culture media is added to inactivate the TrypLE™ Express reagent. Cells were counted using a TC20™ Automated Cell Counter (BioRad), by combining 10 µL of cell solution with 10 µL Trypan Blue stain (Thermo 15250061).

The K562 leukemia suspension cell line was handled as described for the adherent cell lines, except for the splitting and seeding procedure. For K562 cells, the cells were spun down at 200 x g for 5 minutes and the media was aspirated from the cell culture carefully so as not to disturb the cell pellet, and replaced with 10 mL of complete media. The cell pellet was then resuspended and diluted to the desired seeding density using complete media.

2.2.4 Cell Lysis Method 1 (AC Lysis Buffer Freeze/Thaw)

Adherent cells were cultured in Nunclon Delta 10 cm^2 dishes (VWR 10171744) and lysed by removing the media and washing with 1X PBS, followed by addition of 1 mL PBS and cell scraping. Cells were collected in a 1.5 mL Eppendorf brand centrifuge tubes (Cat. No. 022363204) and spun down at 14,000 x g for 45 seconds. Supernatant was removed, and the cells were resuspended in 50 µL of AC lysis buffer (150 mM NaCl, 1.5 mM $MgCl_2$, 5% glycerol, 0.8% NP40, 1mM DTT, 50 mM HEPES, 25 mM NaF, 1 mM Na_3PO_4) with 3X HALT/EDTA protease inhibitor (Thermo 78438) and 0.2 mM phenylmethylsulfonylfluoride (PMSF) (Goldbio). The cells were then frozen in liquid

nitrogen and thawed in a 37 °C bead bath three times with gentle vortexing between thaws, followed by a 14,000 x g spin for 15 minutes. Supernatant was transferred to a new tube and a portion was taken for protein quantification using a Bradford assay (Bio-Rad Protein Assay Dye Reagent Concentrate #5000006, BSA-Santa Cruz sc-2323). After protein quantification, the lysates were diluted to the desired concentration using AC lysis buffer and 4X Laemmli buffer (1 M Tris pH 6.8, 8% SDS, 40% glycerol, 20% β-mercaptoethanol, and 0.2% bromophenol blue), followed by dry bath heating at 95 °C for 10 minutes.

Adherent cells cultured on 6-well plates (Greiner 657160) were lysed by removing media, washed with 1X PBS, followed by adding 0.5 mL TrypLE^{TM} Express (Gibco 12605-010) and incubated at 37 °C for 5 minutes. TrypLE^{TM} Express was neutralized using 0.5 mL of media and cells were then transferred to a 1.5 mL Eppendorf tube and spun down at 14,000 x g for 45 seconds. Supernatant was removed, and 1 mL of PBS was added to wash the cells. Cells were spun down at 14,000 x g for 45 seconds, supernatant was removed, and the cells were resuspended in 50 µL of AC lysis buffer. Freeze/thaw method was continued as described above.

2.2.5 Cell Lysis Method 2 (MPER Lysis)

Mammalian protein extraction reagent, MPER (Thermo 78501), was used as an alternative lysis method for 10 cm^2 dishes. Media was removed from the cells, and 5 mL of 1X PBS was added to wash cells. 1 mL of MPER was added to the plate and was shaken in a room temperature (Innova 42 incubator) at 250 rpm for 5 minutes. The solution was collected and spun down at max speed (~4470 x g) for 1 hour. Supernatant

was placed in a new tube and the protein concentration and sample preparation was conducted as previously described.

2.2.6 Western Blotting

SDS-PAGE gels (8.5%) containing 25 µg of total protein per well were transferred to 0.45 µm nitrocellulose (Bio-Rad 1620115) using constant voltage (100V) for 1 hour at 4 °C in 1X transfer buffer with 10% ethanol. After transferring, the nitrocellulose membrane was blocked with 5% milk in 1X TBST at room temperature for 30 minutes. The membranes were then washed 3 times, 5 minutes each, with 1X TBST. Primary incubation with antibodies was done overnight at 4 °C. After primary incubation, the blots were washed 5 times, 5 minutes each, with 1X TBST and then incubated in secondary antibody in 1% milk TBST for 30 minutes at room temperature. After secondary antibody incubation, the blots were washed 5 times, 5 minutes each, with 1X TBST and then once with 1X TBS for 10 minutes. TBS was removed, and the blots were incubated in Clarity™ Western ECL substrate (Bio-Rad 1705061) and imaged on the Bio-Rad ChemiDoc™ Touch Imaging System using the chemiluminescence setting with 2x2 binning. Ladder images were taken using the colorimetric setting. After development, the membranes were washed with 1X TBST two times for 5 minutes each. 1:1000 β-actin HRP (Santa Cruz sc-47778 HRP) in 1% milk in TBST was added as a loading control and incubated for 1.5 hours at room temperature. Western blot development was then performed as described above. Primary antibodies used were 1:500 OSBP A-5 (Santa Cruz sc-365771), 1:500 p21 C-19 (Santa Cruz sc-397), and 1:1000 OSBP2 B-1 (Santa

Cruz sc-365922). Secondary antibodies used were 1:1000-1:3000 goat anti-mouse IgG1-HRP (Santa Cruz sc-2060), and 1:3000 goat anti-rabbit IgG-HRP (Santa Cruz sc-2004).

2.2.7 Washout Experiment

Cells were treated with 1 nM OSW-1, 1 nM Taxol, or DMSO containing media for 6 hours, or as indicated. Media was removed and the cells were gently washed with 5 mL of complete media 3 times and then 10 mL of fresh compound-free media was added back to the cells. The cells were then allowed to recover in compound-free media for the indicated times (0-72 hours), and were lysed as previously described and analyzed.

2.2.8 Cycloheximide Chase Experiment

HCT-116 and HEK293 cells were seeded at $1.6x10^5$ cell per well into 6-well plates (Greiner 657160) and left to rest for 20 hours. Media containing 177 µM cycloheximide (Sigma C7698-1G) was added to the plates and the cells were incubated for the times indicated before the cells were lysed via AC lysis as described previously, and analyzed by Western blotting.

2.2.9 Cytotoxic Assay Protocol

HCT-116 and HEK293 cells were seeded at 2,000 cells per well and HeLa cells were seeded at 5,000 cells per well into opaque 96-well Falcon plates (VWR 25382-208). Cells were allowed to rest for 20 hour before treatments. Day 0 control plate was created by adding 25 µL of media containing either 0.1% DMSO or 1% DMSO and 20 µL of cell titer blue (Promega G8081) to each of the wells containing cells and incubated at 37 °C,

5% CO_2 for 1 hour and 30 minutes. Plates were read using a GloMax® Discover Microplate Reader using the Cell Titer Blue protocol. Remaining plates with cells were treated with various dilutions of compounds and incubated at 37 °C for 48 hours under 5% CO_2. After 48-hour incubation, 20 µL of cell titer blue was added to the each well and the plates were incubated and analyzed as described above. The control plate was subtracted from the treatment plate and the values were analyzed using GraphPad Prism software. Co-incubation experiments were done using the same protocol described above with the following changes: the OSW-1-compound was serially diluted in media containing 10µM of ITZ, TTP, or THEV, and this mixture was then added to the plate for the 48 hour treatment.

2.2.10 Antiviral Experiments

HeLa cells were grown to >75% confluency (healthy log phase cells) in complete media, DMEM (Hyclone SH30081.0) with 10% FBS (Atlanta Biological S11550) and 1% penicillin-streptomycin (Gibco 15140-122). For experiments, cells were trypsinized, counted using a hemocytometer, and seeded into 20 wells of two 24-well trays (Falcon 3047) with 1.0 x 10^5 cells per well, in 1.0 mL complete media. Each treatment is performed using quadruplicate wells (n=4) and each virus was on a separate plate. After seeding, cells were incubated 20 hours at 37 ºC, 5% CO_2, at which point cells have grown to a near confluent monolayer.

For the antiviral continual treatment experiments, the media was gently removed from each well and CoxA9-01 or Echo2-01 viruses, diluted in serum-free DMEM with a M.O.I. of 1.0, was added to the culture. The 1.0 x 10^5 cells per well was assumed to

double during incubation so 2.0 x 10^5 pfu/well of virus was used for an M.O.I. of 1.0. The virus and cells were incubated for 30 minutes at 37 ºC, 5% CO_2. Then, the virus inoculum was removed, and the culture washed one time with 1.0 mL of serum-free media per well. 1 mL of media was added to each well containing either 10,000 nM ITZ, TTP, THEV, or the indicated concentration of OSW-1 (for the comparative OSBP-targeting antiviral compounds experiment OSW-1 was dosed at 10 nM). The infected cells were then incubated in media with the indicated compound for 10 hours at 37 ºC, 5% CO_2. After 10 hours, the plate was stored at -80 ºC until the TCID-50 titration. This experiment was performed independently 3 times to generate the data in the figure.

For the antiviral washout treatment experiments, cells were seeded as described above. After 20-hour incubation the media was gently removed from each well, and 1 mL of media was added containing either 10,000 nM ITZ, TTP, THEV, or the indicated concentration of OSW-1 (for the comparative OSBP-targeting antiviral compounds experiment OSW-1 was dosed at 10 nM). Cells were incubated for 6 hours, after which time the media was removed and cells were gently washed three times with 1.0 mL of FBS-free DMEM media. Media was replaced with complete compound-free media and cells were allowed to incubate and recover from compound treatment for 24 hours. After the media was removed, CoxA9-01 or Echo2-01 viruses, diluted in serum-free DMEM with a M.O.I. of 1.0 was added to the culture. The 1.0 x 10^5 cells per well was assumed to double and double again during incubation so 4.0 x 10^5 pfu/well of virus was used for an M.O.I. of 1.0. The virus and cells were incubated for 30 mins at 37 ºC, 5% CO_2. Then, the virus inoculum was removed, and the culture washed one time with 1.0 mL of serum-

free media per well. Then, 1.0 mL of complete media was added to the well, and the infected cells were then incubated for 10 hours at 37 ºC, 5% CO_2.

After 10-hour incubation, the plate was stored at -80 ºC until processing. Then, the plates were rapidly thawed, the cells in media were scraped from the wells into sterile 1.5 mL centrifuge tubes and the suspension then centrifuged at 10,000 x g at 4 ºC to produce the virus containing supernatant, which is assayed for TCID-50 titration on sub-confluent RD cells. This experiment was performed independently three times to generate the data in the figure. The TCID-50 titration was performed according to the protocol described by Reed et al.[213]. This experiment was performed independently 3 times to generate the data in the figure.

2.2.11 Immunofluorescent Microscopy

HCT-116 cells were seeded at 50,000 cells onto sterile 18 mm cover slips in 12-well plates for treatments lasting 24 hours. The cells were incubated for 24 hours before treatment to ensure attachment. Once treatments were completed, media was removed and the cells were washed with warm 1X PBS. PBS was removed and 0.5 mL of freshly prepared 4% paraformaldehyde in PBS was added. Cover slips were incubated at 37 °C for 20 minutes and then the paraformaldehyde was removed followed by three 1X PBS washes. Permeabilization of the cells was done with 0.5 mL of 0.5% Triton X-100 in PBS at room temperature for 10 minutes. 1X PBS was used to wash the cells three times. ImageiT FX signal enhancer (Thermo I36933) was added onto the cover slips, and incubated at room temperature for 30 minutes followed by three 1X PBS washes. Coverslips were blocked with 0.5 mL of 1% BSA in PBS at room temperature for 30

minutes followed by 3 washes with 1X PBS. Primary antibody was added and the slips were incubated overnight at 4 °C. The primary antibody solution was removed and the cover slips were washed three times with 1X PBS. The secondary antibody was incubated in darkness at room temperature for 1 hour. The secondary antibody solution was removed and the slips were washed 3 times with 1% BSA-PBS, 3 times with 1X PBS, and then soaked the cover slip in 300 nM DAPI (Thermo D1306) solution for 10 minutes. The slips were mounted onto glass slides using VECTASHEILD HardSet Antifade mounting media (VECTOR labs H-1400). Slides were stored at -20 °C until imaging was conducted. Primary antibodies used were 1:100 OSBP1 1F2 (Novus NBP2-00935) and 1:500 TGN46 (Novus NBP1-49643). Secondary antibodies used were 1:500 goat anti-mouse IgG H&L Alexa Fluor® 488 (Abcam 6 ab150113) and donkey anti-rabbit IgG H&L Alexa Fluor® 594 (Abcam ab150076). Imaging was done with a Lecia SP8 using a 63x objective with 2x digital zoom. Images were analyzed with ImageJ software [214].

2.2.12 iTRAQ Proteomic Mass Spectrometry

HEK293 cells were seeded and treated according to the 0-72 hour recovery washout experimental procedure previously described (1 nM OSW-1 or DMSO, 6-hour treatment). After the desired post-washout time point, the cells were lysed according to the AC lysis protocol using modified AC lysis buffer. The modified AC lysis buffer contained no DTT and only 3X HALT (no EDTA or PMSF) for protease inhibitor. Free thiols can interfere with the cysteine blocking step prior to iTRAQ tagging and protease inhibitors were kept to a minimum to avoid inhibiting trypsin during the digestion process. Effective treatment was confirmed via Western blot using OSBP antibody and

β-Actin antibody as a loading control. A Multiplex Buffer Kit (Sciex 4381664) was used for the denaturing, reducing, and blocking steps. Trypsin with $CaCl_2$ (Sciex 4352157) was used for digestion; and iTRAQ Reagent-8Plex Multiplex Kit (Sciex 4390812) was used for iTRAQ labeling. These kits were utilized according to the iTRAQ Reagents-8plex protocol. After tagging, the pH of the samples was lowered to approximately 3 using 1N Phosphoric Acid, and ran through a cation-exchange cartridge system (Sciex cation exchange cartridge 4326747, cartridge holder 4326688, outlet connector 4326690, and needleport adapter 4326689) to remove any substances that could interfere with LC/MS/MS analysis. The protein eluate was quantified using a NanoDrop OneC (Thermo). Samples were normalized to a "mixed" sample that contained 5.5 µg of protein from each sample. Only shared proteins in all 3 biological replicates were used to test for changes in different conditions. P-values were generated using multiple t-tests in GraphPad Prism 7 (p-value <0.05 for significantly changed proteins). Volcano plots were also generated in GraphPad Prism 7 to display p-value against fold changes between the two treatment conditions (DMSO and OSW-1).

2.2.13 LC-MS/MS Analysis of iTRAQ Labeled Peptides

Mixed peptide samples were analyzed using the LC-MS/MS following previously published protocol [215,216]. Peptide samples were desalted, dried in a SpeedVac, and resuspended in buffer A (0.1% formic acid in water). 1 µg of the digested sample was injected onto a custom-packed C18 RPLC column (75 µm i.d., 150 mm length, 2 µm C18 resin, Thermo) using a Waters (Milford, MA, USA) nano-Acquity UPLC system, which is online coupled with a LTQ Orbitrap Velos Pro mass spectrometer (Thermo) through a

custom nano-ESI interface. For peptide separation, a 100-min gradient was applied from 3% buffer A to 35% buffer B (0.1% formic acid in acetonitrile). Full MS spectra were acquired at a resolution of 60K (m/z range between 350 and 2000). The data-dependent higher-energy collisional dissociation (HCD) based MS/MS spectra were acquired at a resolution of 15K with a normalized collisional energy of 33% using the ten most abundant parent ions. Peptides were identified using MSGF+ to search LC-MS/MS against the annotated Uniprot human protein database [217,218]. Peptide identifications were filtered with a MSGF cut-off score lower than the calculated FDR<1% at the unique peptide level against decoy database. The iTRAQ reporter ion intensities of each HCD scan were extracted and analyzed using the in-house developed software.

2.2.14 Mass Spectrometry Label-Free 2D OSBP Quantification

The first-dimension high-pH (pH=10) separation was performed on a Thermo Accela HPLC system (Thermo Scientific, Hanover Park, IL) with an ACQUITY UPLC BEH300 C18 column (50mm, Waters, Milford, MA, USA). The mobile phase A (MPA) was 20 mM ammonium formate in water and the mobile phase B (MPB) was 20 mM ammonium formate in acetonitrile. The mobile phases were adjusted to pH 10. A 60 minute gradient from 3% to 70% (3% to 10% in a minute) mobile phase B was applied for peptide separation, and 60 fractions were collected (1 minute per fraction). Fraction concatenation was performed following Yang et al. [219]. A total of 12 fractions were obtained for the second-dimension low-pH LC-MS/MS analysis.

2.2.15 [^{3}H]25-OHC Competitive Binding Assay Procedure

The [^{3}H]25-hydroxycholesterol competitive binding assay is based on the procedure from Taylor and Kandutsch [220] and performed according to the method outlined by Burgett et al. [52]. The binding data was analyzed on GraphPad Prism 7 using non-linear regression. Binding curve R^2 values of 0.85 were the cutoff to report binding values. K_D and K_i values and standard deviation were calculated using at least 3 independent replicates unless otherwise specified.

2.2.16 OSW-1-Compound Generation and Preparation

The OSW-1 compound was obtained through total synthesis in the Burgett lab or from isolation from the natural source. OSW-1 used in the experiments was of >95% purity as determined through ^{1}H-NMR and LCMS analysis. Solid OSW-1 compound was dissolved in analytical grade DMSO solution to produce 10 mM stocks for experimentation. The 10 mM OSW-1 stock solution was aliquoted into Eppendorf brand 1.5 mL centrifuge tubes; Each individual 10mM OSW-1 aliquots were thawed no more than three times.

2.2.17 Statistical Analysis

All results are expressed as mean ± SD and are $n \geq 3$ unless otherwise stated. All statistical tests were performed using GraphPad Prism 7.0. Comparison between groups was made by using a one-way ANOVA with a follow up Dunnett's test. The p-values are reported using GraphPad Prism: *$p \leq 0.05$, **$p \leq 0.01$ ***$p \leq 0.001$, and ****$p \leq 0.0001$.

2.3 Results

2.3.1 Continual OSW-1-compound treatment results in time and proteasome-dependent loss of OSBP and ORP4 in the cell

The OSW-1-compound targets both OSBP and ORP4 with similar binding values (K_i values of 26 ± 9 nM and 54 ± 11 nM, respectively) as measured by [^{3}H]25-hydroxycholesterol competitive binding experiments [52] (see **Chapter 4** for more

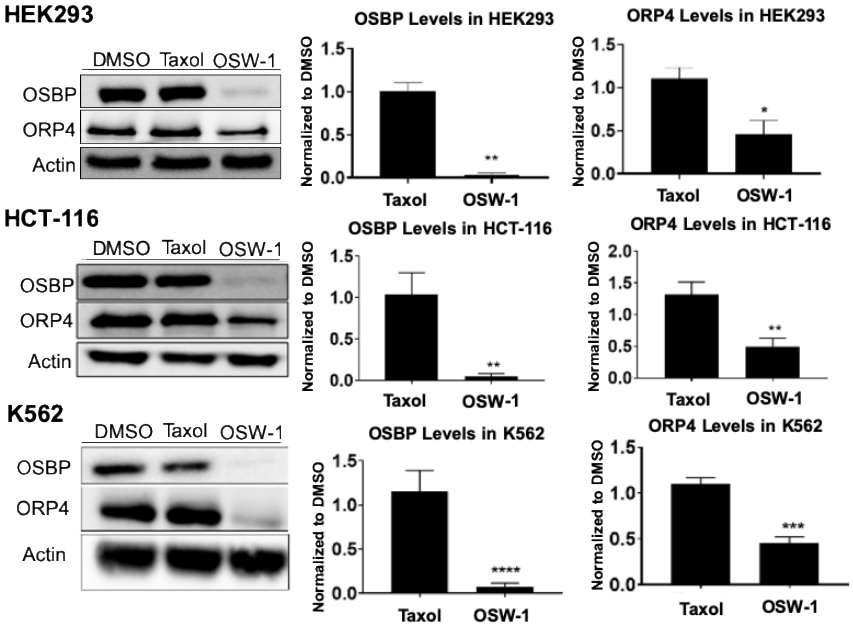

Figure 6: Cellular OSBP and ORP4 levels decrease after OSW-1-compound treatment.
A 1 nM, 24-hour OSW-1-compound treatment results in >90% decrease in cellular OSBP levels, and ~50% decrease in ORP4 levels.

information). Treatment of cells with low nanomolar concentrations of the OSW-1-compound has previously been reported to lead to the time-dependent and proteasome-dependent loss of OSBP levels in the cell [52]. However, the effects of the OSW-1-compound on the levels of the precision anticancer target, ORP4, were unknown. Importantly, determining the effect of OSW-1-compound treatment on ORP4 levels will

be critical for optimizing OSW-1-compound treatment to circumvent the cytotoxicity and growth arrest associated with ORP4 loss [76]. This will be a necessary requirement to effectively probe the cellular function(s), regulation, and disease contributions of OSBP for development as an antiviral target, as well as further study the OSW-1-compound as an antiviral therapeutic. Treatment with 1 nM of the OSW-1-compound for 24 hours in multiple human cell lines resulted in >90% decrease in OSBP and ~50% decrease in ORP4 levels (**Figure 6**).

Inhibition of the proteasome using 25 nM treatment of the proteasome inhibitor, bortezomib, significantly rescues the loss of ORP4 after OSW-1-compound treatment, revealing ORP4 loss is proteasome-dependent, consistent with the previously determined mechanism of loss for OSBP levels (**Figure 7**) [52].

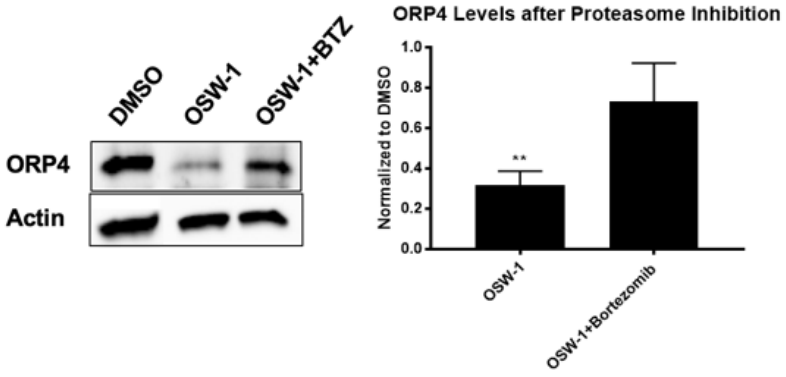

Figure 7: OSBP and ORP4 loss is proteasome-dependent. A 1 nM, 24-hour continual treatment of the OSW-1-compound in K562 cells results in ORP4 loss that can be significantly abrogated by co-administration of the OSW-1-compound with 25 nM of the proteasome inhibitor, bortezomib. This experiment reveals that OSW-1-compound induced ORP4 loss is also proteasome-dependent, similar to OSBP.

This is the first reported analysis of cellular ORP4 levels after OSW-1-compound treatment, as well as the first evidence that ORP4 responds to OSW-1-compound

treatment in a similar manner as OSBP. However, OSBP levels appear much more sensitive to the effects of OSW-1-compound treatment than ORP4 levels after 24 hour treatment (**Figure 6**). To further probe the difference in the rate of disappearance between OSBP and ORP4, protein levels were monitored after 1 nM OSW-1-compound treatment at 2-hour intervals over the course of 24 hours (**Figure 8**). The results of this experiment confirmed that OSBP levels are substantially more affected by OSW-1-compound treatment than ORP4 levels, with ~90% decrease in OSBP levels after just 12 hours of continual treatment (**Figure 8A**). In contrast, ORP4 levels are not significantly affected until after 12 hours of continual treatment, with 24-hour continual treatment resulting in ~50% decrease (**Figure 8B**). OSW-1-compound treatment in K562 cells appears to result in lower ORP4 levels compared to HCT-116 and HEK293 cells (**Figure 8B**). The observed difference in the rate of OSBP and ORP4 loss after OSW-1-compound treatment can be exploited to probe the antiviral OSBP targeting effects of the OSW-1-compound, while circumventing the cytotoxicity and growth arrest associated with ORP4 loss [76].

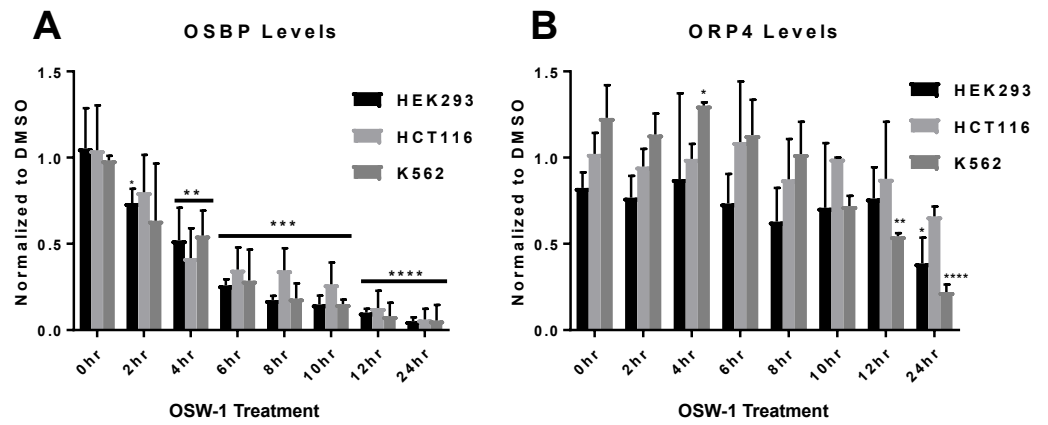

Figure 8: OSBP levels are more substantially decreased than ORP4 levels after OSW-1-compound treatment.

A) A 1 nM, 24-hour continual treatment with the OSW-1-compound results in ~90% decrease in cellular OSBP levels. **B)** In contrast, ORP4 levels are only reduced, on average, ~50% after 1 nM, 24-hour treatment with the OSW-1-compound. [189]

2.3.2 Transient exposure to non-toxic, low nanomolar concentrations of the OSW-1-compound (i.e., "the washout experiment") induces a specific, persistent and multigenerational decrease in cellular OSBP levels

Utilizing the observed difference in the rate of OSBP and ORP4 loss after OSW-1-compound treatment (**Figure 8**), we introduced what we coined as the "washout experiment" (abbreviated WO) (**Figure 9**). The WO experiment exposes cells to low dose (1 nM), transient (6 hours) OSW-1-compound treatment, an exposure time and concentration that resulted in significant OSBP loss without affecting ORP4 levels (**Figure 8**). After 6-hour treatment, the OSW-1-compound is removed from the cell culture and the cells are thoroughly washed to remove any residual OSW-1-compound. The cells are lysed immediately after the OSW-1-compound is removed (0-hour post-washout (pWO)), or re-incubated in new, compound-free media and allowed to recover for 24-72 hours after the OSW-1-compound has been removed, or "washed out" (i.e., 24-

72 hours post-washout (pWO)) (**Figure 9**).

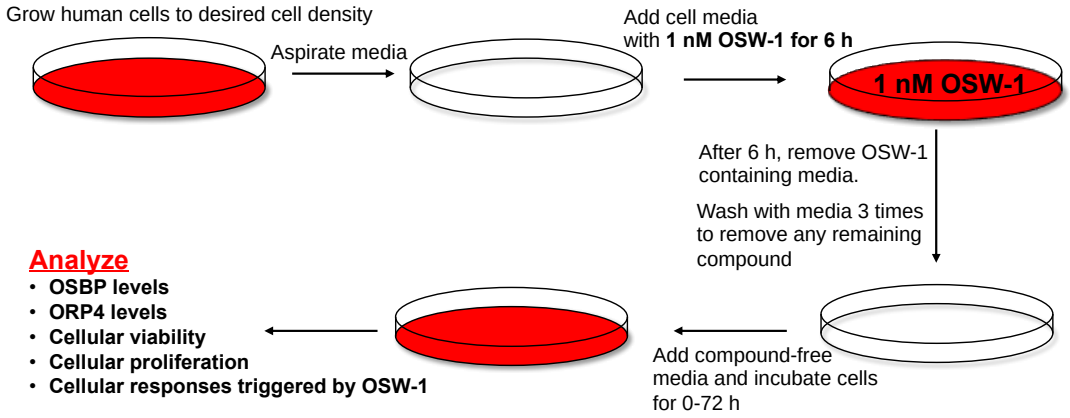

Figure 9: Experimental workflow for "the washout experiment".
The washout (WO) experiment uses low dose (1 nM), transient (6 hours) treatment of the OSW-1-compound, followed by OSW-1-compound washout and 0-72 hours post-washout (pWO) recovery in compound-free media.

The goal of the WO experiment is to circumvent the cytotoxicity and growth arrest associated with ORP4 loss [76], as well as probe the cellular responses triggered by, but not continually caused by, the presence of the OSW-1-compound in cells.

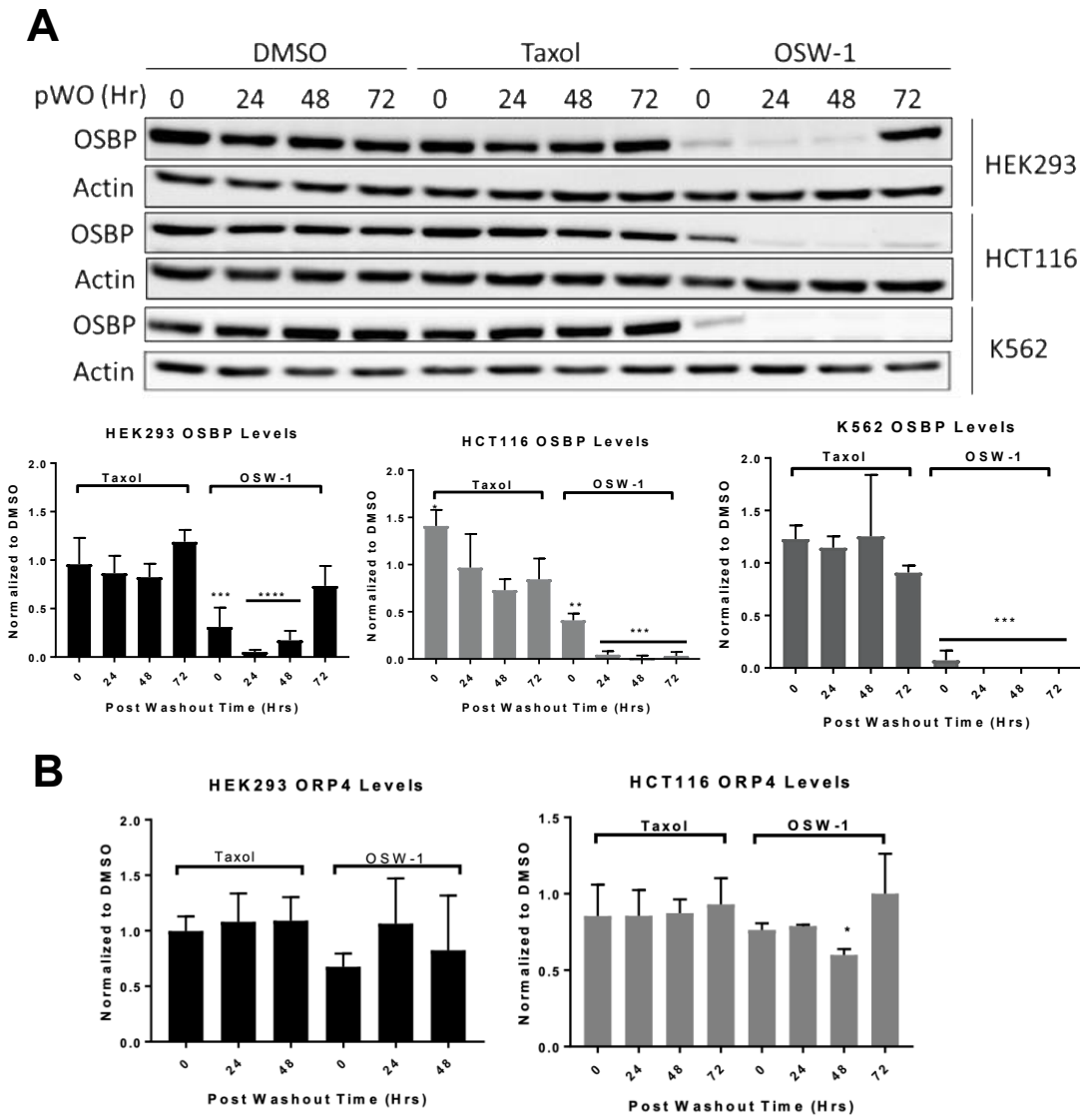

Figure 10: Low dose (1 nM), transient treatment (6-hour) with the OSW-1-compound results in a persistent, multigenerational decrease in OSBP levels.
A) Human cell lines treated with the OSW-1-compound for 6 hours, followed by 0-72-hour pWO recovery (i.e., "the WO experiment") reveals that OSBP levels are still approximately 90% or more reduced in HCT-116 and K562 cell lines 72 hours after the OSW-1-compound was removed from culture; while HEK293 cells are ~90% reduced for over 48 hours after the compound was removed from culture. This decrease is multigenerational as the division time of these cells lines is ~16 hours. **B)** Under the WO experimental conditions, ORP4 levels are not significantly affected; consequently, these treatment conditions did not decrease cellular viability, proliferation, or alter cellular morphology.[189]

Under these experimental conditions, cellular OSBP levels were significantly reduced by ~90%, with no significant change in ORP4 levels (**Figure 10**). Importantly, under washout (WO) conditions there was also no significant cytotoxicity, reduction in cellular proliferation, or observable change in cellular morphology at any time-point analyzed (data not shown) [189]. This indicates not only that washout conditions circumvent the negative effects associated with ORP4 loss, but also that reduction of OSBP levels by ~90% in cells for multiple days is non-toxic to the cell, a critical requirement for a host-cell antiviral target. Bottom-up proteomic mass spectrometry (MS) also showed a significant loss of OSBP peptides after OSW-1-compound treatment (**Figure 11**), confirming the reduction in OSBP levels as seen by Western blot (**Figure 10**). The OSBP loss was additionally confirmed by the decrease in OSBP immunofluorescent signal after OSW-1-compound treatment using immunofluorescent confocal microscopy imaging (data not shown) [189].

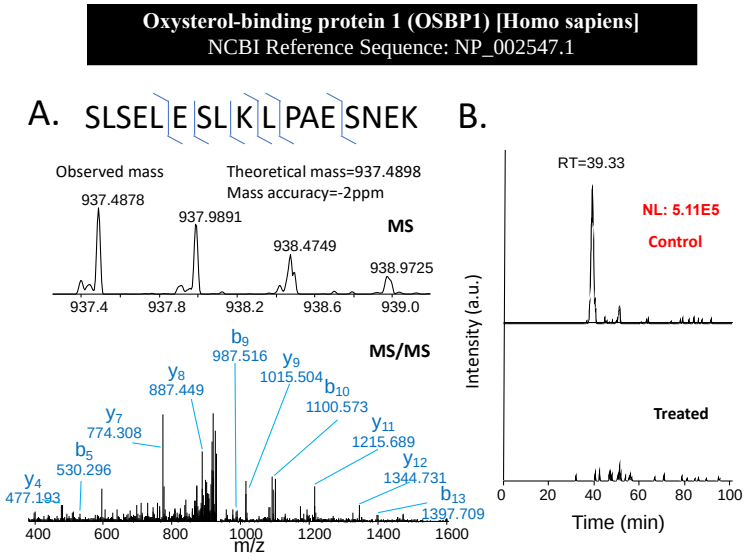

Figure 11: Mass spectrometry confirms OSBP loss in cells after OSW-1-compound treatment.
A) and **B)** Bottom-up proteomic MS of OSBP peptides confirms OSBP loss in cells after OSW-1-compound treatment seen via Western blot. [189]

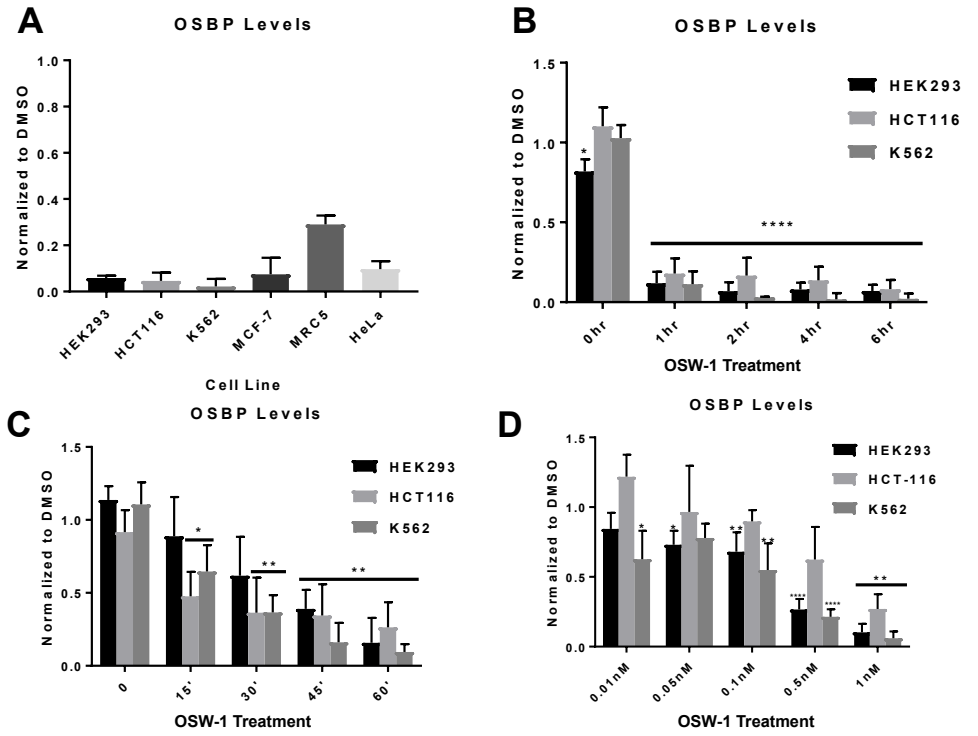

Figure 12: OSBP loss occurs in all cell lines tested under WO conditions and OSW-1-compound treatment with concentrations less than 1 nM and exposure times less than 1-hour result in significant OSBP loss.
A) Highlighting the ubiquity of OSW-1-compound induced OSBP loss, significant OSBP loss occurs with 6-hour treatment, 24-hour pWO recovery in all cell lines tested. **B)** and **C)** Highlighting the potency of OSW-1-compound induced OSBP loss, treatment times as low as 1-hour with 24-hour pWO recovery result in ~75% reduction in OSBP levels. Treatment times less than 1-hour also significantly decrease OSBP levels. **D)** Treatment concentrations as low as 0.5 nM for 6 hours, with 24-hour pWO recovery results in ~50% decrease in OSBP levels in the cell. [189]

A 1 nM treatment of the OSW-1-compound for 6 hours, followed by 24 hours pWO recovery resulted in substantial OSBP loss in all cell lines tested (**Figure 12A**). Multiple human cell lines were tested in this experiment including the non-tumorigenic cell line, HEK293 (**Figure 10, 12**), the lung fibroblast cell line, MRC-5 (**Figure 12A**),

and numerous cancer cell lines (HCT-116, K562 (**Figure 10, 12**), MCF-7, HeLa (**Figure 12A**)). A 1 nM OSW-1-compound treatment as brief as 1-hour with 24-hour pWO recovery reduced OSBP levels ~75% (**Figure 12B**). Treatment times for less than 1-hour with 24-hour pWO recovery also significantly reduced OSBP levels (**Figure 12C**). 6-hour treatment with concentrations as minimal as 0.5 nM, with 24-hour pWO recovery also led to significant OSBP loss (~50% decrease) in cells (**Figure 12D**). These results highlight both the potency and ubiquity of the observed OSW-1-compound induced OSBP loss response in human cells (**Figure 12**).

Curiously, the significant reduction in OSBP levels in the WO experiment persists for over 72 hours after the OSW-1-compound is removed in multiple human cell lines (**Figure 10A**). In HEK293 cells, OSBP levels begin to return 72 hours pWO; however, in HCT116 and K562 cells, OSBP levels remain ~90% repressed 72 hours after the OSW-1-compound is removed from the cell culture (**Figure 10A**). Additionally, the loss of OSBP continues after the OSW-1-compound is removed, bottoming out at ~95% reduction 24 hours pWO (**Figure 10A**). The long-term repression of OSBP levels in the absence of the compound, coupled with the continued decrease in OSBP levels after the compound is removed, indicates the triggering of a cellular response by OSW-1-compound treatment that persists long after the compound has been removed. The reduction of OSBP levels is specific to the OSW-1-compound, as cell treatment with the antimitotic compound, Taxol, did not alter OSBP levels (**Figure 10A**). The OSW-1-compound induced long-term repression of OSBP levels is multigenerational, as the cells in this experiment have divided multiple times after the OSW-1-compound was removed and still contain minimal cellular OSBP. The cell lines used in this experiment divide

every ~16-20 hours, therefore a vast majority of the cell population present at 72 hours pWO were never directly exposed to the OSW-1-compound. OSW-1-compound washout treatment of the leukemia suspension cell line, K562, allowed for transfer of WO treated cells to new culture flasks. The transfer of K562 cells to new flasks eliminated the possibility of residual OSW-1-compound being released from the plasticware and inducing long-term OSBP repression. (**Figure 10A**).

To determine if the sustained OSBP loss is due to persistent residual intracellular OSW-1-compound, both quantitative liquid chromatography mass spectrometry (LCMS) and single cell mass spectrometry (SCMS) were utilized. Using these analytical techniques in combination with a deuterated OSW-1-compound standard allows for the relative quantification of OSW-1-compound levels remaining in the cell after washout. The OSW-1-compound and potential metabolites were not detectable in either MS analytical approach 24 hours after the OSW-1-compound was removed from culture (i.e., 24 hours pWO) [189]. The OSW-1-compound MS detection limit in this analysis was determined to be ~100 pM [189]. This result indicates that persistent residual intracellular OSW-1-compound is not continually repressing OSBP levels, but rather the OSW-1-compound triggers an effect in cells that regulates OSBP levels for multiple days after the OSW-1 compound is removed.

We next wanted to determine if this regulation was specific to OSBP, or if this response occurs with ORP4 and other cellular proteins as well. To test this, cycloheximide chase experiments were performed to determine the half-lives of OSBP and ORP4, which had not previously been reported (**Figure 13A**). Cycloheximide treatment inhibits global protein translation in the cell and is therefore cytotoxic after 24 hours, limiting half-life

measurements exceeding 24 hours. OSBP and ORP4 were shown to have similar half-lives of >24 hours (**Figure 13A**). Next, K562 cells were treated with 1 nM OSW-1-compound for 24-hour continual treatment to significantly decrease ORP4 levels and monitor the return of the protein over the course of 72 hours (**Figure 13B**). K562 cells were chosen for this experiment as this cell line has the most significant decrease in ORP4 levels upon OSW-1-compound treatment. Despite similar half-lives, interestingly, OSBP levels remain ~90% decreased 72 hour pWO, while ORP4 levels begin to return immediately after the OSW-1-compound is removed (**Figure 13B**).

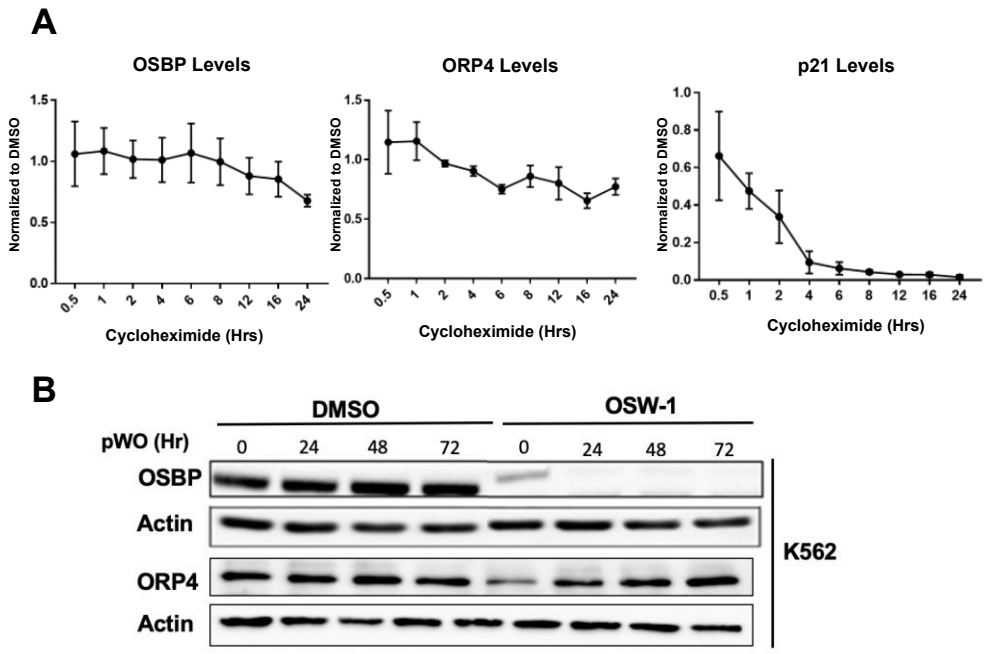

Figure 13: OSBP and ORP4 levels are regulated differently after OSW-1-compound treatment despite the same mechanism of loss and similar half-lives.
A) Cycloheximide chase experiment to determine OSBP and ORP4 half-life in the cell using 177 nM cycloheximide as a translational inhibitor. p21 levels were used as a control for translational inhibition, with the p21 half-life generated from this experiment consistent with previously reported values [291]. The results indicate that OSBP and ORP4 both have similar half-lives that are >24 hours. **B)** Monitoring the return of OSBP and ORP4 levels after OSW-1-compound treatment over the course of 72 hours pWO. OSBP levels remain repressed ~90% 72 pWO, while ORP4 levels begin to return immediately after the OSW-1-compound is removed. [189]

Additionally, iTRAQ quantitative proteomic mass spectrometry analysis was performed to quantify global protein level changes after OSW-1-compound treatment. We found that the OSW-1-compound does not broadly alter the cellular proteome, suggesting the existence of an unrecognized endogenous OSBP-specific regulation system that may be triggered upon the binding of certain ligands to OSBP (i.e., OSW-1) (**Figure 14**).

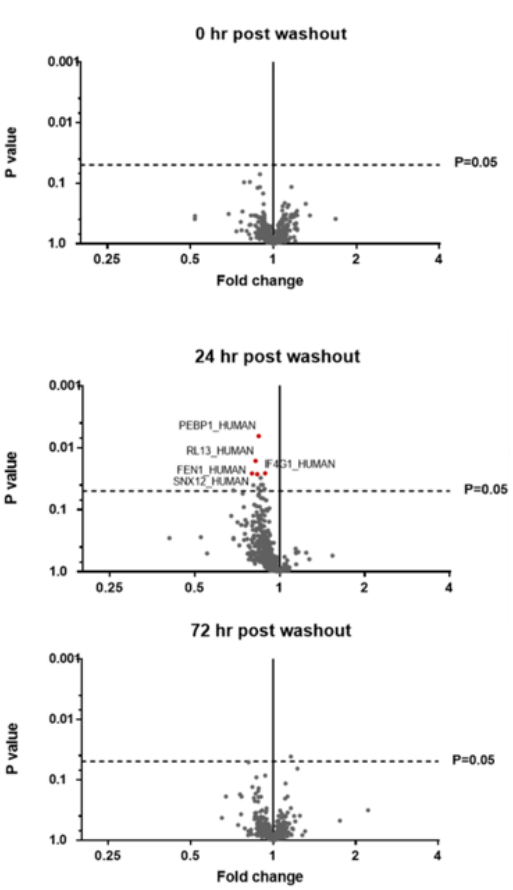

Significantly Changed Proteins after OSW-1-Compound Washout Treatment

Gene ID	Protein	P value
24 hrs pWO		
PEBP1	Phosphatidylethanolamine-binding protein 1	0.0065
RPL13	60s ribosomal protein L13	0.0163
EIF4G1	Eukaryotic translation initiation factor 4 gamma 1	0.0258
FEN1	Flap endonuclease 1	0.0260
SNX12	Sorting nexin-12	0.0266
YWHAB	14-3-3 protein beta	0.0306
RCN1	Reticulocalbin-1	0.0394
PSMA7	Proteasome subunit alpha type-7	0.0395
EEF1A2	Translational Elongation factor 1-alpha 2	0.0401
RDX	Radixin	0.0446
TUBB1	Tubulin beta-1 chain	0.0459
PRPS1	Ribose-phosphate pyrophosphokinase 1	0.0468
DARS2	Aspartate-tRNA ligase, mitochondrial	0.0483
PSMD2	26S proteasome non-ATPase regulatory subunit 2	0.0489
72 hrs pWO		
SSBP1	Single-stranded DNA-binding protein, mitochondrial	0.0414

Figure 14: iTRAQ proteomic mass spectrometry reveals OSW-1-compound treatment does not broadly alter the cellular proteome.
WO experimental conditions (1 nM, 6-hour treatment, 0-72-hour recovery) analysis by iTRAQ proteomic MS/MS reveals that the cellular proteome is not broadly affected by OSW-1-compound treatment (n=3). [189]

Overall, these results suggest the existence of an active cellular process, triggered by OSW-1-compound treatment, that persistently and specifically reduces OSBP levels in the cell for multiple days after the initial stimuli is removed. Mechanistic studies investigating the processes underlying this regulation have determined that the long-term repression is not caused by canonical proteolytic mechanisms (i.e., proteasome or autophagy); and RNA Seq and qPCR analysis of mRNA transcript levels determined that OSBP mRNA transcription is not significantly changed after OSW-1-compound treatment, indicating long-term OSBP repression is mediated by regulation on an RNA level (see **Chapter 3** for more information).

The persistent, multigenerational decrease in OSBP levels in the absence of the OSW-1-compound, with no change in cell viability or morphology, combined with the necessity of OSBP for the replication a number of highly relevant human RNA viral pathogens [84–89,92], provided a unique opportunity to test the efficacy of the OSW-1-compound as a novel *prophylactic* antiviral compound. We hypothesized that the OSBP regulatory response triggered by the OSW-1-compound may be part of an unidentified innate antiviral response in cells. Therefore, if our innate antiviral hypothesis is correct, the washout treatment should induce an antiviral response in cells that persists for days after the OSW-1-compound has been removed, conferring prophylactic antiviral activity in cells.

2.3.3 Transient treatment with the OSW-1-compound induces antiviral prophylaxis against clinically isolated Enteroviruses

The OSW-1-compound has previously been show to display anti-*Enterovirus* activity in cells [89]. Consistent with this report, we observed that the OSW-1-compound inhibited the replication of two clinically isolated *Enteroviruses*, Echo2 and Coxsackievirus A9, in a concentration dependent manner. A 10-hour continual OSW-1-compound treatment at the indicated concentrations (0.1-30 nM) reduced viral titers ~10,000-fold in HeLa cells (**Figure 15A**). To test whether the WO experiment confers prophylactic antiviral activity in cells, HeLa cells were treated with the indicated concentration of the OSW-1-compound (0.1-30 nM) for 6 hours. After 6 hours, the cells were thoroughly washed to remove residual OSW-1-compound and re-incubated in compound-free media for 24 hours. After 24-hour recovery, the cells were then inoculated with the virus for 30 minutes and then incubated in compound-free media for 10 hours, after which viral titers were measured. Despite not being exposed to the OSW-1-compound for 24 hours prior to viral inoculation, the WO cells reduced Echo2 viral titers ~100-fold and Coxsackievirus A9 viral titers ~1,000-fold compared to the vehicle control (**Figure 15B**). Importantly, HeLa cells divide approximately every 16 hours [221]; therefore, a number of the virally inoculated cells were never directly exposed to the OSW-1-compound and still displayed significant antiviral activity, suggesting this novel approach could be exploited as a preventative antiviral treatment. To our knowledge, this report is the first identification of a small-molecule antiviral *prophylactic* that exerts its effect through modulating a host protein (i.e., OSBP).

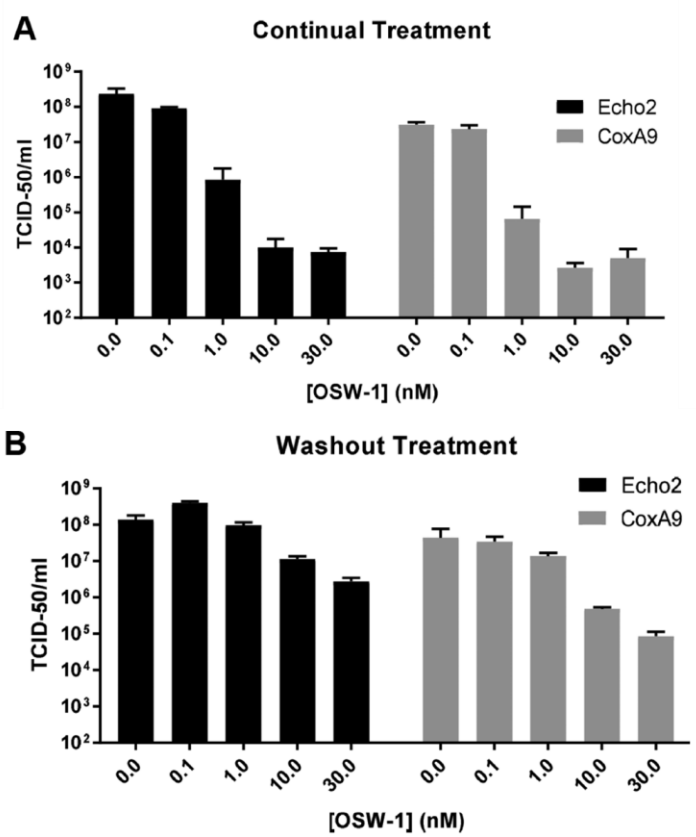

Figure 15: OSW-1-compound treatment induces prophylactic antiviral activity against clinically isolated *Enteroviruses*.
A) Viral titer levels in HeLa cells inoculated with the clinically isolated *Enteroviruses*, Coxsackie A9 and Echo 2, under normal treatment conditions. Cells were treated with the indicated concentration of OSW-1-compound for 6 hours, inoculated with virus for 30 minutes (multiplicity of infection (M.O.I.)=1), and then re-incubated in the indicated concentration of OSW-1-compound for 10 hours. **B)** Viral titer levels in HeLa cells inoculated with the *Enteroviruses*, Coxsackie A9 and Echo 2, under washout treatment conditions. Cells were treated with the indicated concentration of OSW-1-compound for 6 hours, the OSW-1-compound was then removed and the cells recovered in compound-free media for 24 hours. After 24 hours, the cells were inoculated with virus for 30 minutes and incubated in compound-free media for 10 hours. [189]

2.3.4 The loss and long-term repression of OSBP is unique to the OSW-1-compound and not other OSBP-targeting antiviral compounds

Several other structurally-diverse small molecules with antiviral activity reported to target OSBP have been identified including: T-00127-HEV2 (THEV) (**3**) [85], itraconazole (ITZ) (**4**) [84], and TTP-8307 (TTP) (**5**) [87] (**Figure 5**). The effect of these OSBP-targeting antiviral compounds on cellular OSBP levels was analyzed to determine if OSBP loss and long-term repression was unique to the OSW-1-compound, or if it is a generalized response to exogenous small-molecule targeting of OSBP. Treatment with 10,000 nM ITZ, TTP, or THEV for 24 hours caused no decrease in cellular OSBP levels (**Figure 16**). In contrast, 1 nM, 24 hour treatment with the OSW-1-compound resulted in ~90% decrease in cellular OSBP levels (**Figure 16**). These results indicate that the OSW-1-compound is the only OSBP-targeting antiviral compound that causes OSBP loss and long-term repression in cells, indicating the observed response is unique to the OSW-1-compound. Additionally, this result suggests that these structurally-diverse antiviral compounds may be targeting OSBP in multiple ways, resulting in distinct perturbances of OSBP in the cell.

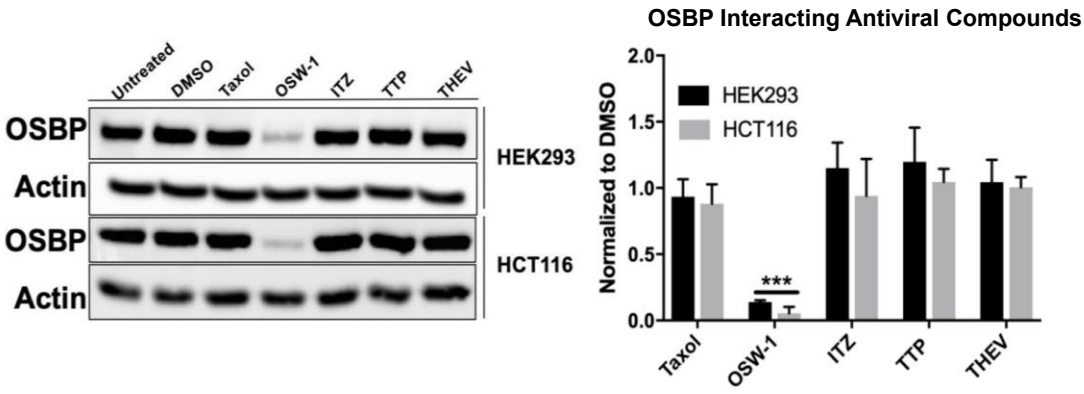

Figure 16: The OSW-1-compound is the only OSBP-targeting antiviral compound that decreases cellular OSBP levels.
A 1 nM continual treatment for 24 hours with the OSW-1-compound decreased OSBP levels ~90%, while 10,000 nM continual treatment for 24 hours with THEV, TTP and ITZ had no effect on OSBP levels. [190]

2.3.5 The OSW-1-compound is the only OSBP-targeting antiviral compound capable of inducing prophylactic antiviral activity in cells

To determine if the prophylactic antiviral activity of the OSW-1-compound is also unique, we analyzed the antiviral efficacy of the OSBP-targeting antiviral compounds (**Figure 17**). Continual treatment with 10,000 nM ITZ, TTP, THEV, or 10 nM OSW-1-compound for 10 hours resulted in antiviral activity consistent with previous literature reports (**Figure 17A**) [84,61,63,65,142]. Comparatively, despite the OSW-1-compound treatment being 1,000-fold less concentrated than the other OSBP-targeting compounds tested, the OSW-1-compound still displayed the highest level of antiviral activity (**Figure 17A**). Importantly, the OSW-1-compound was the only OSBP-targeting antiviral compound that displayed *prophylactic* antiviral activity. HeLa cells were treated with 10,000 nM ITZ, TTP, THEV, or 10 nM OSW-1-compound for 6 hours, followed by removal of the compounds and 24-hour recovery in compound-free media. After 24

hours, the cells were inoculated with the indicated virus and incubated in compound-free media for 10 hours, after which viral titer levels were analyzed. The OSW-1-compound was the only compound possessing antiviral activity 24 hours after the compound treatment had ceased, decreasing viral proliferation ~10,000-fold (**Figure 17B**). At the time of viral inoculation, OSBP levels in the washout cells are reduced >90% by OSW-1-compound treatment, while the other OSBP-targeting antiviral compounds had no effect on cellular OSBP levels (**Figure 17C**). This highlights the unique effects of the OSW-1-compound on cellular OSBP level, regulation, and antiviral activity.

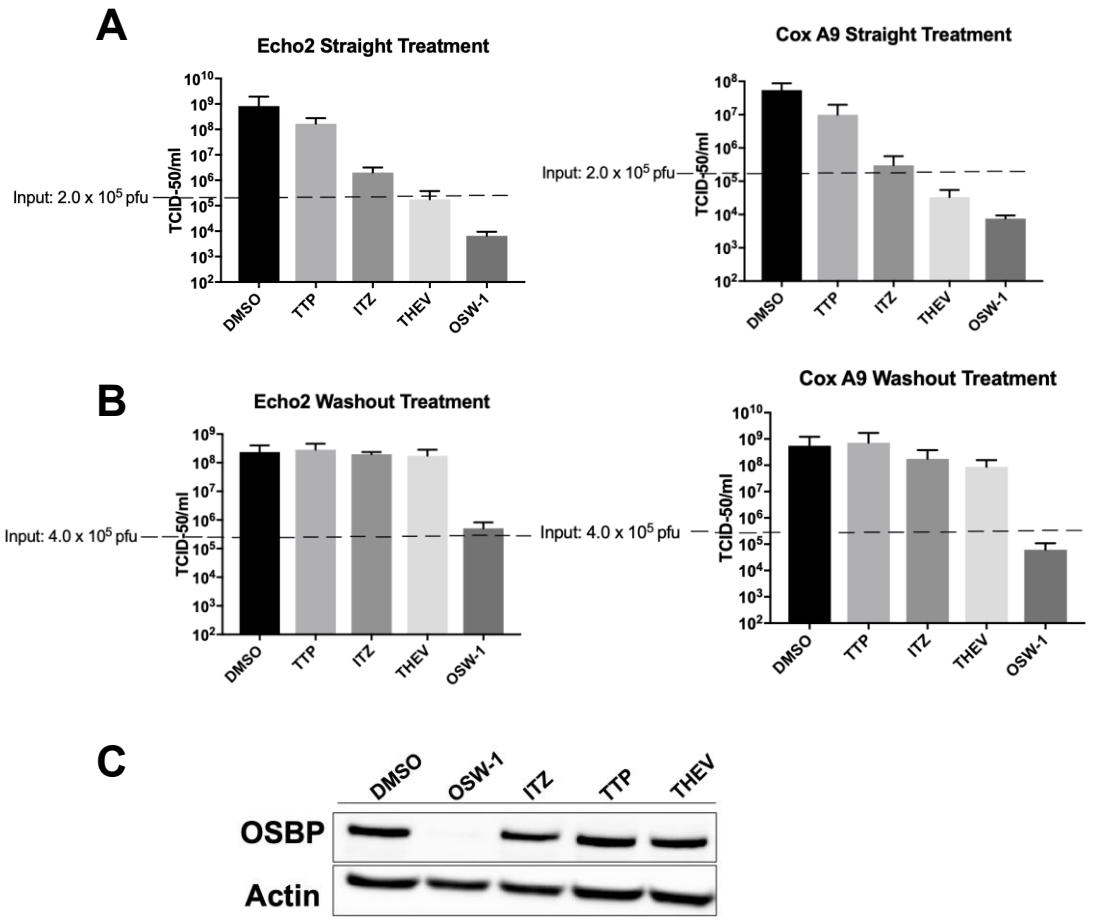

Figure 17: The OSW-1-compound is the only OSBP-targeting compound that induces prophylactic antiviral activity.

A) Levels of viral titers in HeLa cells inoculated with the clinically isolated *Enteroviruses*, Coxsackie A9, and Echo 2. HeLa cells were inoculated with virus for 30 minutes (M.O.I.=1) followed by treatment with either 10 nM OSW-1-compound or 10,000 nM THEV, ITZ, or TTP for 10 hours. **B)** HeLa cells were treated with 10 nM OSW-1-compound, or 10,000 nM THEV, ITZ, or TTP for 6 hours. The compounds were removed and the cells were incubated in compound-free media for 24 hours followed by viral inoculation for 30 minutes (MOI =1). Cells were then incubated for 10 hours in compound-free media. The OSW-1-compound is the only compound that possessed antiviral activity 24 hours after the compound was removed from culture. **C)** OSBP levels in HeLa cells at the time of viral inoculation under washout conditions in Fig. 17B. [190]

2.3.6 The OSW-1-compound and the other OSBP-targeting antiviral compounds interact with OSBP through multiple modes of binding and have distinct effects on OSBP activity in the cell

The difference in effect of the OSBP-targeting antiviral compounds on cellular OSBP levels and antiviral activity suggests that these compounds are targeting OSBP in multiple ways and may have distinct effects on OSBP cellular activity. The only previous binding measurement reported for any of the OSBP-targeting antiviral compounds was for ITZ. ITZ has a reported K_D of 430 nM against full-length OSBP-GFP as measured using microscale thermophoresis, however, the binding site of ITZ on OSBP was not identified [84]. The OSW-1-compound directly competes with oxysterol binding in the OSBP and ORP4 sterol binding pocket [52]. The sterol binding pocket is located in the C-terminal OSBP-related ligand-binding domain (ORD) of OSBP and ORP4 [2] (see **Chapter 4** for more information on the ORP-ORD).

To determine if the other OSBP-targeting antiviral compounds interact with OSBP in the same manner, an established [^{3}H]25-hydroxycholesterol ([^{3}H]25-OHC) competitive binding assay was employed. If a compound interacts with OSBP through the sterol binding pocket, the binding of the [^{3}H]25-OHC radioligand reporter to the sterol binding pocket will be competitively inhibited as the concentration of a ligand of interest (e.g. OSW-1) increases. This results in a sigmoidal dose-response curve which can be utilized to calculate an inhibition constant (K_i). Due to the competitive nature of this assay, only binding to the sterol binding pocket of the ORD can be detected, and not interaction with the protein at other locations (for more information on the [^{3}H]25-OHC competitive binding assay procedure and analysis, see **Chapter 4**). OSW-1, ITZ, THEV,

and TTP were tested for binding against human OSBP and ORP4 using the [^{3}H]25-OHC competitive binding assay. These are the first binding values reported for human OSBP, as previous OSBP binding values used rabbit, or other animal OSBP [52]. The OSW-1-compound produced an OSBP K_i of 16 ± 4 nM and an ORP4 K_i of 71 ± 6 nM (**Figure 18 A, B, C**). Similar to OSW-1, THEV interacts with the sterol binding pocket of OSBP and ORP4 with K_i binding values of 22 ± 15 nM and 98 ± 14 nM, respectively (**Figure 18 A, B, C**). In contrast, there was no detectable competitive [^{3}H]25-OHC binding inhibition at any concentration tested for the ITZ and TTP compounds, indicating that ITZ and TTP interact with OSBP at a location other than the sterol binding pocket (**Figure 18 A, B, C**).

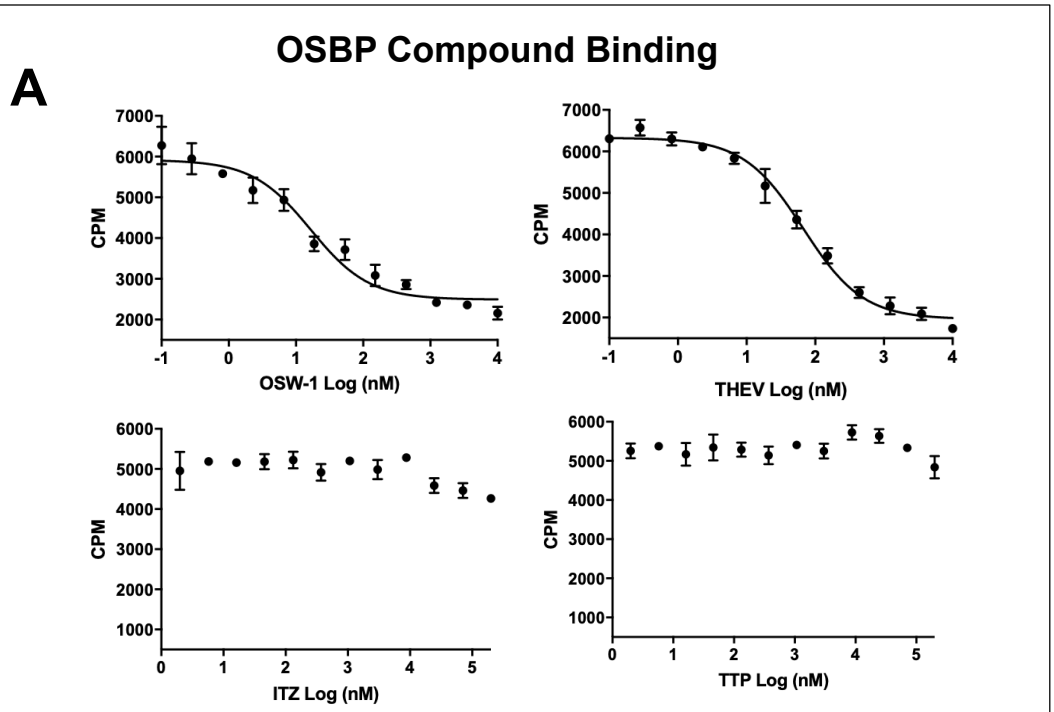

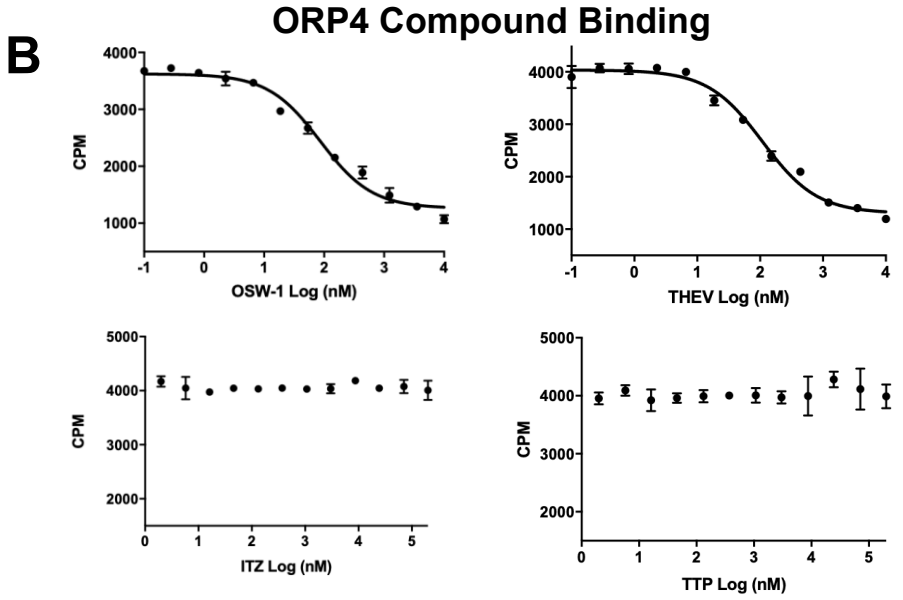

C

Compound	OSBP K_i (nM)	ORP4 K_i (nM)
OSW-1	16 ± 4	71 ± 6
THEV	22 ± 15	98 ± 14
Itraconazole	-	-
TTP	-	-

Figure 18: The OSBP-targeting antiviral compounds interact with OSBP through different modes of binding.

A) OSBP and **B)** ORP4 interact with the OSW-1-compound and THEV through the sterol binding pocket and TTP and ITZ do not, as determined using a competitive [^{3}H]25-OHC binding assay. Representative binding curves shown. **C)** Average K_i binding values from at least three independent experiments with internal technical triplicates within each experiment. [190]

To further confirm that the OSW-1-compound and THEV both interact with the OSBP sterol binding pocket, 1 nM of the OSW-1-compound was co-administered with 10,000 nM THEV, TTP, or ITZ (**Figure 19**). Co-administration of the OSW-1-compound and THEV significantly rescued OSBP levels in both cell lines tested compared to OSW-1-compound treatment alone (**Figure 19A**). This result indicates that THEV is able to out compete the OSW-1-compound for OSBP sterol pocket binding and therefore prevent degradation of the protein, confirming the competitive binding result. OSW-1 and TTP co-administration had no effect on rescuing OSBP levels (**Figure 19A**).

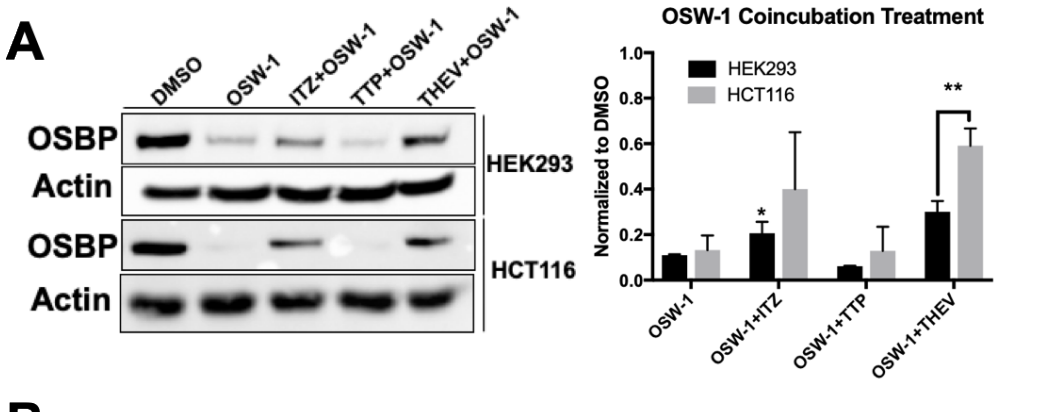

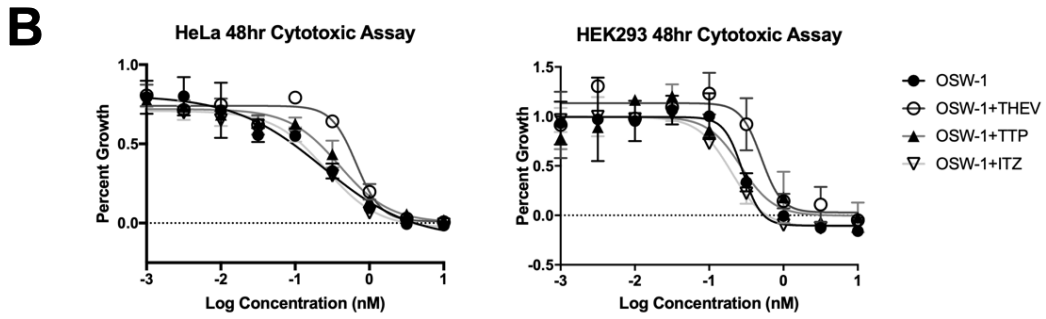

	Average GI_{50} (nM)			
	OSW-1	**OSW-1+THEV**	**OSW-1+TTP**	**OSW-1+ITZ**
HeLa	0.33 ± 0.18	0.63 ± 0.18	0.29 ± 0.11	0.28 ± 0.16
HEK293	0.22 ± 0.09	0.29 ± 0.14	0.16 ± 0.03	0.19 ± 0.11

Figure 19: THEV co-incubation with the OSW-1-compound rescues OSW-1-compound induced OSBP loss and ORP4-targeting associated cytotoxicity.
A) Co-incubation with 1 nM OSW-1-compound and 10,000 nM THEV, TTP, or ITZ for 24 hours reveals THEV, and to a lesser extent, ITZ, is able to abrogate the OSW-1-compound induced loss of OSBP, indicating these compounds inhibit the ability of the OSW-1-compound to interact with OSBP. Representative Western blot shown with the average of three independent replicates. **B)** Cytotoxicity assay using co-incubation with the indicated concentration of OSW-1-compound and 10,000 nM THEV, TTP, or ITZ for 48 hours show OSW-1/THEV co-incubation approximately doubles the GI_{50} of OSW-1 in HeLa cells. Representative cytotoxicity curves and averages from three independent experiments with technical triplicates within each experiment. [190]

Interestingly, ITZ also rescued OSW-1-compound induced degradation of OSBP despite not competitively inhibiting [^{3}H]25-OHC in the binding assay (**Figure 18, 19**). OSBP homology models published by Bauer et al. in 2018 used to investigate the structure-

activity relationships (SAR) between ITZ and OSBP showed two predicted docking orientations of ITZ; one of which is abutting the fingerprint region of OSBP, which is in close proximity to the sterol binding pocket of OSBP [223]. Therefore, even though ITZ is unable to competitively inhibit [^{3}H]25-OHC in the binding assay, it is still possible that the close proximity of ITZ to the sterol binding pocket may interfere with the ability of the much larger OSW-1-compound to access the binding pocket when co-administered.

To validate the sterol pocket binding interaction between THEV and ORP4, 48-hour cytotoxic assays were conducted with co-incubation of the OSW-1-compound and 10,000 nM of THEV, TTP, or ITZ (**Figure 19B**). THEV, ITZ, and TTP are not cytotoxic at the concentration administered in the cytotoxicity assay (data not shown) [190]. THEV is able to rescue OSW-1-compound induced cytotoxicity, approximately doubling the GI_{50} of the OSW-1-compound in HeLa cells, presumably by outcompeting the OSW-1-compound for binding to ORP4 (**Figure 19B**); however, this increase is not statistically significant using a one-way ANOVA with a follow up Dunnett's test . These results reveal OSBP is targeted by antiviral small molecules through multiple modes of binding, suggesting OSBP could be targeted for antiviral development in multiple ways.

Immunofluorescent confocal microscopy showed that the different OSBP-targeting antiviral compounds caused distinct effects on OSBP cellular activity (**Figure 20**). OSBP cellular localization patterns have previously been shown to be altered by ligand binding, including through interaction with oxysterols like 25-OHC [15,52,50], OSW-1 [52,224], ITZ [84,63], THEV [85], and TTP [87]. Additionally, OSBP localization experiments have previously been performed in HCT-116 cells [52]. OSBP is predominately co-localized to the Golgi marker which is consistent with reports of OSBP localizing to the

ER-Golgi interface under certain stimuli [15]. In our results, 10,000 nM 25-OHC treatment for 24 hours results in strong co-localization of OSBP (green) with the Golgi marker, TGN46 (red) (**Figure 20A**). Treatment with 1 nM OSW-1-compound results in a significant reduction in OSBP signal after 24 hours, as expected based on Western blot and proteomic mass spectrometry results, while the remaining OSBP is tightly grouped and the Golgi marker is diffuse (**Figure 20A**). 10,000 nM ITZ treatment results in a punctate OSBP pattern that is closely associated with the Golgi marker, while the Golgi marker signal appears to be more diffuse in the cytoplasm (**Figure 20A**). 10,000 nM TTP treatment results in tight colocalization of OSBP to the Golgi marker, with a signal similar to the DMSO treated vehicle control (**Figure 20A**). 10,000 nM THEV treatment results in OSBP co-localization with the Golgi marker in a tight pattern, similar to the 25-OHC-induced OSBP localization. Co-administration of 1 nM OSW-1-compound with 10,000 nM THEV, ITZ, or TTP reveals that THEV and ITZ alter the localization pattern induced by the OSW-1-compound (**Figure 20B**). The localization pattern of OSW-1+ITZ treated cells is a mixture of the results of the individual treatments, but possesses a stronger OSBP signal, confirming the OSW-1+ITZ Western blot results that showed ITZ prevented the loss of OSBP induced by the OSW-1-compound (**Figure 20A**). Likewise, OSW-1+THEV co-administration resulted in a mixture of the results of the individual treatments (**Figure 20B**), also resulting in a stronger OSBP signal, once again confirming the Western blot results (**Figure 20A**). OSW-1+TTP resulted in low expression OSBP, presumably due to the inability of TTP to rescue OSW-1-compound induced OSBP loss (**Figure 20A**), and produced a pattern not consistent with the individual treatments (**Figure 20B**).

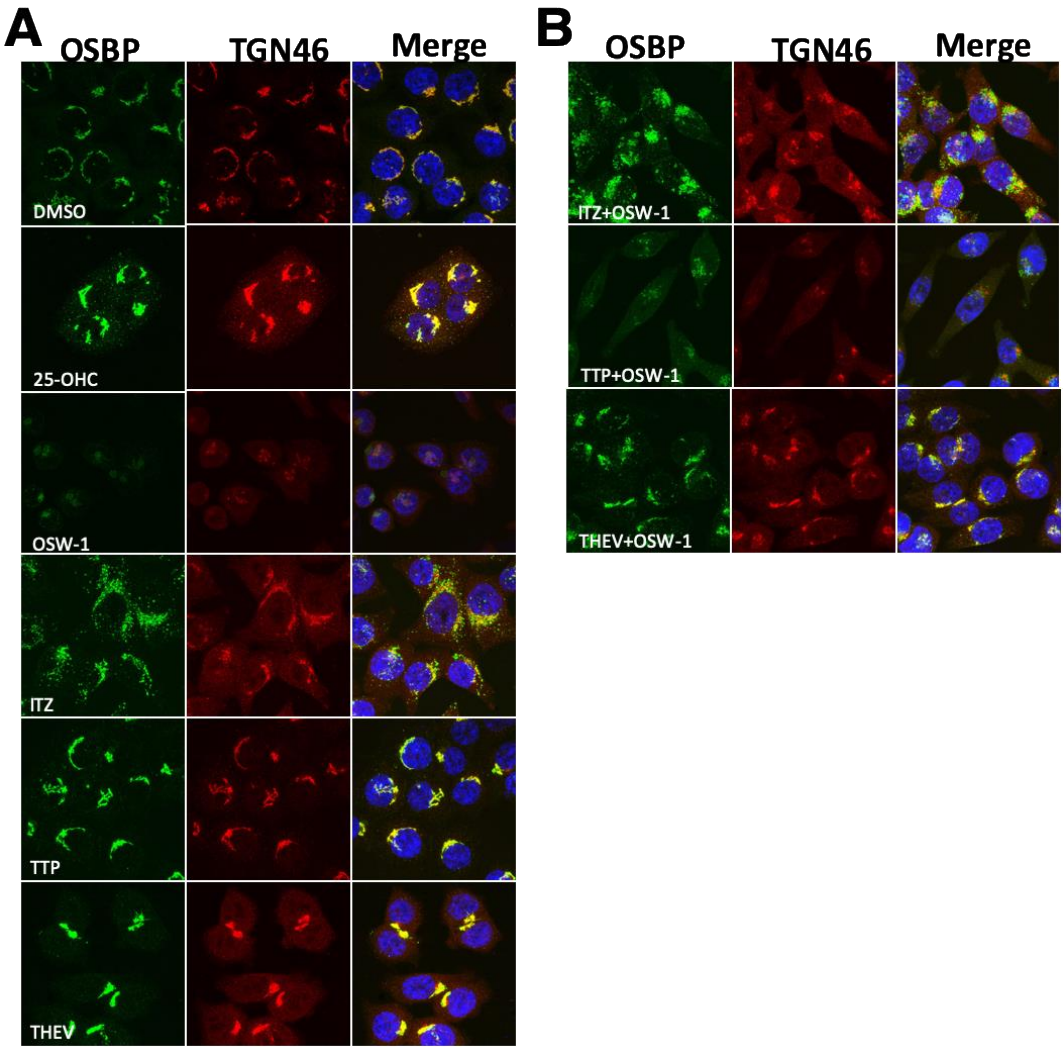

Figure 20: The OSBP-interacting antiviral compounds have distinct effects on OSBP localization in cells.
Immunofluorescent confocal microscopy in HCT-116 cells reveals OSBP (green) localization patterns change with respect to the Golgi marker TGN 46 (red), and nucleus (blue) after **A)** administration of 1 nM OSW-1-compound or 10,000 nM THEV, TTP, and ITZ, or **B)** a combination of the treatments. [190]

2.4 Discussion

The results of this chapter reveal the discovery that transient exposure to non-toxic, low nanomolar concentrations of the OSW-1-compound triggers an unrecognized OSBP-specific regulatory response in cells. The triggering of this response by OSW-1-

compound treatment causes an ~90% decrease in cellular OSBP levels that persists for multiple days after the compound has been removed from cell culture, resulting in the long-term repression of OSBP levels in the cell (**Figure 10**). The multigenerational persistence of this regulatory response indicates that it can be stably passed down to subsequent cell generations that were never directly exposed to the OSW-1-compound.

The OSW-1-compound washout treatment conditions do not result in a decrease in cellular viability, cellular proliferation, or change in morphology (data not shown) [189]. The discovery that an ~90% reduction of cellular OSBP levels for multiple days is not toxic to the cell suggests OSBP could be targeted for antiviral drug development without causing toxicity to the host. Long-term OSBP repression was shown not to be the result of persistent residual intracellular OSW-1-compound (data not shown) [189], indicating that the OSW-1-compound triggers the long-term regulation of OSBP levels, rather than persistently repressing OSBP levels by its presence in cells. Our results show that ORP4 levels also decrease after OSW-1-compound treatment in the same time and proteasome-dependent manner as OSBP after OSW-1-compound treatment (**Figure 6, 7**), but OSBP levels are much more sensitive to OSW-1-compound treatment than ORP4 (**Figure 8**). Importantly, despite the same mechanism of loss after OSW-1-compound treatment and similar half-lives for both OSBP and ORP4, OSBP levels remain repressed for multiple days after the OSW-1-compound treatment has ceased, while ORP4 levels do not (**Figure 13**). Additionally, iTRAQ proteomic mass spectrometry revealed that OSW-1-compound treatment does not broadly alter the cellular proteome (**Figure 14**). Together, these results indicate that OSW-1-compound treatment triggers an effect in cells that uniquely and specifically regulates OSBP levels for multiple days after the initial stimuli (i.e., OSW-

1) is removed. These findings suggests the existence of an unidentified endogenous OSBP-specific regulatory response that may be triggered by the binding of certain ligands to OSBP (i.e., OSW-1).

OSBP levels are significantly decreased 24 hours after the OSW-1-compound has been removed (i.e., 24 hours post-washout (pWO)) in all cell lines tested, and treatment concentrations of less than 1 nM and exposure to the OSW-1-compound as brief as 1-hour significantly reduces cellular OSBP levels 24 hours pWO, highlighting the ubiquity and potency of this novel response (**Figure 12**).

Leveraging this discovery, we show that long-term OSBP repression can be exploited to induce *prophylactic* antiviral activity in cells (**Figure 15**). To the best of our knowledge, we report the OSW-1-compound as the first identified small-molecule antiviral prophylactic that exerts activity through modulating a host protein (i.e., OSBP).

We hypothesize that the observed regulatory response uniquely triggered by the OSW-1-compound may be part of a larger, unrecognized arm of innate antiviral response in cells. Due to the necessity of OSBP for the replication of a number of highly relevant human RNA viral pathogens [84–89,92], a cellular response mechanism for specifically decreasing OSBP levels in the cell for multiple days during a viral infection could create a cellular environment that is not toxic to the host cell itself, but not conducive to viral replication for multiple days; allowing for the host immune system to more efficiently and effectively clear the viral infection from the host (see **Chapter 3** and **Chapter 5** for more information on the innate antiviral response hypothesis). The ability to exogenously trigger and harness this unrecognized response with a small molecule, like the OSW-1-compound, could introduce an entirely new paradigm in antiviral treatment. Antiviral

targeting of OSBP in this manner would circumvent the high probability of mutational resistance associated with targeting elements of the highly mutable virus itself, and could lead to a broad-spectrum *preventative* antiviral therapy. The broad necessity of OSBP among RNA viruses indicates this novel antiviral mechanism would not only be effective against many existing RNA viruses that are already established public health menaces with no current treatments, but also newly emergent RNA viruses (i.e., SARS-CoV-2) and RNA viruses that have not yet emerged.

This chapter also shows that long-term repression of OSBP levels and prophylactic antiviral activity are specific to the OSW-1-compound, and not generally a consequence of OSBP binding of small molecules, or other OSBP-targeting antiviral compounds (**Figure 16, 17**). Additionally, we reveal that the OSBP-targeting antiviral compounds (**Figure 5**) target OSBP through multiple modes of binding (**Figure 18, 19**) and have distinct effects on OSBP cellular localization (**Figure 20**). These results highlight not only the unique effect of the OSW-1-compound on cellular OSBP levels and regulation, but also the ability of OSBP to be targeted by structurally-diverse antiviral small molecules through multiple distinct mechanisms that allow OSBP activity to be modulated in a variety of distinct ways for antiviral therapeutic development.

2.5 Conclusions

Overall, these results reveal important insights into OSBP cellular biology and OSBP-targeted antiviral drug development. This chapter not only reports the discovery of an unrecognized cellular regulatory process that specifically represses OSBP levels for multiple days, but also introduces a novel approach to induce antiviral prophylaxis in human cells through exploiting this unrecognized response. The prophylactic antiviral

activity of the OSW-1-compound suggests that this response can be harnessed using exogenous small molecules and exploited to develop novel broad-spectrum preventative antiviral treatments. We hypothesize that this regulatory response may be part of a larger, undiscovered arm of innate antiviral response in cells. Additionally, this chapter shows that OSBP is targeted by structurally-diverse antiviral small molecules through multiple mechanisms with distinct effects on OSBP cellular activity, indicating that OSBP could be targeted for antiviral development in multiple ways. These discoveries lay the foundation for a new paradigm in antiviral treatment that could potentially not only treat, but also possibly prevent RNA viral pandemics like the COVID-19 pandemic, as well as pandemics that have not yet occurred.

Chapter 3: Mechanistic studies on the cellular responses triggered by the OSW-1-compound

Abstract

The naturally occurring small molecule OSW-1 targets the broad-spectrum antiviral target oxysterol-binding protein (OSBP) with high affinity. We discovered that transient (6h), non-toxic (1 nM) treatment with the OSW-1-compound triggers an ~90% multigenerational decrease in cellular OSBP levels that persists for over 72 hours after the OSW-1-compound has been removed from cell culture. The OSW-1-compound triggered long-term repression of cellular OSBP levels induces *prophylactic* antiviral activity in cells. The long-term OSBP repression induced by the OSW-1-compound is specific for OSBP and does not repress other cellular proteins, including the closest protein relative to OSBP, ORP4. These results suggest the existence of an endogenous OSBP-specific regulatory response that is triggered by the binding of certain ligands to OSBP (i.e., OSW-1). The mechanisms underlying this response remain enigmatic. This chapter investigates the mechanism of OSBP regulation leading to long-term OSBP repression, and other responses triggered by the OSW-1-compound. We show that OSBP is not repressed by canonical mechanisms of protein regulation, including transcriptional repression and post-translational proteolysis by the proteasome or autophagy. Instead, the OSW-1-compound triggers OSBP regulation on an RNA level, and also causes significant changes to an RNA regulatory pathway and antiviral host defense mechanism called nonsense-mediated decay (NMD). Additionally, it was determined that OSW-1-compound treatment induces cellular autophagy through mTORc1 inhibition. Overall, utilizing the OSW-1-compound as a small-molecule probe, we discovered a unique endogenous OSBP regulatory process that can be exploited to induce broad-spectrum antiviral *prophylaxis* in cells. The combined effects of the OSW-1-compound to: decrease and repress cellular OSBP levels for multiple days, inhibit mTORc1, induce cellular autophagy, and modulate NMD host defense processes, creates a multifaceted innate antiviral environment in the cell that can persist while a viral infection is cleared. Together, these results suggest that long-term OSBP repression, and other related responses triggered by the OSW-1-compound, may comprise an unrecognized innate antiviral response pathway in the cell that could be exploited to create a new class of broad-spectrum preventative antiviral treatments.

Allocation of Contribution

The following chapter (Chapter 3) is reproduced with permission in part from (i) "Transient Compound Treatment Induces a Multigenerational Reduction of Oxysterol-Binding Protein (OSBP) Levels and Prophylactic Antiviral Activity," Roberts, B. L.; **Severance, Z. C.**; Bensen, R. C.; Le, A. T.; Kothapalli, N. R.; Nunez, J. I.; Ma, H.; Wu, S.; Standke, S. J.; Yang, Z.; Reddig, W. J.; Blewett, E. L.; Burgett, A. W. G. *ACS Chem. Biol.* **2019**, 14 (2), 276–287: DOI: 10.1021/acschembio.8b00984, https://pubs.acs.org/doi/full/10.1021/acschembio.8b00984 [189]. Further permissions related to the material excerpted in this chapter should be directed to the American Chemical Society (ACS).

I produced the results presented in this chapter with the following exceptions. Dr. Brett Roberts conducted the experiments in **Figure 23A, C,** and **E**. Dr. Ryan Bensen conducted the experiments in **Figure 21** and **23A**. **Figure 21** was performed in collaboration with Dr. Shawna Standke and the Yang Research Group at the University of Oklahoma. Dr. Anh Le-McClain synthesized the deuterated OSW-1 standard used in **Figure 21**. Dr. Zhe Wang from the Wu Research Group at the University of Oklahoma performed the mass spectrometry analysis for **Figure 28A**. Dr. Fares Najar from the University of Oklahoma performed the RNA Seq bioinformatics analysis in **Figure 28B**.

3.1 Introduction

Oxysterol-binding protein (OSBP) is a lipid binding protein expressed ubiquitously in humans and other eukaryotes [2,9]. OSBP is involved in diverse cellular activities such as lipid transport, metabolism, and signaling; however, the overall function(s) of OSBP in the cell remain unclear (see **Section 1.4: OSBP biology** for more information) [1,2,9]. OSBP is also an evolutionarily conserved host factor required for the proliferation of a broad spectrum of human pathogenic RNA viruses [84–89,92]. Although cholesterol transport to the viral replication compartment (VRC) by OSBP has been shown to be required for viral proliferation, OSBP may also provide other critical contributions to RNA viral infection that have not yet been elucidated (see **Section 1.6.1: OSBP as a broad-spectrum antiviral target** for more information) [84–89,92].

The naturally occurring small molecule, OSW-1, selectively targets OSBP and ORP4 with high affinity (see **Section 1.7.1: ORPphilins** for more information on OSW-1) [52]. Our discovery of the long-term multigenerational repression of cellular OSBP levels, triggered by OSW-1-compound treatment, is a unique and novel response to exogenous small molecule treatment that we call the "washout effect" [189,190]. We were able to leverage the discovery of this OSBP regulatory response to confer *prophylactic* antiviral activity in cells. This is a novel method of inducing antiviral prophylaxis that could potentially be exploited to develop broad-spectrum preventative RNA antiviral treatments (see **Chapter 2** for more information).

The initial ~90% decrease of cellular OSBP levels induced by OSW-1-compound treatment is proteasome-dependent [52,189]; however, the mechanism of OSBP repression that causes this ~90% reduction to persist for multiple generations of cells for multiple

days in the absence of the compound remains unknown. We have previously shown that this long-term repression is unique to OSBP, and not other cellular proteins, even OSBP's closest protein relative, ORP4. These results indicate that OSW-1-compound treatment triggers an effect in cells that uniquely and specifically regulates OSBP levels for multiple days after the initial stimuli is removed, suggesting the existence of an endogenous OSBP-specific regulatory response that is triggered by the binding of certain ligands to OSBP (i.e., OSW-1). We hypothesize this response may be part of an unrecognized arm of innate antiviral response in cells that could be harnessed by small molecules and exploited to create an entirely new class of preventative broad-spectrum RNA antiviral therapies. Elucidating the mechanism(s) underlying this regulatory response may not only be a route to discovering novel cellular biology, but also provide the basis for new medicines that exploit this response to create RNA antiviral treatments against many human RNA viral pathogens that currently have no treatment. Harnessing and understanding this response could introduce a new paradigm in antiviral therapeutics that could potentially not only treat, but possibly also prevent existing and new viral RNA pandemics, such as the COVID-19 pandemic.

Protein expression is regulated and repressed through various cellular mechanisms [225–228]. The regulation of protein expression in the cell is critical for cellular function and thus protein expression is subject to regulation at multiple layers: transcription, translation, and post-translation [225–228]. Transcriptional regulation involves varying the transcription of a certain gene from DNA into mRNA [226]. Transcriptional regulation occurs on two levels: regulation of chromatin structure, which controls the accessibility of transcriptional machinery to certain genes, and regulation of

transcriptional machinery that bind to genes (when accessible) and promote or repress gene transcription into mRNA [226]. Translational regulation is a step down from transcriptional regulation and involves regulating the ability of the mRNA transcript to be translated into protein [227]. Eukaryotic translation occurs in three stages: initiation, elongation, and termination, with most translational regulation occurring at the initiation step [227,229]. Translational regulation typically involves RNA binding proteins (RBPs) that interact with non-exonic components of the mRNA transcript (i.e., introns, or 3' or 5' untranslated regions (UTRs)), and regulate the RNA to either promote or inhibit its translation [227,230,231]. Therefore, the presence of mRNA in a cell does not necessarily mean an mRNA transcript will be translated into protein [227]. Post-translational regulation involves either reversible post-translational modifications (e.g. phosphorylation) that can regulate protein function, or the irreversible post-translational selective degradation of a protein [228,232]. In the latter case, post-translational protein regulation involves the use of proteolytic pathways to degrade the protein target, such as the proteasome or autophagy [228].

Herein, we investigate the mechanism of OSBP regulation leading to long-term OSBP repression in the cell, as well as identify other cellular responses caused by OSW-1-compound treatment. Our results indicate that the OSW-1-compound triggers OSBP regulation on an RNA level, and also causes sweeping changes to an RNA regulatory pathway known as nonsense-mediated decay (NMD). NMD is not only a pervasive post-transcriptional regulatory system used to adjust the specific expression of a protein under various stimuli, but also a known host antiviral defense mechanism against RNA viruses [233–237]. Additionally, it is revealed that OSW-1-compound treatment induces cellular

autophagy through inhibition of mTORc1. mTORc1 is also involved in host innate antiviral response [238–241]. Collectively, our results indicate that OSW-1-compound treatment creates a multifaceted innate antiviral environment in the cell that may comprise an unrecognized cellular innate antiviral response that could be induced simply by modulating cellular OSBP levels.

3.2 Methods and Materials

3.2.1 Cell Lines and Viruses

Same as **Chapter 2 Methods Section 2.2.2: Cell Lines and Viruses**.

3.2.2 General Cell Culture

Same as **Chapter 2 Methods Section 2.2.3: General Cell Culture**

3.2.3 Cell Lysis Method 1 (AC Lysis Buffer Freeze/Thaw)

Same as **Chapter 2 Methods Section 2.2.4: Cell Lysis Method 1 (AC Lysis Buffer Freeze/Thaw)**

3.2.4 Cell Lysis Method 2 (MPER Lysis)

Same as **Chapter 2 Methods Section 2.2.5: Cell Lysis Method 2 (MPER Lysis)**

3.2.5 Western Blots

Same as **Chapter 2 Methods Section 2.2.6: Western Blots**, with the addition of the following antibodies: primary antibodies, 1:100 SQSTM1 (p62) D-3 (Santa Cruz sc-28359) and 1:1000 LC3A/B D3U4C XP® (Cell Signaling 12741). Secondary antibodies, 1:2000 goat antirabbit IgG-HRP (Cell Signaling 7074S).

3.2.6 Washout Experiment

Same as **Chapter 2 Methods Section 2.2.7: Washout Experiment**

3.2.7 Cycloheximide Chase Experiment

Same as **Chapter 2 Methods Section 2.2.8: Cycloheximide Chase Experiment**

3.2.8 iTRAQ Proteomic Mass Spectrometry

Same as **Chapter 2 Methods Section 2.2.12: iTRAQ Proteomic Mass Spectrometry**

3.2.9 LC-MS/MS Analysis of iTRAQ Labeled Peptides

Same as **Chapter 2 Methods Section 2.2.13: LC-MS/MS Analysis of iTRAQ Labeled Peptides**

3.2.10 OSW-1-Compound Generation and Preparation

Same as **Chapter 2 Methods Section 2.2.16: OSW-1-Compound Generation and Preparation**

3.2.11 Synthesis of Deuterated OSW-1 Standard

The deuterated OSW-1 analog was produced via total synthesis of OSW-1 adapted from literature procedure [242,243]. During the synthesis of the xylose component, a benzoate group containing the deuterated methyl substituent was introduced.

3.2.12 Intracellular OSW-1 Quantification using LC-MS and Single-Cell MS Methods

nano-UPLC/MS: HCT-116 cells ($1.5x10^5$) were seeded in a 6-well plate. Upon 60% confluency, cell lysate was created following a 1-hour treatment of 100 nM OSW-1, with or without a 24 hour post-washout recovery (pWO). Trypsin (0.5 mL) was used to detach the cells, with additional McCoy's media (0.5 mL) to stop digestion. Cell count was performed using a Bio-Rad TC20™ Automated Cell Counter with trypan blue viability staining. Cells were spun at 500 x g for 5 minutes followed by a 1 mL PBS wash. The cell pellet was lysed using 1 mL of 50 nM d-OSW-1 dissolved in cold acetonitrile and methanol (1:1) with brief vortexing on ice for 10 minutes. The cell pellet was spun at 15000 xg at 4°C for 15 minutes. The supernatant was transferred to a new tube and dried using a speed vacuum (Savant SPD11V, Thermo) at 70 °C. Prior to analysis, cells are resuspended in 150 µL of ACN: H_2O (1:10). Analysis was performed using a Waters nanoAQUITY BEH C-18 column (100 µm x 100 mm, 1.7 µm) coupled with a mass spectrometer (Thermo LTQ Orbitrap XL, Waltham, MA) using a flow rate of 0.3 uL/min. Mobile phase A is ACN with 0.1% formic acid, and mobile phase B is H_2O with 0.1% formic acid. The time/%A are as follows: 0/0, 1/50, 2/100, 3/100, and 4/0 for a total runtime of 5 minutes [244].

3.2.13 Single-Cell MS Analysis

HCT-116 cells ($1.5x10^5$) were seeded on to a glass microchip (18 mm diameter) with chemically-etched microwells (55 µm diameter; 25 µm deep) placed into each well of a 6-well plate. Upon 60% cell confluency, cells were treated as described for nano-

UPLC/MS. Following treatment, the microchip was washed with 5 mL of FBS-free McCoy's media and placed on an X, Y, Z-translational stage for quantification. MS analysis was performed as previously described [245]. Briefly, single probes were coupled to the mass spectrometer by using a flexible arm clamp to position the nano-ESI emitter in front of the inlet. The solvent-providing capillary was connected to the solvent through the conductive union. For quantification, 50 nM d-OSW-1 was added into the solvent. High voltage (~4.5 kV) was used for SCMS experiments in the positive ion mode with a mass resolution (m/Δm) of 60,000. A flow rate of ~5 nL/s was used (the actual flowrate is optimized for each single-probe). Data was collected using Xcaliber software and exported into Excel for analysis [244].

3.2.14 Proteasome Inhibitor Experiment

HCT-116 cells were seeded out into plates and incubated for 20 hours. For the co-incubation experiments, the cells were treated with DMSO (Sigma 472301), 1 nM OSW-1, 25 nM bortezomib (Sigma 5043140001), 25 nM carfilzomib (AdooQ Bioscience A11278), 170 nM MG-132 (Sigma 474787), or a combination of treatments for 24 hours. Cells were lysed and analyzed by Western blotting. For the washout experiments, the cells were treated with media containing DMSO or 1 nM OSW-1 for 6 hours, washed 3 times with 5 mL of media, and then allowed to recover for 24 hours. After the 24-hour recovery, one set of treatments were lysed as a control to ensure OSBP loss, while the other cells were treated with media containing 25 nM bortezomib, 25 nM carfilzomib, 170 nM MG-132, or DMSO for 24 hours. Cells were lysed and analyzed via Western blot [214].

3.2.15 Calpain Inhibitor Experiment

Under the washout experimental conditions, cells were treated with DMSO or 1 nM OSW-1 for 6 hours. Cells were washed out according to the washout experimental method previously described (see **Chapter 2 Methods Section 2.2.7: Washout Experiment)**. After 24-hour recovery, one set of DMSO and OSW-1 treated cultures were lysed following the 6-well lysis method (see **Chapter 2 Methods Section 2.2.4: AC Lysis**). At the same time (24 hour post-washout (pWO), ALLN (10 μM) was added to one set of DMSO and one set of OSW-1 treated cells. The cells continued to incubate until 48-hour pWO, at which point they were lysed and analyzed via Western blot [244].

3.2.16 Autophagy Experiment

HEK293 cells were seeded into 10 cm^2 plates. Upon 70% confluency, cells were treated with DMSO as a vehicle control, 1 nM OSW-1, 25 μM chloroquine, or 100 nM rapamycin, or a combination of treatments for 6 hours in 10 mL DMEM media for each 10 cm^2 plate. After 6 hours, the media containing the OSW-1-compound was washed out with three separate 5 mL compound-free media washes (same as the washout experimental protocol). Cells were then treated with either drug free media, 100 nM rapamycin, 25 μM chloroquine, or a combination of treatments, and allowed to recover from OSW-1-compound treatment for 6, 15, or 24 hours. After the indicated post-washout time point, the cells were lysed using AC lysis buffer according to the cell lysis protocol described previously. Lysates were analyzed via Western blot using OSBP, SQSTM1 (p62), and LC3-A/B antibodies, with β-actin antibody used as a loading control for

quantification (antibody information can be found in 'Western blotting' experimental methods).

3.2.17 RT-PCR Analysis

HCT-116 and HEK293 cells were seeded at $0.85x10^5$ cells/mL into 10 cm^2 plates and left to rest for 20 hours. Cells were treated in the same manner as the washout with 1 nM Taxol, 1 nM OSW-1, and DMSO and left to recover for 0-72 hours. Once each time point was reached, media was removed from cell plates and 1 mL of TRIzol (Thermo 15596026) was added to the plates and cells were scraped and collected in a 1.5 mL Eppendorf tube and incubated at room temperature for 5 minutes to ensure nucleoprotein complex dissociation. To each tube, 0.2 mL of chloroform was added and incubated for 2.5 minutes at room temperature. The samples were then spun down at 12,000 x g for 15 minutes at 4°C. After spinning the upper aqueous phase was transferred into a fresh 1.5 mL Eppendorf tube. 0.5 mL of 100% isopropanol was added and the tubes were mixed by inversion followed by a 10 minute incubation at room temperature. Samples were then spun down at 12,000 x g for 10 minutes at 4°C. Supernatant was discarded and 1 mL of 75% ethanol was added to the pellet to wash the RNA. The sample was vortexed briefly to dislodge pellet and then spun down at 7,500 x g for 5 minutes at 4°C. Supernatant was discarded and pellets were left to air dry for 5 minutes, after which 100 µL of MQ H_2O were added to resuspend the RNA. Samples were then heated at 60 °C for 10 minutes. RNA concentration was taken using a nano-drop before being stored at -80 °C. cDNA was made by using the Maxima First Strand cDNA Synthesis Kit (Thermo K1671). 4 µg of RNA was added to a PCR tube containing 1 µL of dsDNase, 1 µL of 10x dsDNase

buffer, and MQ H_2O to 10 µL. PCR tube was then incubated at 37 °C for 2 minutes, placed on ice, spun down briefly, and placed back on ice. 1 µL of 100 mM DTT was added to the tube and incubated at 55 °C for 5 minutes, placed on ice, spun down briefly, and placed back on ice. 1 µL of 10 mM dNTPs, 1 µL random primers, and MQ H_2O to 15 µL. Tubes were briefly mixed and incubated at 65°C for 5 minutes, put on ice, spun down, and put back on ice. 4 µL of 5X RT buffer and 1 µL of Maxima enzyme were added to the tube and then incubated at 25 °C for 20 minutes, 50 °C for 30 minutes, followed by an inactivation at 85°C for 5 minutes. cDNA was stored at -20 °C. cDNA synthesis was confirmed by PCR with intron spanning β-Actin primers. Once verification was confirmed, RT-PCR was set up using Fast SYBR Green (Thermo 4385612) with intron spanning primers (OSBP, ORP4, and β-Actin). 10 µL of Fast SYBR Green was mixed with 0.3 µL of 100 µmoles forward and reverse primer solution, 1 µL of cDNA, and MQ H_2O to 20 µL. Each gene was done in triplicate for each time point. The plate was then run on a Roche LightCycler® 480 system using SYBR green protocol [214].

3.2.18 RNA Seq Analysis

HEK293 cells were seeded and treated with 1 nM OSW-1 or DMSO according to the washout experimental procedure described previously. After 24 hours post-washout (pWO), the samples were lysed in TRIzol and shipped on dry ice to Omega Bioservices (Norcross, GA). Omega Bioservices first isolated total RNA using E.N.Z.A. Total RNA Isolation Kit II (Product Number R6934-01) and sample extraction QC was analyzed via Nanodrop and Agilent Tapestation. mRNA isolation/library prep was performed by Poly-T oligonucleotide mediated mRNA extraction through hybridization of the mature

mRNA Poly-A tail using Illumina TruSeq stranded mRNA library prep kit (Product Number 20020595). Library QC was then be analyzed using an Agilent Tapestation. The RNA was sequenced using Illumina HiSeq4000/X Ten sequencing platform using a PE150 sequencing format. Sequencing depth was performed at 200M reads per samples, generating ~30GB of data per sample. The data was downloaded from the Illumina BaseSpace website as a fastq file. Data analysis was performed by Dr. Fares Najar at the University of Oklahoma Dept. Chemistry/Biochemistry, as outlined in Anders S., McCarthy D.J., Chen, Y et al., 2013 [246].

3.2.19 Cell Media Analysis for OSBP Levels

Media was aspirated from four HEK293 cell tissue culture plates: two DMSO treated and two OSW-1 treated (1 nM, 24-hour continuous treatment)). The media from the two DMSO plates were combined and the media for the two OSW-1 treated plates were combined for a total of 20 mL media for each treatment condition. The media was then separated into two aliquots for each treatment: two 10 mL DMSO media aliquots and two 10 mL OSW-1 media aliquots. Media was filtered using a 0.2 µm pore filter (VWR 28145-501) to remove any cells that may have detached and were removed with the media. One aliquot for each treatment was centrifuge filter concentrated using a 10 kDa cut off filter (Sigma Z648027) to a final volume of 500 µL. The remaining aliquot was concentrated using ammonium sulfate precipitation (2.91 g ammonium sulfate per 10mL media). Samples were then diluted in Laemmli buffer and 18 µL of each sample was added to each well of the 8.5% SDS PAGE gel; 25 µg of protein was added for positive and negative controls (same control lysates as the cell pellet analysis). Western

blot analysis was performed as previously described (see **Chapter 2 Methods Section 2.2.6: Western Blots)**.

3.2.20 Cell Pellet Analysis for OSBP Levels

Cell pellets were procured from 1 nM, 24-hour OSW-1 treatment treated HEK293 cells lysed using either the AC lysis (Lysis Method 1) or the MPER method (Lysis Method 2) of cell lysis described previously (see **Chapter 2 Methods Section 2.2.4 and 2.2.5** for lysis procedures). Pellets were gently washed with PBS and resuspended to remove any residual lysate from the exterior of the pellet. The samples were then repelleted using a microcentrifuge centrifuge (14,000 x g for 45 seconds). The PBS was removed and the cell pellets were resuspended in 29 µL of Fast Digest buffer (Thermo B64) and 1 µL of DNase and incubated at 65 °C for 5 minutes; twice the volume was used for MPER lysed pellets due to larger pellet size. 10 µL of Laemmli buffer was then added to the samples and samples were incubated at 95 °C for 10 minutes. 18 µL of each sample was loaded into an SDS PAGE gel (8.5%). Samples were loaded immediately off the heat block to increase solubility. 25 µg of protein was added for the positive control (i.e., DMSO 24-hour continual treatment) and negative control (i.e., 1 nM 24-hour OSW-1 treatment). Western blots were performed as described previously (see **Chapter 2 Methods Section 2.2.6: Western Blots)**.

3.2.21 Statistical Analysis

All results are expressed as mean ± SD and are $n \geq 3$ unless otherwise stated. All statistical tests were performed using GraphPad Prism 7.0. Comparison between groups

was made by using a one-way ANOVA with a follow up Dunnett's test. The p values are reported using GraphPad Prism: *$p \leq 0.05$, **$p \leq 0.01$ ***$p \leq 0.001$, and ****$p \leq 0.0001$.

3.3 Results

3.3.1 Persistent intracellular OSW-1-compound is not responsible for long-term OSBP repression

Liquid chromatography mass spectrometry (LCMS) was used to quantify the amount of OSW-1-compound remaining in the cell 24 hours after the OSW-1-compound was removed from cell culture (i.e., 24 hours post-washout (pWO)) to determine if persistent residual intracellular OSW-1-compound was responsible for the observed OSBP repression (**Figure 21**). Using a deuterated standard allows for the quantification of OSW-1-compound remaining in the cell after compound washout. We determined that the OSW-1-compound is no longer detectable 24 hours pWO, with the detectable limit of this method ~100 pM (**Figure 21A**). The absence of detectable intracellular OSW-1-compound was confirmed using single-cell mass spectrometry (SCMS) (**Figure 21B**). These results confirm that the OSW-1-compound is not continually repressing OSBP levels through its persistent presence in the cell, but rather triggers an effect that regulates OSBP levels for multiple days after the initial stimuli (i.e., OSW-1) is removed.

A

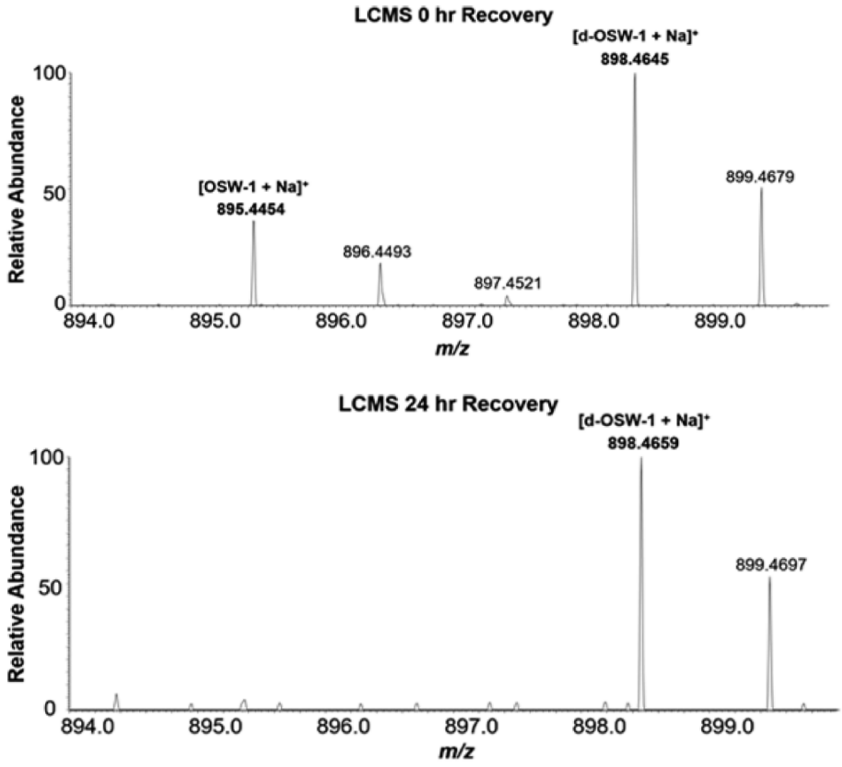

B

	LCMS	
Time Post Washout	*Moles (x10 $^{-18}$)*	*Concentration (μM)*
0 hr	5.66 ± 2.41	1.74 ± 0.74
24 hr	NQ	NQ

Figure 21: Intracellular OSW-1-compound levels are undetectable 24 hours post-washout (pWO).

A) Liquid chromatography mass spectrometry (LCMS) quantification of intracellular OSW-1-compound levels 0 hours pWO and 24 hours pWO after 100 nM OSW-1-compound treatment for 1-hour in HCT-116 cells using a deuterated OSW-1 standard for quantification. OSW-1-compound levels are undetectable 24 hours pWO. **B)** Single-cell LCMS quantification of intracellular OSW-1-compound levels 0 hours and 24 hours pWO confirm that intracellular OSW-1-compound levels are undetectable 24 hours pWO. Average of 3 biological replicates (n=3), detectable limit ~100 pM, NQ = not quantifiable. [189]

3.3.2 Verification of long-term OSBP repression results

In an effort to be as thorough, systematic, and parsimonious as possible, alternative repression explanations were investigated such as whether the long-term repression of OSBP was an experimental artifact, for example, by OSBP being retained in the cell pellet after lysis (**Figure 22A**). To determine if OSBP is retained in the cell pellet after lysis, DMSO, Taxol, and OSW-1-compound treated HEK293 cell pellets were analyzed after lysis using two different lysis methods (i.e., AC lysis and MPER lysis) (**Figure 22A**). The cell pellets were loaded into the Western blot directly from the heat block to increase pellet solubility. No significant OSBP was found remaining in the cell pellet under any of the treatment or lysis conditions (**Figure 22A**).

The cell culture media was also probed to determine if OSBP was being released into the media after OSW-1-compound treatment (**Figure 22B**). Cell culture media from DMSO and OSW-1-compound treated HEK293 cells was analyzed via Western blot after media concentration using either centrifuge column concentration, or ammonium sulfate precipitation. There is no significant OSBP present in the cell media, and no significant difference between DMSO or OSW-1 treated cell media (**Figure 22B**).

Together, these results indicate that OSBP is not trapped in the cell pellet during lysis, or released into the cell culture media after OSW-1-compound treatment, confirming that the observed long-term OSBP repression is not an experimental artifact (**Figure 22**).

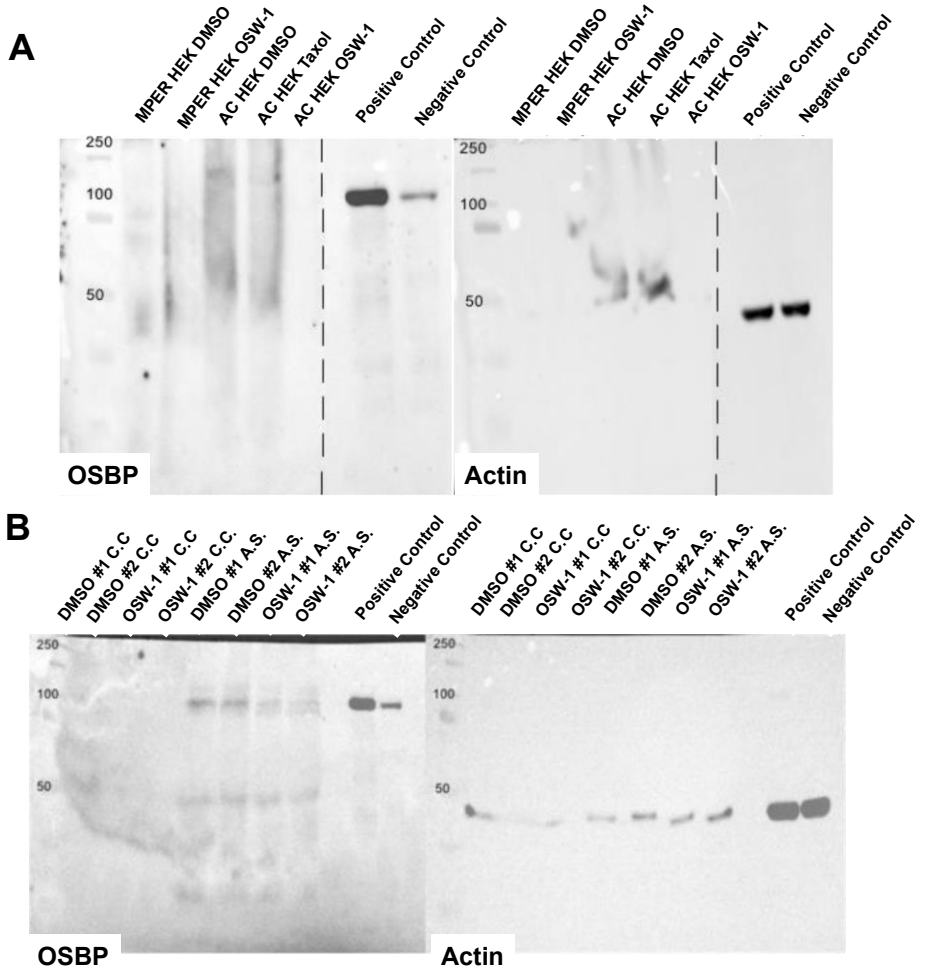

Figure 22: OSBP is not trapped in the cell pellet, or released into the cell media after OSW-1-compound treatment.

A) HEK293 cell pellets lysed using either the AC lysis method or MPER lysis method, treated with DMSO, OSW-1-compound, or Taxol and analyzed via Western blot. There is no OSBP detected in the cell pellet after lysis, or difference between conditions, indicating OSBP is not sequestered in the cell pellet after OSW-1-compound treatment. **B)** DMSO and OSW-1-comound treated HEK293 cell culture media was concentrated using either centrifuge column concentration (C.C.), or ammonium sulfate precipitation (A.S.) and analyzed via Western blot. There is no significant OSBP detected in the media, and no significant difference between treatment groups, revealing OSBP is not released into the cell culture media after treatment. Positive and negative controls used were DMSO vehicle control samples and 1 nM, 24-hour OSW-1-compound treated samples, respectively [189].

3.3.3 Long-term OSBP repression does not occur through canonical mechanisms and is mediated through RNA regulation

To elucidate the regulatory mechanism(s) mediating the long-term repression of OSBP levels in the cell after OSW-1-compound washout treatment, we began systematically testing and eliminating some of the more likely regulation mechanisms, including inhibition of transcription and post-translational proteolysis by the proteasome or autophagy (**Figure 23**). Since the initial loss of OSBP in the cell is proteasome-dependent, we examined whether the long-term repression of OSBP was a consequence of continual proteasome degradation (**Figure 23A**) [52]. The proteasome was inhibited using three different well-studied proteasome inhibitors, bortezomib, carfilzomib, and MG132. The results showed that although the initial decrease in OSBP levels is proteasome-dependent, the subsequent long-term OSBP repression was not significantly rescued by any of the proteasome inhibitors, indicating that the proteasome is not responsible for the long-term OSBP repression triggered by the OSW-1-compound (**Figure 23A**). Additionally, calcium-dependent proteases called calpains have been implicated in the cellular activity of the OSW-1-compound in HL-60 cells, resulting in the calpain-dependent degradation of the ER chaperone protein, GRP78, after OSW-1-compound treatment [191]. Inhibition of calpains using the calpain inhibitor, ALLN, also did not rescue long-term OSBP repression, indicating calpain-dependent degradation is not responsible for the persistent OSBP reduction (**Figure 23A**). We next tested whether the other canonical proteolytic pathway in the cell, autophagy, was responsible for the repression (**Figure 23B**). Inhibition of cellular autophagy using the autophagy inhibitor, chloroquine (CQ), did not rescue OSW-1-compound triggered long-term OSBP

repression (**Figure 23B**). Collectively, these results indicate that OSBP repression is not regulated by post-translational proteolysis.

We next investigated whether long-term OSBP repression was regulated at a transcriptional level (**Figure 23C, D**). qPCR and RNA Seq analyses were both employed to quantify changes in OSBP mRNA levels after OSW-1-compound washout treatment. These analyses revealed that OSBP mRNA levels are not significantly changed compared to the vehicle control at any pWO timepoint measured (**Figure 23C, D**). Additionally, using an RNA Seq sequencing depth of 200M reads/sample allowed for detection of all 12 OSBP/ORP transcripts and showed that no other ORP transcript significantly changed in expression after OSW-1-compound washout treatment (**Figure 23D**). The results of the qPCR and RNA Seq analysis reveal that OSBP mRNA is still being transcribed normally after OSW-1-compound washout treatment, despite an almost complete absence of OSBP at the protein level, indicating long-term OSBP repression is not regulated on a transcriptional level.

To determine if the observed OSBP repression was the result of rapid OSBP turnover in the cell, a cycloheximide chase experiment was performed to investigate the normal turnover rate and half-life of OSBP, both of which had not been previously reported (**Figure 23E**). Cycloheximide treatment inhibits global protein translation in the cell and is therefore cytotoxic after 24 hours. The results indicate that OSBP is not rapidly turned over in the cell and possesses a half-life of >24 hours (**Figure 23E**).

The low turnover rate of OSBP under normal conditions, in combination with the inability of proteasome and autophagy inhibitors to rescue long-term OSBP repression under washout conditions, indicates that this repression is most likely not regulated at the

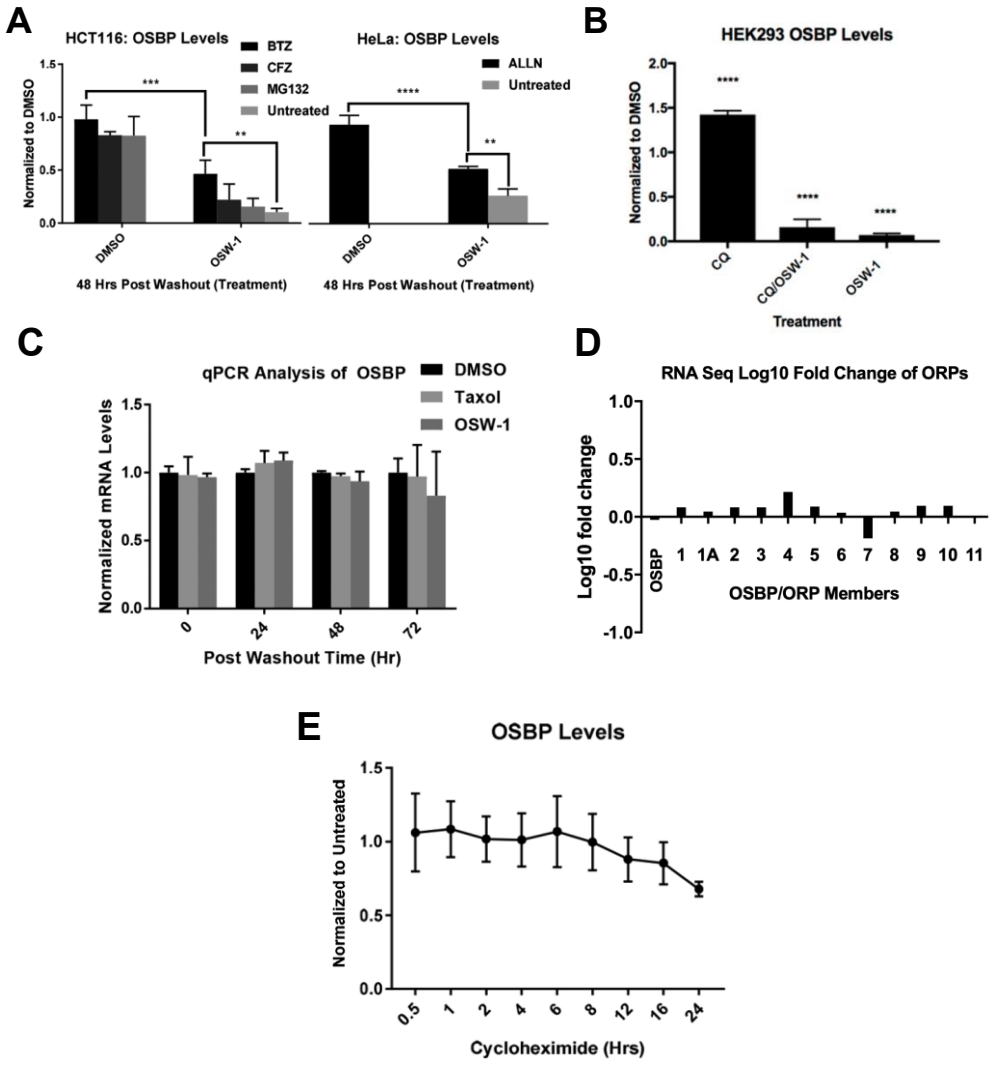

Figure 23: Long-term OSBP repression is not regulated on a transcriptional or post-translational level.

A) Cells were treated with 1 nM OSW-1-compound for 6 hours, followed by 24-hour pWO recovery, allowing OSBP levels to reduce ~90%. After 24 hours pWO, cell were treated with the proteasome inhibitors bortezomib (25 nM), carfilzomib (25 nM), MG132 (170 nM), or the calpain inhibitor ALLN (10 µM) for 24 hours, after which OSBP levels were quantified via Western blot. Results show that proteasome and calpain inhibition do not rescue OSBP repression. **B)** Autophagy inhibition using the autophagy inhibitor chloroquine (CQ) (25 µM) also did not significantly increase OSBP levels pWO. **C)** qPCR analysis of OSBP mRNA levels 0-72 hr pWO and **D)** RNA Seq analysis of OSBP/ORP mRNA 24 hours pWO reveal that OSBP mRNA is still being transcribed normally relative to vehicle control after OSW-1-compound treatment. **E)** Cycloheximide-chase experiment to determine OSBP half-life in the cell using 177 nM cycloheximide as a translational inhibitor. p21 levels were used as a control for translational inhibition, with the p21 half-life generated from this experiment consistent with previously reported values [291]. OSBP half-life was determined to be >24 hours.
189

post-translational level. Additionally, the observation that OSBP mRNA is still being transcribed normally after OSW-1-compound treatment indicates that OSBP repression is most likely regulated on an OSBP mRNA level.

To confirm that long-term OSBP repression is regulated on an RNA level, HEK293 cells were transfected with exogenous Myc-His tagged OSBP (**Figure 24**). OSBP Myc-His cDNA contains only exons and does not possess regulatory elements such as introns, or 3' and 5' UTRs; therefore, exogenous OSBP-Myc-His cannot be regulated by RNA binding proteins and other translational regulatory proteins that typically target non-exon portions of the mRNA transcript to regulate translation [230,231]. We found that exogenous OSBP-Myc-His responds differently to OSW-1-compound treatment than endogenous OSBP, with only an ~50% decrease in exogenous OSBP-Myc-His levels 24 hours pWO after 6-hour, 100 nM OSW-1-compound treatment (**Figure 24**). Similarly, 50 nM, 24-hour continual OSW-1-compound treatment decreased exogenous OSBP-Myc-His levels by only 50% (**Figure 24**). OSW-1-compound treatment concentrations greater than 50 nM for 24-hour continual treatment was too cytotoxic to obtain viable results (data not shown). Comparatively, endogenous OSBP levels decrease ~90% after only 1 nM OSW-1-compound treatment for 6 hours, followed by 24-hour pWO recovery (**Figure 23A, B**). These results indicate that exogenous OSBP-Myc-His is resistant to OSW-1-compound induced long-term repression, consistent with the mechanism of repression being regulated at the RNA level.

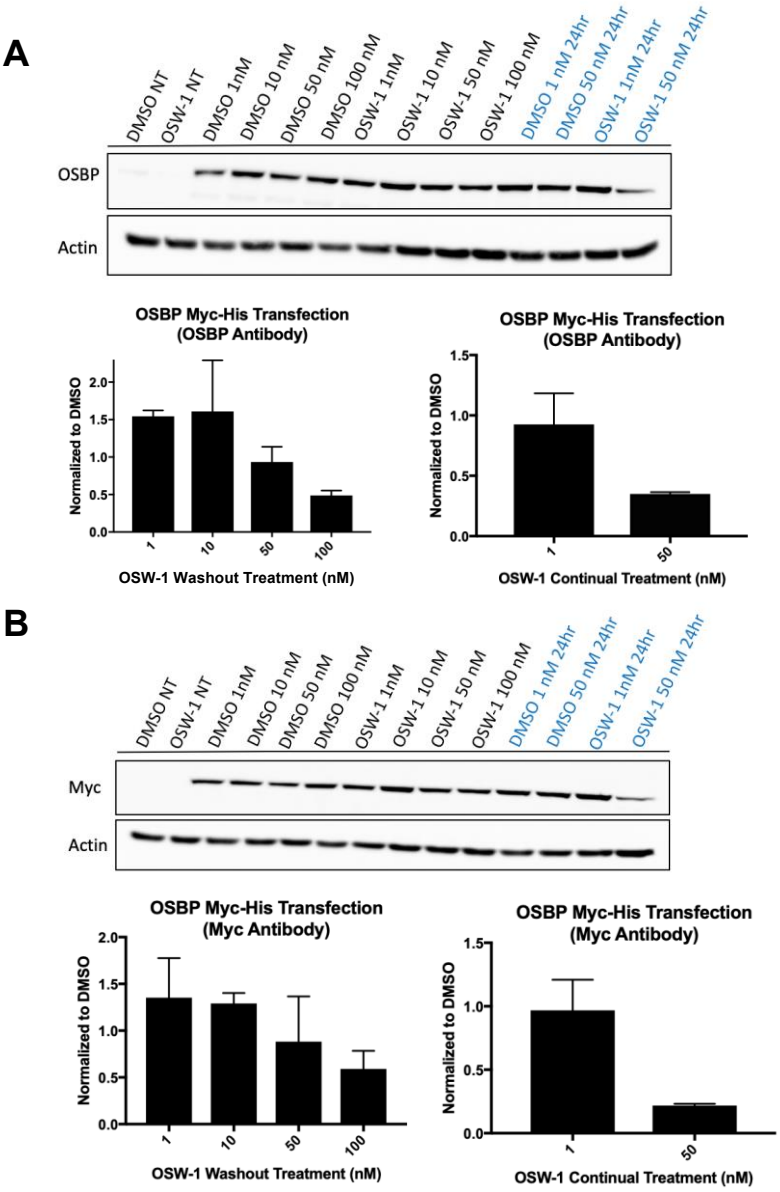

Figure 24: Exogenous OSBP-Myc-His is not regulated in the same manner as endogenous OSBP.

HEK293 cells were subject to low-dose transfection (1 µg OSBP-Myc-His cDNA in 10 cm^2 plates) followed by OSW-1-compound washout treatment at the indicated concentration (i.e., 6-hour OSW-1-compound treatment followed by 24-hour pWO recovery), or 24-hour continual OSW-1-compound treatment at the indicated concentration. OSBP levels after treatment were analyzed via **A)** an OSBP-specific antibody capable of detecting both endogenous and exogenous OSBP and **B)** Myc tag-specific antibody, capable of detecting only exogenous OSBP-Myc-His. NT=Not Transfected. Black text above the Western blot indicates washout conditions, while blue text indicate 24-hour continual treatment. Experiments were performed in duplicate.

3.3.4 OSW-1-compound treatment induces cellular autophagy through mTORc1 inhibition.

Although autophagy is not responsible for the long-term repression of OSBP levels (**Figure 23B, 25A**), the controls used to determine that CQ treatment effectively inhibited cellular autophagy indicated that OSW-1-compound treatment was inducing cellular autophagy (**Figure 25B, C**). During autophagy, the protein, p62, binds autophagic substrates destined for degradation and returns it to the autophagosome through interaction with the protein, LC3B, located on the autophagosome membrane [247]. During the autophagic process, p62 is degraded by the autolysosome along with the autophagic substrates, while the membrane-bound LC3B is not degraded [247]. Consequently, a decrease in cellular p62 levels is indicative of an increase in autophagic flux (i.e., degradation of autophagic substrates), and an increase in LC3B levels is indicative of an increase in autophagosome formation. The quantification of both cellular p62 and LC3B levels therefore allows for the monitoring of cellular autophagy induction [247,248]. Rapamycin, a well-studied inducer of autophagy, was used as a positive control to induce autophagy, while CQ was used as a negative control to inhibit autophagy [247,248].

Cellular p62 levels were found to decrease ~50% 0 hours pWO and steadily increase in a time-dependent manner after the removal of the OSW-1-compound (**Figure 25B**). Additionally, LC3B levels in OSW-1/CQ treated cells are comparable to the positive control rapamycin/CQ treated cells 0 hour pWO, and by 24 hour pWO, there is significantly more LC3B in the OSW-1/CQ treated cells compared to the rapamycin/CQ treated positive control cells (**Figure 25C**). These results are consistent with the induction of cellular autophagy after OSW-1-compund treatment. Importantly, co-incubation of

OSW-1 and CQ greatly potentiated the cytotoxicity of OSW-1, suggesting autophagy may be induced as a cytoprotective mechanism against OSW-1-compound treatment (data not shown).

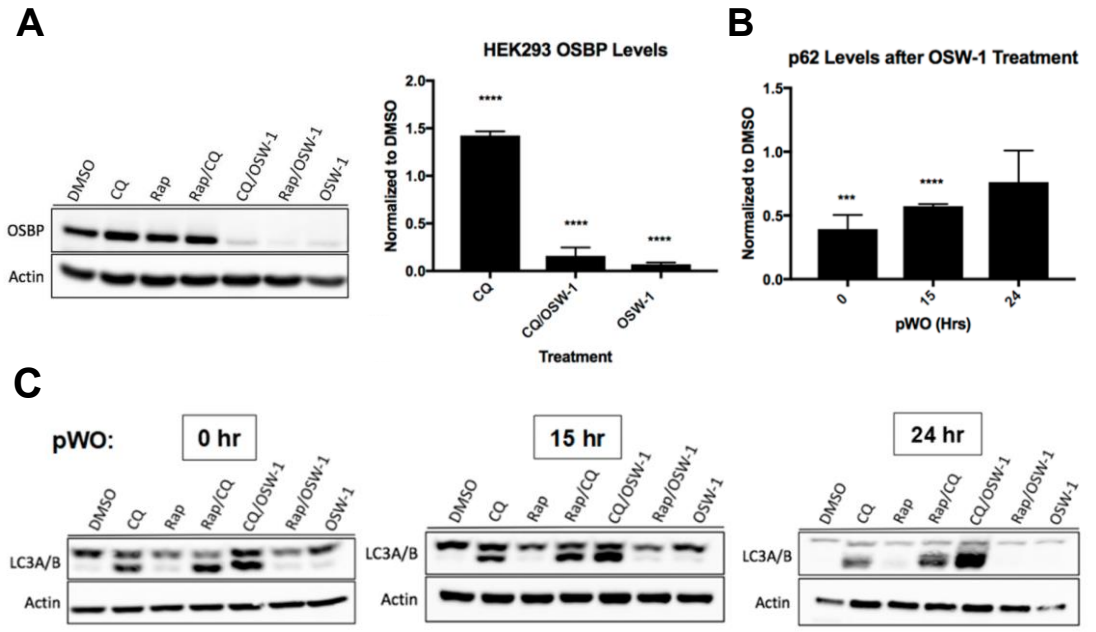

Figure 25: OSW-1-compound treatment induces cellular autophagy.
A) Autophagy inhibition via chloroquine (CQ) treatment (25 μM) does not significantly increase OSBP levels 24 hr pWO. Rapamycin (Rap) (100 nM) was used as a positive control to induce autophagy. **B)** OSW-1-compound treatment decreases cellular p62 levels ~50% 0 hours pWO, indicative of an increase in autophagic flux. **C)** OSW-1-compound treatment significantly increases cellular LC3B levels (bottom band). OSW-1/CQ treated cells possess significantly more cellular LC3B than CQ treated cells alone, and comparable levels to the positive control Rap/CQ treated cells at 0 hour pWO. By 24 hours pWO, OSW-1/CQ treated cells possess significantly more LC3B than even the positive control, indicating a significant increase in autophagosome formation after OSW-1-compound treatment [189].

mTORc1 is a cellular protein complex that functions as a signaling hub in cells, integrating various cellular inputs and directing cellular anabolic and catabolic processes (**Figure 26A**). Inhibition of mTORc1 induces catabolic processes in cells, such as

autophagy [249]. Small molecule schweinfurthins, which target OSBP and ORP4 similar to the OSW-1-compound, have previously been reported to cause mTORc1 inhibition in cells (see **Section 1.7.1: ORPphilins** for more information) [250]. Therefore, OSW-1-compound induced inhibition of mTORc1 was investigated as the mechanism leading to the observed autophagy induction after OSW-1-compound treatment [249]. mTORc1 activity was monitored by measuring REDD1 levels and phosphorylation of p70S6K at T-389 as a proxy for mTORc1 activity (**Figure 26A**) [251,252].

REDD1 is an endogenous inhibitor of mTORc1 that is also regulated by mTORc1 [251]. When mTORc1 is inhibited (e.g. after rapamycin treatment) REDD1 is decreased on both a protein and transcript level (**Figure 26A**) [251]. Under OSW-1-compound washout conditions, REDD1 protein levels were found to decrease ~50% 24 hours pWO (**Figure 26B**). Additionally, RNA Seq analysis showed that the REDD1 transcript was one of the most significantly downregulated transcripts detected under OSW-1-compound washout conditions 24 hours pWO (~5-fold decrease in expression, p-value: 2.13E-06, FDR: 4.45E-03), consistent with OSW-1-compound treatment inhibiting mTORc1 (**Figure 28B**).

p70S6K is a kinase downstream of mTORc1 and is regulated by mTORc1 (**Figure 26A**) [252]. Phosphorylation of p70S6K at T-389 by mTORc1 is a hallmark of mTORc1 activation and leads to an increase in global protein synthesis and autophagy inhibition (**Figure 26A**) [252]. Conversely, a decrease in p70S6K T-389 phosphorylation is correlated with autophagy induction, decrease in protein synthesis, and mTORc1 inhibition [252]. Phosphorylation of p70S6K at T-389 was also found to decrease ~50% under OSW-1-

compound washout conditions 24 hours pWO, confirming that OSW-1-compound treatment inhibits mTORc1 (**Figure 26C**).

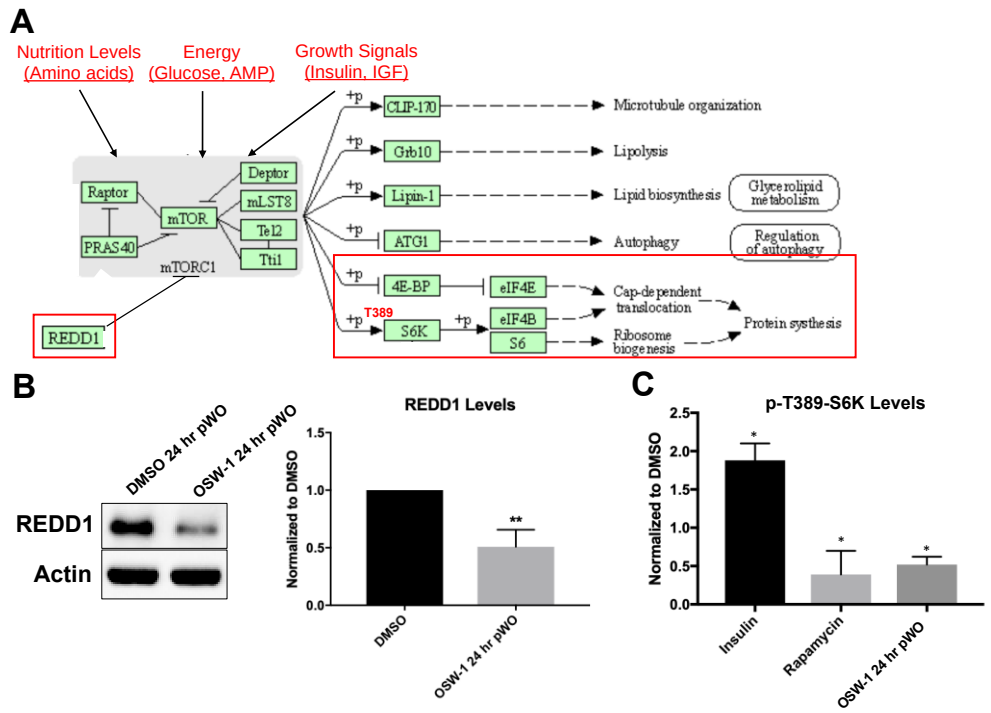

Figure 26: OSW-1-compound treatment inhibits mTORc1.
A) Outline of mTORc1 signaling, with emphasis on mTORc1 signaling connections to REDD1 and p70S6K, used for monitoring mTORc1 activity in the cell. Figure adapted from mTORc1 KEGG pathway map. **B)** Western blot and quantification of REDD1 levels reveal REDD1 protein levels decrease ~50% 24 hours pWO. **C)** Western blot quantification of p70S6K phosphorylation at T-389 using a T-389 phospho-specific antibody. Insulin was used as a positive control to activate mTORc1 and rapamycin was used as a negative control to inhibit mTORc1. *p70S6K results were performed in duplicate.

Additional lines of evidence that OSW-1-compound treatment inhibits mTORc1 can be found in our iTRAQ proteomic mass spectrometry and RNA Seq analyses of OSW-1-compound washout cells (**Figure 27, 28**). As previously mentioned, mTORc1 inhibition causes a decrease in global protein synthesis and ribosome biogenesis (**Figure 26A**) [252,253]. In the iTRAQ analysis, of the 243 significantly changed proteins detected in the 2D iTRAQ analysis 24 hours pWO, over 30 were ribosomal subunits, all of which significantly decreased after treatment (**Figure 27A, Figure 28A**). This decrease in ribosome subunit production also occurred on a transcript level in the RNA Seq analysis, with over 15 ribosomal subunits detected also decreasing on a transcript level (**Figure 27B**).

Furthermore, both the 1D and 2D iTRAQ analyses indicated that global protein synthesis is decreased 24 hours pWO, as evidence by the shift left of almost all cellular proteins detected in the volcano plot (**Figure 14**, **28A**). Both the decrease in ribosome production and the decrease in protein synthesis is consistent with OSW-1-compound induced mTORc1 inhibition [252,253]. The decrease in protein synthesis in the iTRAQ analyses are resolved 72 hours pWO, which is consistent with the reemergence of OSBP in this cell line (HEK293) (**Figure 10, 14**, **28A**). This result suggests that mTORc1 inhibition occurs due to the chemical knockdown of OSBP by the OSW-1-compound. During this time while my research was underway, a paper came out in *Nature Cell Biology* confirming these results, also showing that OSBP is required for mTORc1 activation, and chemical or genetic knockdown of OSBP leads to mTORc1 inhibition and subsequent autophagy in cells [59].

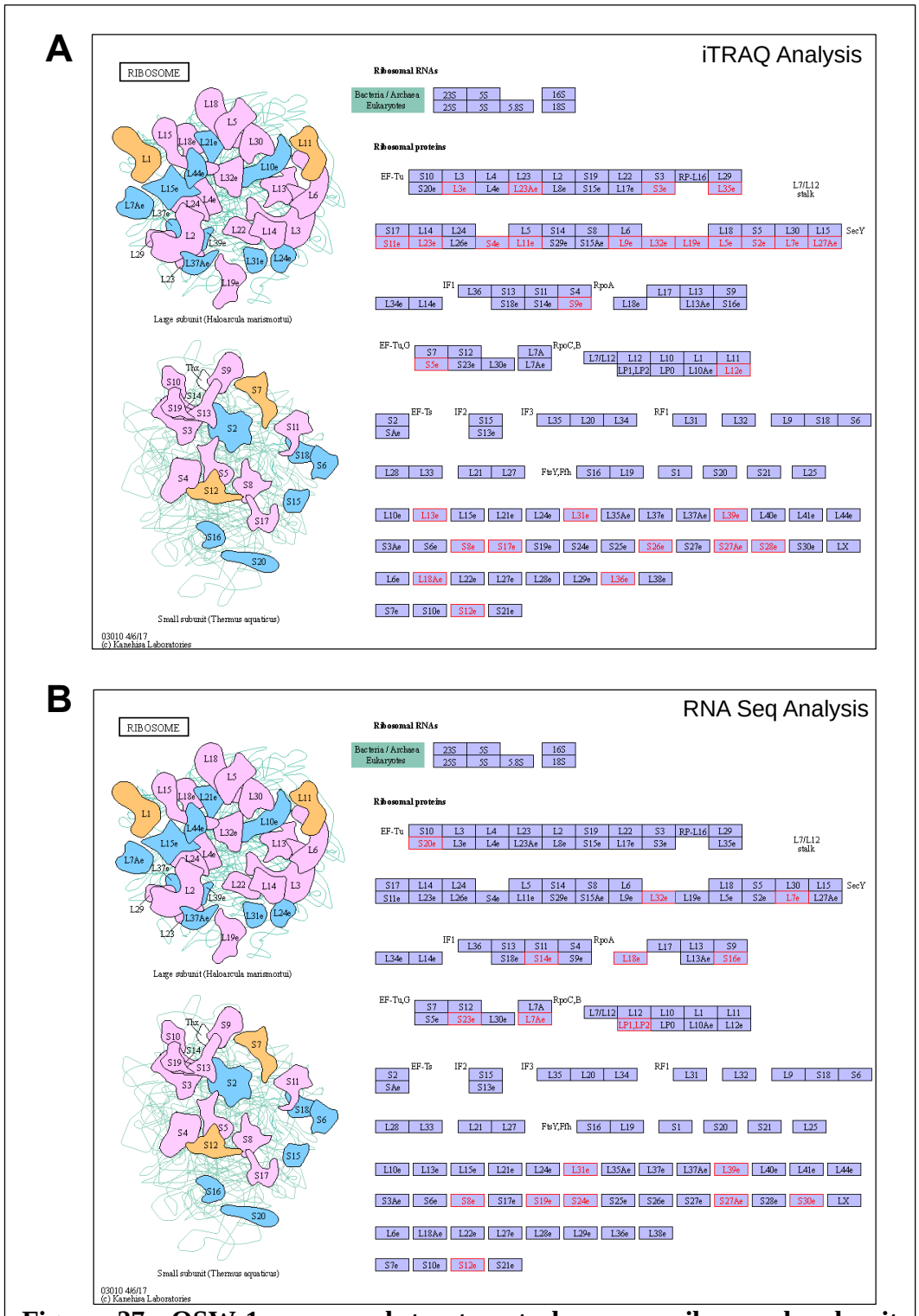

Figure 27: OSW-1-compound treatment decreases ribosomal subunit production on both a transcript and protein level.
KEGG pathway maps of significantly changed ribosomal subunits after OSW-1-compound treatment, all of which significantly decreased 24 hours pWO. Significantly changed ribosomal subunits are shown in red. **A)** Significantly decreased ribosomal subunit proteins from 2D iTRAQ analysis. **B)** Significantly decreased ribosomal subunit transcripts from RNA Seq analysis.

3.3.5 Global transcriptomic and proteomic analysis reveal significant changes to RNA regulation after OSW-1-compound treatment

RNA Seq and iTRAQ proteomic mass spectrometry analyses were utilized to identify global changes to the cellular transcriptome and proteome after OSW-1-compound washout treatment that may provide clues to the mechanism of RNA regulation mediating OSBP repression (**Figure 28**).

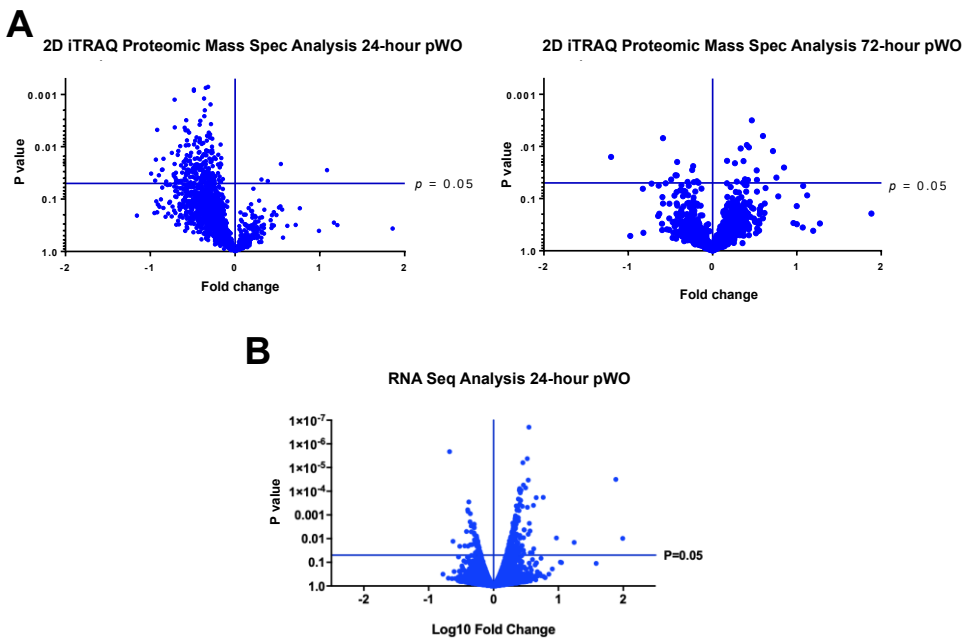

Figure 28: Proteomic and transcriptomic analysis after OSW-1-compound washout treatment.
A) 2D iTRAQ proteomic mass spectrometry analysis of global protein changes in HEK293 cells after OSW-1-compound washout treatment 24 hours and 72 hours pWO. **B)** RNA seq analysis of global transcript changes in HEK293 cells after OSW-1-compound washout treatment 24 hours pWO. Both analyses were performed using three independent biological replicates (n=3).

2D mass spectrometry analysis involves using an additional chromatography method that further separates components in the sample prior to MS analysis, allowing for the detection of more peptides [216]. The 2D iTRAQ proteomic mass spectrometry

analysis detected and identified a total of 2045 cellular proteins. 243 of those proteins were significantly changed 24 hours pWO, with all but 4 proteins decreasing in abundance relative to the DMSO vehicle control (**Figure 28A**). In contrast, only 32 proteins were found to significantly change 72 hours pWO, most of which increased in abundance relative to the DMSO vehicle control (**Figure 28A**). Note the previously mentioned 'shift left' in the volcano plot in 24-hour pWO samples is consistent with a slight global decrease in protein synthesis. The 'shift left' is resolved 72 hours pWO, consistent with the reemergence of OSBP levels in this cell line (HEK293). The 1D iTRAQ analysis (**Figure 14**), also displays this global 'shift left' 24 hours pWO. Almost all peptides detected in both 1D and 2D iTRAQ analyses 24 hours pWO were decreased relative to the DMSO vehicle control (**Figure 14, 28A**).

The RNA Seq analysis detected over 12,500 transcripts, with approximately 300 transcripts significantly changed 24 hours pWO (**Figure 28B**). Approximately 230 of these transcripts increased in expression, while approximately 70 transcripts decreased in expression (**Figure 28B**). In contrast to the iTRAQ proteomic analysis, there is no 'shift left' in the RNA Seq volcano plot. This indicates that the almost ubiquitous moderate decrease in peptides detected 24 hours pWO in the iTRAQ analyses are occurring on the protein level, but this decrease is not reflected on the transcript level, indicating a change in global RNA regulation after OSW-1-compound treatment (**Figure 14, 28**). Additionally, many of the significantly decreased proteins 24 hours pWO in the iTRAQ analysis were associated with translational machinery (i.e., ribosomal subunits and translational initiation factors etc.). Together, these observations are consistent with our previously obtained results indicating that OSW-1-compound treatment triggers

regulation of OSBP on an RNA level to mediate long-term OSBP repression (**Figure 23, 24**).

The iTRAQ and RNA Seq datasets of OSW-1-compound treated washout cells were analyzed using a combination of gene ontology and KEGG pathway analysis to more precisely identify significantly changed biological processes (**Figure 29**). Gene ontology analysis provides a list of significantly changed biological processes with associated p-values, which indicate the likelihood of the annotation of a particular process to a group of changed proteins/transcripts to occur by chance (**Figure 29**) [254]. Gene ontology and KEGG analyses identified significantly changed biological processes consistent with our previous results: changes in translation, particularly at the initiation level, ribosome subunit biogenesis, and proteasome associated degradation (**Figure 29**). However, one process was the most significantly changed in both the iTRAQ and RNA Seq analyses, an RNA regulation pathway called nonsense-mediated decay (NMD) (**Figure 29**). NMD was originally implicated as an RNA surveillance pathway that detects aberrant mRNA transcripts with premature termination codons (PTCs), hence the name. More recently, NMD has been recognized as a pervasive post-transcriptional regulation pathway commonly used by cells to adjust the specific expression of a protein under various stimuli [233,234]. Importantly, the introduction of a PTC does not have to occur through genetic mutation, but can be generated through alternative splicing, a process known as Regulated Unproductive Splicing and Translation (RUST), or alternative splicing NMD (AS-NMD) [233,234,255]. Interestingly, NMD is also a host defense mechanism used against RNA viruses, which are the same viruses that OSBP targeting inhibits [235–237].

Biological Process	P-Value	FDR
Nuclear Transcribed mRNA catabolic processes, non-sense mediated decay	iTRAQ:**5.25E-31** RNA Seq:**6.32E-16**	iTRAQ:**9.28E-28** RNA Seq:**6.29E-13**
SRP Dependent Co-translational protein targeting to membrane	iTRAQ:**4.82E-28** RNA Seq:**2.44E-13**	iTRAQ:**4.26E-25** RNA Seq:**1.02E-10**
Translation	iTRAQ:**2.74E-17** RNA Seq:**1.03E-03**	iTRAQ:**6.69E-15** RNA Seq:**4.37E-02**
Translational Initiation	iTRAQ:**1.32E-07** RNA Seq:**1.30E-11**	iTRAQ:**2.93E-31** RNA Seq:**3.61E-09**
Regulation of Proteasomal Ubiquitination-Dependent Protein Catabolic Processes	iTRAQ:**4.28E-04** RNA Seq:**1.14E-03**	iTRAQ:**2.16E-02** RNA Seq:**4.85E-02**
Ribosomal Small Subunit Biogenesis	iTRAQ:**2.55E-04** RNA Seq:**1.15E-03**	iTRAQ:**1.48E-02** RNA Seq:**4.85E-02**

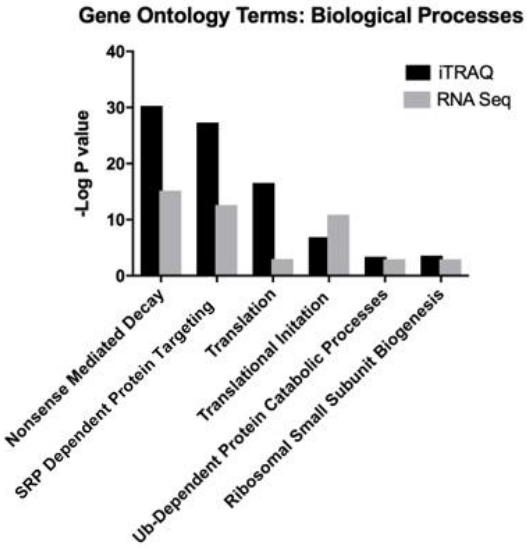

Figure 29: Gene ontology analysis of iTRAQ and RNA Seq datasets. Gene ontology analysis of biological processes that are significantly changed after OSW-1-compound washout treatment 24 hours pWO in both iTRAQ and RNA Seq analyses with associated p-values and False Discovery Rate (FDR) values. Results generated from http://geneontology.org/ and confirmed using KEGG Pathway analysis.

Probing alternative splicing databases revealed OSBP, but not ORP4, possesses an NMD-responsive alternative transcript (**Figure 30**). This transcript is generated by removing exon 9, which contains half of the ORP fingerprint region, including the two histidine residues required for phospholipid binding (**Figure 30**). Removal of this exon also introduces a frameshift and a downstream PTC, generating the NMD-responsive

OSBP transcript variant. There are no published reports about this OSBP NMD transcript, or how it contributes to OSBP regulation. The existence of an OSBP NMD-responsive transcript, but not ORP4, may explain why OSW-1-compound treatment triggers the long-term repression of OSBP, but not ORP4 (see **Chapter 2**). The significant changes to NMD on both a transcript and protein level (**Figure 29**) suggests that OSW-1-compound treatment may activate cellular NMD processes, which may also cause the alternative splicing of OSBP to the NMD-responsive transcript. NMD targeting of the alternatively spliced OSBP NMD-responsive transcript would result in repression of OSBP on the protein level, which continues in the absence of the OSW-1-compound. In total, our results indicate long-term repression of OSBP is regulated by the RNA regulatory pathway, NMD; however, furthers studies are necessary to confirm this hypothesis.

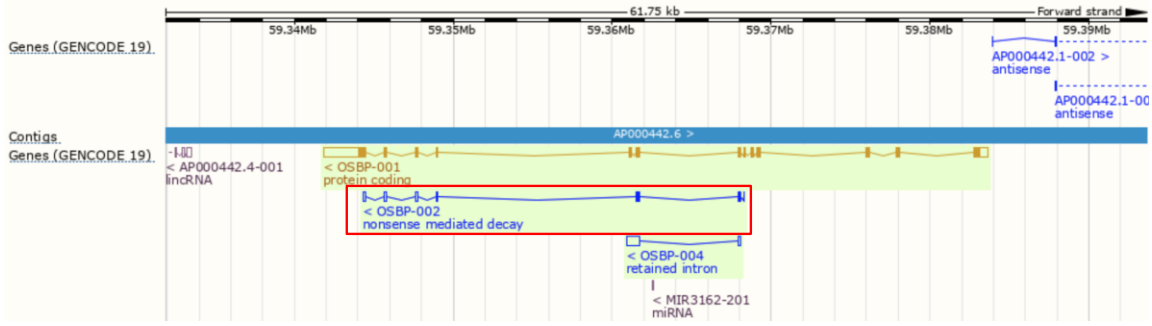

Figure 30: OSBP transcript variants.
Transcript variants of OSBP reveal that OSBP possesses an NMD-responsive alternative transcript (highlighted in red), while ORP4 does not. Image obtained from http://grch37.ensembl.org/.

3.4 Discussion

In this chapter, the mechanism(s) underlying the long-term repression of OSBP and other cellular responses triggered by the OSW-1-compound were investigated. We

found that long-term OSBP repression is not due to persistent residual OSW-1-compound in the cell, with intracellular OSW-1-compound levels undetectable 24 hours pWO (**Figure 21**). OSBP long-term repression was also found not to be a result of OSBP sequestration in cell pellets during the lysis process, and OSBP is not released into the cell culture media after OSW-1-compound treatment (**Figure 22**). Collectively, these results confirm that OSBP is repressed in cells in the absence of the OSW-1-compound, and OSW-1-compound treatment triggers a cellular mechanism that regulates OSBP levels for multiple day after the OSW-1-compound is no longer detectable in cells.

The mechanism of OSBP repression is not regulated on a post-translational level, as OSBP is shown not to be rapidly turned over in the cell under normal conditions, and inhibition of the two canonical post-translational proteolytic pathways, autophagy and the proteasome, did not rescue OSBP repression (**Figure 23 A, B, E**). Furthermore, qPCR and RNA Seq analysis revealed that OSBP mRNA is still being transcribed at a rate comparable to untreated cells after OSW-1-compound washout treatment (**Figure 23 C, D**). The continued transcription of OSBP mRNA, in combination with the failure of inhibitors of the major post-translational proteolytic pathways to rescue the repression, indicates that long-term OSBP repression is mediated on an OSBP mRNA level. Consistent with these results, exogenous Myc-His tagged OSBP containing only exons, but not regulatory elements commonly targeted by RNA binding regulatory proteins (i.e., introns or 3' and 5' UTRs), was resistant to the washout effect, implying endogenous and exogenous OSBP are regulated differently after OSW-1-compound washout treatment (**Figure 24**) [231].

While investigating autophagy as the possible repression mechanism, OSW-1-compound treatment was found to induce cellular autophagy, as evidenced by the monitoring of cellular p62 and LC3B levels, which are both well-studied indicators of autophagic flux and autophagosome formation, respectively (**Figure 25**). A previously published report showed that treatment with small molecule schweinfurthins, a member of the ORPphilin family like the OSW-1-compound (see **Section 1.7.1: ORPphilins** for more information), leads to mTORc1 inhibition in the cell [250]. The connection between mTORc1 inhibition and autophagy induction in the cell led us to investigate whether OSW-1-compound treatment also inhibited mTORc1, resulting in the observed autophagy induction [249]. Under OSW-1-compound washout conditions, both REDD1 and pT389-p70S6K levels were decreased ~50% 24 hours pWO, and RNA Seq analysis revealed REDD1 is one of the most downregulated transcripts detected 24 hours pWO, all consistent with mTORc1 inhibition in the cell (**Figure 26**) [251,252]. Additionally, iTRAQ proteomic mass spectrometry analysis revealed a significant decrease in ribosomal subunit production, and a decrease in global protein synthesis 24 hours pWO, also consistent with mTORc1 inhibition (**Figure 27, 28**) [252,253]. The decrease in protein synthesis and ribosomal subunits was resolved 72 hours pWO, correlating with the reemergence of OSBP levels in this cell line (HEK293), and suggesting that specifically the chemical knockdown of OSBP by OSW-1 was responsible for the mTORc1 inhibition.

Shortly after obtaining these results, a paper was published in *Nature Cell Biology* by the Zoncu lab at UC Berkley confirming these findings [59]. mTORc1 is a cellular protein complex that functions as one of the cell's main sensors and effectors, integrating

various cellular inputs like nutrition levels and growth factors and subsequently activating or inhibiting downstream cellular processes in response (**Figure 26A**) [249]. mTORc1 activation occurs at the lysosome, and the Zoncu group found that this localization and subsequent activation of mTORc1 required cholesterol trafficked from the ER to the lysosome via OSBP [59]. Therefore, OSBP levels are *directly* coupled to mTORc1 activity, and the chemical or genetic knockdown of OSBP leads to mTORc1 inhibition and subsequent autophagy [59]. Although we were the first group to publish that OSW-1-compound treatment induces cellular autophagy [189], the Zoncu group was the first group to publish the direct connection between OSBP levels and mTORc1 activity that leads to the autophagy induction [59].

However, the confirmation that OSBP levels are directly coupled to mTORc1 activity is an important finding for our innate antiviral response hypothesis (see **Chapter 2** for more information on the innate antiviral hypothesis). mTORc1 is involved in cellular innate antiviral response in cells and RNA viruses commonly subvert mTORc1 through various mechanisms, resulting in constitutive activation of mTORc1 in cells during viral infection [238–241]. In response to viral infection, host cells commonly induce autophagy to eliminate invading viruses, decrease protein synthesis and ribosome biogenesis to inhibit viral protein production, or induce apoptosis to contain the viral infection; all processes mediated by the inhibition of mTORc1 [238,256]. Viral subversion and constitutive activation of mTORc1 counteracts these host defenses, as mTORc1 activation inhibits autophagy, inhibits apoptosis, and increases protein synthesis and ribosome biogenesis to increase viral protein production [238]. The long-term repression of OSBP by the OSW-1-compound would therefore not only inhibit cholesterol transfer to

the viral replication compartment (VRC), consequently inhibiting viral proliferation, but also directly inhibit mTORc1, thus countering viral subversion and constitutive activation of mTORc1 and inducing the antiviral effects associated with mTORc1 inhibition (i.e, autophagy induction, decrease in viral protein production etc.). A multifaceted antiviral response that can be triggered simply by regulating OSBP levels in the cell.

iTRAQ proteomic mass spectrometry and RNA Seq were also used to quantify global proteomic and transcriptomic changes after OSW-1-compound washout treatment. Analysis of these datasets using gene ontology and KEGG pathway analysis allowed for the identification of significantly changed biological processes in OSW-1-compound washout treated cells (**Figure 29**). Many of the significantly changed biological processes after OSW-1-compound washout treatment detected in both analyses were consistent with our previous results: changes in translation, particularly at the initiation level, ribosome subunit biogenesis, and proteasome associated degradation (**Figure 29**). However, one process was the most significantly changed in both iTRAQ and RNA Seq analyses, an RNA regulation pathway called nonsense-mediated decay or (NMD) (**Figure 29**). NMD was originally implicated as merely an RNA surveillance mechanism for detecting aberrant mRNA containing premature termination codons (PTCs) [233,234]. More recently, NMD has been recognized as a pervasive post-transcriptional regulation pathway commonly used by cells to adjust the specific expression of a protein under various stimuli [233,234]. However, the introduction of a PTC does not have to occur through genetic mutation, but can be brought about through alternative splicing, a process known as Regulated Unproductive Splicing and Translation (RUST), or alternative splicing NMD (AS-NMD) [233,234,255].

Additionally, probing alternative splicing databases revealed OSBP, but not ORP4, possesses an NMD-responsive alternative transcript (**Figure 30**). There are no published reports about this OSBP NMD transcript, or how it contributes to OSBP regulation (**Figure 30**). The existence of an OSBP NMD-responsive transcript, but not ORP4, may explain why both proteins decrease in a time and proteasome-dependent manner after OSW-1-compound treatment, but only OSBP levels remain repressed after the compound is removed (see **Chapter 2**). The significant changes to the NMD pathway on both a transcript and protein level, suggests that OSW-1-compound treatment activates cellular NMD processes, which may also cause the alternative splicing of OSBP to the NMD-responsive transcript. NMD targeting of the OSBP NMD-responsive transcript would then result in repression of OSBP on the protein level that persists in the absence of the OSW-1-compound. In total, our results indicate long-term repression of OSBP is regulated by the RNA regulatory pathway, NMD; however, furthers studies are necessary to confirm this hypothesis. It is worth noting that we cannot currently rule out miRNA regulation of the OSBP transcript, as OSBP has been reported to be targeted by the brain-specific, miR-124, and miRNA have previously been shown to have a role in sterol regulation and innate antiviral response in cells [181,257].

The connection between how OSW-1-compound treatment induces alternative splicing and NMD processes may lie in the OSBP repression induced mTORc1 inhibition. Recently, rapamycin, which as previously mentioned is an mTORc1 inhibitor, was shown to modulate NMD processes in cells; increasing the quantity of PTC-containing NMD transcripts, as well as decreasing the expression of NMD substrates [258]. These results indicate that mTORc1 inhibition can not only induce alternative splicing to increase

NMD-responsive transcript expression, but also augment NMD of particular transcripts [258]. Additionally, mTORc1 has been reported to interact with splicing factors and regulate their activity [259,260]. However, whether this is the mechanism leading to alternative splicing and NMD modulation in the context of our studies remains to be determined. Additionally, the connection between mTORc1 inhibition, alternative splicing and NMD augmentation remains unclear [258].

Importantly, NMD was also recently identified as a host defense mechanism used against (+)ssRNA viruses, which are the same viruses that targeting OSBP inhibits [235–237]. (+)ssRNA viruses have mRNA-like genomes (i.e., mRNA is (+)ssRNA), and typically contain multiple open reading frames, necessary to maximize genome size and express as many proteins as possible in a condensed viral genome [261]. These mRNA-like genomes with multiple open reading frames resemble endogenous NMD substrates and are consequently degraded by the NMD pathway, making NMD an ideal pathway for targeting invading viral RNA [261]. The effect of OSW-1-compound washout treatment on the NMD pathway in the cell may be another facet of the innate antiviral response hypothesis, in addition to inhibition of cholesterol transport to the VRC and mTORc1 inhibition.

3.5 Conclusions

Overall, utilizing the OSW-1-compound as a small-molecule probe, we discovered a unique cellular OSBP regulatory process, triggered by the OSW-1-compound, that can be exploited to induce broad-spectrum antiviral prophylaxis in cells. The combined effects of the OSW-1-compound to trigger: a decrease and repression of cellular OSBP levels for multiple days, consequently inhibiting mTORc1 (decreasing

global protein synthesis and inducing autophagy), and modulate NMD host defense processes, creates a multifaceted innate antiviral environment in the cell that can persist while a viral infection is cleared. We hypothesize that the long-term repression of OSBP, and the other antiviral associated responses induced as a result of this repression, may be part of an unrecognized innate antiviral response pathway in the cell. The ability to trigger and exploit this response for antiviral prophylaxis using the OSW-1-compound, indicates this multifaceted innate antiviral response can be harnessed with exogenous small molecules. This chapter elucidates important insights into OSBP cellular biology and provides the basis for the creation and development of an entirely new class of broad-spectrum RNA antiviral compounds. The broad-spectrum, preventative potential of this novel approach may introduce a new paradigm in RNA antiviral therapeutics that would greatly increase our currently limited capacity to prevent and treat RNA viral pandemics like COVID-19.

Chapter 4: Ligand binding profiling and structure-activity relationship (SAR) of ORP subfamily 1: OSBP and ORP4

Abstract

OSBP and the ORPs all possess an ~50 kDa C-terminal OSBP-related ligand-binding domain (ORD). The ORD has the ability to bind both sterols (i.e., cholesterol and oxysterols) and phospholipids. In addition to endogenous lipids, a collection of structurally diverse, biologically-active modified oxysterol compounds have been shown to target OSBP and ORP4 through the ORD sterol binding pocket, including OSW-1, cephalostatin 1, ritterazine B, and T-00127-HEV2. OSBP and ORP4 have also been implicated in human disease biology: OSBP is essential for the proliferation of a broad spectrum of viral pathogens and ORP4 expression drives cancer cell proliferation and survival. OSBP and ORP4 are therefore potentially druggable targets to create novel antiviral and anticancer drugs. However, drug development against OSBP and ORP4 is limited by the lack of defined structure-activity relationship (SAR) between OSBP and ORP4 and their oxysterol ligands. There are no solved protein structures for OSBP or ORP4. Herein, we report the first comprehensive SAR study of oxysterol ligand binding to OSBP and ORP4. Using a library of various non-cholesterol oxysterols (e.g. cardiac glycoside and glucocorticoid drugs), cholesterol oxysterols, and oxysterol side chain analogs, we show that OSBP and ORP4 only interact with cholesterol oxysterols, and tolerate various side chain hydroxylation positions (i.e., C-20, C-24, C-25 and C-27) and side chain stereochemistry. The ability of OSBP and ORP4 to bind various side chain hydroxylated oxysterols does not apply to C-22 hydroxylation; C-22 hydroxylated oxysterols do not interact with OSBP or ORP4. We also show that any modification in the length of the isohexyl sterol side chain significantly impairs binding to OSBP and ORP4. This apparent side chain requirement is contradicted by the high affinity binding of T-00127-HEV2, a steroidal compound completely lacking a side chain. Our results indicate that the THEV C-3 THP group may function as an isostere for the sterol side chain, suggesting that OSBP and ORP4 can accommodate sterol interaction through multiple modes of binding. The characterization of oxysterol ligand binding to OSBP and ORP4 performed in this chapter provides critical information necessary to guide the development of novel small-molecule antiviral and anticancer therapeutics.

Allocation of Contribution

I produced the results presented in this chapter with the following exceptions. Dr. Juan Nuñez conducted binding experiments that contributed to the data in **Tables 1**, **2**, and **3**, and performed the experiments for the full binding curves for 20-OHC and SA-9 in **Figure 34**. Dr. Ryan Bensen also assisted in some of the compound serial dilutions for some of the binding experiments. Mr. Kevin Snead from the Bourne Research Group at

the University of Oklahoma conducted the homology modeling and docking experiments in **Figure 35** and **36**, and also prepared the procedure for the homology modeling and docking in the Methods section. The side chain analog (SA) compounds were synthesized by Dr. Anh Le-McClain and Dr. Cori Malinky with the assistance of Ms. Sophia Sakers, Ms. Hailee Rau, and Mr. Gianni Manginelli.

4.1 Introduction

OSBP and the ORPs bind lipids, particularly sterols (i.e., cholesterol and oxysterols) and phospholipids, using ~50 kDa C-terminal OSBP-related ligand-binding domain (ORD). Several structurally diverse, biologically-active small molecules have previously been reported to target both OSBP and ORP4 in the ORD sterol binding pocket, including the natural product compounds OSW-1 (**3**), cephalostatin 1 (**4**), schweinfurthin A (**5**), and ritterazine B (**6**) (**Figure 4B**) [52]. Additionally, multiple antiviral small molecules have been shown to target OSBP, including OSW-1 (**3**) (**Figure 4B**), itraconazole (ITZ) (**7**), T-00127-HEV2 (THEV) (**8**), and TTP-8307 (TTP) (**9**) (**Figure 4C**) [84,85,87,89,190]. We have previously shown that the OSBP-targeting antiviral small molecules (**Figure 4C**) interact with OSBP through multiple modes of binding that results in distinct effects in OSBP cellular activity [190]. The evident roles of OSBP in viral replication and ORP4 in cancer cell survival and proliferation (**see Section 1.6: OSBP and ORP4 in human disease biology** for more information), in combination with the ability of biologically-active small molecules to interact with OSBP and ORP4 through multiple modes of binding (**see Section 1.7: Small-molecule targeting of OSBP and ORP4** and **Chapter 2** for more information), highlights the potential druggability of this protein family. However, the lack of defined structure-activity relationships (SAR) of ligand binding to OSBP and ORP4 limits potential drug development targeting these proteins.

OSBP and ORP4 ligand binding SAR is particularly important for the development of small molecules that selectively bind OSBP for antiviral drug targeting or ORP4 for precision anticancer drug targeting. No protein structure of OSBP or ORP4 has been reported. However, there are crystal structures of the ORD of certain ORP homologs in yeast, known as Osh proteins, from *S. cerevisiae* (Osh3, Osh4, and Osh6), and *K. Lactis* (Osh1) [16–19]. More recently, crystal structures were determined for the ORD of ORP subfamily II members, ORP1 and ORP2, complexed with cholesterol and PI(4,5)P_2, respectively [11,20]. Collectively, these structures reveal that sterols bind in the ORD sterol binding pocket in a conserved "head-down" binding orientation. The C-3 hydroxyl of the sterol A-ring (i.e., the sterol "head") is at the bottom of the hydrophobic binding tunnel and the sterol side chain extends toward the top of the tunnel, interacting with the N-terminal lid (**Figure 3**). Interestingly, ligand-hydroxyl interactions with these proteins, both at the sterol A-ring C-3 position, as well as side chain hydroxylation in oxysterols, are not directly contacting the protein, but instead all occur through water-mediated hydrogen bonds [17,20,262]. The presence of only indirect water-mediated hydrogen bonding to the proteins indicates that oxysterol binding by OSBP and ORP4 may be flexible and able to accommodate the binding of various oxysterols with different hydroxylation positions [25] (see **Section 1.2: Overview of OSBP/ORP ligand binding** for more information).

The high affinity binding of 25-OHC (**1**) to OSBP and ORP4, relative to the reported binding of cholesterol (**2**) (**Figure 4A**) [52,53,76], indicates hydroxylation of the sterol side chain may be important for developing high affinity compounds targeting OSBP and ORP4. Many of the biologically-active small molecules targeting OSBP and

ORP4, such as OSW-1 (**3**), cephalostatin 1 (**4**), ritterazine B (**6**), and THEV (**8**) are structurally modified oxysterol compounds that inhibit the binding of [^{3}H]25-hydroxycholesterol ([^{3}H]25-OHC) to OSBP and ORP4 (**Figure 4B, C**). Therefore, understanding the SAR of oxysterol binding to OSBP and ORP4, particularly of the oxidized side chain component, may be important in developing improved lead compounds for drug development.

Importantly, the binding of oxysterols to OSBP and ORP4 has not been extensively characterized, particularly using human OSBP and ORP4. Previously reported oxysterol binding values for OSBP utilized mouse, rabbit, or hamster, but not human OSBP [52,263,41,25,264,265,53,266]. Only one previous report of oxysterol binding used human ORP4, but this report examined binding of only the structurally modified oxysterol compounds in **Figure 4B**, and not oxysterols in general [52]. The limited reports examining oxysterol binding to the OSBP/ORP family used enriched lysate produced from animal tissue (e.g. hamster liver extract), and therefore might not be selective to individual OSBP/ORP members or even to the OSBP/ORP family [4,41].

Despite sparse binding information within this protein family, several other ORPs have binding values determined for various oxysterols. ORP1L has been reported to bind 25-OHC (K_D 83 nM) and also 22(*R*)-OHC [26,266,267]. The truncated isoform, ORP1S, has been shown to bind, 25-OHC (K_D 84 to 167 nM), 22(*R*)-OHC (K_D 96 nM), and cholesterol (K_D 393 nM) [25,268]. ORP transfection in COS7 cells was also reported to result in ORP1L photo-crosslinking to photo-cholesterol and photo-25-OHC [25]. ORP2 does not display a high affinity for 25-OHC (K_D 3.9 μM) and showed no binding of 27-OHC, but binds 22(*R*)-OHC with high affinity (K_D 14 nM) and 7-KC (K_D 140 nM) and was also

shown to bind cholesterol [26]. ORP transfection in COS7 cells was reported to result in ORP3 photo-crosslinking to photo-cholesterol [25]. Additionally, ORP3 and ORP6 were found to photo-crosslink photo-25-OHC, suggesting ORP3 has the ability to bind both cholesterol and 25-OHC, while ORP6 has the ability to bind 25-OHC [25]. ORP7 showed only a weak, inconsistent signal when tested against photo-cholesterol and photo-25-OHC [25]. The ORD of ORP5 was reported to extract and transfer dehydroergosterol during liposomal exchange assays, suggesting ORP5 can also bind sterols, however no binding values have been determined [269]. ORP8 binds 25-OHC and weakly binds 24(*S*)-OHC, but does not bind 7-KC [26,270]. When transfected in COS7 cells, both ORP5 and ORP8 were shown to photo-crosslink photo-cholesterol and photo-25-OHC [25]. Binding values for ORP9 or ORP10 have not been established, but both have been shown to extract cholesterol from liposomes [271,272]. ORP9S has also been shown to extract the fluorescent sterols, cholestatrienol and dehydroergosterol [273]. Reports indicate that ORP9L and ORP9S cannot bind cholesterol or 25-OHC in solution, therefore a competition assay was not possible and no binding values have been reported [272,273]. Binding values for ORP10 and ORP11 have not been established. When transfected in COS7 cells, ORP10 and ORP11 were shown to photo-crosslink photo-25-OHC, but only observed a weak, inconsistent signal in the presence of photo-cholesterol [25]. Additionally, ORP10 has been reported to extract cholesterol from membranes [271]. There are no current reports of ORP11 ligand binding other than the previously mentioned photo-crosslinking experiment [25].

This chapter provides the first comprehensive report of the SAR of oxysterol ligand binding to human OSBP and ORP4 (subfamily 1). Our results indicate that hydroxylation at multiple side chain positions (i.e., C-20, C-24, C-25, C-27), with the

exception of C-22, confers high affinity binding to both OSBP and ORP4. The stereochemistry of the side chain hydroxylation provides modest selectivity between OSBP and ORP4, with the stereochemical preference between epimers depending on the hydroxylation position. Additionally, the sterol isohexyl side chain is required for binding, and any modification in the length of the side chain impairs binding to both OSBP and ORP4. This apparent side chain binding requirement is contradicted by the high affinity binding of THEV (**8**) (**Figure 4C**), a steroidal compound which completely lacks a side chain. Our results indicate that THEV interacts with OSBP and ORP4 in a manner similar to oxysterols, with the THEV C-3 THP group functioning as a possible isostere for the sterol side chain. These results indicate OSBP and ORP4 can interact with oxysterols and structurally modified oxysterols through multiple modes of binding that could be exploited for antiviral and precision anticancer therapeutic development.

4.2 Materials and Methods

4.2.1 Plasmids and Cloning

Same as **Chapter 2 Methods Section 2.2.1: Plasmids and Cloning**

4.2.2 General Cell Culture and Cell Lines

All cells were handled using aseptic technique and cultured at 37 °C in 5% CO_2. HEK293T cells (ATCC CRL-3216) were grown in 10 cm^2 dishes (Thermo 172931) in complete Dulbecco's Modified Eagle's Medium (DMEM) with 10% Hyclone (Fisher Sci SH3006603) and 1% penicillin-streptomycin (Thermo 15140122) at 37 °C and 5% CO_2. Cells were passaged and seeded by aspirating media followed by washing with 5 mL of

1X PBS (Thermo 10010-023). The PBS was aspirated and the cells were incubated with 2.5 mL TrypLE™ Express (Thermo 12605-010) for a ~5-10 minute incubation at 37 °C. After the cells have detached, the TrypLE™ Express was quenched using 7.5 mL of media and gently pipetted until the cell solution was homogenized. Cell counts and viability was determined by using a TC20^{TM} Automated Cell Counter (Biorad) by mixing 10 μL of cell solution with 10 μL of Trypan Blue stain (Thermo 15250061). Cells were then seeded in a 10 cm^2 dish at the desired cell density.

4.2.3 Transfection Procedure

HEK293T cells were cultured and seeded as previously described previously. $4x10^6$ HEK293T cells were seeded in a 10 cm^2 dish. After 24 hours, 60 μL of Lipofectamine 2000 (Thermo 11668-019) was added to 1.5 mL of pre-warmed Opti-MEM Reduced Serum Media (Thermo 31985-070) and incubated at room temperature for 5 minutes. During this time, 24 μg OSBP or ORP4 cDNA was added to a separate 1.5 mL aliquot of pre-warmed Opti-MEM Reduced Serum Media. The Opti-MEM aliquot containing cDNA was then gently added to the Opti-MEM containing tube containing Lipofectamine (3 mL total per 10 cm^2 dish), gently mixed, and then incubated at room temperature for 30 minutes. After 30 minutes, the media was aspirated from the HEK293T cells and the OPTI-MEM mixture was gently added to the cells and incubated for 4 hours at 37 °C. After 4 hours, 12 mL of antibiotic-free DMEM media was added to each plate for a total volume of 15 mL per plate. The cells were then incubated for 48 hours and then lysed with MPER.

4.2.4 MPER Cell Lysis for Binding Assay Procedure

Mammalian protein extraction reagent, MPER (Thermo 78501) was used for the lysis of transfected cells for the generation of binding lysate. The media was aspirated from the culture and the cells were washed once with 5 mL 1X PBS. The PBS was aspirated and 2 mL of MPER with 1X HALT™ Protease Inhibitor and 1X EDTA (Thermo 78438) was added to the plate and was shaken at room temperature (Innova 42 incubator) at 250 rpm for 5 minutes. All remaining steps were performed at 4 °C to minimize protein degradation. The lysate was then transferred to pre-cooled ultracentrifuge tubes and spun at 100,000 xg for 1 h (Beckman Coulter Optima TLX Ultracentrifuge). The supernatant was collected and the concentration was determining via Bradford assay using a BSA standard curve (Santa Cruz sc-2323). The lysate was diluted to 0.2 mg/mL in Binding Buffer (50 mM HEPES pH 7.4, 50 mM KCl, 5 mM DTT, 1X HALT™ Protease Inhibitor, 1X EDTA) and a small aliquot of the concentrated lysate was kept for Western blot analysis. The diluted lysate was then divided into aliquots, frozen with LN_2 and stored at -80 °C.

4.2.5 [^{3}H]25-OHC Competitive Binding Assay Procedure

The [^{3}H]25-hydroxycholesterol competitive binding assay is based on the procedure from Taylor and Kandutsch [220] and performed according to the method outlined by Burgett et al. [52]. The binding data was analyzed on GraphPad Prism 7 using non-linear regression. Binding curves generating R^2 values of 0.85 were the cutoff to report binding values. K_D, K_i values and standard deviation values were calculated using at least 3 independent replicates unless otherwise stated. Compounds that did not bind

were tested in at least 2 independent replicates unless otherwise stated. Full binding curves can be found in Appendix 3. Dr. Juan Nuñez performed binding experiments that generated binding curves contained in Appendix 3; binding curves that did not generate a definitive K_i due to weak competitive [^{3}H]25-OHC inhibition binding were reanalyzed resulting in more conservative apparent $>K_i$ values [212].

4.2.6 Western Blot

OSBP or ORP4L transfected protein lysate (10 μg) was loaded onto a 8.5% SDS PAGE gel and ran at 150V for 1 hour. The gel was then transferred to a 0.45 μm nitrocellulose membrane (Biorad 1620115) using a Trans-blot® Turbo™ Semi-Dry Transfer System (Biorad 170-4155) at 1.3 A, 25V for 15 minutes. The membrane was then blocked in 5% non-fat dry milk dissolved in 1X Tris-buffered saline with 0.2% Tween-20 (TBST). After 30 minutes, the membrane was washed 3 times for 5 minutes each with 1X TBST and then incubated in primary antibody overnight with 1% milk in 1X TBST at 4 °C. The blot was then washed 3 times for 5 minutes each and incubated in secondary antibody for 30 minutes with 1% milk in 1X TBST at room temperature. The membrane was then washed 5 times for 3 minutes each with TBST with a final 3 minute wash in TBS. The TBS was removed, and the blots were incubated in Clarity™ Western ECL substrate (Bio-Rad 1705061) and imaged on the Bio-Rad ChemiDoc™ Touch Imaging System using the chemiluminescence setting with 2x2 binning. Ladder images were taken using the colorimetric setting. After development, the membranes were washed with 1X TBST 3 times for 5 minutes each. 1:1000 β-actin HRP (Santa Cruz sc-47778 HRP) with 1% milk in 1X TBST was added as a loading control and incubated for

1-hour at room temperature. The actin Western blot was developed as described above. Primary antibodies used were 1:2000 OSBP A-5 (Santa Cruz sc-365771), 1:2000 OSBP2 B-1 (Santa Cruz sc-365922), or 1:25,000 Myc-c antibody (Novus NB600-335). Secondary antibodies used were 1:3000 goat anti mouse IgG1-HRP (Santa Cruz sc-2005), or 1:5000 dilution of a donkey anti-goat antibody (Novus NB7357).

4.2.7 OSBP/ORP4 Homology Modeling and Docking Studies

A homology model of OSBP was built using the online tool SWISS-MODEL, which selected the crystal structure of human ORP2 as the most similar template (PDB code: 5ZM8, 40% sequence similarity and 48% sequence coverage) [11,274]. In order to remove clashes, the initial OSBP homology model was subjected to one round of energy minimization using the Sander program from AmberTools18 [275]. The minimization protocol included 2500 steps of steepest descent followed by 2500 steps of conjugate gradient minimization. The starting ORP4 homology model was obtained from Zhong et al. [77]. The initial search box was determined by superimposing *Saccharomyces cerevisiae* OSH4 bound to 25-hydroxycholesterol (PDB code: 1ZHX) [17] onto the ORP4 and OSBP homology models. The homology models and ligand files were prepared for docking using AutoDockTools-1.5.6 [276]. The ligand binding pockets of ORP4 and OSBP were prepared by docking cholesterol into the binding pocket and performing a round of energy minimization with 100 steps of steepest descent followed by 10 steps of conjugate gradient minimization, with the ligand atom positions fixed. After minimization, the ligand was deleted, and the models were subjected to molecular docking with 25-OHC and THEV. All docking was performed using Autodock Vina [277] against a rigid receptor, and docking results were visualized using UCSF Chimera [278].

4.3 Results

4.3.1 OSBP and ORP4 do not bind non-cholesterol oxysterols

Ligand binding to OSBP and ORP4 was determined using a well-established [^{3}H]25-hydroxycholesterol ([^{3}H]25-OHC) competitive binding assay [76,25,52,53,189,190,220,264,266]. Compounds were assayed for the inhibition of [^{3}H]25-OHC binding to cloned and overexpressed human OSBP or ORP4 in S100 HEK293T lysate. HEK293T lysate overexpressing the negative control, LacZ, does not show detectable specific [^{3}H]25-OHC binding (data not shown) [52,212]. The background HEK293T S100 lysate is capable of solubilizing the oxysterols during the binding assays, producing reliable and reproducible sigmoidal dose-response curves [220]. The equilibrium dissociation constant (K_D) for human OSBP binding 25-OHC is 22 ± 5 nM in this assay (**Figure 4A**) [212], which is consistent with previously reported values generated using rabbit OSBP [52]. The [^{3}H]25-OHC K_D for human ORP4 is reported to be 54 ± 23 (**Figure 4A**) [52]. In our assay, 25-OHC has a K_i of 26 ± 7 for human OSBP and 55 ± 8 nM for human ORP4, which is consistent with previous reports (**Table 2**) [52,212].

A series of non-cholesterol oxysterol compounds were tested for binding interactions to OSBP and ORP4, including bile acids, plant sterols, azacholesterol, cardiac glycoside drugs, and glucocorticoid drugs (**Figure 31**). These compounds did not show any inhibition of [^{3}H]25-OHC binding to OSBP or ORP4 at concentrations < 30 μM (**Table 1)**. These results indicate that OSBP and ORP4 sterol binding pocket

interactions are limited to cholesterol-derived oxysterol compounds and not general steroid structures.

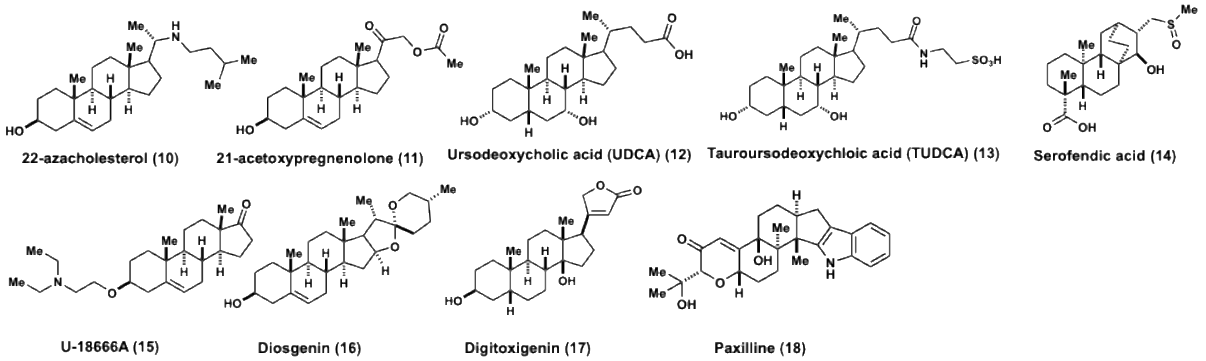

Figure 31: Non-cholesterol oxysterol compounds do not competitively inhibit [^{3}H]25-OHC binding to OSBP or ORP4.

Library of non-cholesterol oxysterols consisting of bile acids, plant sterols, azacholesterol, cardiac glycoside drugs, and glucocorticoid drugs do not inhibit [^{3}H]25-OHC binding to OSBP or ORP4 at concentrations < 30 μM. These results suggest that OSBP and ORP4 do not generally bind all molecules with a sterol core. Full binding curves for each compound can be found in Appendix 3. *21-acetoxypregnenolone was only tested for OSBP and ORP4 binding in 1 independent experiment.

Table 1. K_i binding values (nM) of non-cholesterol oxysterol compounds

Compound	OSBP	ORP4
22-Azacholesterol **(10)**	>100,000	NT
21-Acetoxypregnenolone **(11)**	>100,000	>100,000
Ursodeoxycholic Acid **(12)**	-	-
Tauroursodeoxycholic Acid **(13)**	-	-
Serofendic Acid **(14)**	-	-
U-18666A **(15)**	>100,000	>50,000
Diosgenin **(16)**	>100,000	-
Digitoxigenin **(17)**	-	NT
Paxilline **(18)**	>50,000	>30,000

- Indicates no detectable competitive inhibition
NT = Not Tested

4.3.2 OSBP and ORP4 bind a variety of cholesterol oxysterols with varying oxidation position and stereochemistry

A series of cholesterol oxysterol analogs were tested for interactions to OSBP and ORP4 using the [^{3}H]25-OHC competitive binding assay. 5α-hydroxy-6-ketocholesterol (5α-6KC) (**21**), which is produced through oxidation of the cholesterol C5-C6-alkene upon reaction with ozone in lung epithelial cells [279], displayed weak to no detectable inhibition in the [^{3}H]25-OHC competitive binding assay (**Figure 32**, **Table 2**). Hydrogenation of the C5-C6 alkene of the 25-OHC sterol skeleton (resulting in trans stereochemistry) to produce 25-hydroxycholestanol (**19**) did not affect binding interactions (OSBP K_i = 24 ± 16 nM; ORP4 K_i = 51 ± 26 nM (**Figure 32**, **Table 2**)). 7α-25-dihydroxycholesterol (7α-25-diOHC (**20**)), which differs from 25-OHC through the introduction of an additional hydroxylation at the C7 position, exhibited competitive

binding to OSBP and ORP4, but slightly attenuated compared to 25-OHC (7α-25-diOHC OSBP K_i = 78 ± 42 nM; ORP4 K_i = 92 ± 55 nM (**Figure 32**, **Table 2**)). These results suggest that the high affinity oxysterol interaction with OSBP and ORP4 in the sterol binding pocket are dependent on side chain hydroxylation and not hydroxylation on the sterol core.

A library of cholesterol oxysterols with varying side chain hydroxylation positions and stereochemistry were tested for [^{3}H]25-OHC competitive binding to human OSBP and ORP4 (**Figure 32**, **Table 2**). 20(*S*)-OHC (**29**), 24(*R*)-OHC (**24**), and 24(*S*)-OHC (**25**) displayed strong competitive inhibition against OSBP, although with K_i values higher than 25-OHC (**Figure 32**, **Table 2**) (i.e., 25-OHC K_i = 26 ± 7 nM; 20(*S*)-OHC K_i = 130 ± 35 nM; 24(*S*)-OHC K_i = 330 ± 80 nM; and 24(*R*)-OHC K_i = 120 ± 60 nM). Interestingly, 24(*R*)-OHC (**24**) displayed a significantly lower K_i against OSBP than the 24(*S*)-OHC epimer (i.e., 120 ± 60 nM versus 330 ± 80 nM) (**Figure 32**, **Table 2**). Additionally, hydroxylation at the C-27 position modestly effects 25-OHC binding to OSBP. The OSBP K_i for, 25(*R*), 27-diOHC (**22**) is 68 ± 16 nM, and the OSBP K_i for the 25(*S*), 27-diOHC epimer (**23**) is 120 ± 35 nM (**Figure 32**, **Table 2**). The lower K_i values for both 24-OHC and 25, 27 diOHC (*R*) epimers compared to the (*S*) epimers, suggests a modest preference for (*R*) hydroxylation at the C-24 and C-25 positions against OSBP. Importantly, C-22 hydroxylation significantly abrogated OSBP interactions in the [^{3}H]25-OHC competitive binding assay. 22(*R*)-OHC and 22(*S*)-OHC displayed weak interactions with OSBP with apparent K_i values of >10 μM for 22(*S*)-OHC and >20 μM for 22(*R*)-OHC (**Figure 32**, **Table 2**).

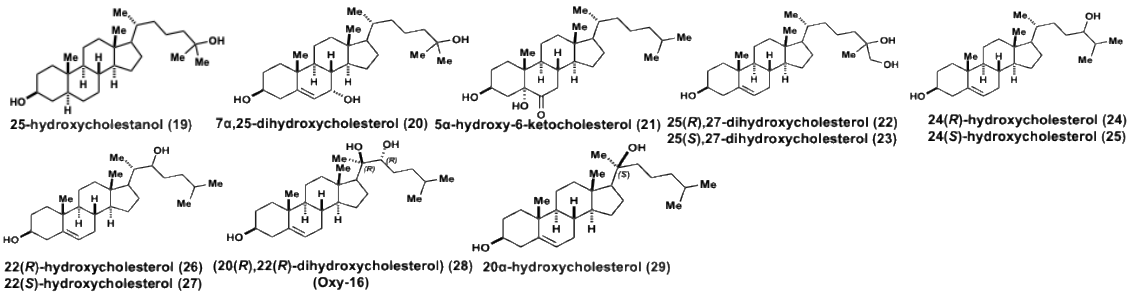

Figure 32: Library of cholesterol oxysterols with varying hydroxylation positions and stereochemistry tested in the [^{3}H]25-OHC competitive binding assay.
Results reveal that oxysterols with hydroxylation at side chain positions C-20, C-24, C-25 and C-27 confers high affinity interaction with OSBP and ORP4. C-22 hydroxylated oxysterols do not produce high affinity interactions with OSBP or ORP4. Full binding curves for each compound can be found in Appendix 3.

Compared to OSBP, ORP4 is more limited in its scope and strength of oxysterol interactions. 20(*S*)-OHC (**29**) interacts with ORP4 with a K_i of 320 ± 90 nM (**Figure 32**, **Table 2**). In ORP4, 24(*S*)-OHC (**25**) increased the K_i approximately 7-fold (400 ± 130 nM) compared to 25-OHC (**Table 2**). For ORP4, 24(*R*)-OHC (**24**) failed to produce a sigmoidal curve indicative of a single binding site for the oxysterol ligand (**Table 2**, **Appendix 3**). Since 24(*R*)-OHC showed dose-dependent binding to OSBP in an identical assay, the failure of 24(*R*)-OHC to produce clear inhibition binding curves against ORP4 is likely not due to solubility or other technical assay issue. 25(*R*), 27-OHC (**22**) also did not produce a sigmoidal inhibition curve for ORP4, similar to 24(*R*)-OHC (**Table 2**, **Appendix 3**). The ability of 24(*R*)-OHC and 25(*R*), 27-diOHC to inhibit [^{3}H]25-OHC binding, but not produce a typical dose-dependent sigmoidal curve, like OSBP, suggests that ORP4 interaction with these ligands may be complex and involve more than a single binding site. In ORP4, 25(*S*), 27-OHC (**23**) displayed micromolar competitive inhibition

(apparent K_i >870 nM). Similar to OSBP, 22(*R*)-OHC showed weak interaction in the binding assay with ORP4 only at high micromolar concentrations, while 22(*S*)-OHC displayed a K_i value of >3 μM (**Figure 32**, **Table 2**). Together, these results indicate 22(*S*)-OHC has a greater capacity to inhibit [^{3}H]25-OHC binding to both OSBP and ORP4 than the (*R*) epimer, albeit with significantly less competitive inhibition than C-20, C-24, C-25, and C-27 side chain hydroxylation (**Figure 32**, **Table 2**).

To better define the role of the C-22 hydroxylation, 20(*R*), 22(*R*)-diOHC (Oxy-16 (**28**) (**Fig. 3**)) was tested. 20(*R*), 22(*R*)-diOHC (**28**), which is identical to 20(*S*)-OHC expect for hydroxylation at C-22, is a reported antagonist in the Hedgehog pathway [280]. Since 20-OHC oxysterols interact with moderately high affinity to OSBP and ORP4, the dihydroxylated 20(*R*), 22(*R*)-diOHC (**28**) analog could define if the poor binding of 22-OHC oxysterols is due to a lack of C-22 hydroxyl positive interactions with the OSBP and ORP4 binding sites, or potential negative clashes with the OSBP and ORP4 binding sites. 20(*R*), 22(*R*)-diOHC (**28**) displayed weak high micromolar binding to OSBP (K_i >30 μM) and ORP4 (K_i >15 μM), suggesting that the detrimental effect of C-22 hydroxylation overrides the positive binding effects of C-20 hydroxylation, potentially through C-22 hydroxylation steric clashing with the sterol binding pocket.

Table 2. K_i binding values (nM) of cholesterol oxysterols.

OHC	OSBP	ORP4
25 **(1)**	26 ± 7	55 ± 8
25 Cholestanol **(19)**	24 ± 16	51 ± 26
7α,25 **(20)**	78 ± 42	92 ± 55
5α,6KC **(21)**	>100,000	NT
25(*R*),27 **(22)**	68 ± 16	>1,000*
25(*S*),27 **(23)**	120 ± 35	>870
24(*R*) **(24)**	120 ± 60	>680*
24(*S*) **(25)**	330 ± 80	400 ± 130
22(*R*) **(26)**	>20,000	>50,000
22(*S*) **(27)**	>10,000	>3,000
20(*R*), 22(*R*) **(28)**	>30,000	>15,000
20(*S*) **(29)**	130 ± 35	320 ± 90

*** Indicates majority of binding curves were not sigmoidal**
\- Indicates no detectable competitive inhibition

4.3.3 Structure-activity relationship (SAR) studies against oxysterol side chain analogs

To better understand the SAR of oxysterol binding to OSBP and ORP4, a library of cholesterol oxysterol side chain analogs were made and tested (**Figure 33**). The analog compounds are derivatives of 20(*S*)-OHC with structurally modified alkyl side chains. 20(*S*)-OHC was selected for derivatization based on its moderate to high competitive binding with both OSBP (K_i 130 ± 35 nM) and ORP4 (320 ± 90 nM) (**Table 2**) and ease of synthetic analog generation. The 20(*S*)-OHC analogs produced varied the side chain lengths and branching positions (i.e., isohexyl, pentyl, isopentyl, butyl, etc.) (**Figure 33**).

The 20(*S*)-OHC analogs were made starting from pregnenolone (data not shown) [281,282]. The 20(*S*)-OHC side chain analog compounds are denoted as 'SA' compounds. The 20(*S*) stereochemistry was preferentially produced over the 20(*R*) analog epimers. For some of the analogs, the 20(*R*) analog epimer was produced in sufficient quantities for biological testing (i.e, SA-2 (**31**), SA-5 (**34**), and SA-7 (**36**) (**Figure 33**). SA-2 ((*R*)-pregenolol (**31**)) and SA-3 ((*S*)-pregenolol (**32**)), which possess no carbon side chain off the C-20 position, displayed no competitive binding for either OSBP or ORP4 at any concentration below 100 μM (**Figure 33**, **Table 3**). The ethyl side chain (*S*)-ethyl-pregenenolol (SA-4, (**33**)) showed only partial competitive binding at high micromolar concentrations (apparent K_i >30 μM) (**Figure 33**, **Table 3**). The butyl side chain present on (*S*)-butyl-pregenenolol (SA-10, **39**) only weakly inhibited [^{3}H]25-OHC binding with micromolar K_i values of >10 μM for OSBP and >30 μM for ORP4 (**Figure 33**, **34**, **Table 3**). The pentyl side chain present on (*S*)-pentyl-pregenenolol (SA-11, **40**) had the highest affinity of any 20-OHC analog compounds tested for both OSBP and ORP4 with K_i values of 600 ± 10 nM for OSBP and 780 ± 180 nM for ORP4 (**Figure 33**, **34**, **Table 3**). 20-OHC oxysterols side chain analogs with octyl side chains were also prepared (**Figure 33**), which extend beyond the typical cholesterol isohexyl side chain. (*R*)-n-octyl-pregenenolol (SA-7, (**36**)) displayed only partial competitive inhibition at high micromolar concentrations (apparent K_i >100 μM); while (*S*)-n-octyl-pregenenolol (SA-8, (**37**)) displayed a greater ability to competitively inhibit [^{3}H]25-OHC binding for both OSBP and ORP4, with a K_i of >10 μM and >20 μM, respectively (**Figure 33, Table 3**). The SAR results indicate that the side chain is optimized at six carbons in order to produce high affinity interaction with

OSBP and ORP4, and any significant oxysterol binding interactions are limited to the isohexyl side chain (**Figure 33, 34, Table 3**).

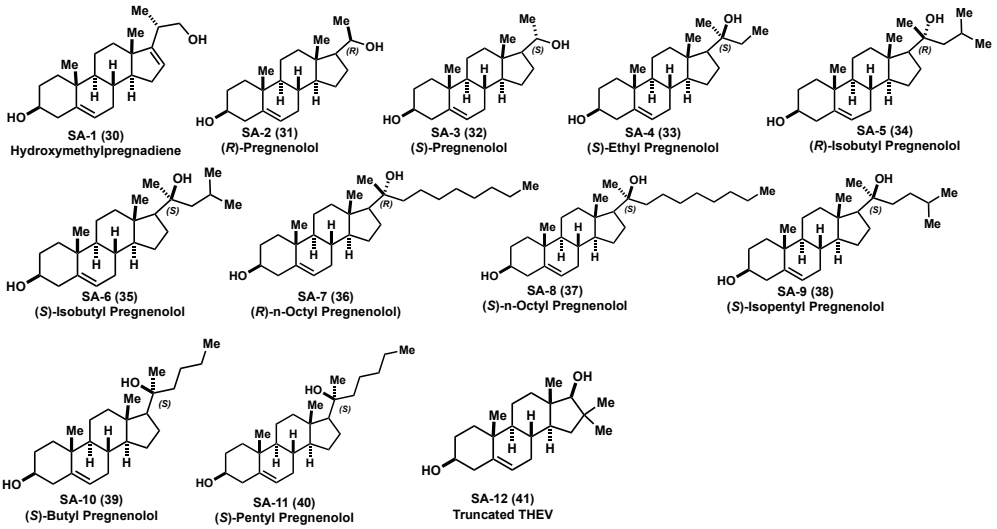

Figure 33: OSBP and ORP4 require the sterol isohexyl side chain for binding. Side chain analogs of 20-OHC reveal that the sterol isohexyl side chain is required for OSBP and ORP4 binding, and any modification in the length of the side chain impairs competitive inhibition of [^{3}H]25-OHC binding. Full binding curves for each compound can be found in Appendix 3.

Table 3. K_i binding values (nM) of oxysterol side chain analogs (SA)

SA	OSBP	ORP4
1 **(30)**	>50,000	>50,000
2 **(31)**	-	-
3 **(32)**	>100,000	>100,000
4 **(33)**	>30,000	>30,000
5 **(34)**	>50,000	>50,000
6 **(35)**	>20,000	>30,000
7 **(36)**	>100,000	>100,000
8 **(37)**	>10,000	>20,000
9 **(38)**	1,300 ± 600	>2,000
10 **(39)**	>10,000	>30,000
11**(40)**	600 ± 10	780 ± 180
12 **(41)**	-	-
THEV **(8)**	22 ± 15	98 ± 14

-Indicates no detectable competitive inhibition

A series of four, five and six carbon branched side chain analogs were also prepared and tested (**Figure 33**). The isobutyl side chains present in (*R*)-isobutyl-pregenenolol (SA-5, (**34**)) showed weak high micromolar binding for both proteins (apparent K_i >50 μM), while (*S*)-isobutyl-pregenenolol inhibited 25-OHC binding at lower concentrations (SA-6, (**35**)) (apparent OSBP K_i > 20 μM and ORP4 K_i > 30 μM) (**Figure 33**, **Table 3**). The increased ability of the (*S*) epimers of n-octyl-pregenenolol and isobutyl-pregenenolol relative to the (*R*) epimers to competitively inhibit [^{3}H]25-OHC binding to both OSBP and ORP4 suggest a preference for (*S*) hydroxylation at the C-20 position; although this observation is limited due to the restricted generation of C-20(*R*) epimers in this analysis. Interestingly, the branched 5-carbon isopentyl side chain, (*S*)-isopentyl-pregenenolol (SA-9, (**38**)), showed moderate OSBP and ORP4 competitive

binding (OSBP K_i =1300 ± 600 nM, ORP4 K_i > 2 μM), which is far lower than the straight chain butyl analog, (*S*)-butyl-pregenenolol, (SA-10 (**39**)), with an OSBP K_i >10 μM and ORP4 K_i >30 μM (**Figure 33**, **34**, **Table 3**). The results of this SAR study indicate that high affinity oxysterol binding to both OSBP and ORP4 is limited to the isohexyl side chain (**Figure 34**, **Table 3)**.

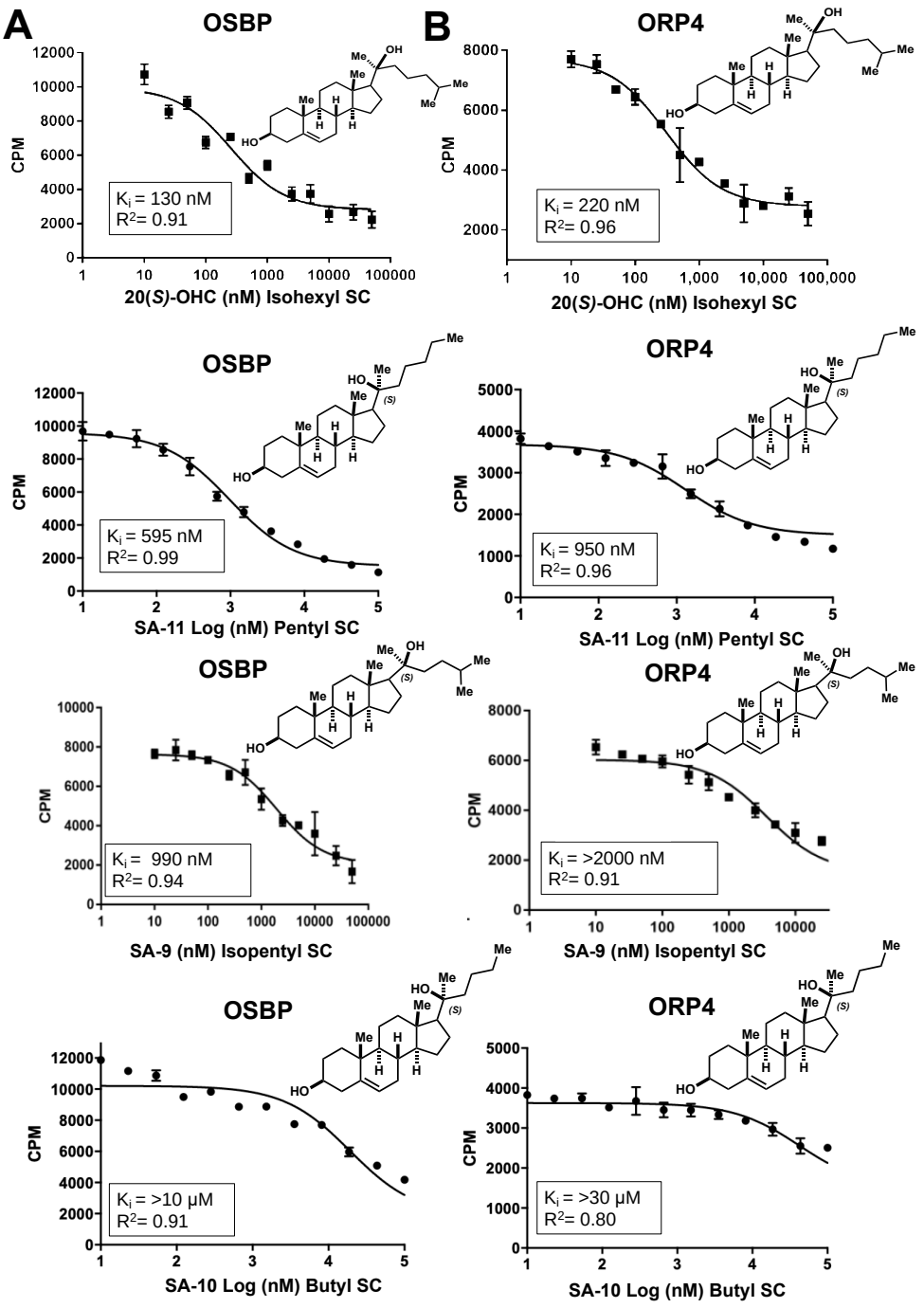

Figure 34: Any modification of the isohexyl sterol side chain length significantly impairs binding to OSBP and ORP4.

Representative binding curves of one of the three independent replicates of 20-OHC, SA-9, SA-10, and SA-11 binding against **A)** OSBP, and **B)** ORP4. 20-OHC is used as the parent molecule with a standard isohexyl side chain. Systematic side chain truncation one carbon at a time from isohexyl (20-OHC), to pentyl (SA-11), to isopentyl (SA-9) side chains results in a steady increase in K_i, until reaching a butyl (SA-10) side chain, which shows almost no detectable inhibition of [^{3}H]25-OHC.

4.3.4 THEV SAR studies against OSBP and ORP4

Despite the apparent necessity of the oxysterol side chain for high affinity interaction with OSBP and ORP4, our group recently reported that the modified oxysterol antiviral compound THEV (T-00127-HEV2) (**Figure 4C**, (**8**)), competes with [^{3}H]25-OHC in the competitive binding assay with a K_i of 22 ± 15 nM for OSBP and a K_i of 98 ± 14 nM for ORP4 (**Table 3**) [190].

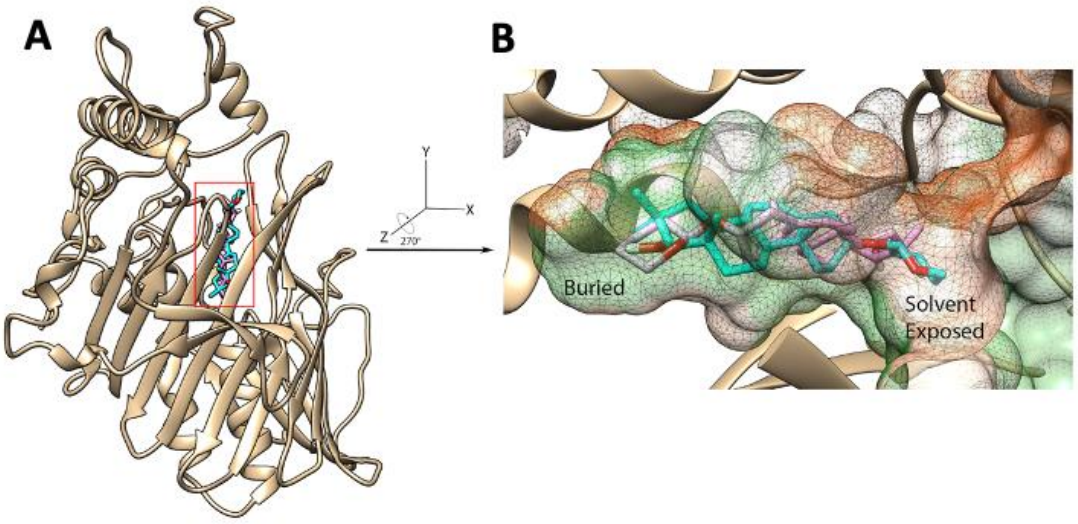

Figure 35: OSBP-THEV homology modeling and docking.
OSBP homology model with THEV docked in the sterol binding pocket located in the ORD β-barrel **A)** External view, and **B)** zoomed into the sterol binding pocket with THEV docked in two orientations. The model suggests that THEV can fit into the sterol binding pocket of OSBP in both a forward and inverted manner. Inverted binding would be necessary for the THEV THP group to act as an isostere for the sterol side chain.

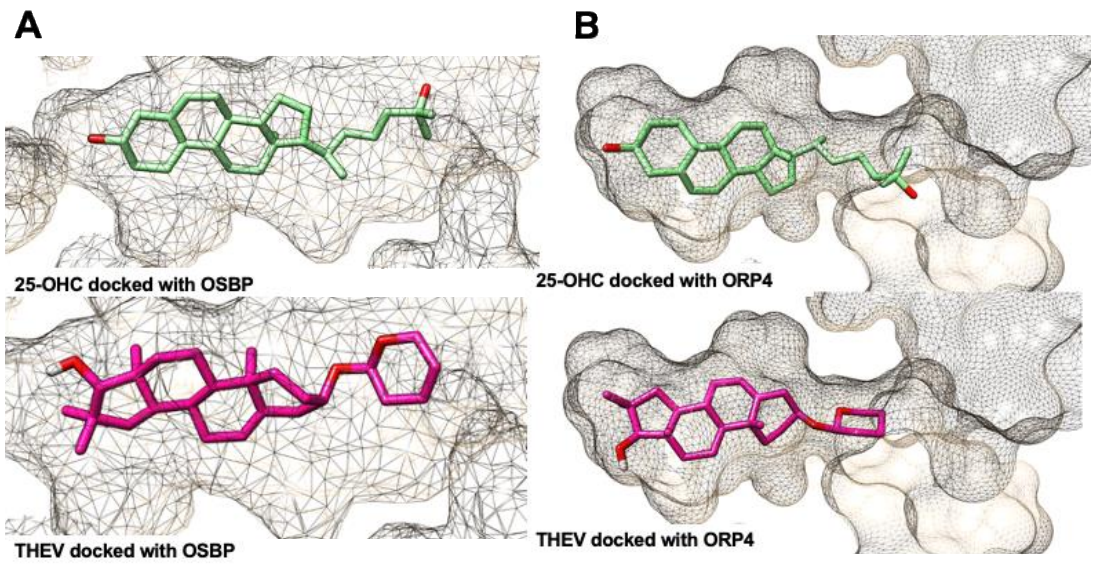

Figure 36: The THEV THP group approximates the sterol side chain in the sterol binding pocket.
Homology modeling with 25-OHC (top) and THEV (bottom) docked in **A)** OSBP homology model, and **B)** ORP4 homology model. The THEV THP group approximates the 25-OHC sterol side chain when docked in the OSBP and ORP4 sterol binding pockets, indicating the high affinity binding of THEV may occur due to the THP group acting as the functional equivalent of the sterol side chain.

The low K_i values for THEV (**8**) clearly contradict the apparent requirement for the isohexyl side chain demonstrated by the 20-OHC side chain analogs (**Figure 4C, Table 3**). Importantly, the THEV compound does possess a C-3 tetrahydropyran (THP) moiety. We hypothesized that the THP group could approximate the cholesterol oxysterol side chain, but only if the THEV compound could interact with OSBP and ORP4 in an inverted matter, with the C-17 hydroxyl entering in the bottom of the binding pocket acting as the functional equivalent of the C-3 hydroxyl of sterols. Our molecular docking studies of the THEV compound against computational models of the OSBP and ORP4 ORD based on homology modeling indicate that the THEV compound could bind in the inverted orientation with the THP group acting as an isostere for the sterol side chain

(**Figure 35**, **36**). To test this hypothesis, we synthesized a truncated THEV analog with the THP moiety cleaved yielding a terminal hydroxyl (SA-12, (**41**))(data not shown) [281]. SA-12 did not show any interaction with either OSBP or ORP4 at any concentration tested (**Figure 36**, **Table 3**). Collectively, these results indicate that the THP moiety of THEV is essential for binding to OSBP and ORP4, and therefore OSBP and ORP4 may accommodate THEV binding with the A-ring THP group in place of the cholesterol side chain.

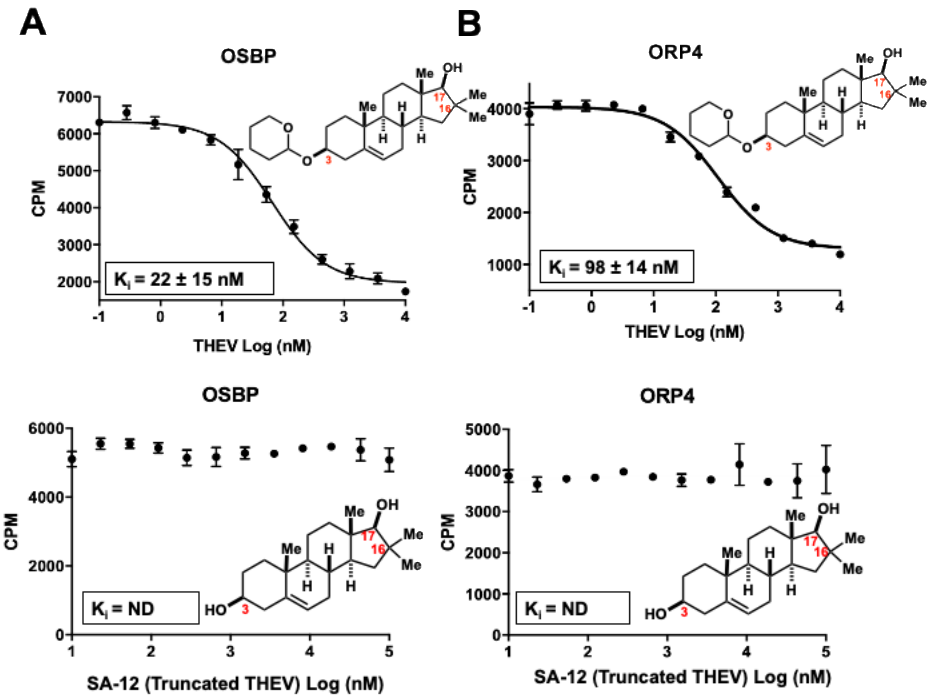

Figure 37: The C-3 THP group of THEV is required for binding to OSBP and ORP4.
Representative binding curves of one independent replicate of THEV and SA-12 (truncated THEV) against **A)** OSBP and **B)** ORP4. Removal of the THEV C-3 THP group abrogates the ability of THEV to competitively inhibit [^{3}H]25-OHC binding. Reported K_i values and standard deviations are the average of three independent experiments. *SA-12 was only tested for ORP4 binding in 1 independent experiment.

4.4 Discussion

Utilizing a small-molecule library of non-cholesterol oxysterols, cholesterol oxysterols, and oxysterol side chain analogs (i.e., SA compounds), we performed the first comprehensive SAR study of oxysterol binding to human OSBP and ORP4. OSBP and ORP4 do not appear to bind non-cholesterol oxysterols in the sterol binding pocket (i.e., bile acids, plant sterols, azacholesterol, cardiac glycoside drugs, and glucocorticoid drugs) (**Figure 31**, **Table 1**). Due to the competitive nature of this binding assay, only ligand binding in the sterol binding pocket that results in competitive inhibition of [^{3}H]25-OHC binding is detected. Therefore, we cannot rule out that these compounds may bind to other locations on OSBP or ORP4. In contrast, OSBP and ORP4 have the ability to bind a variety of cholesterol oxysterols with various side chain hydroxylation positions (i.e., C-20, C-24, C-25 and C-27) and stereochemistry, although ORP4 is more limited than OSBP in both strength and scope of oxysterol interaction (**Figure 32**, **Table 2**). Side chain hydroxylation at C-22 is the only position that significantly impairs binding to both OSBP and ORP4 (**Figure 32**, **Table 2**). 22(*R*)-OHC is an important steroid hormone intermediate and agonist of liver X receptors (LXRs), and 22(*R*)-OHC is bound by ORP subfamily 2 members, ORP1 and ORP2, with low nM affinity (see **Chapter 4 Introduction** for more information) [26,283,284]. Additionally, ORP1S and ORP2 have a role in LXR regulation and ORP2 also plays a role in steroidogenic gene expression and steroid hormone biosynthesis, and does not possess a high affinity for 25-OHC (K_D 3.9 μM) [26,268,285]. The affinity of ORP1 and ORP2 for 22-OHC and lack of affinity for 25-OHC, in combination with their role in LXR regulation and steroid hormone biosynthesis, suggests the impaired binding of oxysterols with C-22 hydroxylation against OSBP and

ORP4 may be a mechanism to avoid influencing LXR regulation and steroid hormone biosynthesis. This also indicates ORP subfamily 1 (i.e., OSBP and ORP4) and 2 (i.e., ORP1 and ORP2) may have complementary, but not redundant functions with respect to oxysterol ligand binding in the cell.

Our results suggest that both OSBP and ORP4 better tolerate (*S*) side chain hydroxylation at the C-20 and C-22 side chain positions over the (*R*) configuration, but OSBP better tolerates (*R*) hydroxylation as the side chain extends ways from the sterol core at the C-24 and C-25 positions (**Figure 32**, **Table 2**). Alternatively, ORP4 interactions with (*R*) hydroxylated ligands at the C-24 and C-25 side chain positions generated non-sigmoidal competitive binding curves, suggestive of a more complex binding interaction with these ligands (**Figure 32**, **Table 2, Appendix**). Additionally, hydroxylation stereochemistry confers modest selectivity between OSBP and ORP4. Sterol core hydroxylation does not appear to increase ligand interaction with OSBP or ORP4 (**Figure 32, Table 2**).

Further probing of side chain binding requirements using a library of side chain analogs (SA) revealed that any change in the length of the sterol isohexyl side chain impairs binding to both OSBP and ORP4 (**Figure 33, 34, Table 3**). The strict requirement of the sterol isohexyl side chain for binding may be a mechanism to distinguish between other biomolecules with similar sterol cores, but different side chain lengths, like bile acids and steroid hormones [28].

In contrast, we previously showed that the OSBP-targeting antiviral compound, THEV (**8**), is a high affinity ligand for OSBP and ORP4 (**Figure 4C**, **Table 3**) [190]. Our competitive binding results using a truncated THEV analog (**41**) and molecular docking

homology modeling indicates that THEV interacts with these proteins in an inverted manner, with the THEV THP moiety acting as a proxy for the sterol side chain (**Figure 35**, **36**, **37**).

4.5 Conclusions

In total, our results indicate that OSBP and ORP4 can be targeted by a variety of oxysterols with differing core and side chain hydroxylation positions, as well as structurally modified oxysterols (i.e., THEV), with varying affinities. However, high affinity oxysterol interaction with OSBP and ORP4 in the sterol binding pocket will require the sterol isohexyl side chain, or the functional equivalent of an isohexyl side chain, as appears to be the case with the THP moiety on THEV.

The ability of OSBP and ORP4 to accommodate the binding of various oxysterols with differing side chain hydroxylation makes sense considering all the protein to ligand hydroxyl group hydrogen bonding interactions in the existing crystal structures of other ORPs and yeast Osh proteins are shown to be mediated through indirect water-mediated hydrogen bonds, and not direct hydrogen bonding to the protein [25]. The lack of direct ligand to protein hydrogen bonding likely allows the binding pocket to be flexible with respect to accommodating different oxysterol hydroxylation positions, and also more or less hydrophobic ligands (i.e., phospholipids) [25]. Additionally, the inability of OSBP and ORP4 (ORP subfamily 1) to tolerate C-22 hydroxylation suggests that ORP subfamily 2 members, ORP1 and ORP2, may have complementary, but not redundant functions in the cell relative to ORP subfamily 1. As previously mentioned, we hypothesize the strict requirement of the isohexyl sterol side chain may be a mechanism to distinguish between

other biomolecules with similar sterol cores, but different side chain lengths (i.e., bile acids and steroid hormones); however, the precise underlying SAR of this mechanism requires further investigation [28].

The characterization of oxysterol ligand binding to OSBP and ORP4 performed in this chapter provides important information necessary to guide the development of novel small-molecule antiviral and anticancer therapeutics that target these proteins through multiple modes of binding. This information is driving anticancer and antiviral drug development in our research group and will be critical for harnessing and developing the OSBP long-term repression response as a novel antiviral therapeutic approach.

Chapter 5: Conclusions and Future Directions

The work in this dissertation outlines the discovery and elucidation of novel OSBP cellular biology that can be triggered by exogenous small molecules and exploited as a novel OSBP-centered prophylactic antiviral therapeutic approach (**Chapters 2** and **3**). This dissertation also reports the first comprehensive SAR study of oxysterol binding to human OSBP and ORP4 that is necessary for the development of our novel prophylactic antiviral therapeutic approach (**Chapter 4**).

Our results support the existence of an endogenous OSBP regulatory response, triggered by OSW-1-compound treatment, that leads to the long-term repression of cellular OSBP levels. We show that transient, low nanomolar, non-toxic OSW-1-compound treatment results in ~90% decrease in cellular OSBP levels that persists for multiple days (i.e., >72 hours in certain cell lines) after the OSW-1-compound has been removed (**Figure 10**). The multigenerational persistence of this response indicates that it can be stably inherited by subsequent cell generations that were never directly exposed to the OSW-1-compound. LCMS and single-cell MS revealed that intracellular OSW-1-compound levels are undetectable 24 hours pWO, indicating that persistent residual intracellular OSW-1-compound is not responsible for the repression, but rather, compound treatment triggers an active cellular process responsible for the long-term repression of OSBP levels (**Figure 21**). We showed that ORP4 levels also decrease in the same time and proteasome-dependent manner as OSBP levels after OSW-1-compound treatment; however, ORP4 levels do not remain repressed after the compound is removed (**Figure 13**). We also show that OSW-1-compound treatment does not appear to repress other cellular proteins (**Figure 14**). Together, these results suggest the existence of an

unrecognized endogenous OSBP-specific regulatory response that may be triggered upon the binding of certain ligands to OSBP (i.e., OSW-1), which represses cellular OSBP levels in cells for multiple days after the initial stimuli is removed.

Importantly, we were able to leverage the discovery of this unique response to induce *prophylactic* antiviral activity in cells (i.e., the cells retain significant antiviral activity in the absence of the compound) against multiple clinically isolated human pathogenic *Enteroviruses* (**Figure 15**, **17**). Further investigation of three other OSBP-targeting antiviral small molecules (THEV, TTP, ITZ (**Figure 5**)) revealed that the OSW-1-compound is the only OSBP-targeting antiviral compound that results in cellular OSBP loss and long-term repression, and importantly, the only compound capable of inducing antiviral prophylaxis in cells (**Figure 16**, **17**). To the best of our knowledge, we report the OSW-1-compound as the first identified small-molecule antiviral prophylactic that exerts activity through modulating the levels of a host protein. We were also able to show that OSBP is targeted by the OSBP-targeting antiviral compounds through multiple modes of binding that have distinct effects on OSBP activity in the cell (**Figure 18**, **19**, **20**). These results not only reveal that the observed OSBP long-term repression and prophylactic antiviral response is unique to the OSW-1-compound, but also that OSBP may be targeted for antiviral development in multiple, distinct ways.

Additionally, we reveal that OSW-1-compound treatment induces cellular autophagy through mTORc1 inhibition (**Figure 25**, **26**, **27**). These results are consistent with recently published findings from the Zoncu lab at UC Berkley [59]. The Zoncu lab found that OSBP levels are directly coupled to mTORc1 activity and decreases in cellular OSBP levels inhibits mTORc1 and induces cellular autophagy, confirming both our

published and unpublished autophagy/mTORc1 results [59,189]. mTORc1 is also involved in cellular innate antiviral response [238–241]. In response to viral infection, host cells commonly induce autophagy to eliminate invading viruses, decrease protein synthesis and ribosome biogenesis to inhibit viral protein production, or induce apoptosis to contain the viral infection; all processes mediated by the inhibition of mTORc1 [238–241,256]. Consequently, viruses commonly subvert and constitutively activate mTORc1 to counteract this antiviral response [238]. mTORc1 activation inhibits autophagy, inhibits apoptosis, and increases protein synthesis and ribosome biogenesis to aid in the viral infection process [238–241]. The long-term repression of OSBP by the OSW-1-compound would therefore not only inhibit cholesterol transfer to the VRC, inhibiting viral proliferation (see **Section 1.6.1** for more information), but also directly inhibit mTORc1; therefore, countering viral constitutive activation of mTORc1 and inducing mTORc1 inhibition associated antiviral processes (i.e., autophagy, decrease in protein synthesis etc.) Overall, these results suggest the existence of a multifaceted antiviral response in cells that can be triggered simply by regulating cellular OSBP levels.

The role of OSBP in sphingomyelin (SM) regulation in cells may also be a facet of this response. Decreasing cellular OSBP levels also inhibits SM biosynthesis [60–62] (see **Section 1.4.3: Lipid metabolism** for more information). Inhibitors of SM biosynthesis have previously been show to decrease HCV replication [120], and HCV virions are enriched in both cholesterol and SM, indicating a critical role for SM in the HCV life cycle [121,122] (see **Section 1.6.1.3: Role of OSBP in HCV biology** for more information on SM in viral infection).

Investigative studies probing the mechanism of OSBP regulation leading to long-term OSBP repression revealed that this regulation is not mediated on a transcriptional or post-translational level, but rather appears to be regulated on an RNA level (**Figure 23**, **24**). Consistent with this observation, global transcriptomic and proteomic analysis revealed that the most significantly changed biological process after OSW-1-compound washout treatment in both analyses is an RNA regulatory pathway called nonsense-mediated decay (NMD) (**Figure 28**, **29**). NMD is not only a pervasive post-transcriptional regulatory pathway used to adjust the specific expression of a protein under various stimuli, but also a recently identified host antiviral defense mechanism against RNA viruses [233–237]. Viral (+)ssRNA is mRNA-like and resembles endogenous NMD substrates (i.e., mRNA transcripts containing PTCs), allowing NMD to target the viral RNA as a host defense mechanism [261] (see **Chapter 3** for more information on NMD).

Additionally, we discovered that OSBP, but not ORP4, possesses an alternatively spliced, NMD-responsive transcript (**Figure 30**). There are no published reports about this OSBP NMD transcript, or how it contributes to OSBP regulation in the cell. Our results suggest that the OSW-1-compound may induce OSBP alternative splicing, followed by NMD targeting of the alternatively spliced NMD-responsive OSBP mRNA, leading to repression of OSBP on a protein level that persists in the absence of the OSW-1-compound. The primers used for our qPCR analysis were unable to discriminate between the coding OSBP transcript and the OSBP NMD-responsive transcript, therefore we may be detecting the NMD transcript in this analysis, which would explain why there is no significant change in OSBP mRNA levels after OSW-1-compound treatment (**Figure 23C**). The proposed AS-NMD mechanism for OSBP repression triggered by the

OSW-1-compound would explain the lack of repression of ORP4, as ORP4 does not possess an alternatively spliced NMD-responsive transcript (**Figure 13B**). Collectively, our results indicate the long-term repression of OSBP is regulated on an RNA level by NMD; however, further studies are necessary to confirm these finding.

The connection between how OSW-1-compound treatment leads to OSBP alternative splicing and subsequent NMD-mediated repression may lie in the OSBP knockdown induced inhibition of mTORc1. Recently, the mTORc1 inhibitor, rapamycin, was shown to modulate NMD processes in cells, both increasing the abundance of PTC-containing NMD transcripts and decreasing the expression of NMD substrates [258]. This indicates that mTORc1 inhibition can not only induce alternative splicing to increase NMD-responsive transcript expression, but also augment NMD targeting of particular transcripts [258]. Additionally, mTORc1 has previously been reported to interact with splicing factors and regulate their activity [259,260]. Therefore, it is possible that the inhibition of mTORc1 due to OSBP loss in the cell may induce changes to alternative splicing, leading to the expression of the OSBP NMD-responsive transcript; and also augment subsequent NMD targeting of the OSBP NMD-responsive transcript leading to repression of OSBP protein levels. However, the exact connection between mTORc1 inhibition, alternative splicing and NMD augmentation remains unclear [258].

Collectively, the combined effects of the OSW-1-compound to trigger: a decrease and repression of cellular OSBP levels for multiple days, consequently inhibiting mTORc1 (decreasing global protein synthesis and inducing cellular autophagy), and modulate NMD processes, appears to create an innate antiviral environment in the cell that can persist while a viral infection is cleared. We hypothesize that the OSBP

regulation triggered by the OSW-1-compound may be part of a larger, unrecognized innate antiviral response pathway in the cell. OSBP has previously been shown to be involved in an interferon-dependent innate antiviral response that involves interferon-inducible transmembrane protein 3 (IFITM3)-mediated disruption of the OSBP and VAPA interaction, which disrupts cholesterol homeostasis and consequently inhibits viral infection [155]. OSBP may also be involved in the interferon-induced innate antiviral activity of 25-OHC [180–182] (see **Section: 1.6.1.6** for more information on OSBP in innate antiviral response). We hypothesize that the OSBP regulatory response triggered by the OSW-1-compound, and the other antiviral-associated responses induced as a result of the subsequent repression, may be part of an unrecognized interferon-independent arm of cellular innate antiviral response.

Many viruses, such as SARS-CoV, have the ability to inhibit the cell's interferon response in an attempt to dampen the host innate immune response to the virus [286–288] . In these cases, the common innate antiviral sensor, toll-like receptors (TLRs), which normally sense viral invasion and elicit an immune response through signaling for interferon production, would be rendered ineffective [288,289]. The cell would therefore require a new antiviral sensor to mediate an innate antiviral response. Since a hallmark of all (+)ssRNA viruses (the viruses that OSBP targeting inhibits) is host membrane remodeling and alteration of lipid metabolism [94], the lipid sensing abilities of OSBP may be used as a new antiviral sensor. This could occur through either directly sensing virally induced changes to membrane structure and host lipid metabolism, or indirectly, by binding of a lipid-related small molecule that indicates the presence of viral infection (e.g. a chemical signal similar to the OSW-1-compound).

Although our overall model is still speculative and further work is required to validate the precise causal chain of events that unfold to elicit this response, we propose the following model (**Figure 38**). After sensing a viral infection, or exposure to the OSW-1-compound, OSBP levels are decreased in the cell via rapid degradation by the proteasome. The decrease in cellular OSBP inhibits cholesterol trafficking to the viral replication compartment (VRC), consequently inhibiting viral proliferation. Decreasing OSBP levels also inhibits SM biosynthesis and subsequently, the viral processes that require SM. The decrease in cellular OSBP additionally inhibits mTORc1, countering viral subversion and constitutive activation of mTORc1, and inducing antiviral responses such as autophagy to degrade the invading viruses and inhibition of protein synthesis to decrease viral protein production. The inhibition of mTORc1 due to OSBP loss in the cell could then induce changes to alternative splicing and augment NMD activity, resulting in expression of the OSBP NMD-responsive transcript and also subsequent targeting of this transcript by NMD. NMD targeting of the OSBP NMD-responsive transcript would repress OSBP protein levels and sustain this response. Augmentation of NMD by mTORc1 inhibition may also result in NMD-targeting of viral RNA, further suppressing viral infection.

This multifaceted innate antiviral response could therefore be initiated simply by decreasing, inhibiting, or regulating OSBP levels in the cell. The long-term repression of OSBP may be a mechanism to sustain this response to locally restrict viral proliferation and allow the host immune system to more effectively and efficiently clear the viral infection from the host.

Further elucidation of this response and the development of clinically-adaptable small molecules to harness this response, could lead to a new paradigm in broad-spectrum antiviral treatment. The prophylactic (i.e., preventative) potential of this antiviral approach, coupled with its broad-spectrum applicability and low probability of viral mutational resistance may allow for the treatment or prevention of many existing RNA viruses with no current treatments. The evolutionarily conserved viral dependence on OSBP as a host factor indicates that this novel antiviral approach may be effective against RNA viruses that have not yet even emerged. This novel approach could be an essential tool in our currently severely limited RNA antiviral toolbox to fight and eliminate current (i.e., COVID-19) and future RNA viral pandemics.

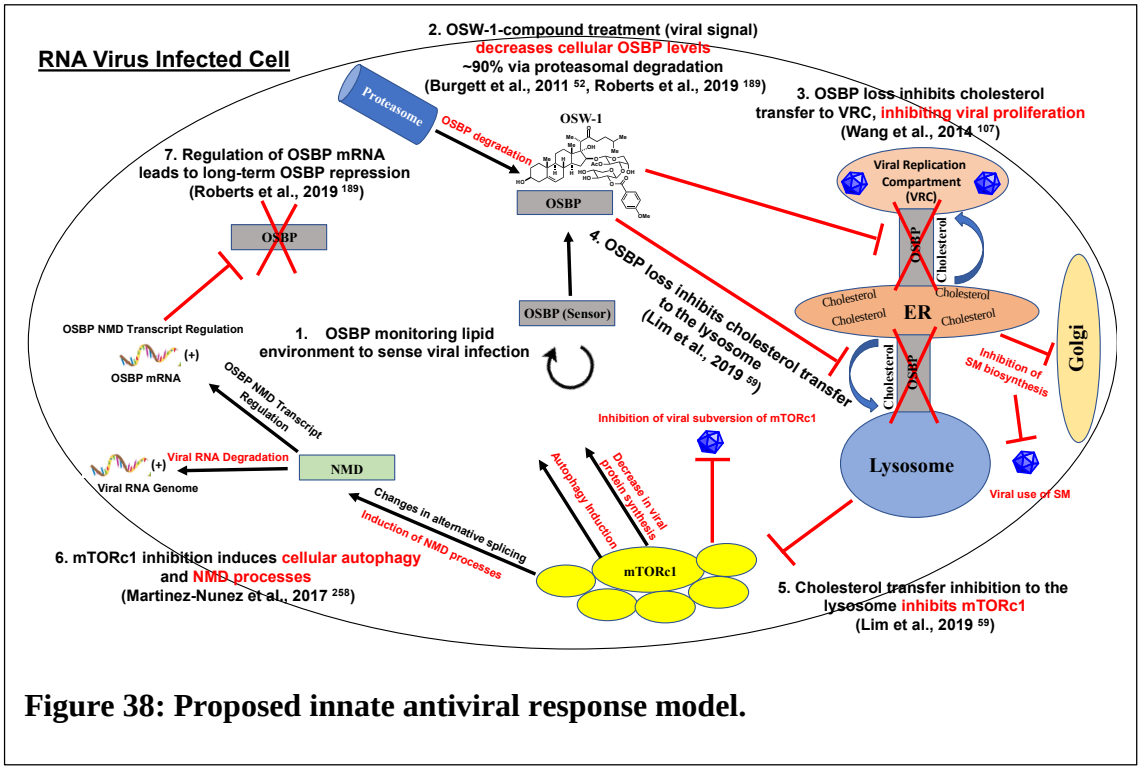

Figure 38: Proposed innate antiviral response model.

References

(1) Raychaudhuri, S.; Prinz, W. A. *Annu. Rev. Cell Dev. Biol.* **2010**, *26* (1), 157–177.

(2) Pietrangelo, A.; Ridgway, N. D. *Cell. Mol. Life Sci.* **2018**, *75* (17), 3079–3098.

(3) Kandutsch, A. A.; Thompson, E. B. *J. Biol. Chem.* **1980**, *255* (22), 10813–10821.

(4) Taylor, F. R.; Kandutsch, A. A. *Chem. Phys. Lipids* **1985**, *38* (1–2), 187–194.

(5) Dawson, P. A.; Ridgway, N. D.; Slaughter, C. A.; Brown, M. S.; Goldstein, J. L. *J. Biol. Chem.* **1989**, *264* (28), 16798–16803.

(6) Levanon, D.; Hsieh, C. L.; Francke, U.; Dawson, P. A.; Ridgway, N. D.; Brown, M. S.; Goldstein, J. L. *Genomics* **1990**, *7* (1), 65–74.

(7) Laitinen, S.; Olkkonen, V. M.; Ehnholm, C.; Ikonen, E. *J. Lipid Res.* **1999**, *40* (12), 2204–2211.

(8) Jaworski, C. J.; Moreira, E.; Li, A.; Lee, R.; Rodriguez, I. R. *Genomics* **2001**, *78* (3), 185–196.

(9) Dye, D. E.; Bieniawski, M. A.; Wright, S. C. E.; Mccauley, A.; Coombe, D. R.; Mousley, C. J. **2018**.

(10) Koriyama, H. Nakagami, H., Ed.; IntechOpen: Rijeka, 2012; p Ch. 7.

(11) Wang, H.; Ma, Q.; Qi, Y.; Dong, J.; Du, X.; Rae, J.; Wang, J.; Wu, W.-F.; Brown, A. J.; Parton, R. G.; Wu, J.-W.; Yang, H. *Mol. Cell* **2019**, *73* (3), 458-473.e7.

(12) Lev, S. *Nat. Rev. Mol. Cell Biol.* **2010**, *11* (10), 739–750.

(13) Funato, K.; Riezman, H.; Muñiz, M. *Biochim. Biophys. acta. Mol. cell Biol. lipids* **2020**, *1865* (1), 158453.

(14) Lev, S. *Cold Spring Harb. Perspect. Biol.* **2012**, *4* (10), a013300.

(15) Mesmin, B.; Bigay, J.; Moser von Filseck, J.; Lacas-Gervais, S.; Drin, G.; Antonny, B. *Cell* **2013**, *155* (4), 830–843.

(16) Manik, M. K.; Yang, H.; Tong, J.; Im, Y. J. *Structure* **2017**, *25* (4), 617-629.e3.

(17) Im, Y. J.; Raychaudhuri, S.; Prinz, W. A.; Hurley, J. H. *Nature* **2005**, *437* (7055), 154–158.

(18) Maeda, K.; Anand, K.; Chiapparino, A.; Kumar, A.; Poletto, M.; Kaksonen, M.; Gavin, A.-C. *Nature* **2013**, *501* (7466), 257–261.

(19) Tong, J.; Yang, H.; Yang, H.; Eom, S. H.; Im, Y. J. *Structure* **2013**, *21* (7), 1203–1213.

(20) Dong, J.; Du, X.; Wang, H.; Wang, J.; Lu, C.; Chen, X.; Zhu, Z.; Luo, Z.; Yu, L.; Brown, A. J.; Yang, H.; Wu, J.-W. *Nat. Commun.* **2019**, *10* (1), 829.

(21) Wyles, J. P.; Perry, R. J.; Ridgway, N. D. *Exp. Cell Res.* **2007**, *313* (7), 1426–1437.

(22) Charman, M.; Colbourne, T. R.; Pietrangelo, A.; Kreplak, L.; Ridgway, N. D. *J. Biol. Chem.* **2014**, *289* (22), 15705–15717.

(23) de Saint-Jean, M.; Delfosse, V.; Douguet, D.; Chicanne, G.; Payrastre, B.; Bourguet, W.; Antonny, B.; Drin, G. *J. Cell Biol.* **2011**, *195* (6), 965–978.

(24) Tong, J.; Yang, H.; Yang, H.; Eom, S. H.; Im, Y. J. *Structure* **2013**, *21* (7), 1203–1213.

(25) Suchanek, M.; Hynynen, R.; Wohlfahrt, G.; Lehto, M.; Johansson, M.; Saarinen, H.; Radzikowska, A.; Thiele, C.; Olkkonen, V. M. *Biochem. J.* **2007**, *405* (3), 473–480.

(26) Ngo, M. H.; Colbourne, T. R.; Ridgway, N. D. *Biochem. J.* **2010**, *429* (1), 13–24.

(27) Fernández-Pérez, E. J.; Sepúlveda, F. J.; Peters, C.; Bascuñán, D.; Riffo-Lepe, N. O.; González-Sanmiguel, J.; Sánchez, S. A.; Peoples, R. W.; Vicente, B.; Aguayo, L. G. *Frontiers in Aging Neuroscience* . 2018, p 226.

(28) Berg JM, T. J. *Biochemistry*, 5th ed.; 2002.

(29) Yan, D.; Olkkonen, V. M. *Int. Rev. Cytol.* **2008**, *265*, 253–285.

(30) Griffiths, W. J.; Wang, Y. *Biochem. Soc. Trans.* **2019**, *47* (2), 517–526.

(31) Wang, B.; Tontonoz, P. *Nat. Rev. Endocrinol.* **2018**, *14* (8), 452–463.

(32) Torocsik, D.; Szanto, A.; Nagy, L. *Mol. Aspects Med.* **2009**, *30* (3), 134–152.

(33) Bielska, A. A.; Schlesinger, P.; Covey, D. F.; Ory, D. S. *Trends Endocrinol. Metab.* **2012**, *23* (3), 99–106.

(34) Nedelcu, D.; Liu, J.; Xu, Y.; Jao, C.; Salic, A. *Nat. Chem. Biol.* **2013**, *9* (9), 557–564.

(35) Emgård, J.; Kammoun, H.; García-Cassani, B.; Chesné, J.; Parigi, S. M.; Jacob, J.-M.; Cheng, H.-W.; Evren, E.; Das, S.; Czarnewski, P.; Sleiers, N.; Melo-Gonzalez, F.; Kvedaraite, E.; Svensson, M.; Scandella, E.; Hepworth, M. R.; Huber, S.; Ludewig, B.; Peduto, L.; Villablanca, E. J.; Veiga-Fernandes, H.; Pereira, J. P.; Flavell, R. A.; Willinger, T. *Immunity* **2018**, *48* (1), 120-132.e8.

(36) Pichot, R.; Watson, R. L.; Norton, I. T. *Int. J. Mol. Sci.* **2013**, *14* (6), 11767–11794.

(37) Decrock, E.; De Bock, M.; Wang, N.; Gadicherla, A. K.; Bol, M.; Delvaeye, T.; Vandenabeele, P.; Vinken, M.; Bultynck, G.; Krysko, D. V; Leybaert, L. *Biochim. Biophys. Acta* **2013**, *1833* (7), 1772–1786.

(38) Zhong, W.; Yi, Q.; Xu, B.; Li, S.; Wang, T.; Liu, F.; Zhu, B.; Hoffmann, P. R.;

Ji, G.; Lei, P.; Li, G.; Li, J.; Li, J.; Olkkonen, V. M.; Yan, D. *Nat. Commun.* **2016**, *7*, 12702.

(39) Antonny, B.; Bigay, J.; Mesmin, B. *Annu. Rev. Biochem.* **2018**, *87*, 809–837.

(40) Chung, J.; Torta, F.; Masai, K.; Lucast, L.; Czapla, H.; Tanner, L. B.; Narayanaswamy, P.; Wenk, M. R.; Nakatsu, F.; De Camilli, P. *Science (80-.).* **2015**, *349* (6246), 428 LP – 432.

(41) Taylor, F. R.; Saucier, S. E.; Shown, E. P.; Parish, E. J.; Kandutsch, A. A. *J. Biol. Chem.* **1984**, *259* (20), 12382–12387.

(42) Dawson, P. A.; Van der Westhuyzen, D. R.; Goldstein, J. L.; Brown, M. S. *J. Biol. Chem.* **1989**, *264* (15), 9046–9052.

(43) Schoenheimer, R.; Breusch, F. *J. Biol. Chem.* **1933**, *103* (2), 439–448.

(44) Yokoyama, C.; Wang, X.; Briggs, M. R.; Admon, A.; Wu, J.; Hua, X.; Goldstein, J. L.; Brown, M. S. *Cell* **1993**, *75* (1), 187–197.

(45) Wang, X.; Sato, R.; Brown, M. S.; Hua, X.; Goldstein, J. L. *Cell* **1994**, *77* (1), 53–62.

(46) Goldstein, J. L.; Brown, M. S. *J. Lipid Res.* **1984**, *25* (13), 1450–1461.

(47) Smith, J. R.; Osborne, T. F.; Goldstein, J. L.; Brown, M. S. *J. Biol. Chem.* **1990**, *265* (4), 2306–2310.

(48) Dawson, P. A.; Hofmann, S. L.; van der Westhuyzen, D. R.; Südhof, T. C.; Brown, M. S.; Goldstein, J. L. *J. Biol. Chem.* **1988**, *263* (7), 3372–3379.

(49) Osborne, T. F.; Gil, G.; Goldstein, J. L.; Brown, M. S. *J. Biol. Chem.* **1988**, *263* (7), 3380–3387.

(50) Ridgway, N. D.; Dawson, P. A.; Ho, Y. K.; Brown, M. S.; Goldstein, J. L. *J. Cell*

Biol. **1992**, *116* (2), 307–319.

(51) Olkkonen, V. M. *Lipid Insights* **2015**, *8* (Suppl 1), 1–9.

(52) Burgett, A. W. G.; Poulsen, T. B.; Wangkanont, K.; Anderson, D. R.; Kikuchi, C.; Shimada, K.; Okubo, S.; Fortner, K. C.; Mimaki, Y.; Kuroda, M.; Murphy, J. P.; Schwalb, D. J.; Petrella, E. C.; Cornella-Taracido, I.; Schirle, M.; Tallarico, J. A.; Shair, M. D. *Nat. Chem. Biol.* **2011**, *7* (9), 639–647.

(53) Wang, P. Y.; Weng, J.; Lee, S.; Anderson, R. G. W. *J. Biol. Chem.* **2008**, *283* (12), 8034–8045.

(54) Weber-Boyvat, M.; Kentala, H.; Peränen, J.; Olkkonen, V. M. *Cell. Mol. Life Sci.* **2015**, *72* (10), 1967–1987.

(55) Storey, M. K.; Byers, D. M.; Cook, H. W.; Ridgway, N. D. *Biochem. J.* **1998**, *336 (Pt 1*, 247–256.

(56) Kentala, H.; Weber-Boyvat, M.; Olkkonen, V. M. *Int. Rev. Cell Mol. Biol.* **2016**, *321*, 299–340.

(57) Charman, M.; Goto, A.; Ridgway, N. D. *Traffic* **2017**, *18* (8), 519–529.

(58) Mesmin, B.; Bigay, J.; Polidori, J.; Jamecna, D.; Lacas-Gervais, S.; Antonny, B. *EMBO J.* **2017**, *36* (21), 3156–3174.

(59) Lim, C.-Y.; Davis, O. B.; Shin, H. R.; Zhang, J.; Berdan, C. A.; Jiang, X.; Counihan, J. L.; Ory, D. S.; Nomura, D. K.; Zoncu, R. *Nat. Cell Biol.* **2019**.

(60) Kawano, M.; Kumagai, K.; Nishijima, M.; Hanada, K. *J. Biol. Chem.* **2006**, *281* (40), 30279–30288.

(61) Perry, R. J.; Ridgway, N. D. *Mol. Biol. Cell* **2006**, *17* (6), 2604–2616.

(62) Peretti, D.; Dahan, N.; Shimoni, E.; Hirschberg, K.; Lev, S. *Mol. Biol. Cell* **2008**.

(63) Nhek, S.; Ngo, M.; Yang, X.; Ng, M. M.; Field, S. J.; Asara, J. M.; Ridgway, N. D.; Toker, A. *Mol. Biol. Cell* **2010**, *21* (13), 2327–2337.

(64) Goto, A.; Liu, X.; Robinson, C.-A.; Ridgway, N. D. *Mol. Biol. Cell* **2012**, *23* (18), 3624–3635.

(65) Wang, P.-Y.; Weng, J.; Anderson, R. G. W. *Science* **2005**, *307* (5714), 1472–1476.

(66) Yan, D.; Lehto, M.; Rasilainen, L.; Metso, J.; Ehnholm, C.; Yla-Herttuala, S.; Jauhiainen, M.; Olkkonen, V. M. *Arterioscler. Thromb. Vasc. Biol.* **2007**, *27* (5), 1108–1114.

(67) Luu, W.; Sharpe, L. J.; Gelissen, I. C.; Brown, A. J. *IUBMB Life* **2013**, *65* (8), 675–684.

(68) Romeo, G. R.; Kazlauskas, A. *J. Biol. Chem.* **2008**, *283* (15), 9595–9605.

(69) Romeo, G.; Frangioni, J. V; Kazlauskas, A. *FASEB J. Off. Publ. Fed. Am. Soc. Exp. Biol.* **2004**, *18* (6), 725–727.

(70) Kim, J.; Guan, K.-L. *Nat. Cell Biol.* **2019**, *21* (1), 63–71.

(71) Moreira, E. F.; Jaworski, C.; Li, A.; Rodriguez, I. R. *J. Biol. Chem.* **2001**, *276* (21), 18570–18578.

(72) Fournier, M. V; Guimaraes da Costa, F.; Paschoal, M. E.; Ronco, L. V; Carvalho, M. G.; Pardee, A. B. *Cancer Res.* **1999**, *59* (15), 3748–3753.

(73) Yan, D.; Olkkonen, V. M. *Future Lipidol.* **2007**, *2* (1), 85–94.

(74) Wang, C.; JeBailey, L.; Ridgway, N. D. *Biochem. J.* **2002**, *361* (Pt 3), 461–472.

(75) Liu, H.; Huang, S. *World J. Clin. cases* **2020**, *8* (1), 1–10.

(76) Charman, M.; Colbourne, T. R.; Pietrangelo, A.; Kreplak, L.; Ridgway, N. D. *J.*

Biol. Chem. **2014**, *289* (22), 15705–15717.

(77) Zhong, W.; Xu, M.; Li, C.; Zhu, B.; Cao, X.; Li, D.; Chen, H.; Hu, C.; Li, R.; Luo, C.; Pan, G.; Zhang, W.; Lai, C.; Wang, T.; Du, X.; Chen, H.; Xu, G.; Olkkonen, V. M.; Lei, P.; Xu, J.; Yan, D. *Cell Rep.* **2019**, *26* (8), 2166-2177.e9.

(78) Pietrangelo, A.; Ridgway, N. D. *J. Cell Sci.* **2018**, *131* (14).

(79) Battaglia, R. A.; Delic, S.; Herrmann, H.; Snider, N. T. *F1000Research* **2018**, *7*, F1000 Faculty Rev-1796.

(80) Evans, R. M. *Trends Cell Biol.* **1994**, *4* (5), 149–151.

(81) Cao, X.; Chen, J.; Li, D.; Xie, P.; Xu, M.; Lin, W.; Li, S.; Pan, G.; Tang, Y.; Xu, J.; Olkkonen, V. M.; Yan, D.; Zhong, W. *FASEB J. Off. Publ. Fed. Am. Soc. Exp. Biol.* **2019**, *33* (12), 13852–13865.

(82) Hilger, D.; Masureel, M.; Kobilka, B. K. *Nat. Struct. Mol. Biol.* **2018**, *25* (1), 4–12.

(83) Li, J.-W.; Xiao, Y.-L.; Lai, C.-F.; Lou, N.; Ma, H.-L.; Zhu, B.-Y.; Zhong, W.-B.; Yan, D.-G. *Oncotarget* **2016**, *7* (40), 65849–65861.

(84) Strating, J. R. P. M.; van der Linden, L.; Albulescu, L.; Bigay, J.; Arita, M.; Delang, L.; Leyssen, P.; van der Schaar, H. M.; Lanke, K. H. W.; Thibaut, H. J.; Ulferts, R.; Drin, G.; Schlinck, N.; Wubbolts, R. W.; Sever, N.; Head, S. A.; Liu, J. O.; Beachy, P. A.; De Matteis, M. A.; Shair, M. D.; Olkkonen, V. M.; Neyts, J.; van Kuppeveld, F. J. M. *Cell Rep.* **2015**, *10* (4), 600–615.

(85) Arita, M.; Kojima, H.; Nagano, T.; Okabe, T.; Wakita, T.; Shimizu, H. *J. Virol.* **2013**, *87* (8), 4252 LP – 4260.

(86) Arita, M. *Microbiol. Immunol.* **2014**, *58* (4), 239–256.

(87) Albulescu, L.; Bigay, J.; Biswas, B.; Weber-Boyvat, M.; Dorobantu, C. M.; Delang, L.; van der Schaar, H. M.; Jung, Y. S.; Neyts, J.; Olkkonen, V. M.; van Kuppeveld, F. J. M.; Strating, J. R. P. M. *Antiviral Res.* **2017**, *140*, 37–44.

(88) Meutiawati, F.; Bezemer, B.; Strating, J. R. P. M.; Overheul, G. J.; Zusinaite, E.; van Kuppeveld, F. J. M.; van Cleef, K. W. R.; van Rij, R. P. *Antiviral Res.* **2018**, *157*, 68–79.

(89) Albulescu, L.; Strating, J. R. P. M.; Thibaut, H. J.; Van Der Linden, L.; Shair, M. D.; Neyts, J.; Van Kuppeveld, F. J. M. *Antiviral Res.* **2015**, *117*, 110–114.

(90) Takano, T.; Akiyama, M.; Doki, T.; Hohdatsu, T. *Vet. Res.* **2019**, *50* (1), 5.

(91) Henriques Silva, N.; Vasconcellos Fournier, M.; Pimenta, G.; Pulcheri, W. A.; Spector, N.; da Costa Carvalho, M. da G. *Int. J. Mol. Med.* **2003**, *12* (4), 663–666.

(92) Dorobantu, C. M.; Albulescu, L.; Lyoo, H.; van Kampen, M.; De Francesco, R.; Lohmann, V.; Harak, C.; van der Schaar, H. M.; Strating, J. R. P. M.; Gorbalenya, A. E.; van Kuppeveld, F. J. M. *mSphere* **2016**, *1* (3).

(93) Nagy, P. D.; Strating, J. R. P. M.; van Kuppeveld, F. J. M. *PLoS Pathog.* **2016**, *12* (10), e1005912–e1005912.

(94) Zhang, Z.; He, G.; Filipowicz, N. A.; Randall, G.; Belov, G. A.; Kopek, B. G.; Wang, X. *Front. Microbiol.* **2019**, *10*, 286.

(95) Kolakofsky, D. *RNA* **2015**, *21* (4), 667–669.

(96) Modrow, S.; Falke, D.; Truyen, U.; Schätzl, H. Modrow, S., Falke, D., Truyen, U., Schätzl, H., Eds.; Springer Berlin Heidelberg: Berlin, Heidelberg, 2013; pp 185–349.

(97) Chazal, N.; Gerlier, D. *Microbiol. Mol. Biol. Rev.* **2003**, *67* (2), 226–237.

(98) Buchmann, J. P.; Holmes, E. C. *Microbiol. Mol. Biol. Rev.* **2015**, *79* (4), 403–418.

(99) Strating, J. R.; van Kuppeveld, F. J. *Curr. Opin. Cell Biol.* **2017**, *47*, 24–33.

(100) Blanchard, E.; Roingeard, P. *Cell. Microbiol.* **2015**, *17* (1), 45–50.

(101) Hsu, N.-Y.; Ilnytska, O.; Belov, G.; Santiana, M.; Chen, Y.-H.; Takvorian, P. M.; Pau, C.; van der Schaar, H.; Kaushik-Basu, N.; Balla, T.; Cameron, C. E.; Ehrenfeld, E.; van Kuppeveld, F. J. M.; Altan-Bonnet, N. *Cell* **2010**, *141* (5), 799–811.

(102) Schlegel, A.; Giddings Jr, T. H.; Ladinsky, M. S.; Kirkegaard, K. *J. Virol.* **1996**, *70* (10), 6576–6588.

(103) Ogawa, K.; Hishiki, T.; Shimizu, Y.; Funami, K.; Sugiyama, K.; Miyanari, Y.; Shimotohno, K. *Proc. Jpn. Acad. Ser. B. Phys. Biol. Sci.* **2009**, *85* (7), 217–228.

(104) Amako, Y.; Syed, G. H.; Siddiqui, A. *J. Biol. Chem.* **2011**, *286* (13), 11265–11274.

(105) Inoue, T.; Tsai, B. *Cold Spring Harb. Perspect. Biol.* **2013**, *5* (1), a013250–a013250.

(106) van der Schaar, H. M.; Dorobantu, C. M.; Albulescu, L.; Strating, J. R. P. M.; van Kuppeveld, F. J. M. *Trends Microbiol.* **2016**, *24* (7), 535–546.

(107) Wang, H.; Perry, J. W.; Lauring, A. S.; Neddermann, P.; De Francesco, R.; Tai, A. W. *Gastroenterology* **2014**, *146* (5), 1373-1385.e11.

(108) Reid, C. R.; Airo, A. M.; Hobman, T. C. *Viruses* **2015**, *7* (8), 4385–4413.

(109) Manns, M. P.; Buti, M.; Gane, E.; Pawlotsky, J.-M.; Razavi, H.; Terrault, N.;

Younossi, Z. *Nat. Rev. Dis. Prim.* **2017**, *3* (1), 17006.

(110) Morozov, V. A.; Lagaye, S. *World J. Hepatol.* **2018**, *10* (2), 186–212.

(111) Kish, T.; Aziz, A.; Sorio, M. *P T* **2017**, *42* (5), 316–329.

(112) Munir, S.; Saleem, S.; Idrees, M.; Tariq, A.; Butt, S.; Rauff, B.; Hussain, A.; Badar, S.; Naudhani, M.; Fatima, Z.; Ali, M.; Ali, L.; Akram, M.; Aftab, M.; Khubaib, B.; Awan, Z. *Virol. J.* **2010**, *7*, 296.

(113) Romero-Brey, I.; Merz, A.; Chiramel, A.; Lee, J.-Y.; Chlanda, P.; Haselman, U.; Santarella-Mellwig, R.; Habermann, A.; Hoppe, S.; Kallis, S.; Walther, P.; Antony, C.; Krijnse-Locker, J.; Bartenschlager, R. *PLoS Pathog.* **2012**, *8* (12), e1003056.

(114) Amako, Y.; Sarkeshik, A.; Hotta, H.; Yates, J. 3rd; Siddiqui, A. *J. Virol.* **2009**, *83* (18), 9237–9246.

(115) Tao, Y. J.; Ye, Q. *PLoS Pathog.* **2010**, *6* (7), e1000943–e1000943.

(116) Wyles, J. P.; McMaster, C. R.; Ridgway, N. D. *J. Biol. Chem.* **2002**, *277* (33), 29908–29918.

(117) Elazar, M.; Cheong, K. H.; Liu, P.; Greenberg, H. B.; Rice, C. M.; Glenn, J. S. *J. Virol.* **2003**, *77* (10), 6055–6061.

(118) Gao, L.; Aizaki, H.; He, J.-W.; Lai, M. M. C. *J. Virol.* **2004**, *78* (7), 3480–3488.

(119) Hamamoto, I.; Nishimura, Y.; Okamoto, T.; Aizaki, H.; Liu, M.; Mori, Y.; Abe, T.; Suzuki, T.; Lai, M. M. C.; Miyamura, T.; Moriishi, K.; Matsuura, Y. *J. Virol.* **2005**, *79* (21), 13473–13482.

(120) Sakamoto, H.; Okamoto, K.; Aoki, M.; Kato, H.; Katsume, A.; Ohta, A.; Tsukuda, T.; Shimma, N.; Aoki, Y.; Arisawa, M.; Kohara, M.; Sudoh, M. *Nat.*

Chem. Biol. **2005**, *1* (6), 333–337.

(121) Merz, A.; Long, G.; Hiet, M.-S.; Brügger, B.; Chlanda, P.; Andre, P.; Wieland, F.; Krijnse-Locker, J.; Bartenschlager, R. *J. Biol. Chem.* **2011**, *286* (4), 3018–3032.

(122) Bishe, B.; Syed, G. H.; Field, S. J.; Siddiqui, A. *J. Biol. Chem.* **2012**, *287* (33), 27637–27647.

(123) Berger, K. L.; Cooper, J. D.; Heaton, N. S.; Yoon, R.; Oakland, T. E.; Jordan, T. X.; Mateu, G.; Grakoui, A.; Randall, G. *Proc. Natl. Acad. Sci. U. S. A.* **2009**, *106* (18), 7577–7582.

(124) Tai, A. W.; Benita, Y.; Peng, L. F.; Kim, S.-S.; Sakamoto, N.; Xavier, R. J.; Chung, R. T. *Cell Host Microbe* **2009**, *5* (3), 298–307.

(125) Reiss, S.; Rebhan, I.; Backes, P.; Romero-Brey, I.; Erfle, H.; Matula, P.; Kaderali, L.; Poenisch, M.; Blankenburg, H.; Hiet, M.-S.; Longerich, T.; Diehl, S.; Ramirez, F.; Balla, T.; Rohr, K.; Kaul, A.; Buhler, S.; Pepperkok, R.; Lengauer, T.; Albrecht, M.; Eils, R.; Schirmacher, P.; Lohmann, V.; Bartenschlager, R. *Cell Host Microbe* **2011**, *9* (1), 32–45.

(126) Trotard, M.; Lepere-Douard, C.; Regeard, M.; Piquet-Pellorce, C.; Lavillette, D.; Cosset, F.-L.; Gripon, P.; Le Seyec, J. *FASEB J. Off. Publ. Fed. Am. Soc. Exp. Biol.* **2009**, *23* (11), 3780–3789.

(127) Borawski, J.; Troke, P.; Puyang, X.; Gibaja, V.; Zhao, S.; Mickanin, C.; Leighton-Davies, J.; Wilson, C. J.; Myer, V.; Cornellataracido, I.; Baryza, J.; Tallarico, J.; Joberty, G.; Bantscheff, M.; Schirle, M.; Bouwmeester, T.; Mathy, J. E.; Lin, K.; Compton, T.; Labow, M.; Wiedmann, B.; Gaither, L. A. *J. Virol.*

2009, *83* (19), 10058–10074.

(128) Vaillancourt, F. H.; Pilote, L.; Cartier, M.; Lippens, J.; Liuzzi, M.; Bethell, R. C.; Cordingley, M. G.; Kukolj, G. *Virology* **2009**, *387* (1), 5–10.

(129) Li, Q.; Brass, A. L.; Ng, A.; Hu, Z.; Xavier, R. J.; Liang, T. J.; Elledge, S. J. *Proc. Natl. Acad. Sci. U. S. A.* **2009**, *106* (38), 16410–16415.

(130) Bishé, B.; Syed, G.; Siddiqui, A. *Viruses* **2012**, *4* (10), 2340–2358.

(131) Aizaki, H.; Morikawa, K.; Fukasawa, M.; Hara, H.; Inoue, Y.; Tani, H.; Saito, K.; Nishijima, M.; Hanada, K.; Matsuura, Y.; Lai, M. M. C.; Miyamura, T.; Wakita, T.; Suzuki, T. *J. Virol.* **2008**, *82* (12), 5715–5724.

(132) Sagan, S. M.; Rouleau, Y.; Leggiadro, C.; Supekova, L.; Schultz, P. G.; Su, A. I.; Pezacki, J. P. *Biochem. Cell Biol.* **2006**, *84* (1), 67–79.

(133) Lim, Y.-S.; Hwang, S. B. *J. Biol. Chem.* **2011**, *286* (13), 11290–11298.

(134) Tai, A. W.; Salloum, S. *PLoS One* **2011**, *6* (10), e26300.

(135) Banerji, S.; Ngo, M.; Lane, C. F.; Robinson, C.-A.; Minogue, S.; Ridgway, N. D. *Mol. Biol. Cell* **2010**, *21* (23), 4141–4150.

(136) Weng, L.; Hirata, Y.; Arai, M.; Kohara, M.; Wakita, T.; Watashi, K.; Shimotohno, K.; He, Y.; Zhong, J.; Toyoda, T. *J. Virol.* **2010**, *84* (22), 11761–11770.

(137) Dorobantu, C. M.; Albulescu, L.; Harak, C.; Feng, Q.; van Kampen, M.; Strating, J. R. P. M.; Gorbalenya, A. E.; Lohmann, V.; van der Schaar, H. M.; van Kuppeveld, F. J. M. *PLoS Pathog.* **2015**, *11* (9), e1005185–e1005185.

(138) Ilnytska, O.; Santiana, M.; Hsu, N.-Y.; Du, W.-L.; Chen, Y.-H.; Viktorova, E. G.; Belov, G.; Brinker, A.; Storch, J.; Moore, C.; Dixon, J. L.; Altan-Bonnet, N. *Cell*

Host Microbe **2013**, *14* (3), 281–293.

(139) Greninger, A. L.; Knudsen, G. M.; Betegon, M.; Burlingame, A. L.; Derisi, J. L. *J. Virol.* **2012**, *86* (7), 3605–3616.

(140) Sasaki, J.; Ishikawa, K.; Arita, M.; Taniguchi, K. *EMBO J.* **2012**, *31* (3), 754–766.

(141) Syed, G. H.; Tang, H.; Khan, M.; Hassanein, T.; Liu, J.; Siddiqui, A. *J. Virol.* **2014**, *88* (5), 2519 LP – 2529.

(142) Grassi, G.; Di Caprio, G.; Fimia, G. M.; Ippolito, G.; Tripodi, M.; Alonzi, T. *World J. Gastroenterol.* **2016**, *22* (6), 1953–1965.

(143) Melia, C. E.; Peddie, C. J.; de Jong, A. W. M.; Snijder, E. J.; Collinson, L. M.; Koster, A. J.; van der Schaar, H. M.; van Kuppeveld, F. J. M.; Bárcena, M. *MBio* **2019**, *10* (3), e00951-19.

(144) Nikonov, O. S.; Chernykh, E. S.; Garber, M. B.; Nikonova, E. Y. *Biochemistry. (Mosc).* **2017**, *82* (13), 1615–1631.

(145) Chen, B.-S.; Lee, H.-C.; Lee, K.-M.; Gong, Y.-N.; Shih, S.-R. *Front. Microbiol.* **2020**, *11*, 261.

(146) Tang, J. W.; Holmes, C. W. *Virulence* **2017**, *8* (7), 1062–1065.

(147) Chen, I.-J.; Hu, S.-C.; Hung, K.-L.; Lo, C.-W. *Medicine (Baltimore).* **2018**, *97* (36), e11831–e11831.

(148) Hohenthal, U.; Vainionpaa, R.; Nikoskelainen, J.; Kotilainen, P. *Thorax*. England July 2008, pp 658–659.

(149) Pons-Salort, M.; Parker, E. P. K.; Grassly, N. C. *Curr. Opin. Infect. Dis.* **2015**, *28* (5), 479–487.

(150) Jacobs, S. E.; Lamson, D. M.; St George, K.; Walsh, T. J. *Clin. Microbiol. Rev.* **2013**, *26* (1), 135–162.

(151) Roulin, P. S.; Lotzerich, M.; Torta, F.; Tanner, L. B.; van Kuppeveld, F. J. M.; Wenk, M. R.; Greber, U. F. *Cell Host Microbe* **2014**, *16* (5), 677–690.

(152) Li, L.; He, Y.; Yang, H.; Zhu, J.; Xu, X.; Dong, J.; Zhu, Y.; Jin, Q. *J. Clin. Microbiol.* **2005**, *43* (8), 3835–3839.

(153) Faleye, T. O. C.; Adewumi, M. O.; Adeniji, J. A. *Viruses* **2016**, *8* (1), 18.

(154) Lugo, D.; Krogstad, P. *Curr. Opin. Pediatr.* **2016**, *28* (1), 107–113.

(155) Amini-Bavil-Olyaee, S.; Choi, Y. J.; Lee, J. H.; Shi, M.; Huang, I.-C.; Farzan, M.; Jung, J. U. *Cell Host Microbe* **2013**, *13* (4), 452–464.

(156) De Palma, A. M.; Thibaut, H. J.; van der Linden, L.; Lanke, K.; Heggermont, W.; Ireland, S.; Andrews, R.; Arimilli, M.; Al-Tel, T. H.; De Clercq, E.; van Kuppeveld, F.; Neyts, J. *Antimicrob. Agents Chemother.* **2009**, *53* (5), 1850–1857.

(157) Arita, M.; Kojima, H.; Nagano, T.; Okabe, T.; Wakita, T.; Shimizu, H. *J. Virol.* **2011**, *85* (5), 2364–2372.

(158) Carocci, M.; Bakkali-Kassimi, L. *Virulence* **2012**, *3* (4), 351–367.

(159) Vansteenkiste, K.; Van Limbergen, T.; Decaluwé, R.; Tignon, M.; Cay, B.; Maes, D. *Porc. Heal. Manag.* **2016**, *2*, 19.

(160) Lanke, K. H. W.; van der Schaar, H. M.; Belov, G. A.; Feng, Q.; Duijsings, D.; Jackson, C. L.; Ehrenfeld, E.; van Kuppeveld, F. J. M. *J. Virol.* **2009**, *83* (22), 11940–11949.

(161) Wessels, E.; Duijsings, D.; Lanke, K. H. W.; van Dooren, S. H. J.; Jackson, C.

L.; Melchers, W. J. G.; van Kuppeveld, F. J. M. *J. Virol.* **2006**, *80* (23), 11852 LP – 11860.

(162) Teterina, N. L.; Pinto, Y.; Weaver, J. D.; Jensen, K. S.; Ehrenfeld, E. *J. Virol.* **2011**, *85* (9), 4284–4296.

(163) Neufeldt, C. J.; Cortese, M.; Acosta, E. G.; Bartenschlager, R. *Nat. Rev. Microbiol.* **2018**, *16* (3), 125–142.

(164) Redoni, M.; Yacoub, S.; Rivino, L.; Giacobbe, D. R.; Luzzati, R.; Di Bella, S. *Rev. Med. Virol.* **2020**, *n/a* (n/a), e2101.

(165) Bollati, M.; Alvarez, K.; Assenberg, R.; Baronti, C.; Canard, B.; Cook, S.; Coutard, B.; Decroly, E.; de Lamballerie, X.; Gould, E. A.; Grard, G.; Grimes, J. M.; Hilgenfeld, R.; Jansson, A. M.; Malet, H.; Mancini, E. J.; Mastrangelo, E.; Mattevi, A.; Milani, M.; Moureau, G.; Neyts, J.; Owens, R. J.; Ren, J.; Selisko, B.; Speroni, S.; Steuber, H.; Stuart, D. I.; Unge, T.; Bolognesi, M. *Antiviral Res.* **2010**, *87* (2), 125–148.

(166) Heaton, N. S.; Perera, R.; Berger, K. L.; Khadka, S.; Lacount, D. J.; Kuhn, R. J.; Randall, G. *Proc. Natl. Acad. Sci. U. S. A.* **2010**, *107* (40), 17345–17350.

(167) Rothwell, C.; Lebreton, A.; Young Ng, C.; Lim, J. Y. H.; Liu, W.; Vasudevan, S.; Labow, M.; Gu, F.; Gaither, L. A. *Virology* **2009**, *389* (1–2), 8–19.

(168) Chukkapalli, V.; Heaton, N. S.; Randall, G. *Curr. Opin. Microbiol.* **2012**, *15* (4), 512–518.

(169) Weiss, S. R.; Navas-Martin, S. *Microbiol. Mol. Biol. Rev.* **2005**, *69* (4), 635–664.

(170) Fung, T. S.; Liu, D. X. *Annu. Rev. Microbiol.* **2019**, *73* (1), 529–557.

(171) Takano, T.; Satomi, Y.; Oyama, Y.; Doki, T.; Hohdatsu, T. *Arch. Virol.* **2016**,

161 (1), 125–133.

(172) Altan-Bonnet, N.; Balla, T. *Trends Biochem. Sci.* **2012**, *37* (7), 293–302.

(173) Sadler, A. J.; Williams, B. R. G. *Nat. Rev. Immunol.* **2008**, *8* (7), 559–568.

(174) Bailey, C. C.; Huang, I.-C.; Kam, C.; Farzan, M. *PLoS Pathog.* **2012**, *8* (9), e1002909.

(175) Brass, A. L.; Huang, I.-C.; Benita, Y.; John, S. P.; Krishnan, M. N.; Feeley, E. M.; Ryan, B. J.; Weyer, J. L.; van der Weyden, L.; Fikrig, E.; Adams, D. J.; Xavier, R. J.; Farzan, M.; Elledge, S. J. *Cell* **2009**, *139* (7), 1243–1254.

(176) Sobo, K.; Le Blanc, I.; Luyet, P.-P.; Fivaz, M.; Ferguson, C.; Parton, R. G.; Gruenberg, J.; van der Goot, F. G. *PLoS One* **2007**, *2* (9), e851–e851.

(177) Chevallier, J.; Chamoun, Z.; Jiang, G.; Prestwich, G.; Sakai, N.; Matile, S.; Parton, R. G.; Gruenberg, J. *J. Biol. Chem.* **2008**, *283* (41), 27871–27880.

(178) Holthuis, J. C. M.; Levine, T. P. *Nat. Rev. Mol. Cell Biol.* **2005**, *6* (3), 209–220.

(179) Tanner, L. B.; Lee, B. *Cell Host Microbe* **2013**, *13* (4), 375–377.

(180) Anggakusuma; Romero-Brey, I.; Berger, C.; Colpitts, C. C.; Boldanova, T.; Engelmann, M.; Todt, D.; Perin, P. M.; Behrendt, P.; Vondran, F. W. R.; Xu, S.; Goffinet, C.; Schang, L. M.; Heim, M. H.; Bartenschlager, R.; Pietschmann, T.; Steinmann, E. *Hepatology* **2015**, *62* (3), 702–714.

(181) Robertson, K. A.; Ghazal, P. *Frontiers in Immunology* . 2016, p 634.

(182) Civra, A.; Francese, R.; Gamba, P.; Testa, G.; Cagno, V.; Poli, G.; Lembo, D. *Redox Biol.* **2018**, *19*, 318–330.

(183) Blanc, M.; Hsieh, W. Y.; Robertson, K. A.; Kropp, K. A.; Forster, T.; Shui, G.; Lacaze, P.; Watterson, S.; Griffiths, S. J.; Spann, N. J.; Meljon, A.; Talbot, S.;

Krishnan, K.; Covey, D. F.; Wenk, M. R.; Craigon, M.; Ruzsics, Z.; Haas, J.; Angulo, A.; Griffiths, W. J.; Glass, C. K.; Wang, Y.; Ghazal, P. *Immunity* **2013**, *38* (1), 106–118.

(184) Liu, S.-Y.; Aliyari, R.; Chikere, K.; Li, G.; Marsden, M. D.; Smith, J. K.; Pernet, O.; Guo, H.; Nusbaum, R.; Zack, J. A.; Freiberg, A. N.; Su, L.; Lee, B.; Cheng, G. *Immunity* **2013**, *38* (1), 92–105.

(185) Civra, A.; Cagno, V.; Donalisio, M.; Biasi, F.; Leonarduzzi, G.; Poli, G.; Lembo, D. *Sci. Rep.* **2014**, *4*, 7487.

(186) Civra, A.; Colzani, M.; Cagno, V.; Francese, R.; Leoni, V.; Aldini, G.; Lembo, D.; Poli, G. *Free Radic. Biol. Med.* **2020**, *149*, 30–36.

(187) Chen, Y.; Wang, S.; Yi, Z.; Tian, H.; Aliyari, R.; Li, Y.; Chen, G.; Liu, P.; Zhong, J.; Chen, X.; Du, P.; Su, L.; Qin, F. X.-F.; Deng, H.; Cheng, G. *Sci. Rep.* **2014**, *4* (1), 7242.

(188) Nishimura, T.; Inoue, T.; Shibata, N.; Sekine, A.; Takabe, W.; Noguchi, N.; Arai, H. *Genes to Cells* **2005**, *10* (8), 793–801.

(189) Roberts, B. L.; Severance, Z. C.; Bensen, R. C.; Le, A. T.; Kothapalli, N. R.; Nunez, J. I.; Ma, H.; Wu, S.; Standke, S. J.; Yang, Z.; Reddig, W. J.; Blewett, E. L.; Burgett, A. W. G. *ACS Chem. Biol.* **2019**, *14* (2), 276–287.

(190) Roberts, B. L.; Severance, Z. C.; Bensen, R. C.; Le-McClain, A. T.; Malinky, C. A.; Mettenbrink, E. M.; Nunez, J. I.; Reddig, W. J.; Blewett, E. L.; Burgett, A. W. G. *Antiviral Res.* **2019**, *170*, 104548.

(191) Garcia-Prieto, C.; Riaz Ahmed, K. B.; Chen, Z.; Zhou, Y.; Hammoudi, N.; Kang, Y.; Lou, C.; Mei, Y.; Jin, Z.; Huang, P. *J. Biol. Chem.* **2013**, *288* (5), 3240–3250.

(192) Shoemaker, R. H. *Nature reviews. Cancer*. England October 2006, pp 813–823.

(193) Rabow, A. A.; Shoemaker, R. H.; Sausville, E. A.; Covell, D. G. *J. Med. Chem.* **2002**, *45* (4), 818–840.

(194) Zhou, Y.; Garcia-Prieto, C.; Carney, D. A.; Xu, R.; Pelicano, H.; Kang, Y.; Yu, W.; Lou, C.; Kondo, S.; Liu, J.; Harris, D. M.; Estrov, Z.; Keating, M. J.; Jin, Z.; Huang, P. *J. Natl. Cancer Inst.* **2005**, *97* (23), 1781–1785.

(195) Dirsch, V. M.; Muller, I. M.; Eichhorst, S. T.; Pettit, G. R.; Kamano, Y.; Inoue, M.; Xu, J.-P.; Ichihara, Y.; Wanner, G.; Vollmar, A. M. *Cancer Res.* **2003**, *63* (24), 8869–8876.

(196) Rudy, A.; Lopez-Anton, N.; Dirsch, V. M.; Vollmar, A. M. *J. Nat. Prod.* **2008**, *71* (3), 482–486.

(197) Beutler, J. A.; Shoemaker, R. H.; Johnson, T.; Boyd, M. R. *J. Nat. Prod.* **1998**, *61* (12), 1509–1512.

(198) Iglesias-Arteaga, M. A.; Morzycki, J. W. *Alkaloids. Chem. Biol.* **2013**, *72*, 153–279.

(199) Heinz, B. A.; Vance, L. M. *J. Virol.* **1995**, *69* (7), 4189–4197.

(200) Brown-Augsburger, P.; Vance, L. M.; Malcolm, S. K.; Hsiung, H.; Smith, D. P.; Heinz, B. A. *Arch. Virol.* **1999**, *144* (8), 1569–1585.

(201) Stockwell, B. R. *Nat. Rev. Genet.* **2000**, *1* (2), 116–125.

(202) Schreiber, S. *C&EN*. 2003, pp 51–61.

(203) Wells, W. A. *J. Cell Biol.* **2005**, *169* (4), 552.

(204) Seto, B. *Clin. Transl. Med.* **2012**, *1* (1), 29.

(205) Feher, M.; Schmidt, J. M. *J. Chem. Inf. Comput. Sci.* **2003**, *43* (1), 218–227.

(206) Colegate, Steven M. Molyneax, R. J. *Bioactive Natural Products: Detection, Isolation, and Structure Determination*, 2nd Editio.; Taylor & Francis Group: Boca Raton, FL, 2008.

(207) Kumar, K.; Waldmann, H. *Isr. J. Chem.* **2019**, *59* (1–2), 41–51.

(208) Lehto, M.; Laitinen, S.; Chinetti, G.; Johansson, M.; Ehnholm, C.; Staels, B.; Ikonen, E.; Olkkonen, V. M. *J. Lipid Res.* **2001**, *42* (8), 1203–1213.

(209) Abzug, M. J. *J. Infect.* **2014**, *68 Suppl 1*, S108-14.

(210) Jin, J.; Jin, X.; Qian, C.; Ruan, Y.; Jiang, H. *Mol. Med. Rep.* **2013**, *7* (5), 1646–1650.

(211) Zhu, J.; Xiong, L.; Yu, B.; Wu, J. *Mol. Pharmacol.* **2005**, *68* (6), 1831–1838.

(212) Nunez, J. I. The Ligand Binding Properties of the Oxysterol-Binding Protein Subfamily 1, University of Oklahoma, 2018.

(213) REED, L. J.; MUENCH, H. *Am. J. Epidemiol.* **1938**, *27* (3), 493–497.

(214) Roberts, B. L. Exploring the Cellular Effects of Small Molecule Inhibitors of Oxysterol-Binding Protein, 2018.

(215) Ma, H.; Delafield, D. G.; Wang, Z.; You, J.; Wu, S. *J. Am. Soc. Mass Spectrom.* **2017**, *28* (4), 655–663.

(216) Wang, Z.; Ma, H.; Smith, K.; Wu, S. *Int. J. Mass Spectrom.* **2018**, *427*, 43–51.

(217) Chen, C.; Huang, H.; Wu, C. H. *Methods Mol. Biol.* **2017**, *1558*, 3–39.

(218) Kim, S.; Pevzner, P. A. *Nat. Commun.* **2014**, *5*, 5277.

(219) Yang, F.; Shen, Y.; Camp, D. G. 2nd; Smith, R. D. *Expert Rev. Proteomics* **2012**, *9* (2), 129–134.

(220) Taylor, F. R.; Kandutsch, A. A. *Methods Enzymol.* **1985**, *110*, 9–19.

(221) Kumei, Y.; Nakajima, T.; Sato, A.; Kamata, N.; Enomoto, S. *J. Cell Sci.* **1989**, *93* (2), 221 LP – 226.

(222) Strating, J. R. P. M.; van der Linden, L.; Albulescu, L.; Bigay, J.; Arita, M.; Delang, L.; Leyssen, P.; van der Schaar, H. M.; Lanke, K. H. W.; Thibaut, H. J.; Ulferts, R.; Drin, G.; Schlinck, N.; Wubbolts, R. W.; Sever, N.; Head, S. A.; Liu, J. O.; Beachy, P. A.; DeMatteis, M. A.; Shair, M. D.; Olkkonen, V. M.; Neyts, J.; van Kuppeveld, F. J. M. *Cell Rep.* **2015**, *10* (4), 600–615.

(223) Bauer, L.; Ferla, S.; Head, S. A.; Bhat, S.; Pasunooti, K. K.; Shi, W. Q.; Albulescu, L.; Liu, J. O.; Brancale, A.; van Kuppeveld, F. J. M.; Strating, J. R. P. M. *Antiviral Res.* **2018**, *156*, 55–63.

(224) Albulescu, L.; Strating, J. R. P. M.; Thibaut, H. J.; van der Linden, L.; Shair, M. D.; Neyts, J.; van Kuppeveld, F. J. M. *Antiviral Res.* **2015**, *117*, 110–114.

(225) Gaston, K.; Jayaraman, P.-S. *Cell. Mol. Life Sci. C.* **2003**, *60* (4), 721–741.

(226) Lee, T. I.; Young, R. A. *Cell* **2013**, *152* (6), 1237–1251.

(227) Spriggs, K. A.; Bushell, M.; Willis, A. E. *Mol. Cell* **2010**, *40* (2), 228–237.

(228) Cooper GM. *The Cell: A Molecular Approach.*, 2nd Editio.; Sinauer Associates: Sunderland, MA, 2000.

(229) Sonenberg, N.; Hinnebusch, A. G. *Cell* **2009**, *136* (4), 731–745.

(230) Mazumder, B.; Seshadri, V.; Fox, P. L. *Trends Biochem. Sci.* **2003**, *28* (2), 91–98.

(231) Barrett, L. W.; Fletcher, S.; Wilton, S. D. *Cell. Mol. Life Sci.* **2012**, *69* (21), 3613–3634.

(232) Knorre, D. G.; Kudryashova, N. V; Godovikova, T. S. *Acta Naturae* **2009**, *1* (3),

29–51.

(233) Karousis, E. D.; Muhlemann, O. *Cold Spring Harb. Perspect. Biol.* **2019**, *11* (2).

(234) Lykke-Andersen, S.; Jensen, T. H. *Nat. Rev. Mol. Cell Biol.* **2015**, *16* (11), 665–677.

(235) Wada, M.; Lokugamage, K. G.; Nakagawa, K.; Narayanan, K.; Makino, S. *Proc. Natl. Acad. Sci.* **2018**, *115* (43), E10157 LP-E10166.

(236) Balistreri, G.; Horvath, P.; Schweingruber, C.; Zund, D.; McInerney, G.; Merits, A.; Muhlemann, O.; Azzalin, C.; Helenius, A. *Cell Host Microbe* **2014**, *16* (3), 403–411.

(237) Fontaine, K. A.; Leon, K. E.; Khalid, M. M.; Tomar, S.; Jimenez-Morales, D.; Dunlap, M.; Kaye, J. A.; Shah, P. S.; Finkbeiner, S.; Krogan, N. J.; Ott, M. *MBio* **2018**, *9* (6), e02126-18.

(238) Le Sage, V.; Cinti, A.; Amorim, R.; Mouland, A. J. *Viruses* **2016**, *8* (6), 152.

(239) Mata, M. A.; Satterly, N.; Versteeg, G. A.; Frantz, D.; Wei, S.; Williams, N.; Schmolke, M.; Peña-Llopis, S.; Brugarolas, J.; Forst, C. V; White, M. A.; García-Sastre, A.; Roth, M. G.; Fontoura, B. M. A. *Nat. Chem. Biol.* **2011**, *7* (10), 712–719.

(240) Weichhart, T.; Hengstschläger, M.; Linke, M. *Nat. Rev. Immunol.* **2015**, *15* (10), 599–614.

(241) Fekete, T.; Pazmandi, K.; Szabo, A.; Bacsi, A.; Koncz, G.; Rajnavölgyi, E. *J. Leukoc. Biol.* **2014**, *96* (4), 579–589.

(242) Deng, S.; Yu, B.; Lou, Y.; Hui, Y. *J. Org. Chem.* **1999**, *64* (1), 202–208.

(243) Xue, J.; Liu, P.; Pan, Y.; Guo, Z. *J. Org. Chem.* **2008**, *73* (1), 157–161.

(244) Bensen, R. C. Personalized Medicine: Developing Precision Antiviral/Anticancer Therapeutics and Bio-Analytical Chemotheropeutic Drug Monitoring, 2020.

(245) Pan, N.; Rao, W.; Kothapalli, N. R.; Liu, R.; Burgett, A. W. G.; Yang, Z. *Anal. Chem.* **2014**, *86* (19), 9376–9380.

(246) Anders, S.; McCarthy, D. J.; Chen, Y.; Okoniewski, M.; Smyth, G. K.; Huber, W.; Robinson, M. D. *Nat. Protoc.* **2013**, *8* (9), 1765–1786.

(247) Glick, D.; Barth, S.; Macleod, K. F. *J. Pathol.* **2010**, *221* (1), 3–12.

(248) González-Rodríguez, Á.; Mayoral, R.; Agra, N.; Valdecantos, M. P.; Pardo, V.; Miquilena-Colina, M. E.; Vargas-Castrillón, J.; Lo Iacono, O.; Corazzari, M.; Fimia, G. M.; Piacentini, M.; Muntané, J.; Boscá, L.; García-Monzón, C.; Martín-Sanz, P.; Valverde, Á. M. *Cell Death Dis.* **2014**, *5* (4), e1179–e1179.

(249) Rabanal-Ruiz, Y.; Otten, E. G.; Korolchuk, V. I. *Essays Biochem.* **2017**, *61* (6), 565–584.

(250) Bao, X.; Zheng, W.; Sugi, N. H.; Agarwala, K. L.; Xu, Q.; Wang, Z.; Tendyke, K.; Lee, W.; Parent, L.; Li, W.; Cheng, H.; Shen, Y.; Taylor, N.; Dezso, Z.; Du, H.; Kotake, Y.; Zhao, N.; Wang, J.; Postema, M.; Woodall-jappe, M.; Takase, Y.; Uenaka, T.; Kingston, D. G. I.; Nomoto, K. **2015**, No. April, 589–601.

(251) Tan, C. Y.; Hagen, T. *PLoS One* **2013**, *8* (5), e63970–e63970.

(252) Gentilella, A.; Kozma, S. C.; Thomas, G. *Biochim. Biophys. Acta* **2015**, *1849* (7), 812–820.

(253) Wang, X.; Proud, C. G. *Physiology* **2006**, *21* (5), 362–369.

(254) http://geneontology.org/.

(255) Hyvonen, M. T.; Uimari, A.; Keinanen, T. A.; Heikkinen, S.; Pellinen, R.;

Wahlfors, T.; Korhonen, A.; Narvanen, A.; Wahlfors, J.; Alhonen, L.; Janne, J. *RNA* **2006**, *12* (8), 1569–1582.

(256) Xu, Y.; Eissa, N. T. *Proc. Am. Thorac. Soc.* **2010**, *7* (1), 22–28.

(257) Gu, X.; Li, A.; Liu, S.; Lin, L.; Xu, S.; Zhang, P.; Li, S.; Li, X.; Tian, B.; Zhu, X.; Wang, X. *Mol. Neurobiol.* **2016**, *53* (9), 6388–6396.

(258) Martinez-Nunez, R. T.; Wallace, A.; Coyne, D.; Jansson, L.; Rush, M.; Ennajdaoui, H.; Katzman, S.; Bailey, J.; Deinhardt, K.; Sanchez-Elsner, T.; Sanford, J. R. *Nucleic Acids Res.* **2017**, *45* (6), 3448–3459.

(259) White, E. S.; Sagana, R. L.; Booth, A. J.; Yan, M.; Cornett, A. M.; Bloomheart, C. A.; Tsui, J. L.; Wilke, C. A.; Moore, B. B.; Ritzenthaler, J. D.; Roman, J.; Muro, A. F. *Exp. Cell Res.* **2010**, *316* (16), 2644–2653.

(260) Ma, X. M.; Yoon, S.-O.; Richardson, C. J.; Jülich, K.; Blenis, J. *Cell* **2008**, *133* (2), 303–313.

(261) Balistreri, G.; Bognanni, C.; Mühlemann, O. *Viruses* **2017**, *9* (1), 24.

(262) Singh, R. P.; Brooks, B. R.; Klauda, J. B. *Proteins* **2009**, *75* (2), 468–477.

(263) Taylor, F. R. In *Regulation of Isopentenoid Metabolism*; ACS Symposium Series; American Chemical Society, 1992; Vol. 497, pp 8–81.

(264) Bowling, N.; Matter, W. F.; Gadski, R. A.; McClure, D. B.; Schreyer, T.; Dawson, P. A.; Vlahos, C. J. *J. Lipid Res.* **1996**, *37* (12), 2586–2598.

(265) Wang, P. -y. *Science (80-.).* **2005**, *307* (5714), 1472–1476.

(266) Yan, D.; Jauhiainen, M.; Hildebrand, R. B.; Willems van Dijk, K.; Van Berkel, T. J. C.; Ehnholm, C.; Van Eck, M.; Olkkonen, V. M. *Arterioscler. Thromb. Vasc. Biol.* **2007**, *27* (7), 1618–1624.

(267) Zhao, K.; Ridgway, N. D. *Cell Rep.* **2017**, *19* (9), 1807–1818.

(268) Lee, S.; Wang, P.-Y.; Jeong, Y.; Mangelsdorf, D. J.; Anderson, R. G. W.; Michaely, P. *Exp. Cell Res.* **2012**, *318* (16), 2128–2142.

(269) Du, X.; Kumar, J.; Ferguson, C.; Schulz, T. A.; Ong, Y. S.; Hong, W.; Prinz, W. A.; Parton, R. G.; Brown, A. J.; Yang, H. *J. Cell Biol.* **2011**, *192* (1), 121–135.

(270) Yan, D.; Mayranpaa, M. I.; Wong, J.; Perttila, J.; Lehto, M.; Jauhiainen, M.; Kovanen, P. T.; Ehnholm, C.; Brown, A. J.; Olkkonen, V. M. *J. Biol. Chem.* **2008**, *283* (1), 332–340.

(271) Nissila, E.; Ohsaki, Y.; Weber-Boyvat, M.; Perttila, J.; Ikonen, E.; Olkkonen, V. M. *Biochim. Biophys. Acta* **2012**, *1821* (12), 1472–1484.

(272) Ngo, M.; Ridgway, N. D. *Mol. Biol. Cell* **2009**, *20* (5), 1388–1399.

(273) Liu, X.; Ridgway, N. D. *PLoS One* **2014**, *9* (9), 1–12.

(274) Waterhouse, A.; Bertoni, M.; Bienert, S.; Studer, G.; Tauriello, G.; Gumienny, R.; Heer, F. T.; de Beer, T. A. P.; Rempfer, C.; Bordoli, L.; Lepore, R.; Schwede, T. *Nucleic Acids Res.* **2018**, *46* (W1), W296–W303.

(275) D.A. Case, K. Belfon, I.Y. Ben-Shalom, S.R. Brozell, D.S. Cerutti, T.E. Cheatham, III, V.W.D. Cruzeiro, T.A. Darden, R.E. Duke, G. Giambasu, M.K. Gilson, H. Gohlke, A.W. Goetz, R Harris, S. Izadi, K. Kasava- jhala, A. Kovalenko, R. Krasny, T. Kurtzman, T., D. M. Y. and P. A. K. *AMBER*; University of California San Francisco, 2018.

(276) Morris, G. M.; Huey, R.; Lindstrom, W.; Sanner, M. F.; Belew, R. K.; Goodsell, D. S.; Olson, A. J. *J. Comput. Chem.* **2009**, *30* (16), 2785–2791.

(277) Trott, O.; Olson, A. J. *J. Comput. Chem.* **2010**, *31* (2), 455–461.

(278) Pettersen, E. F.; Goddard, T. D.; Huang, C. C.; Couch, G. S.; Greenblatt, D. M.; Meng, E. C.; Ferrin, T. E. *J. Comput. Chem.* **2004**, *25* (13), 1605–1612.

(279) Pulfer, M. K.; Murphy, R. C. *J. Biol. Chem.* **2004**, *279* (25), 26331–26338.

(280) Wang, F.; Stappenbeck, F.; Matsui, W.; Parhami, F. *J. Cell. Biochem.* **2017**, *118* (3), 499–509.

(281) Le-McClain, A. T. Design and Synthesis of OSW-1 Analogs and Other Bioactive Small Molecules for Potential Therapeutic Applications, University of Oklahoma, 2018.

(282) Malinky, C. A. Concise Synthesis Methods to Aminosterols and Sterol N-Glycosides for the Development of New OSW-1-Derived Scaffolds, University of Oklahoma, 2020.

(283) Sugano, S.; Miura, R.; Morishima, N. *J. Biochem.* **1996**, *120* (4), 780–787.

(284) Janowski, B. A.; Willy, P. J.; Devi, T. R.; Falck, J. R.; Mangelsdorf, D. J. *Nature* **1996**, *383* (6602), 728–731.

(285) Escajadillo, T.; Wang, H.; Li, L.; Li, D.; Sewer, M. B. *Mol. Cell. Endocrinol.* **2016**, *427*, 73–85.

(286) Devasthanam, A. S. *Virulence* **2014**, *5* (2), 270–277.

(287) Spiegel, M.; Pichlmair, A.; Martínez-Sobrido, L.; Cros, J.; García-Sastre, A.; Haller, O.; Weber, F. *J. Virol.* **2005**, *79* (4), 2079–2086.

(288) Lester, S. N.; Li, K. *J. Mol. Biol.* **2014**, *426* (6), 1246–1264.

(289) Uematsu, S.; Akira, S. *J. Biol. Chem.* **2007**, *282* (21), 15319–15323.

(290) Schroepfer, G. J. *Physiol. Rev.* **2000**, *80* (1), 361–554.

(291) Bloom, J.; Amador, V.; Bartolini, F.; DeMartino, G.; Pagano, M. *Cell* **2003**, *115*

(1), 71–82.

Appendix 1: Chapter 2 Supplemental

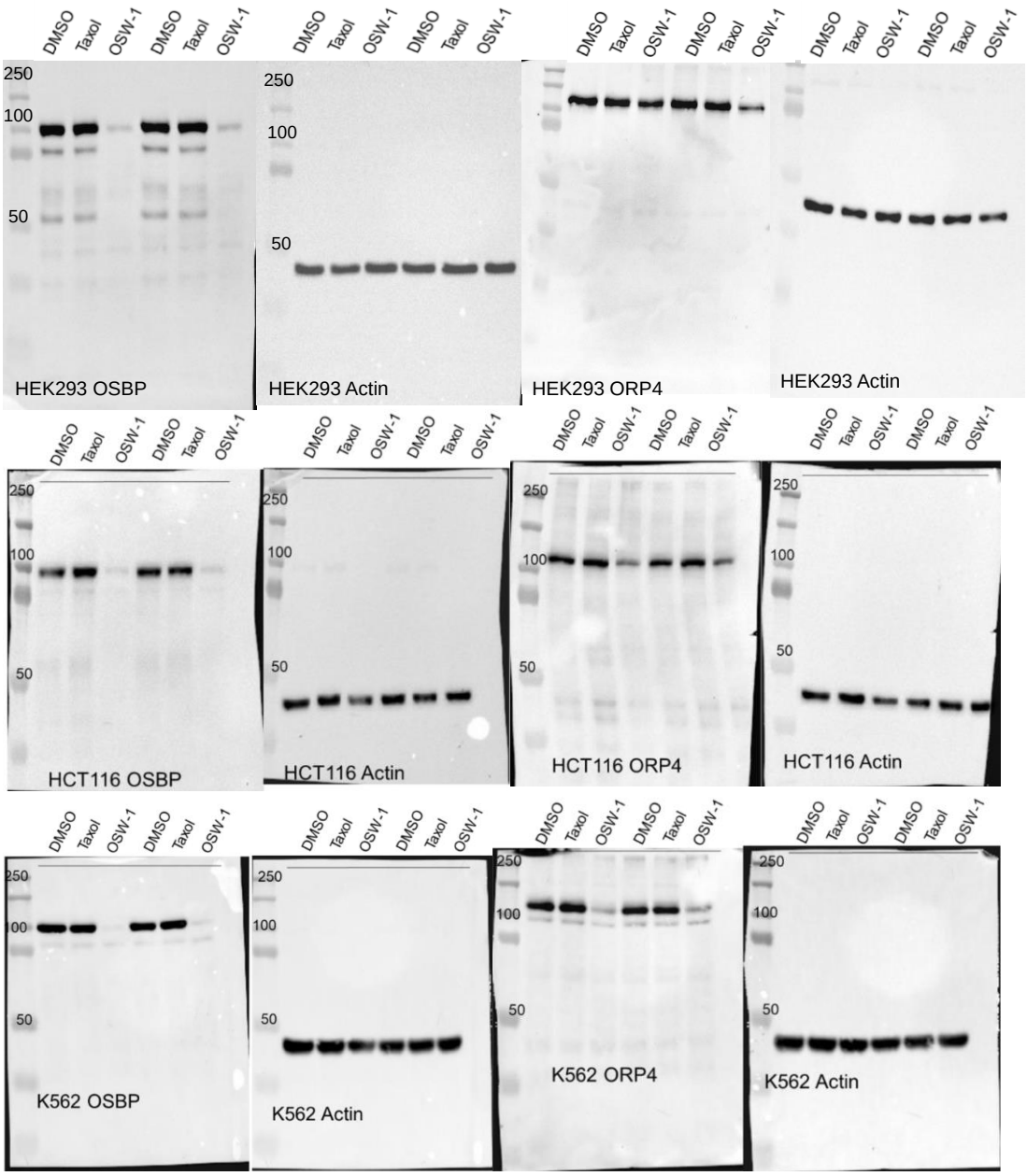

Figure 39: Full Western blots of Figure 6.

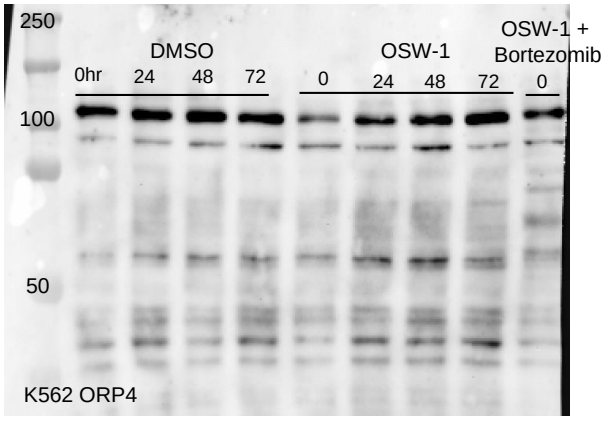

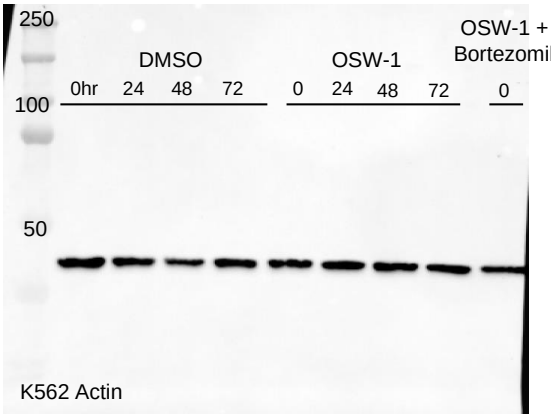

Figure 40: Full Western blots of Figure 7.

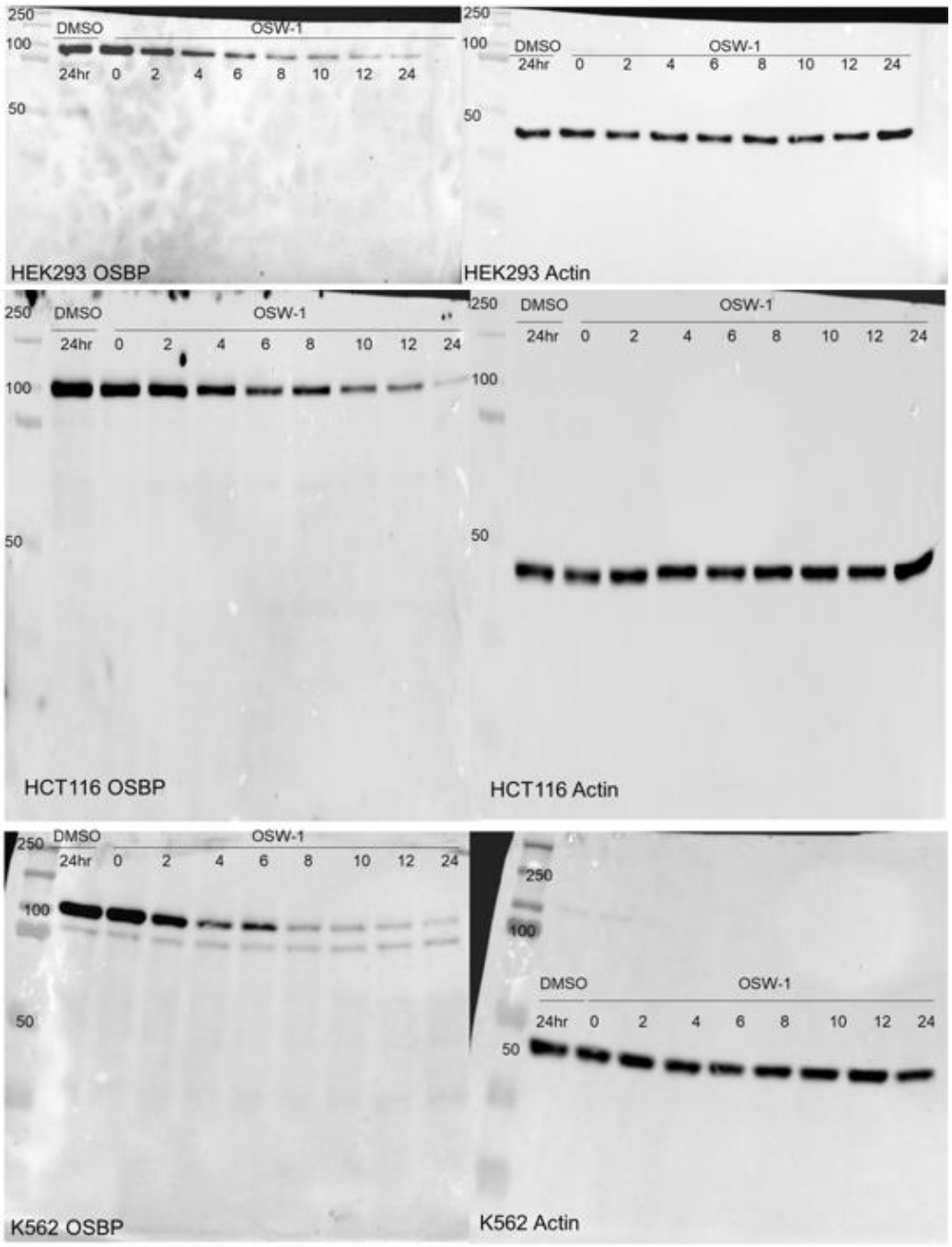

Figure 41: Full OSBP Western blots of Figure 8A.

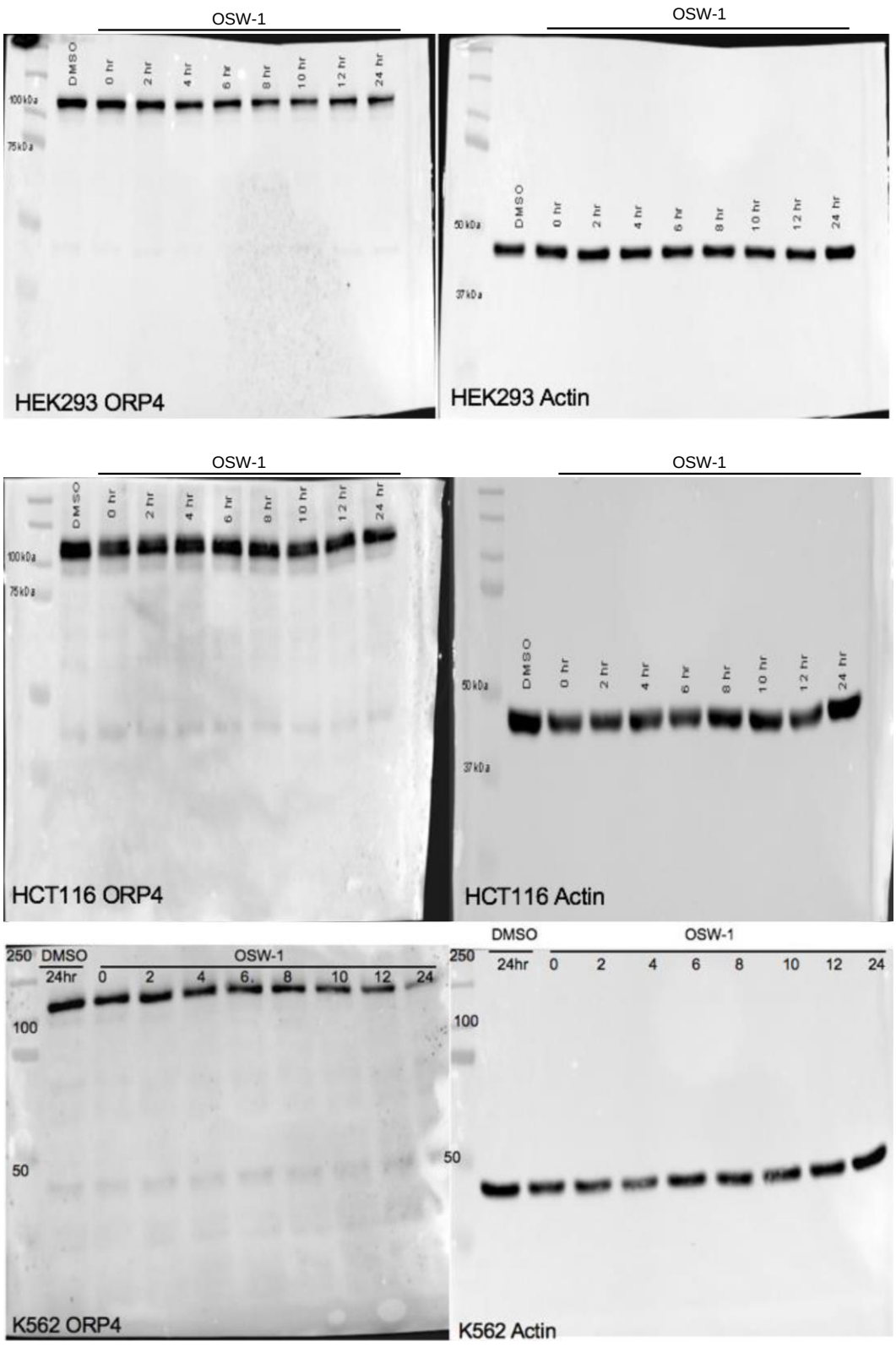

Figure 42: Full ORP4 Western blots of Figure 8B.

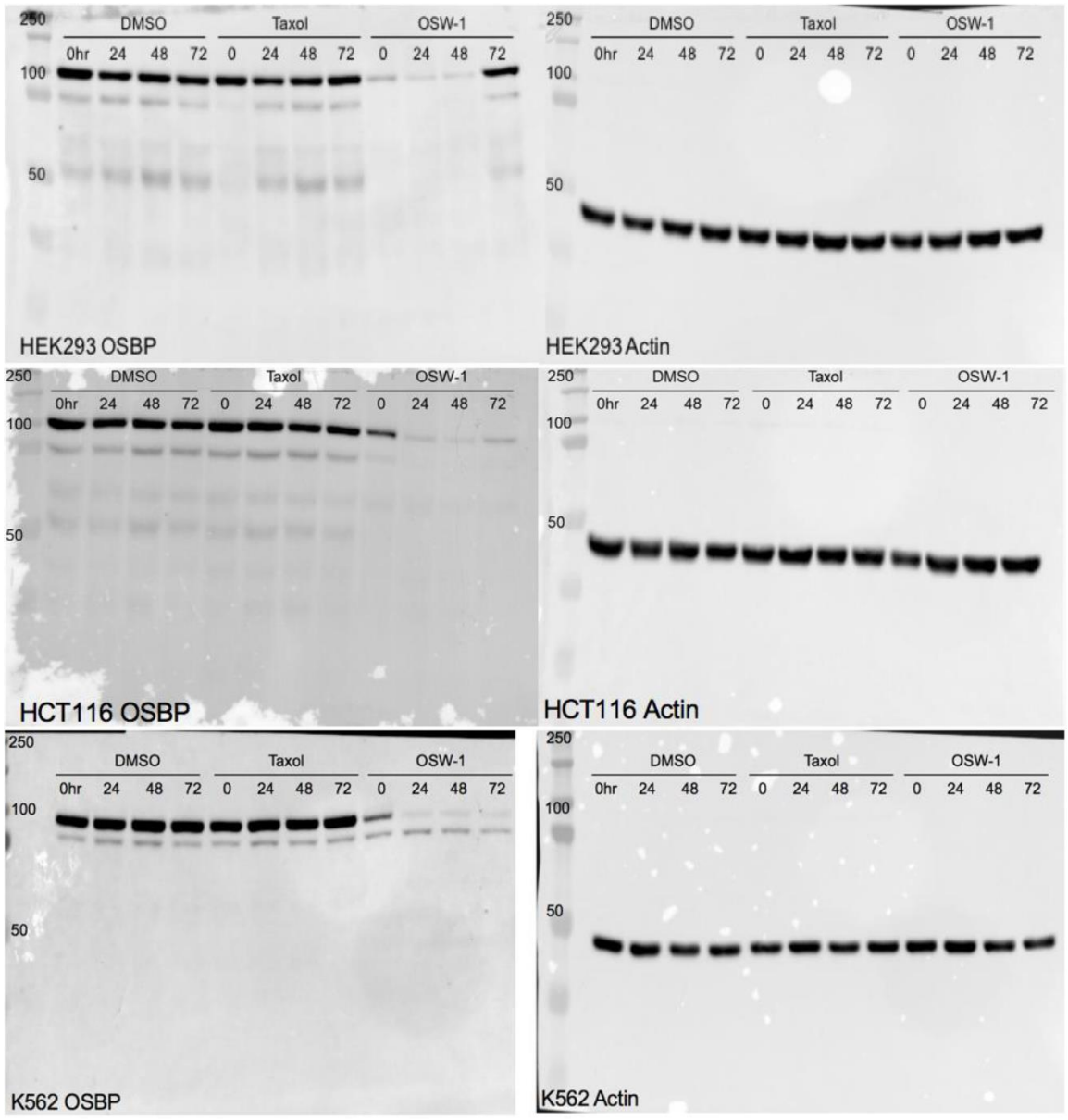

Figure 43: Full Western blots of Figure 10A.

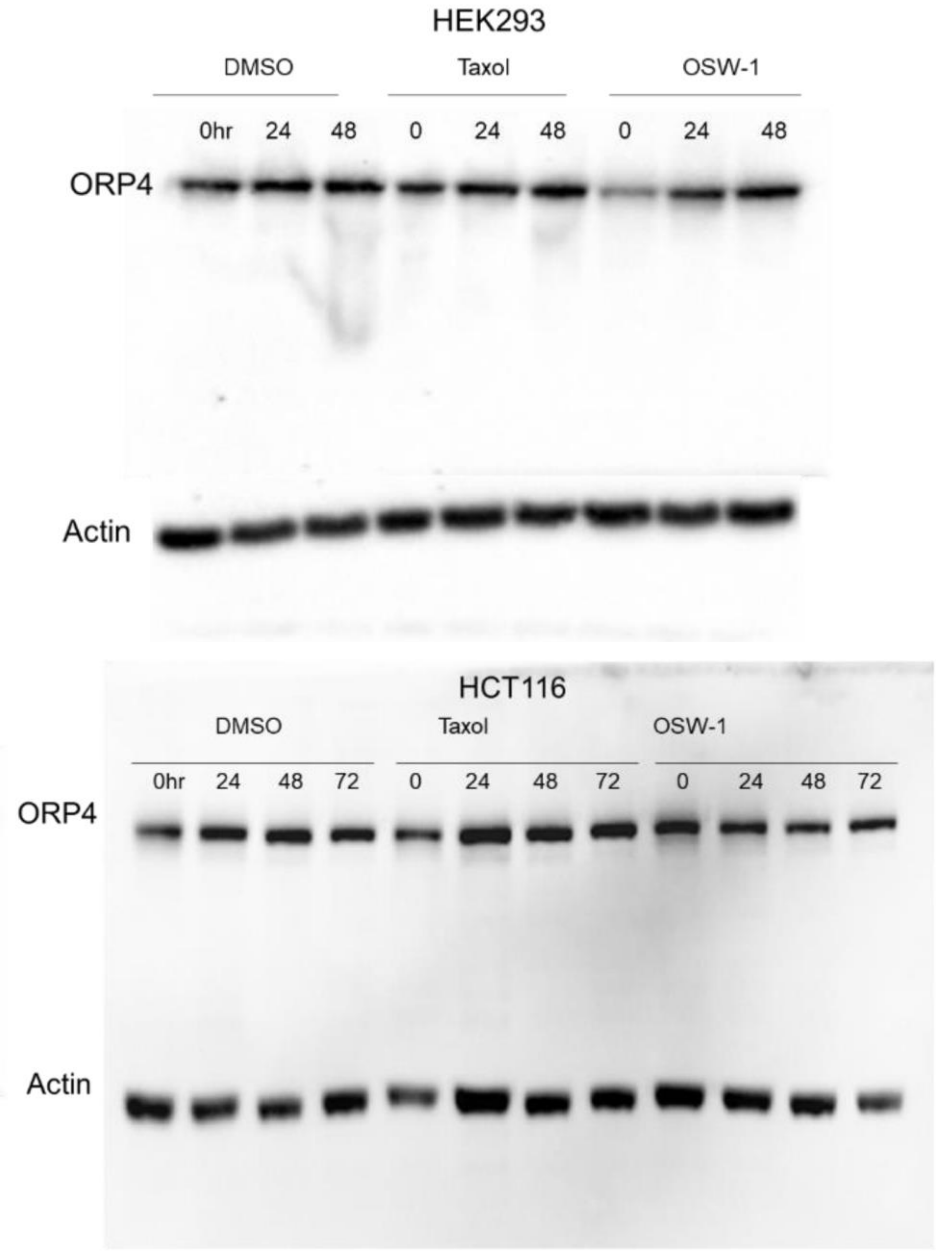

Figure 44: Full Western blots of Figure 10B.

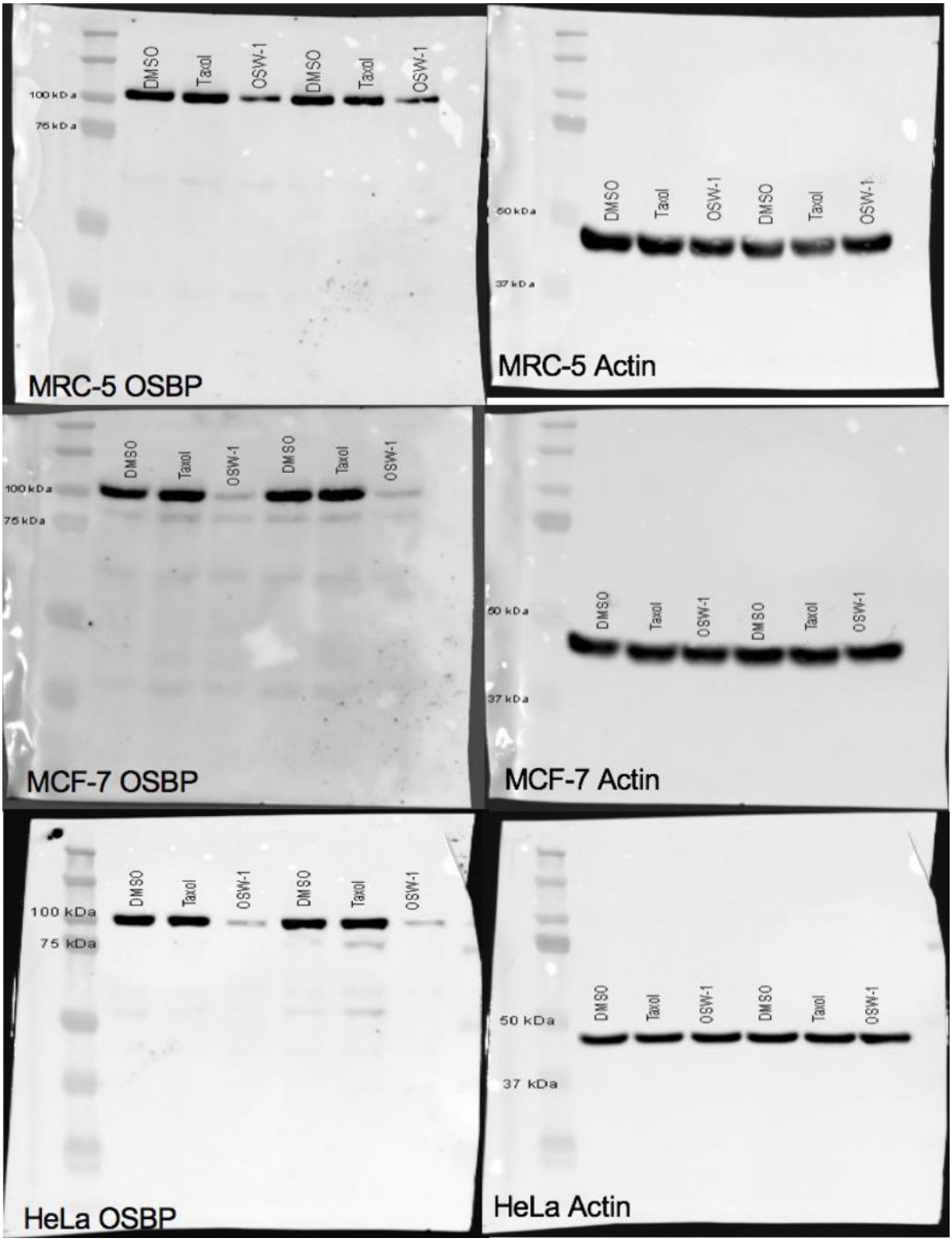

Figure 45: Full Western blots of Figure 12A.

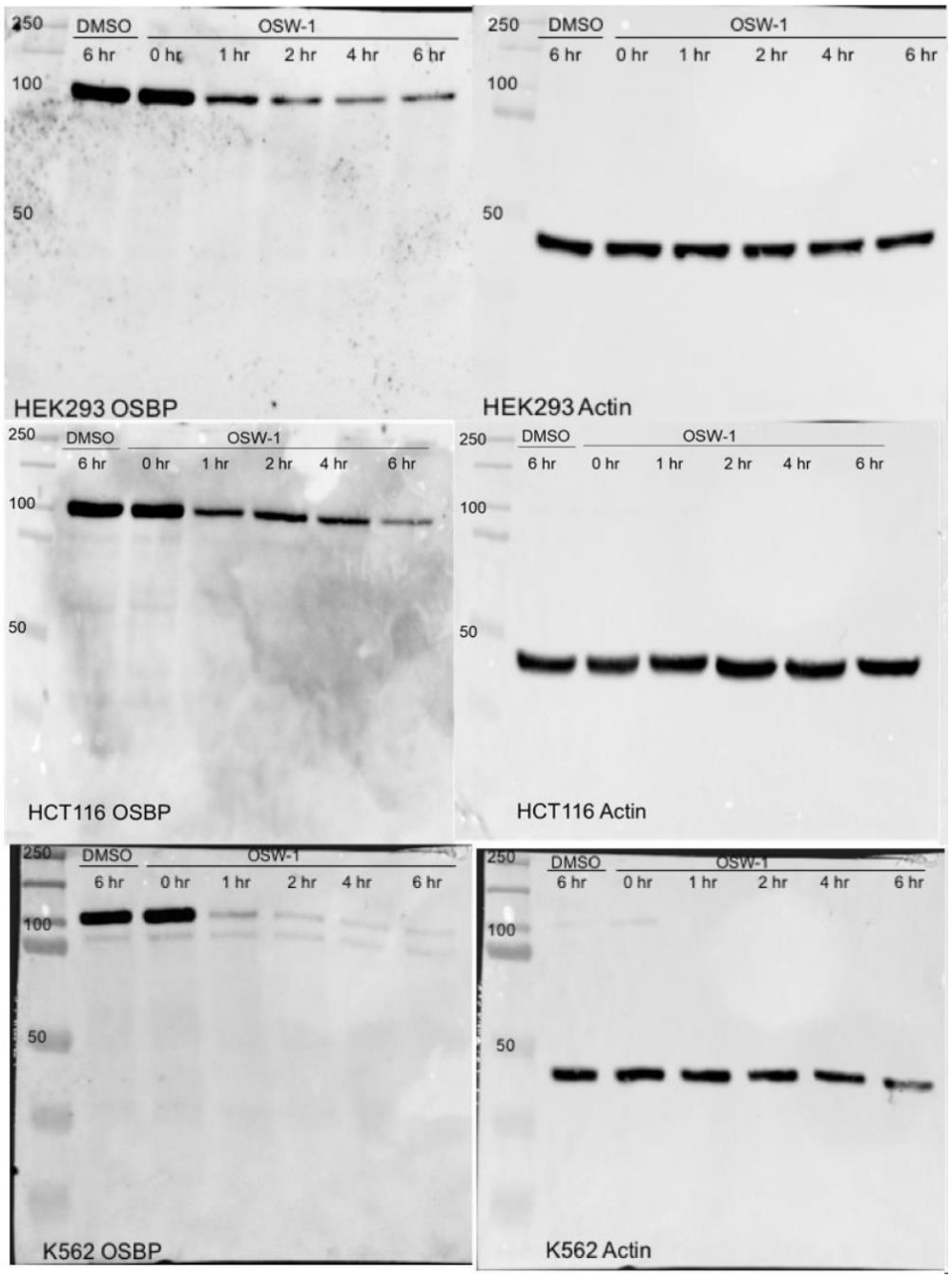

Figure 46: Full Western blots of Figure 12B.

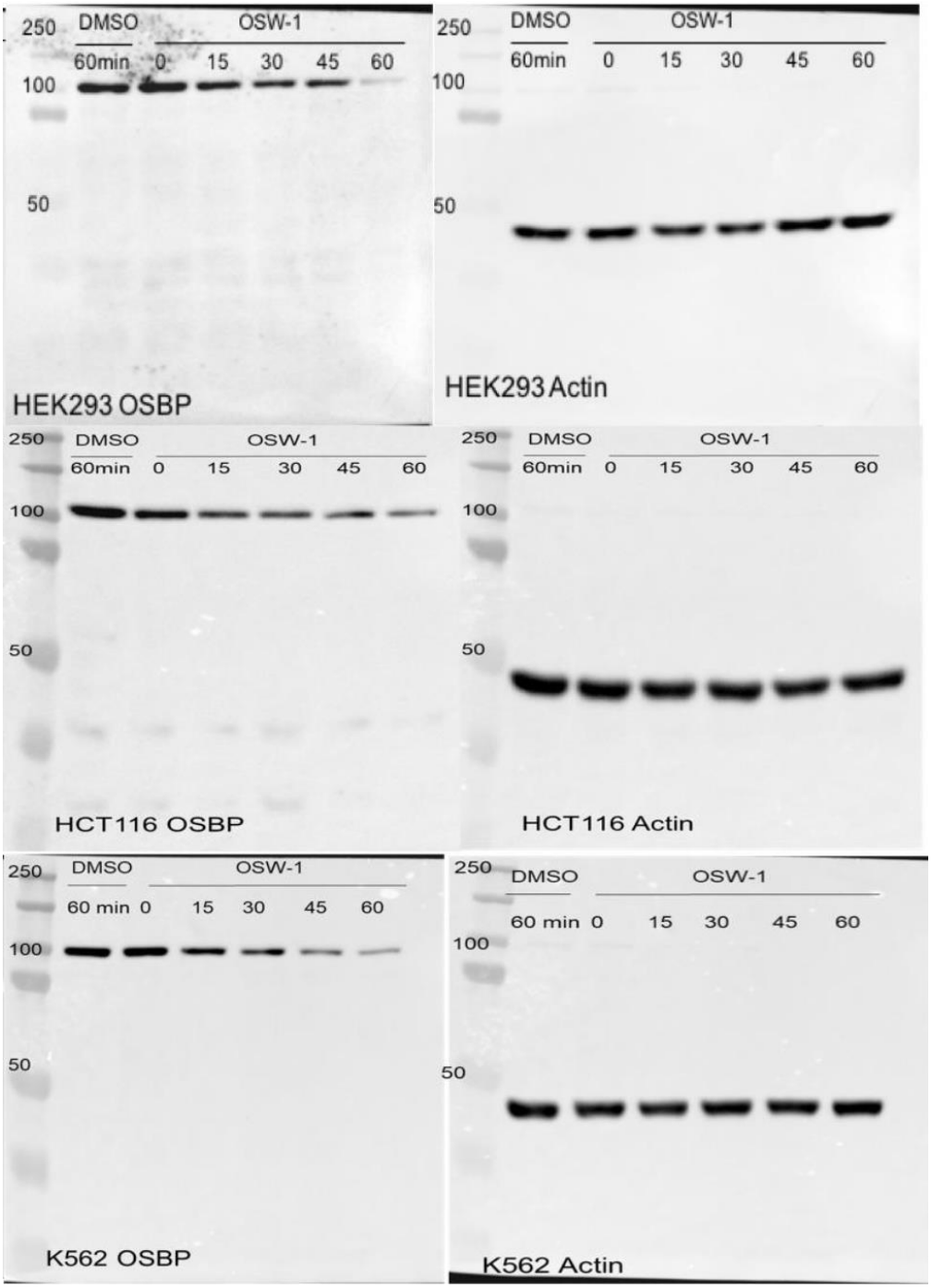

Figure 47: Full Western blots of Figure 12C.

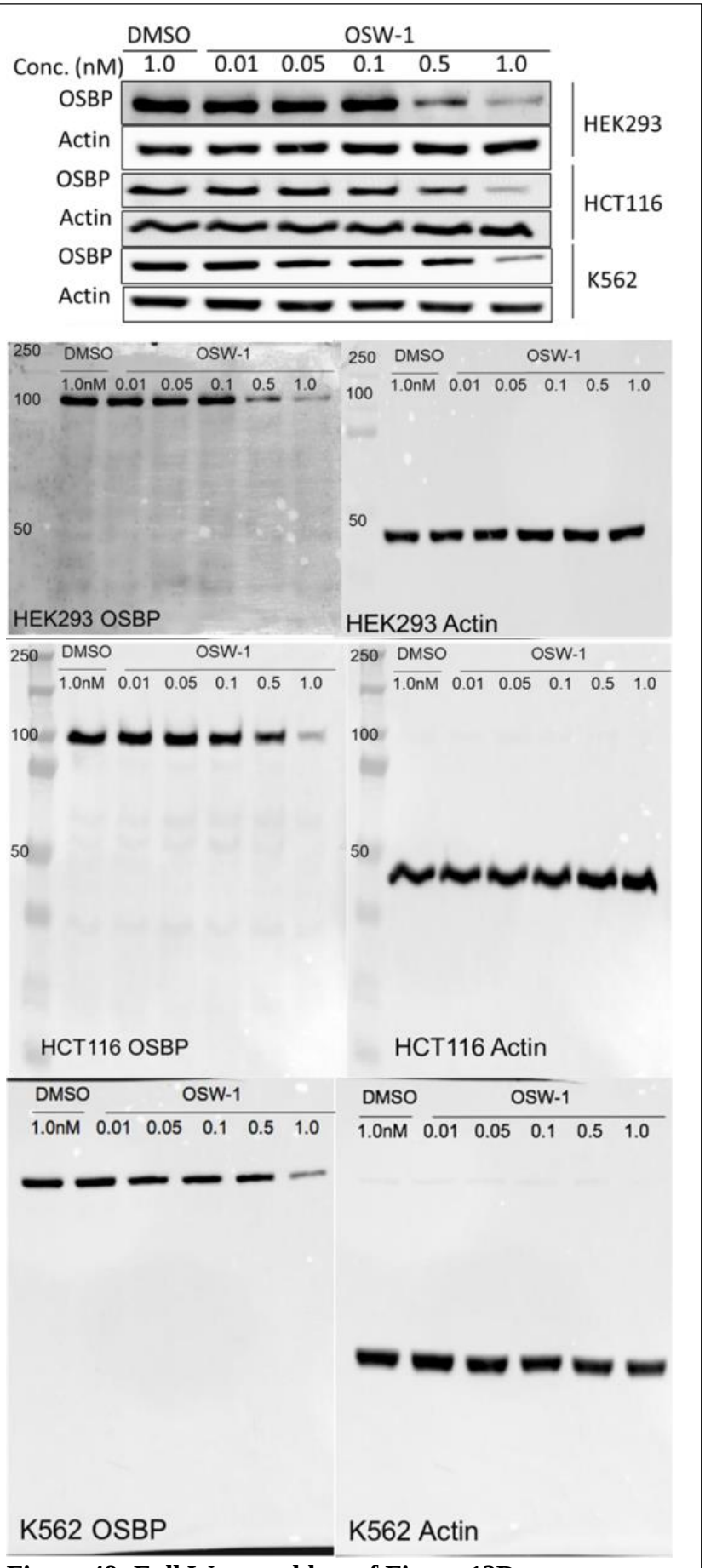

Figure 48: Full Western blots of Figure 12D.

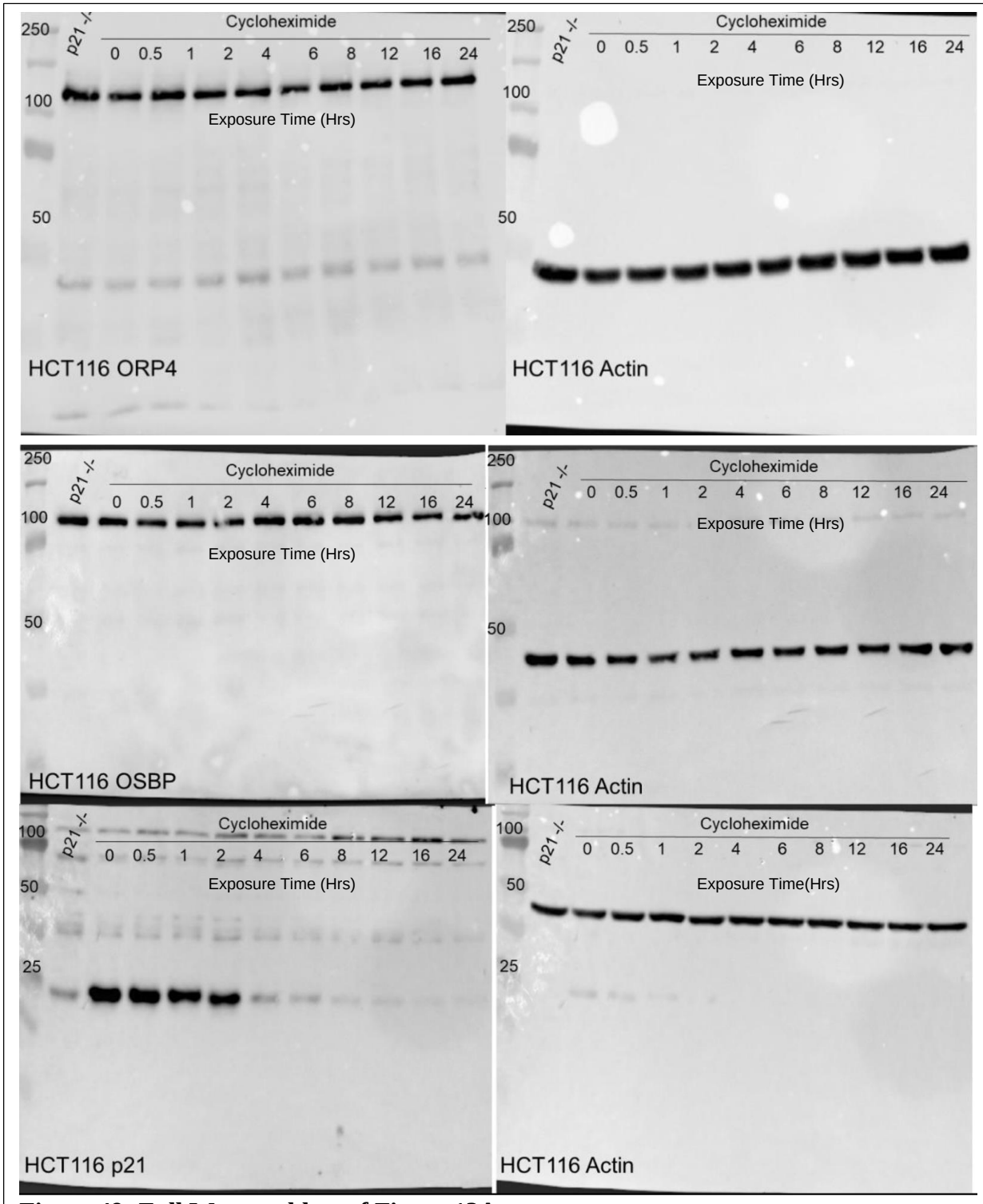

Figure 49: Full Western blots of Figure 13A.

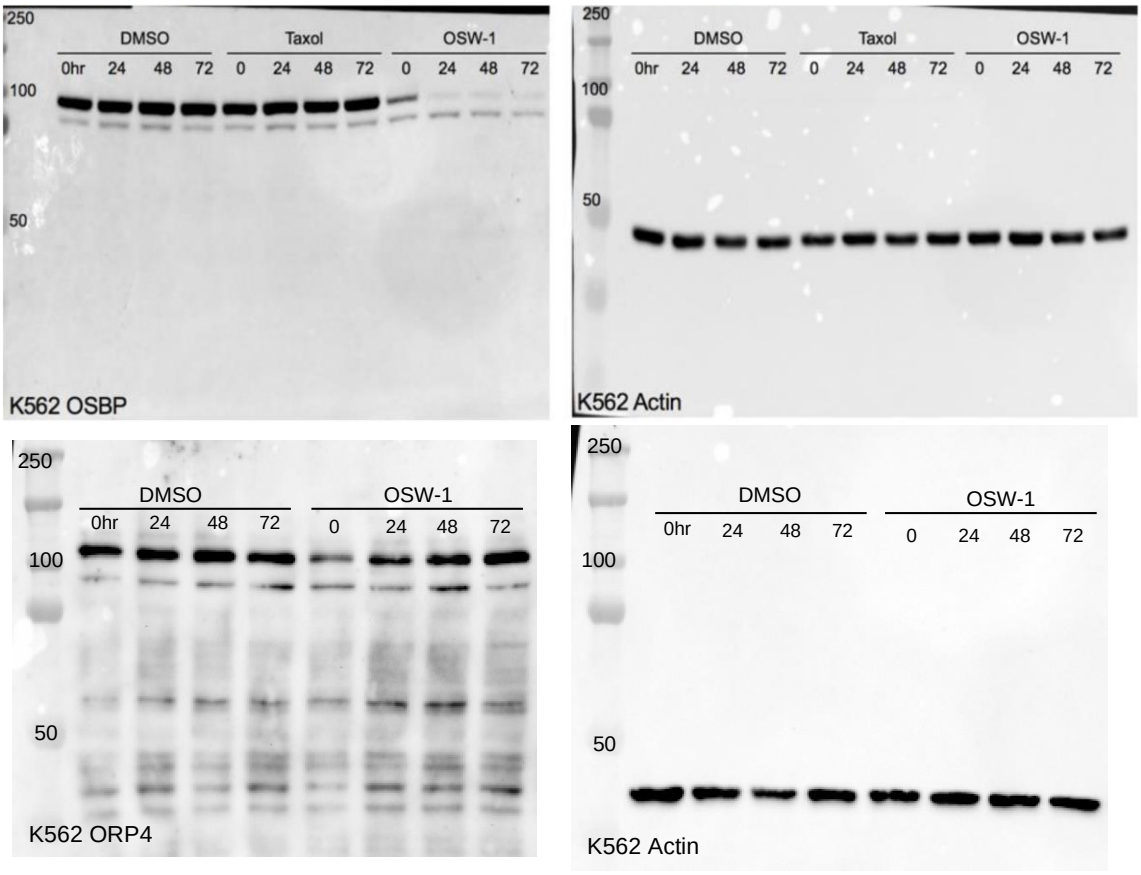

Figure 50: Full Western blots of Figure 13B.

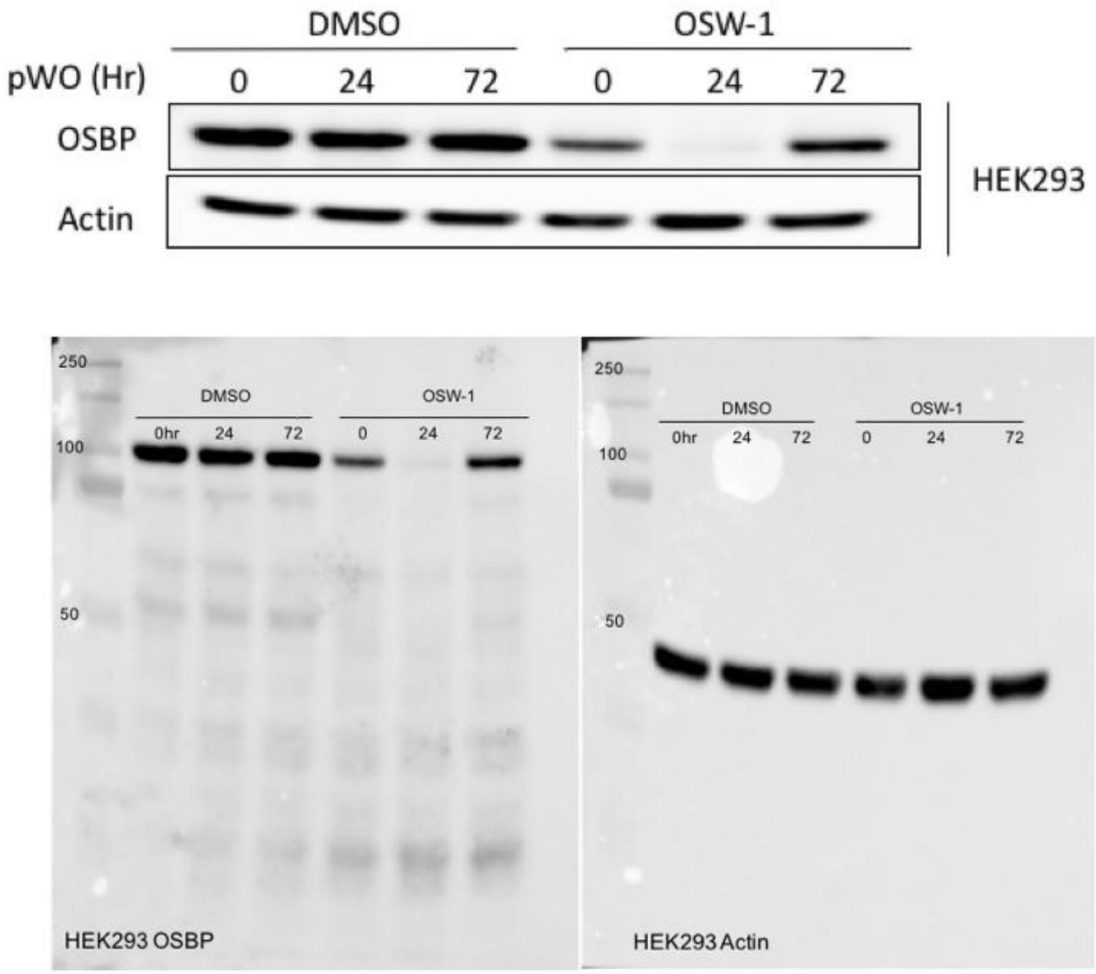

Figure 51: Full Western blot of lysate for iTRAQ proteomic mass spectrometry analysis in Figure 14.

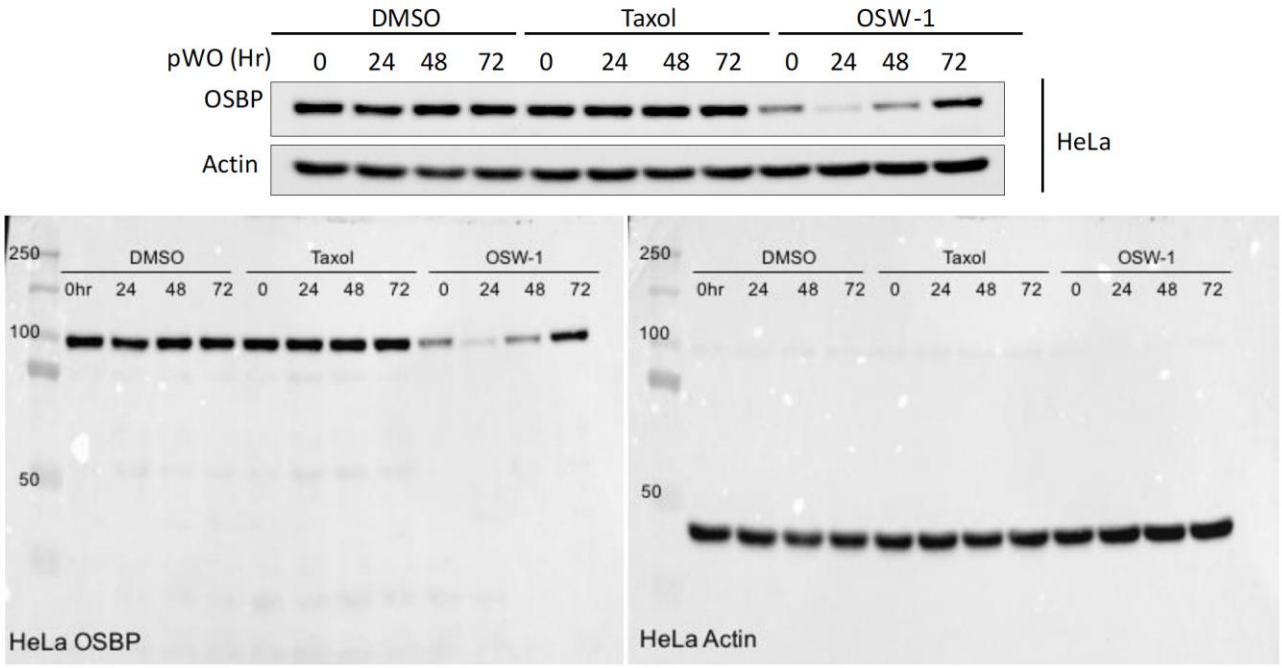

Figure 52: Full Western blot of HeLa cell washout experiment for Figure 15.

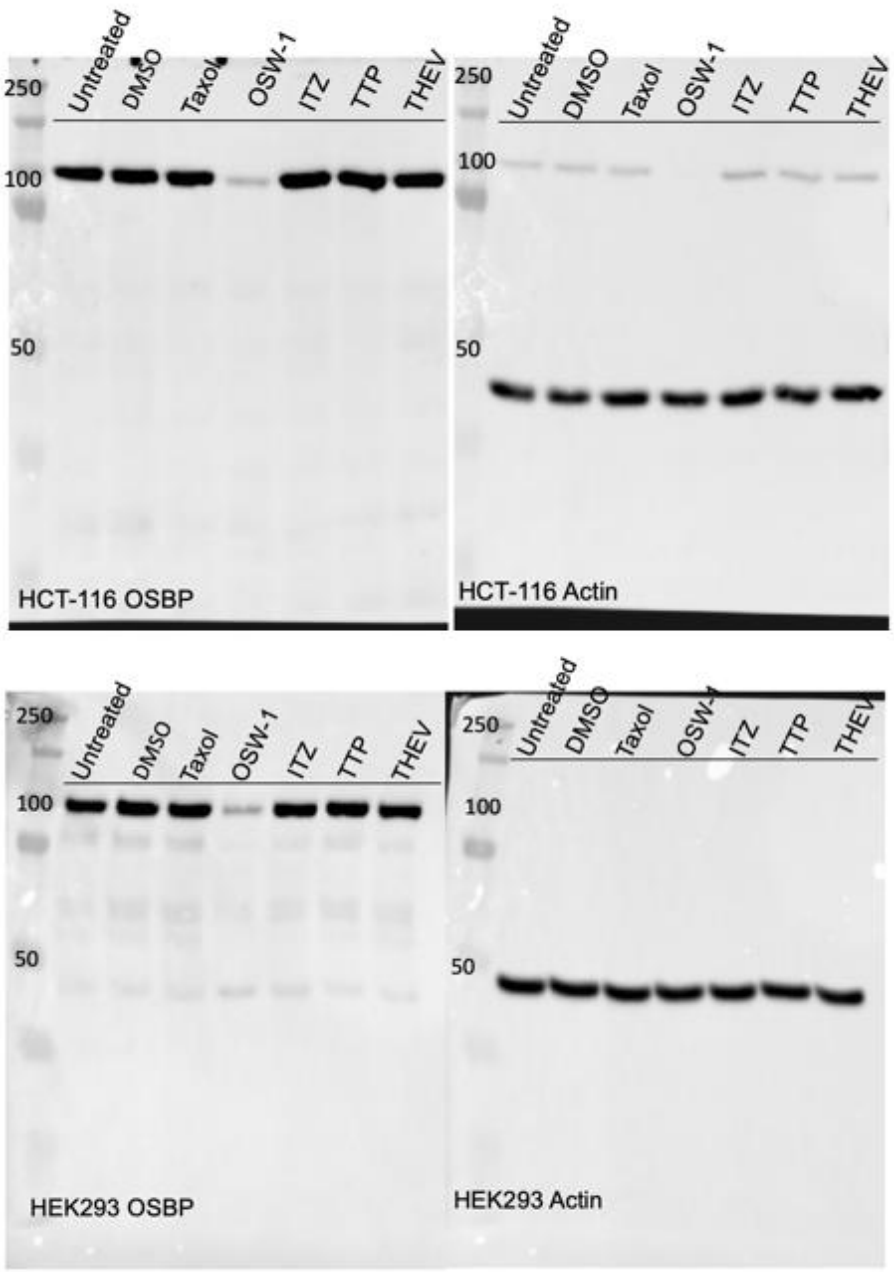

Figure 53: Full Western blots of Figure 16.

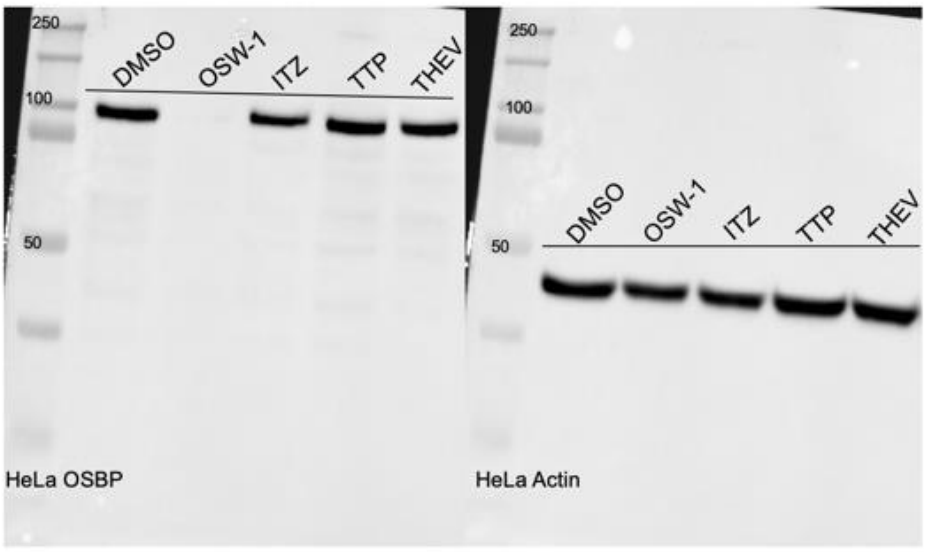

Figure 54: Full Western blots of Figure 17C.

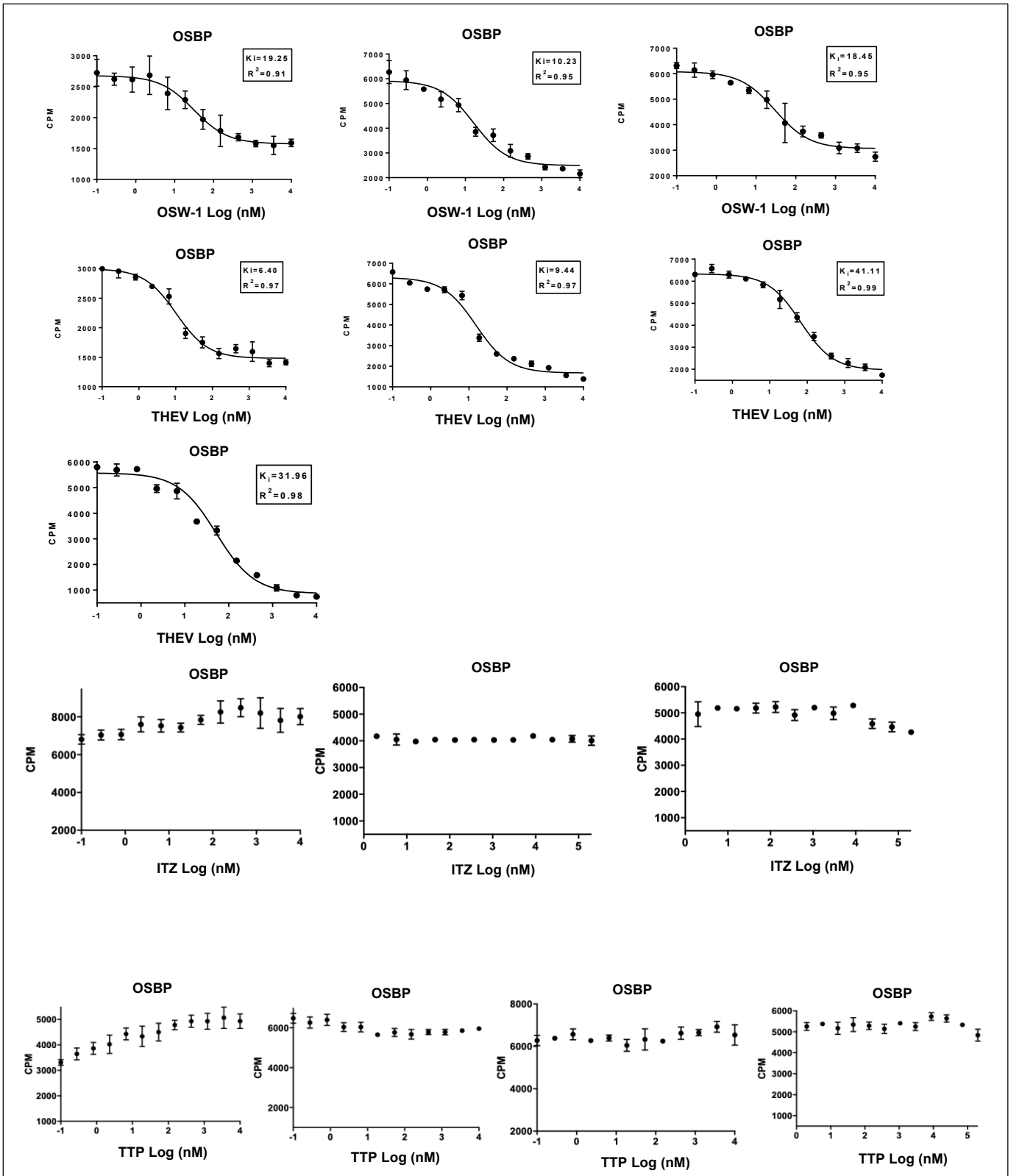

Figure 55: Full OSBP binding curves for Figure 18.

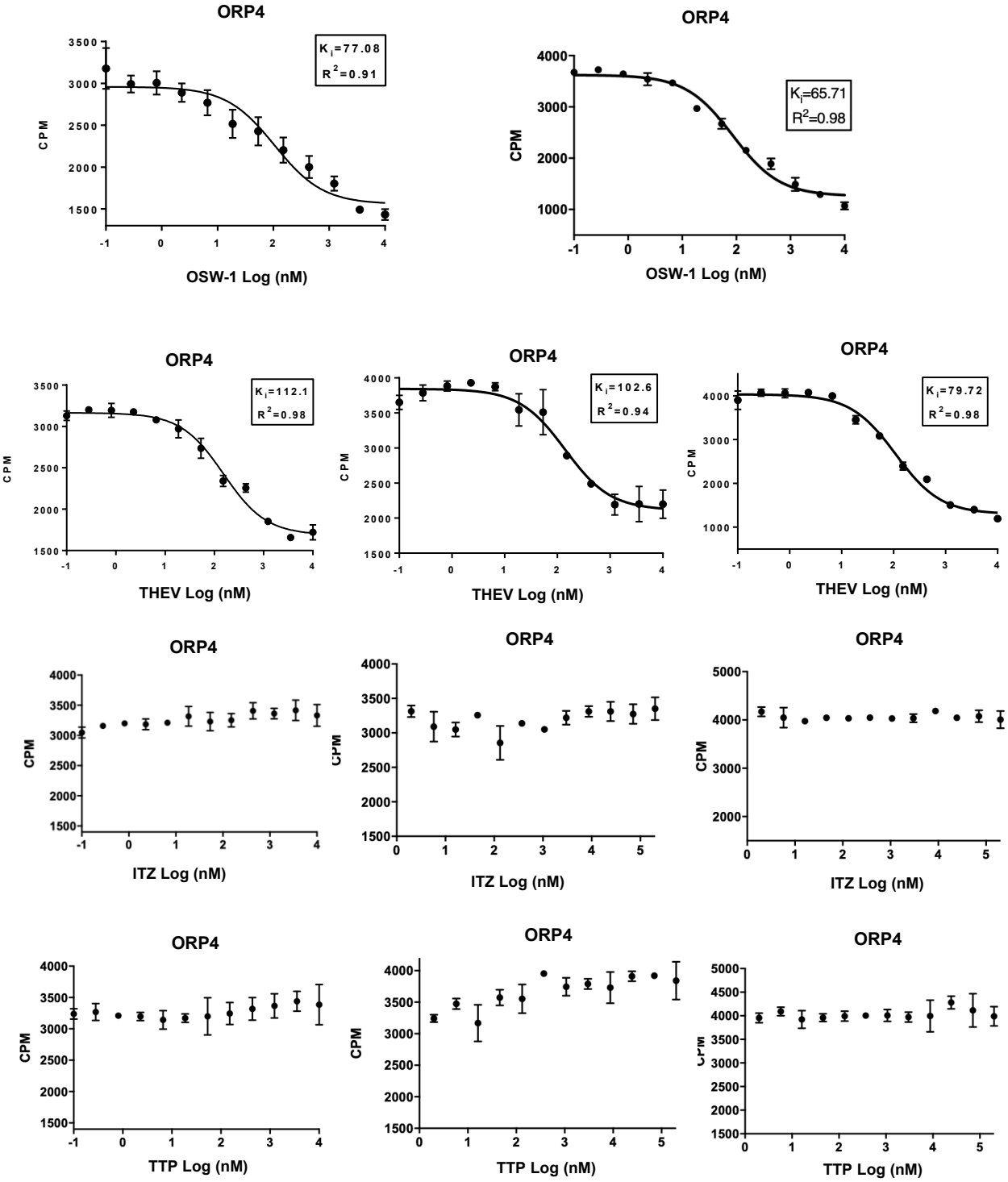

Figure 56: Full ORP4 binding curves for Figure 18.

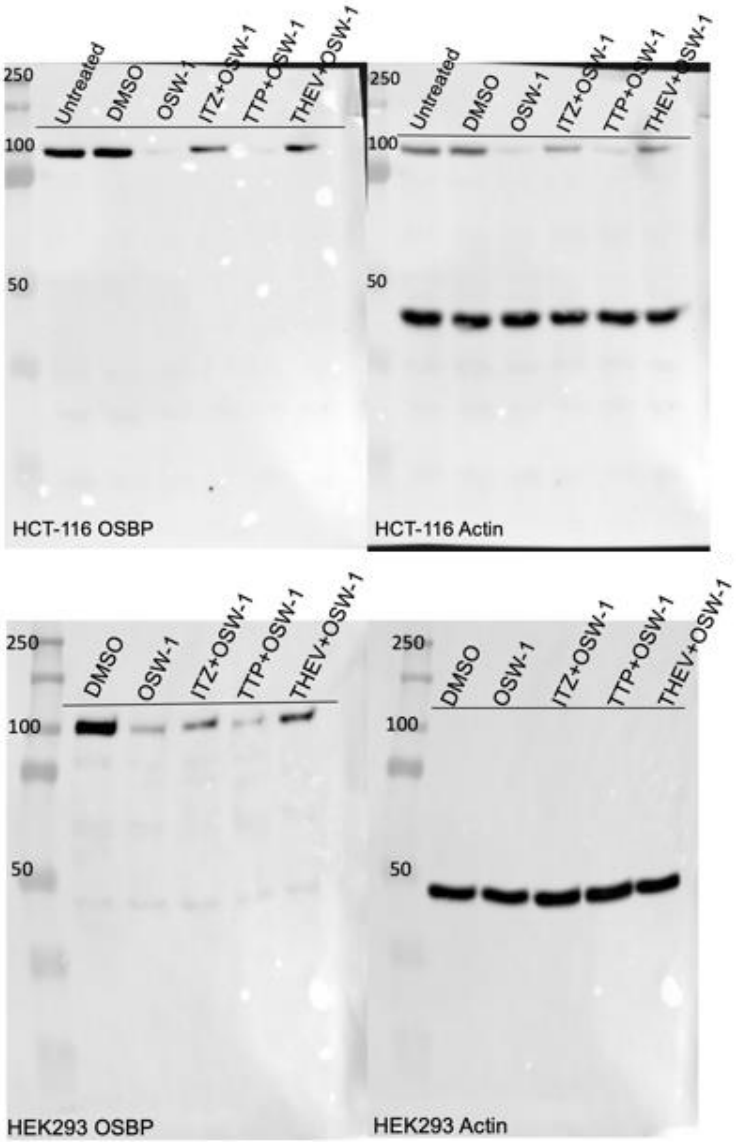

Figure 57: Full Western blot of Figure 19A.

Appendix 2: Chapter 3 Supplemental

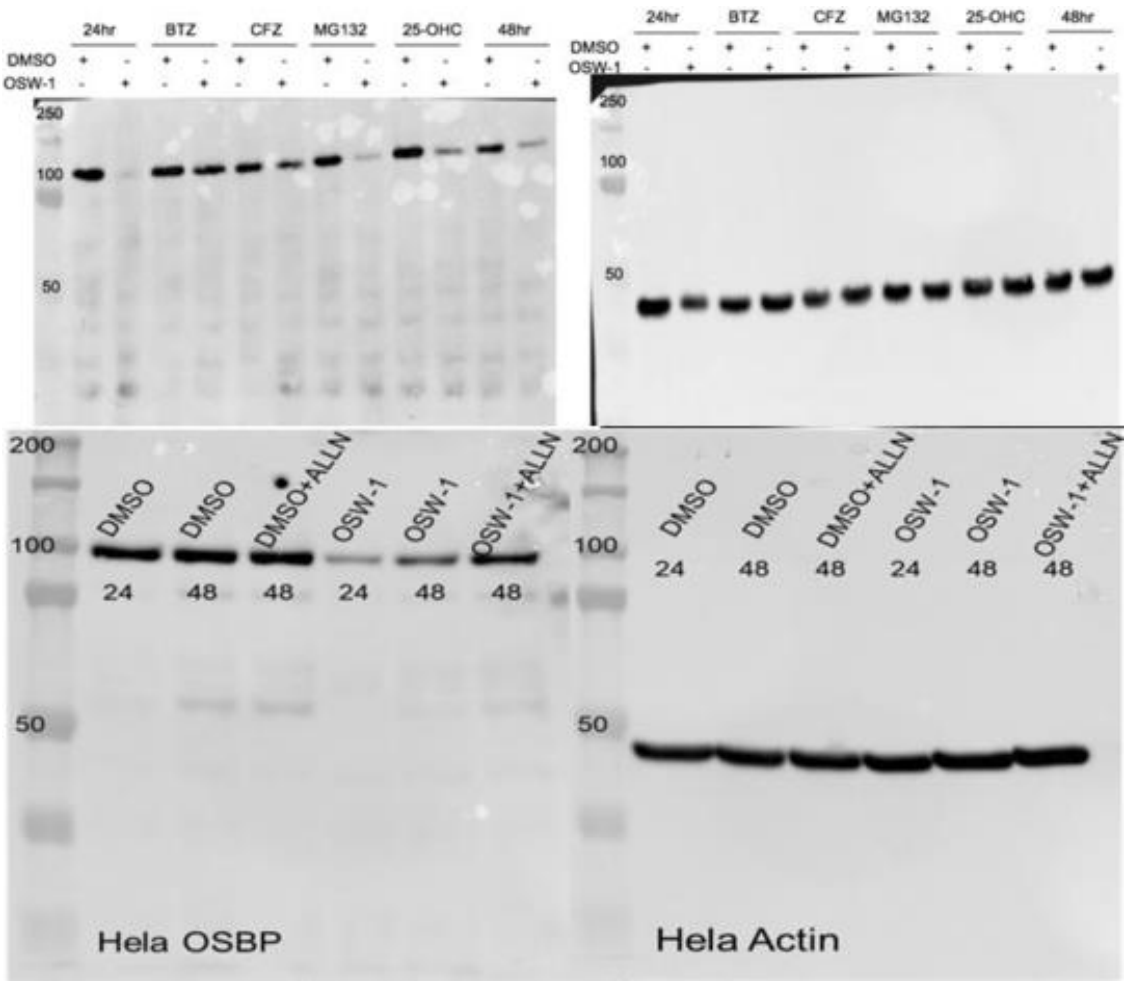

Figure 58: Full Western blots of Figure 23A.

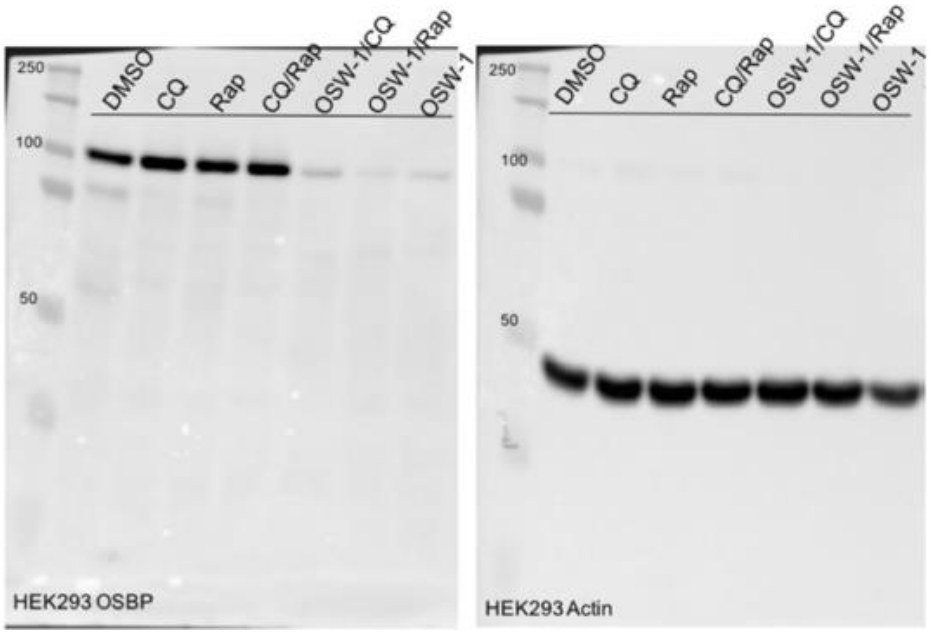

Figure 59: Full Western blots of Figure 23B and Figure 25A.

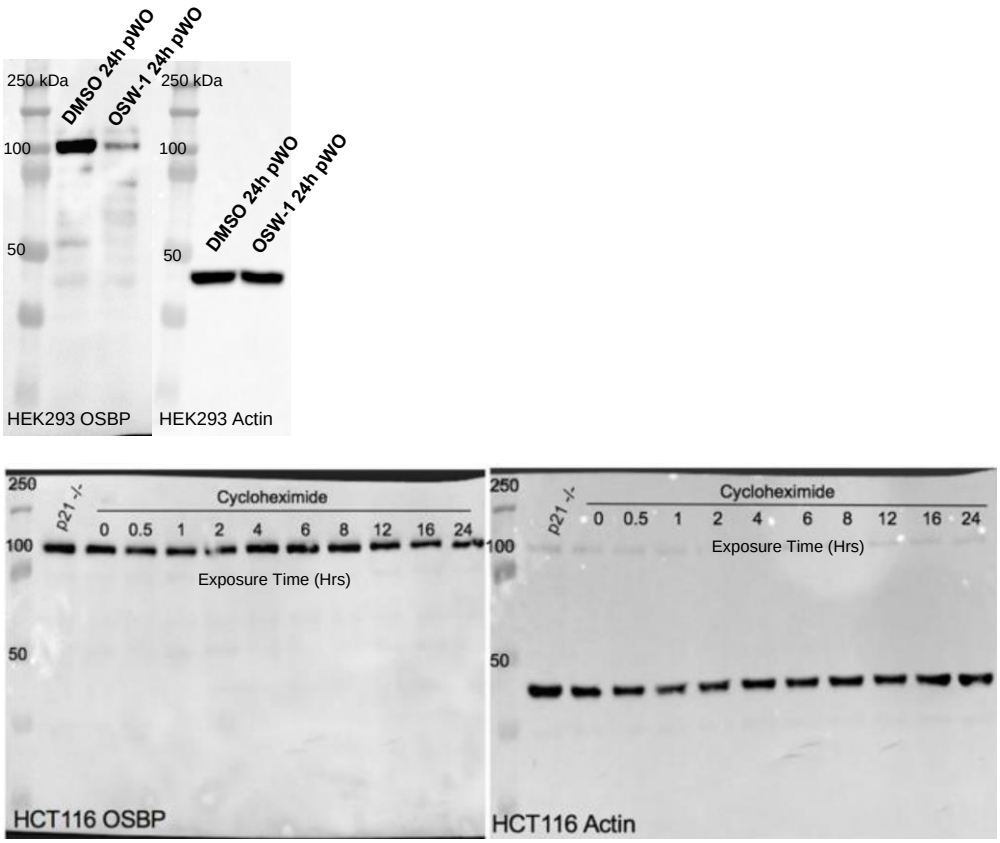

Figure 60: Full Western blots of an RNA Seq sample for Figure 23D (top) and Figure 23E (bottom).

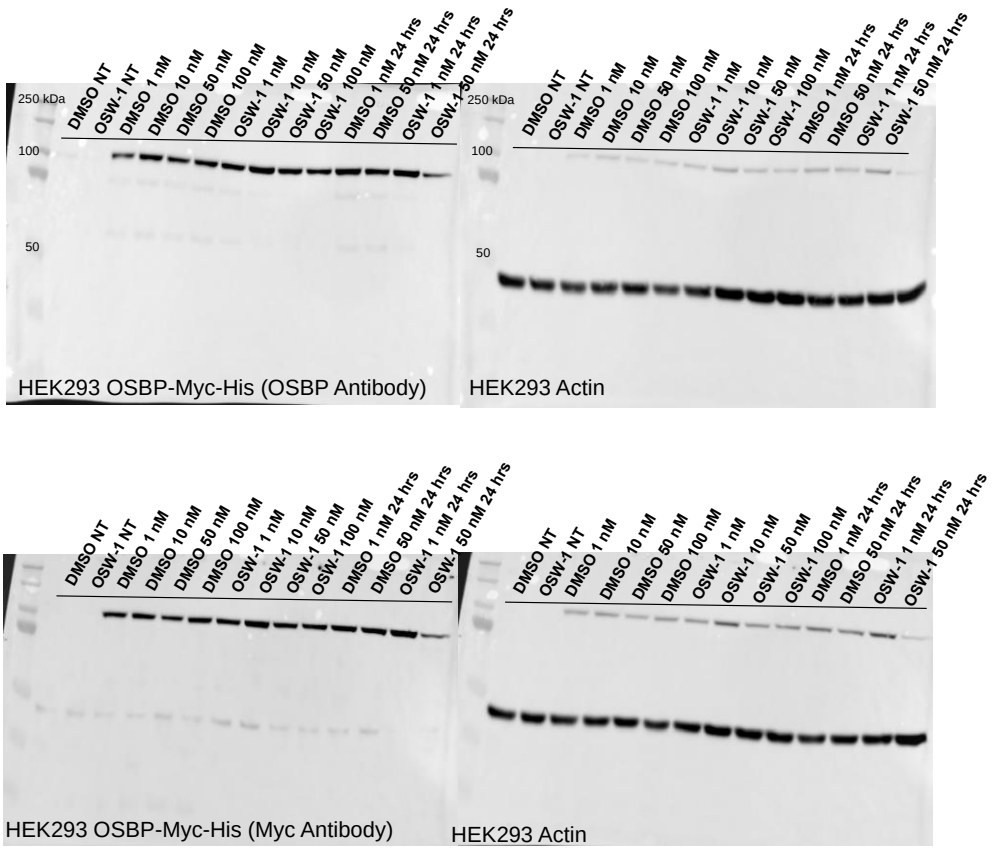

Figure 61: Full Western blots of Figure 24.

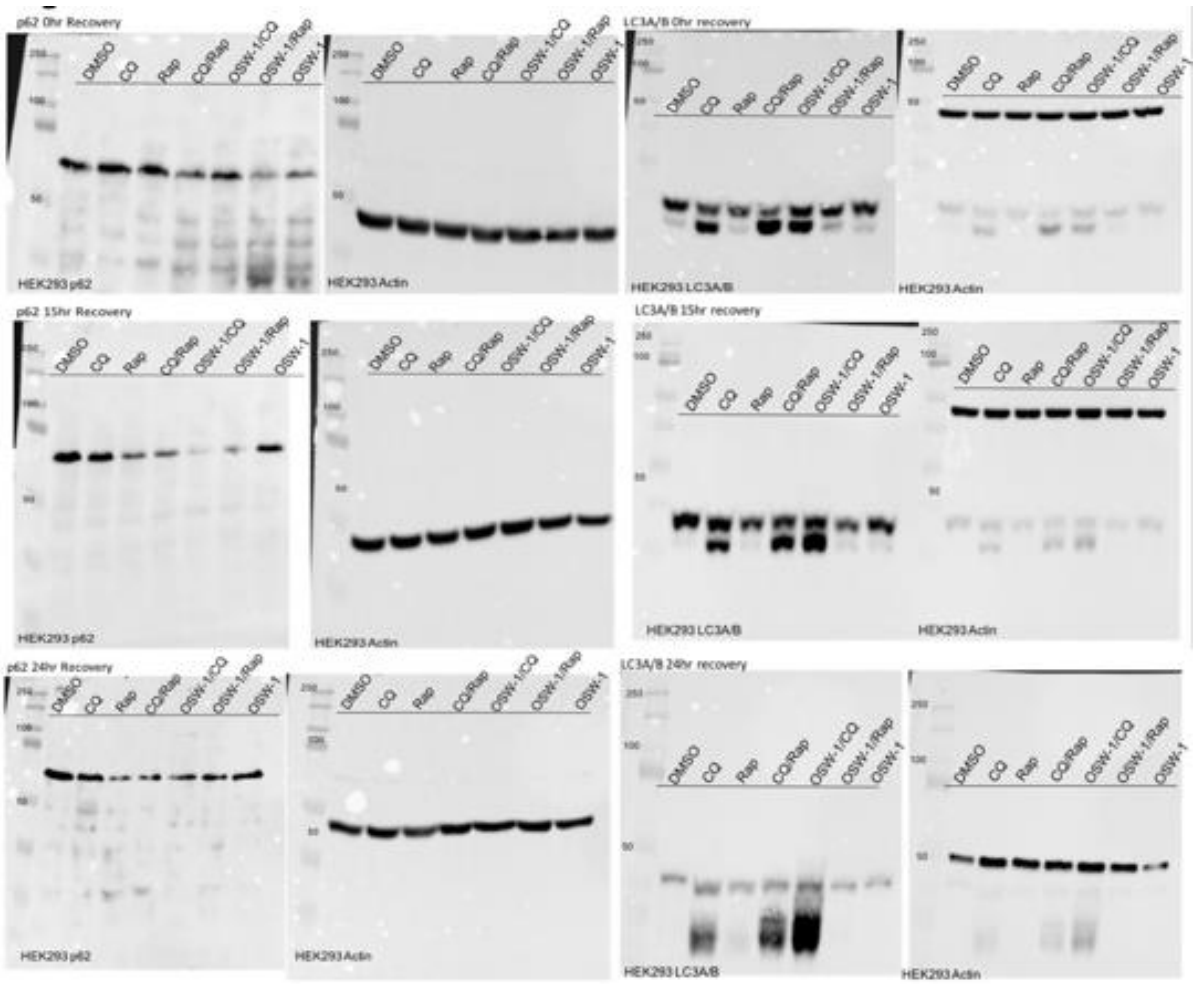

Figure 62: Full Western blots of Figure 25B (left) and Figure 25C (right).

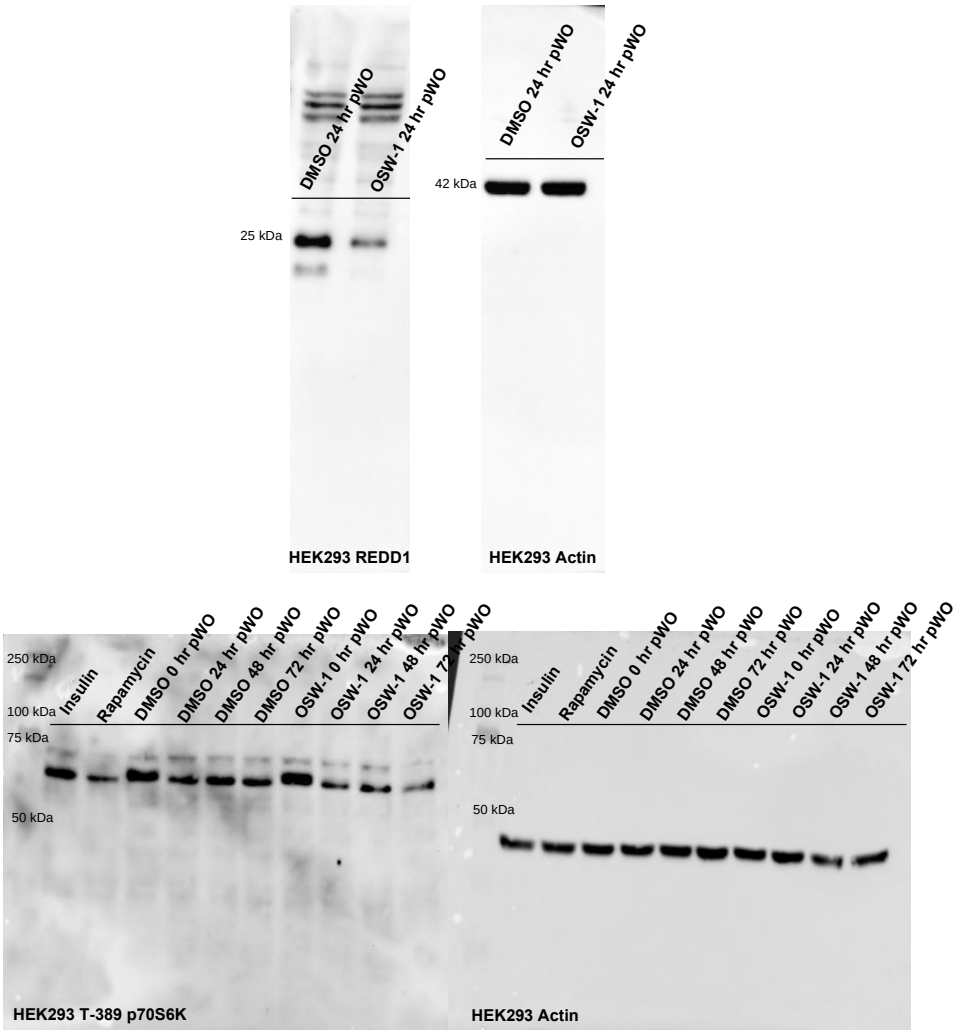

Figure 63: Full Western blots of Figure 26B (top) and Figure 26C (bottom).

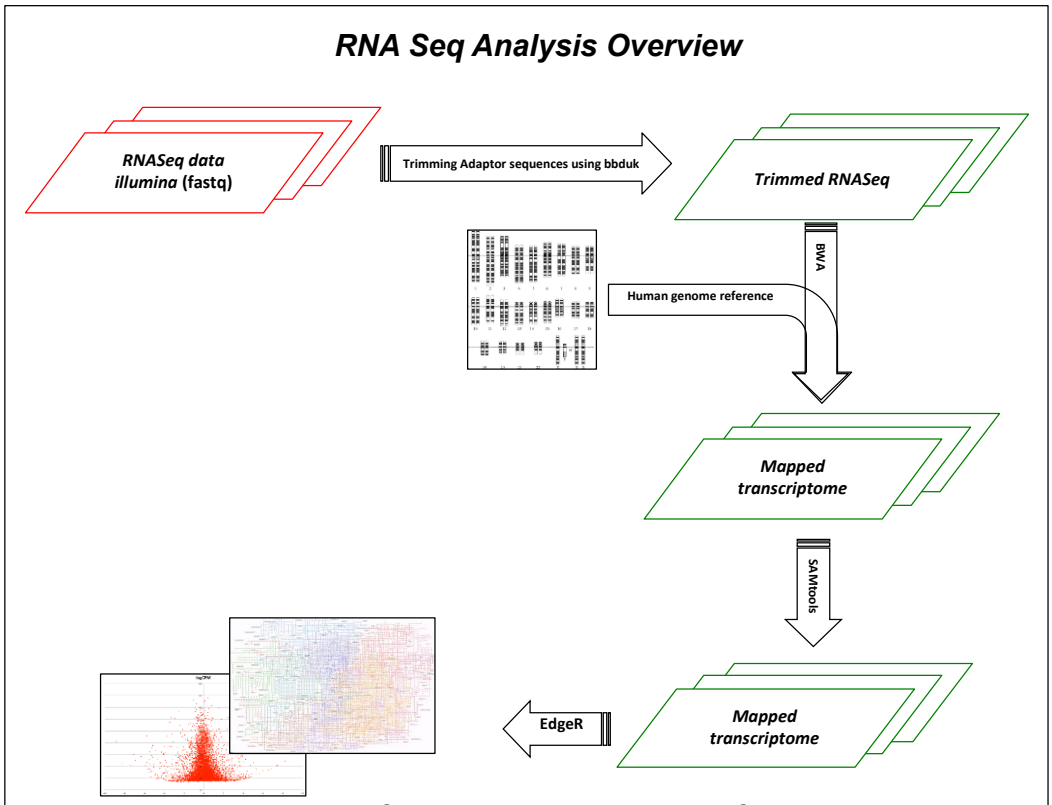

Figure 64: RNA Seq bioinformatics analysis outline for Figure 28B.
The RNA Seq bioinformatics analysis was performed in collaboration with Dr. Fares Najar. Dr. Najar is also credited with the creation of this image.

Appendix 3: Chapter 4 Supplemental

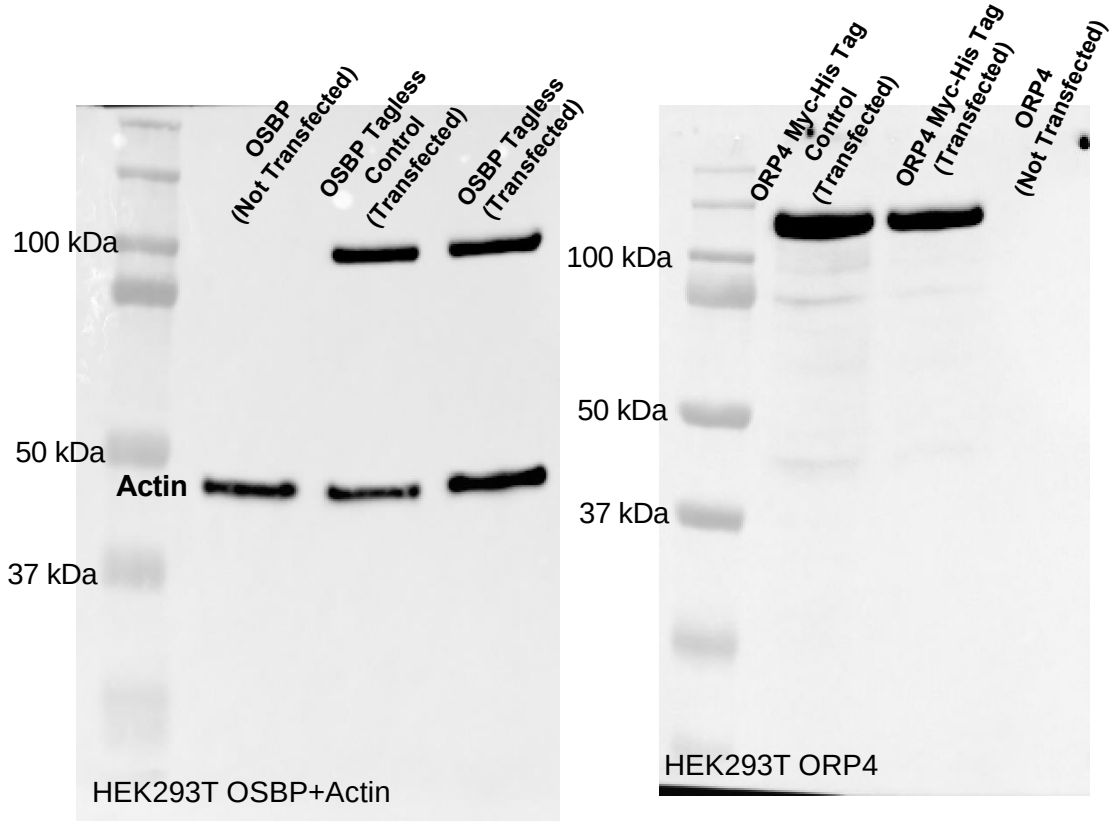

Figure 65: Full Western blots of OSBP and ORP4 binding lysates.

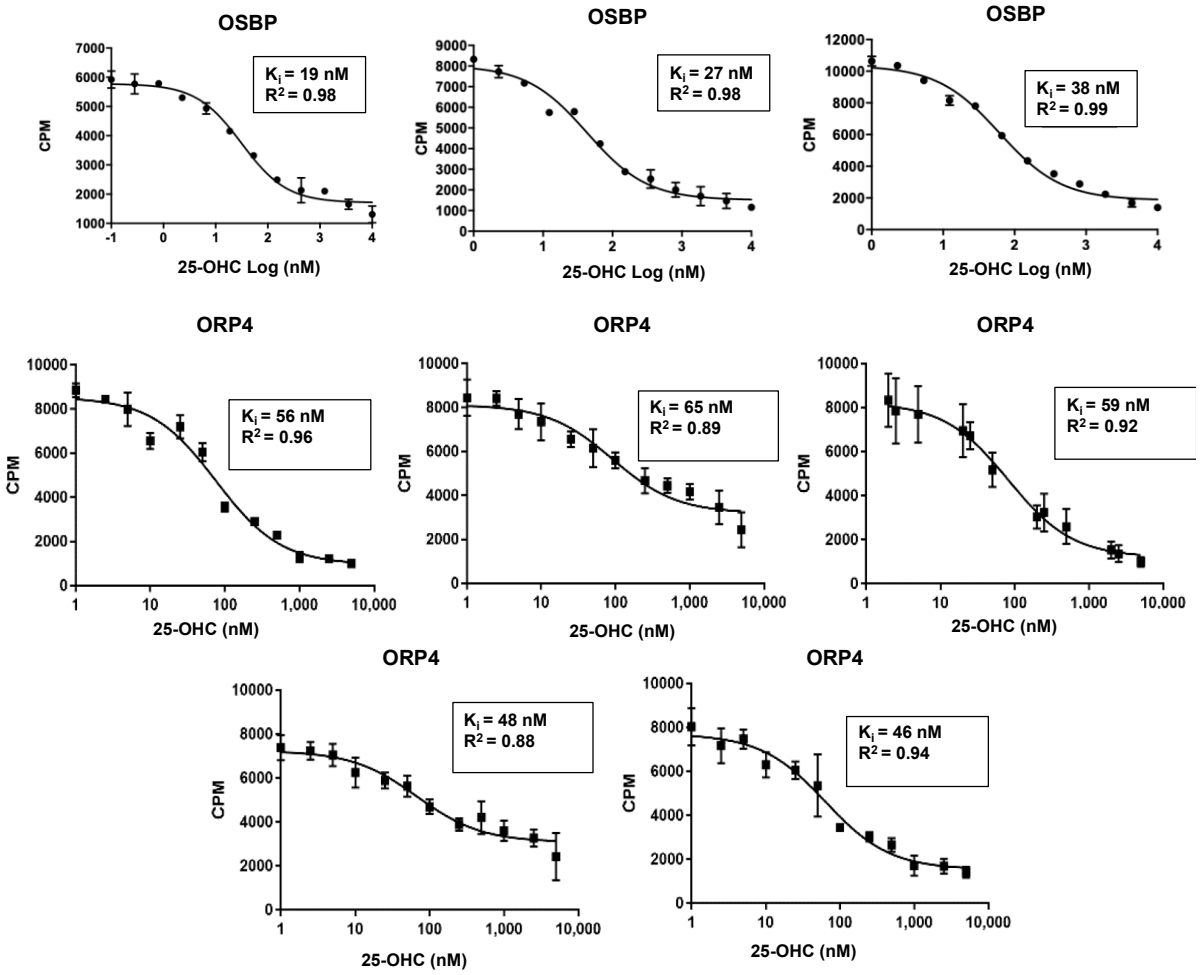

Figure 66: OSBP and ORP4 binding curves for 25-OHC.

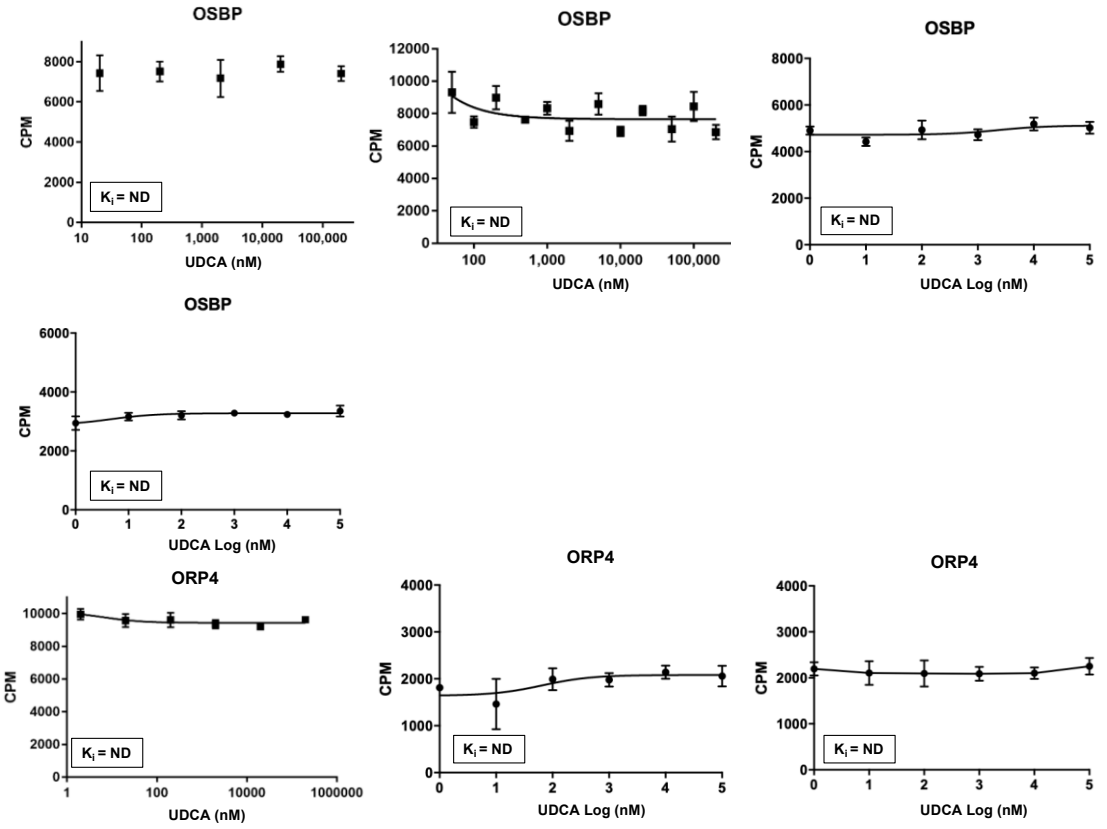

Figure 67: OSBP and ORP4 binding curves for UDCA.

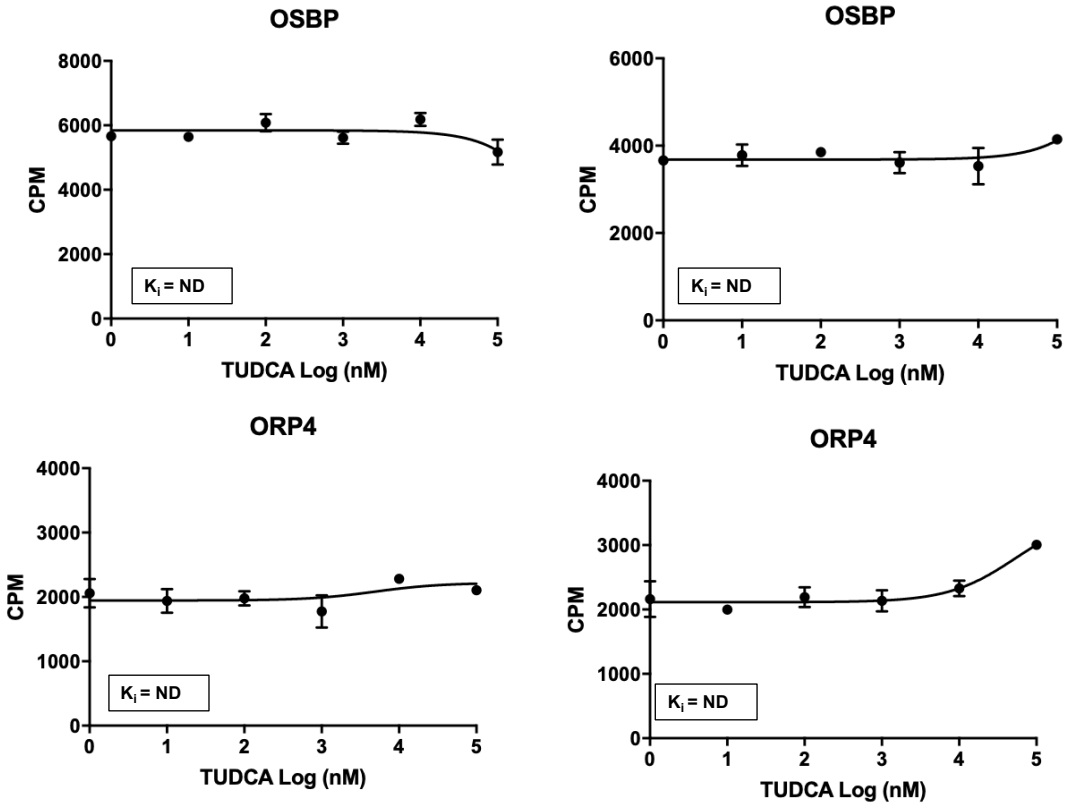

Figure 68: OSBP and ORP4 binding curves for TUDCA.

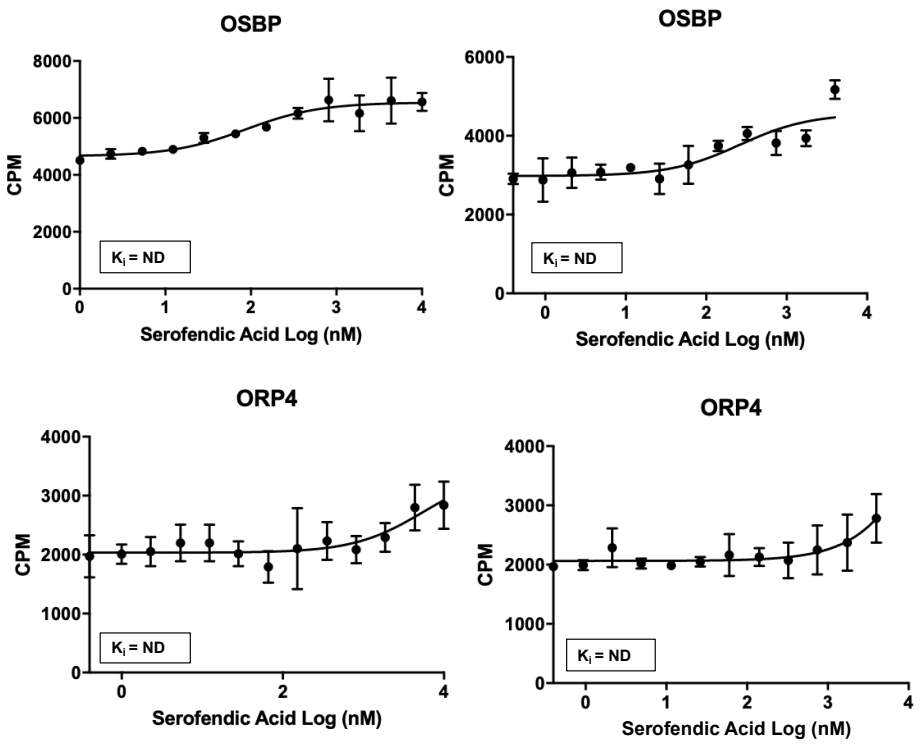

Figure 69: OSBP and ORP4 binding curves for Serofendic Acid

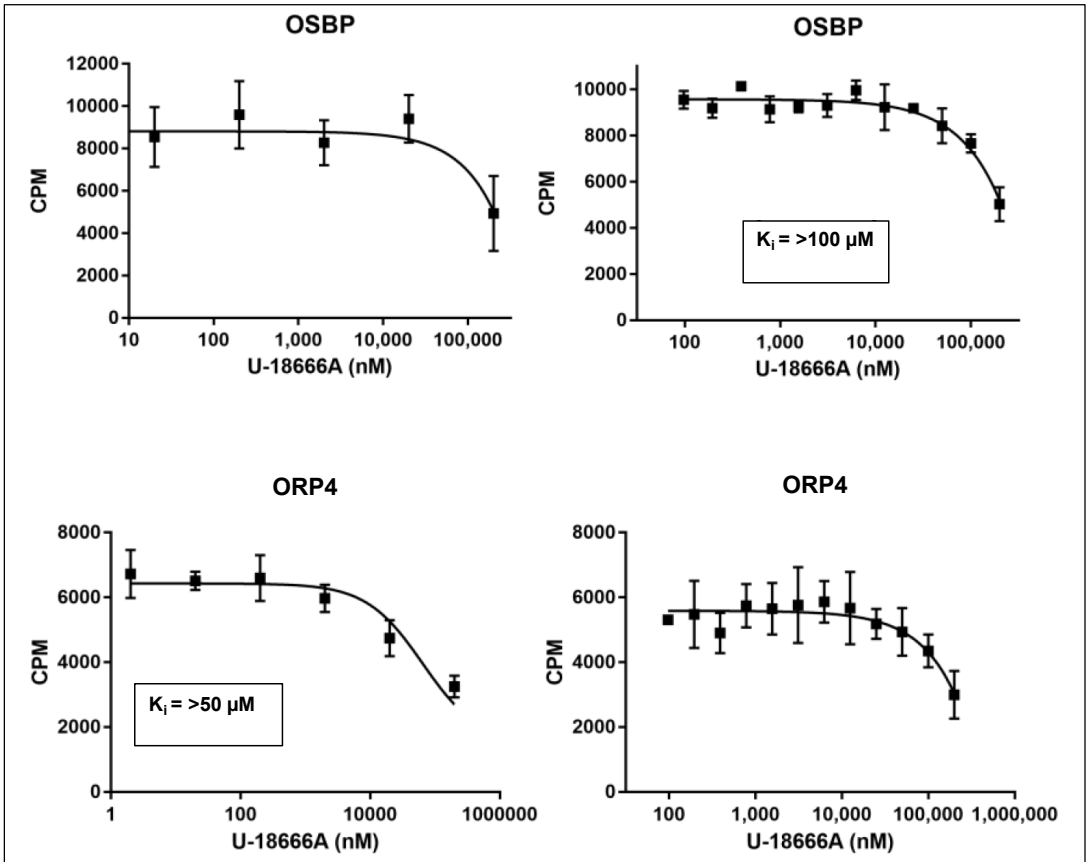

Figure 70: OSBP and ORP4 binding curves for U-18666A.

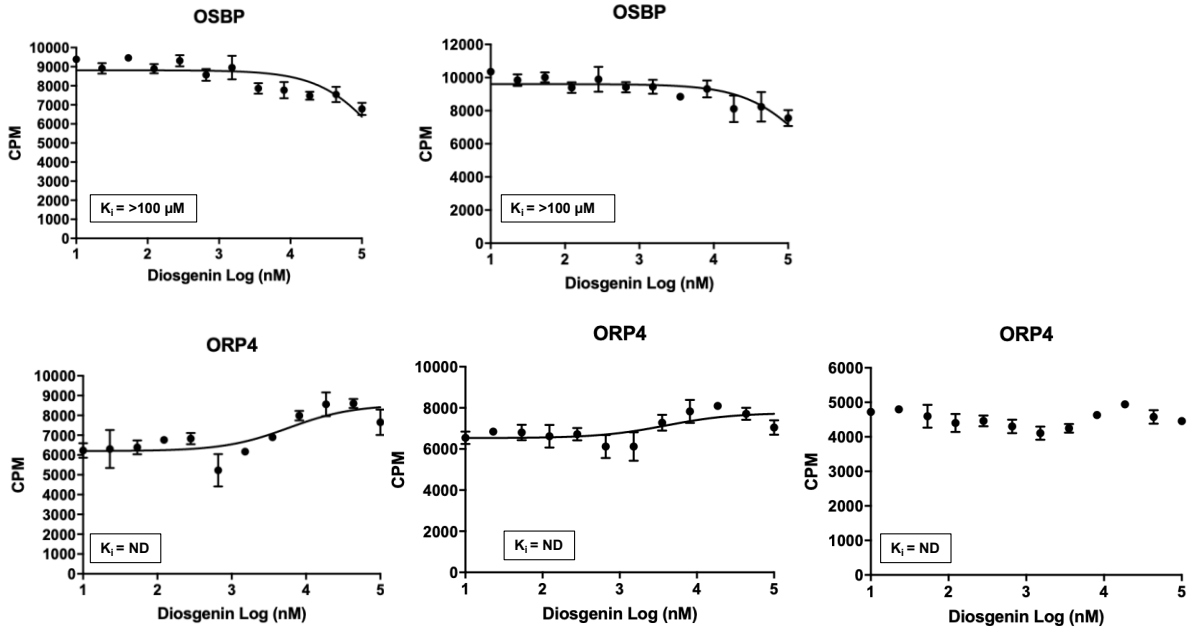

Figure 71: OSBP and ORP4 binding curves for Diosgenin.

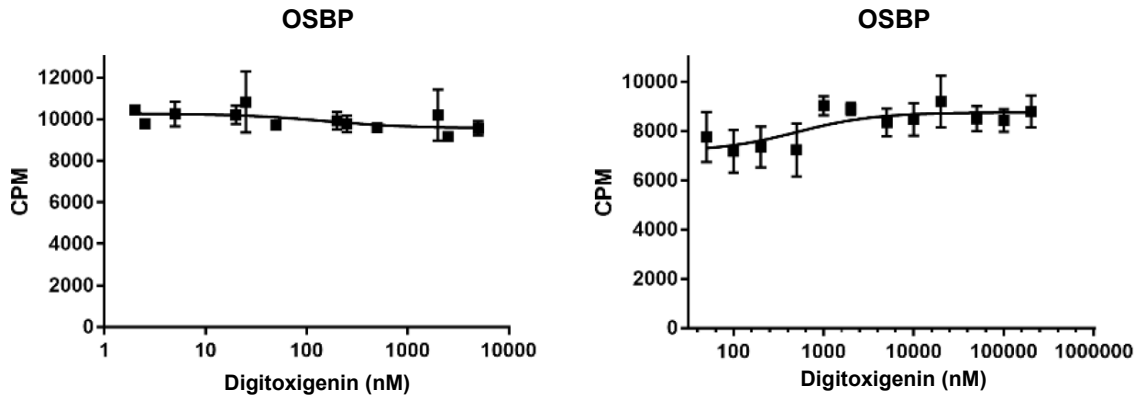

Figure 72: OSBP binding curves for Digitoxigenin

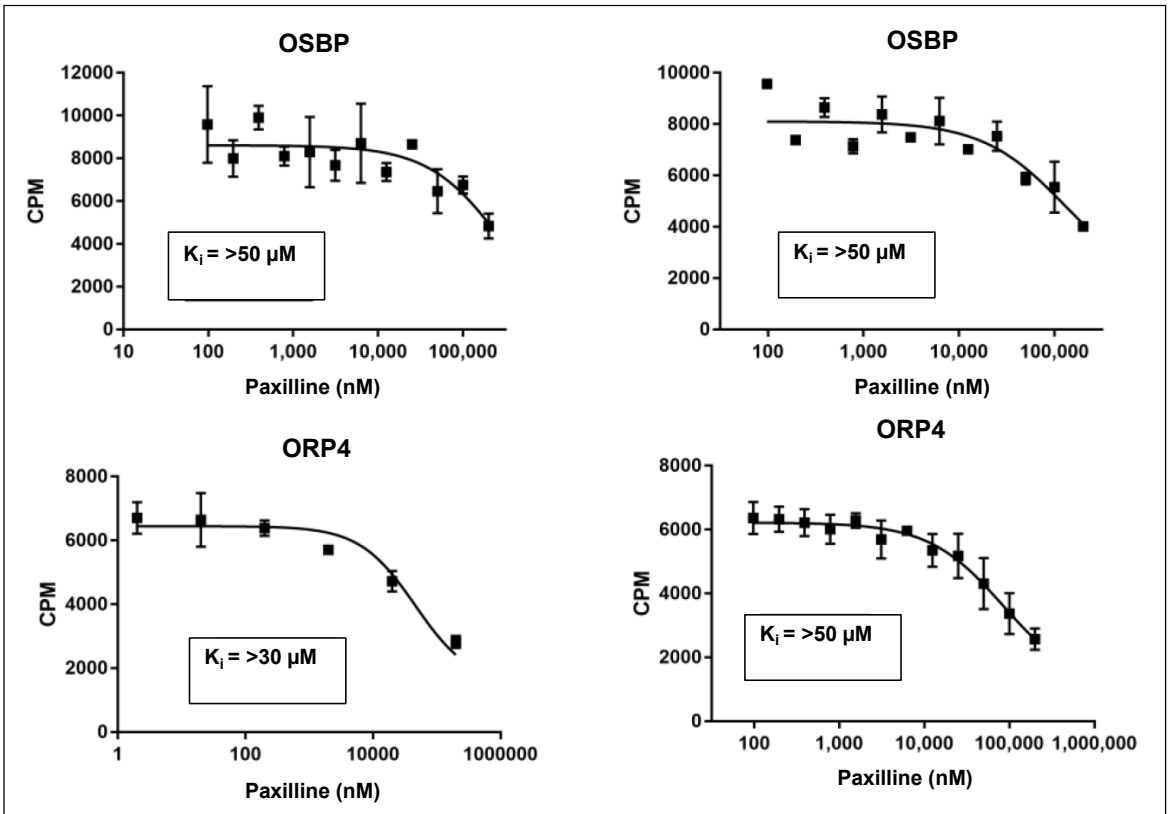

Figure 73: OSBP and ORP4 binding curves for Paxilline.

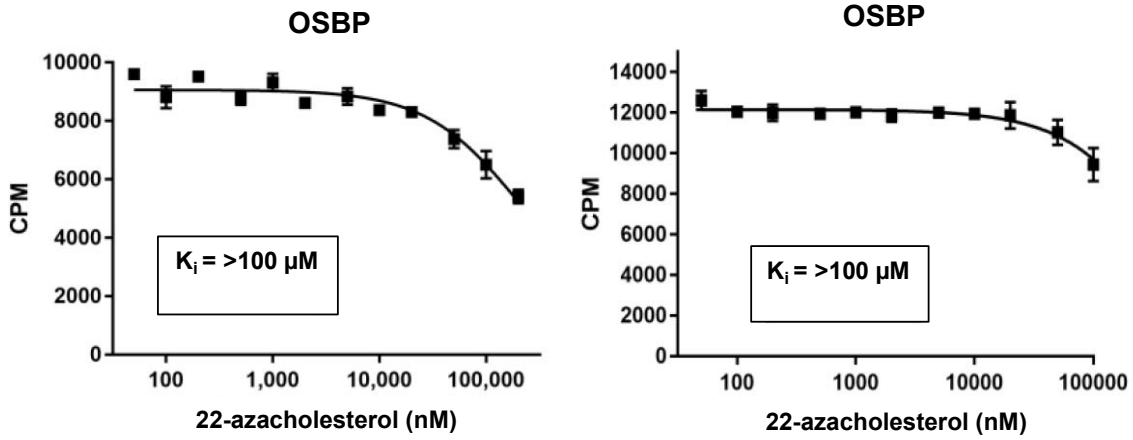

Figure 74: OSBP binding curves for 22-azacholesterol.

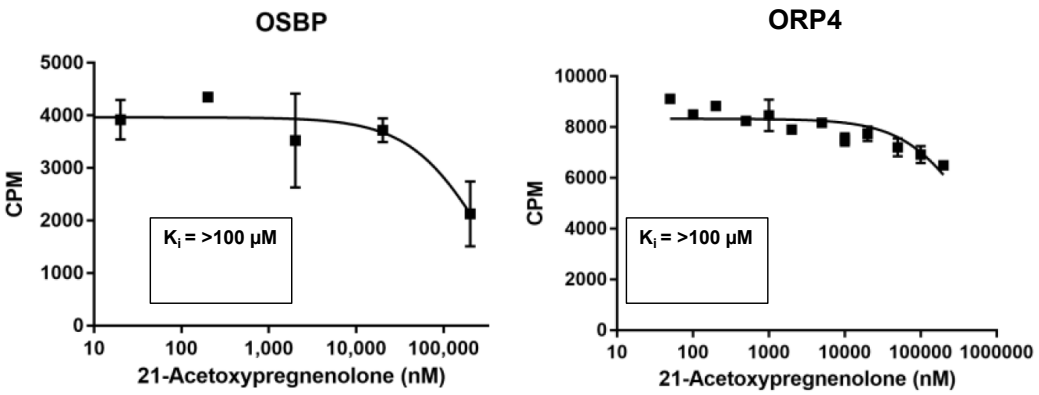

Figure 75: OSBP and ORP4 binding curves for 21-acetoxypregnenolone.

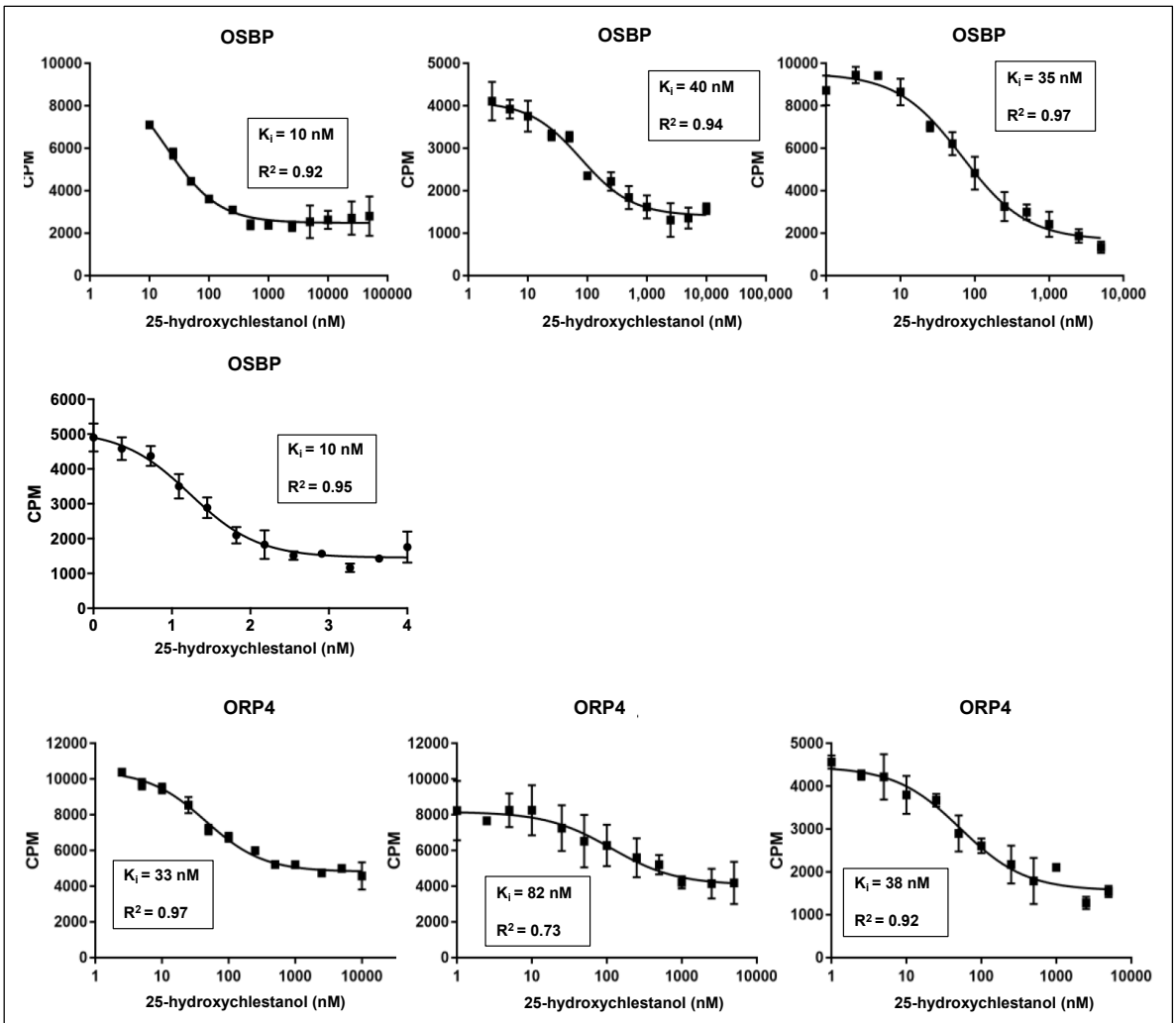

Figure 76: OSBP and ORP4 binding curves for 25-hydroxycholestanol.

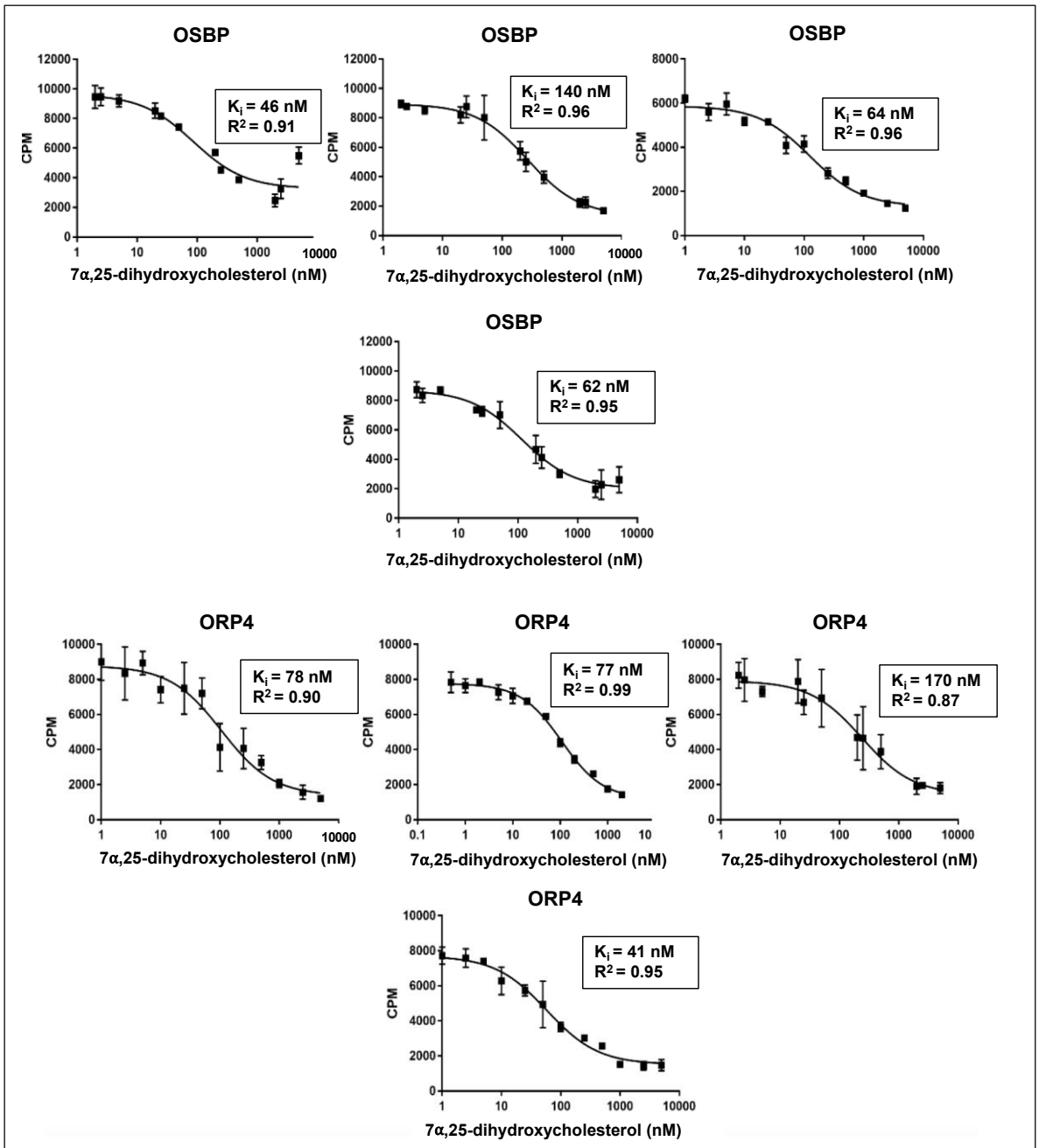

Figure 77: OSBP and ORP4 binding curves for 7α-25-diOHC.

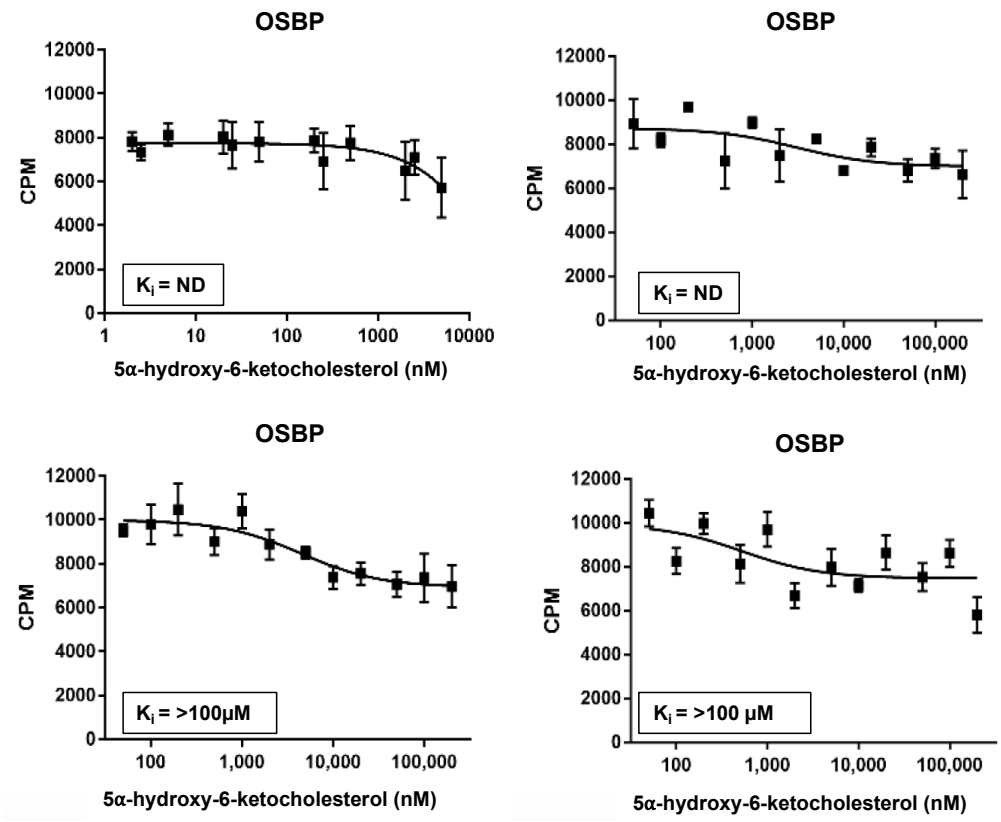

Figure 78: OSBP binding curves for 5α-OHC-6-ketocholesterol.

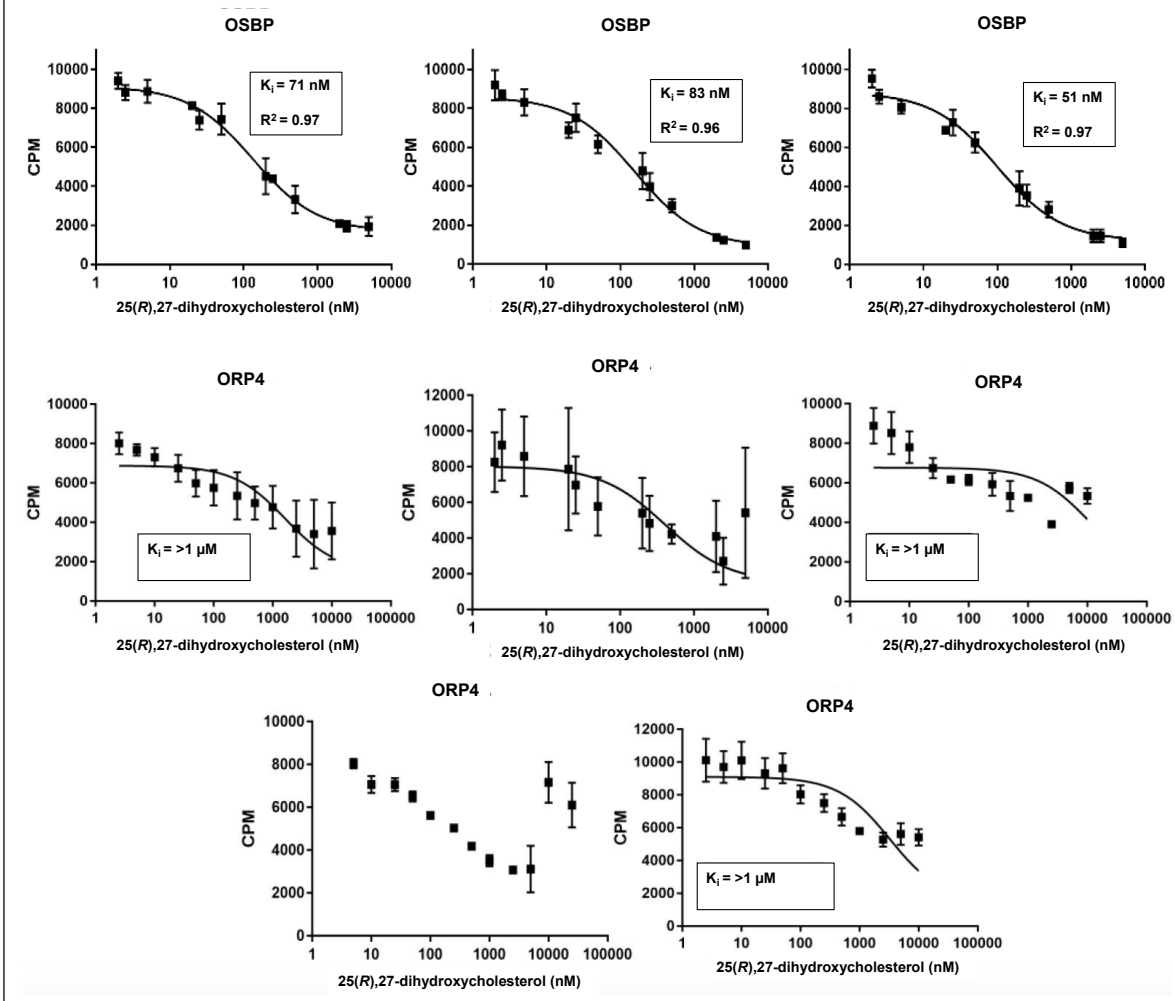

Figure 79: OSBP and ORP4 binding curves for 25(*R*),27-diOHC

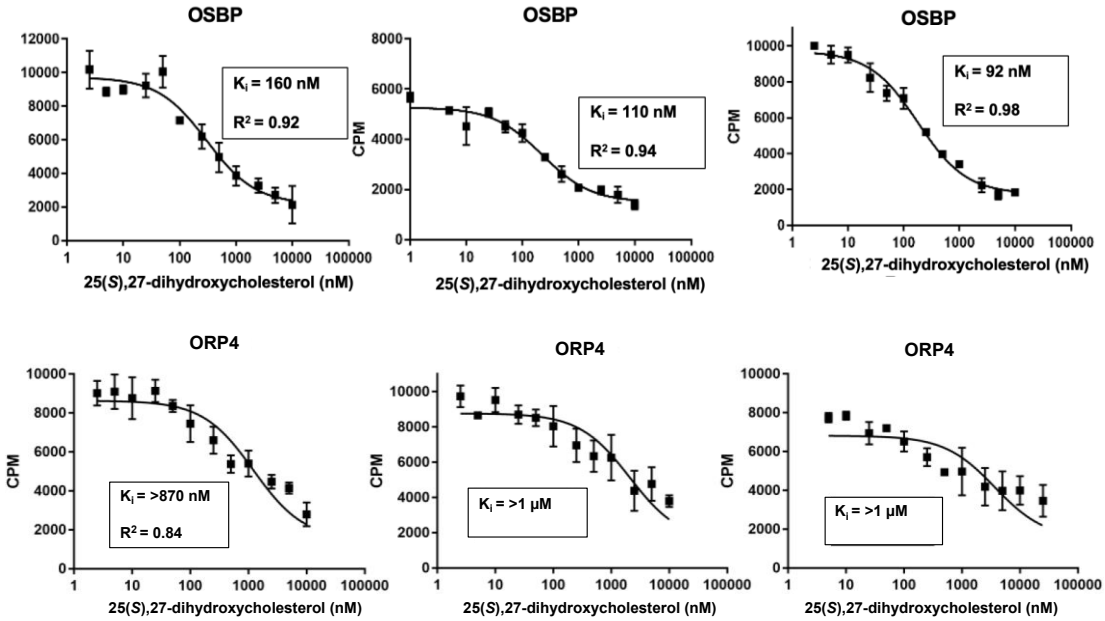

Figure 80: OSBP and ORP4 binding curves for 25(*S*), 27-diOHC.

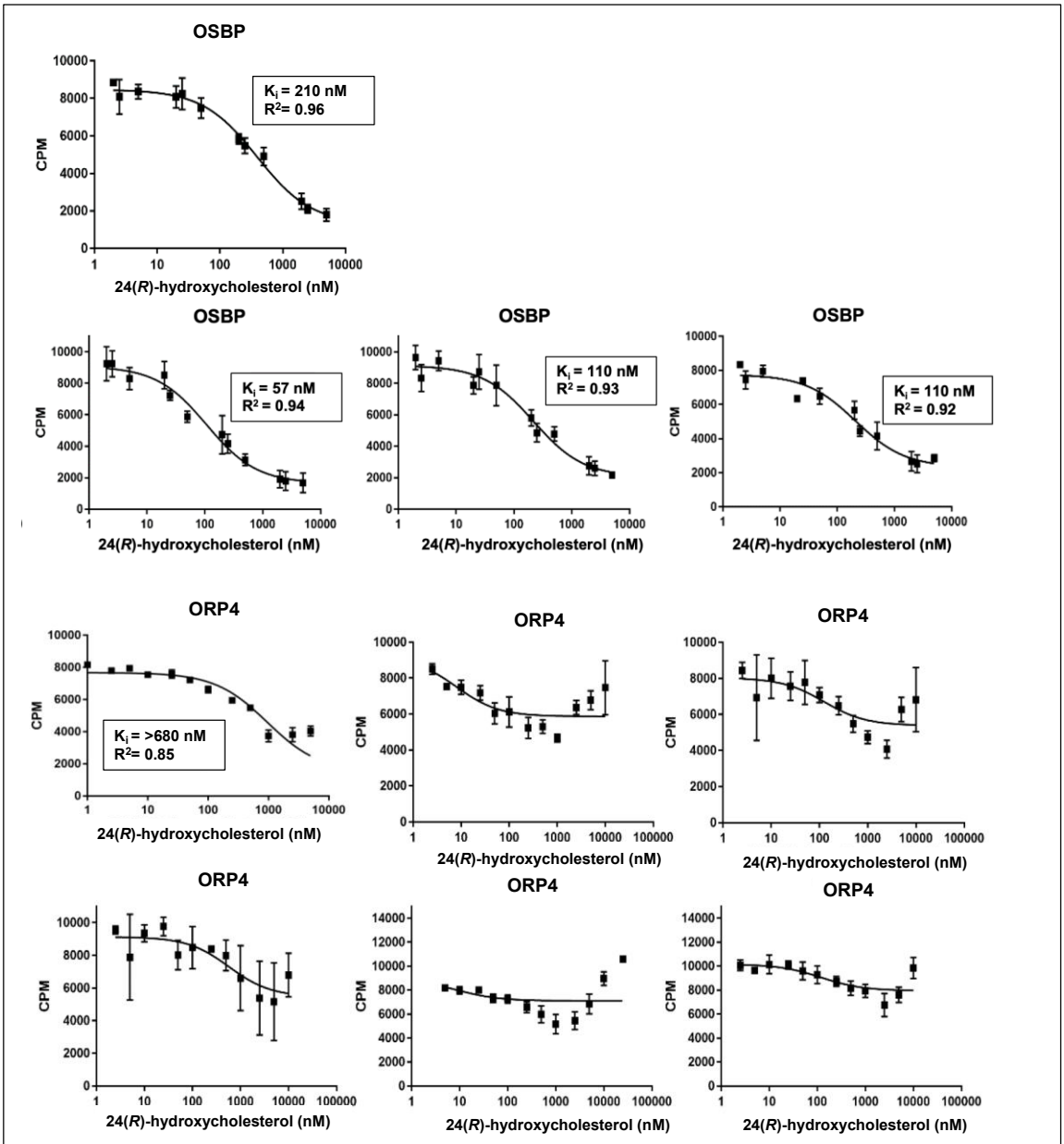

Figure 81: OSBP and ORP4 binding curves for 24(*R*)-OHC.

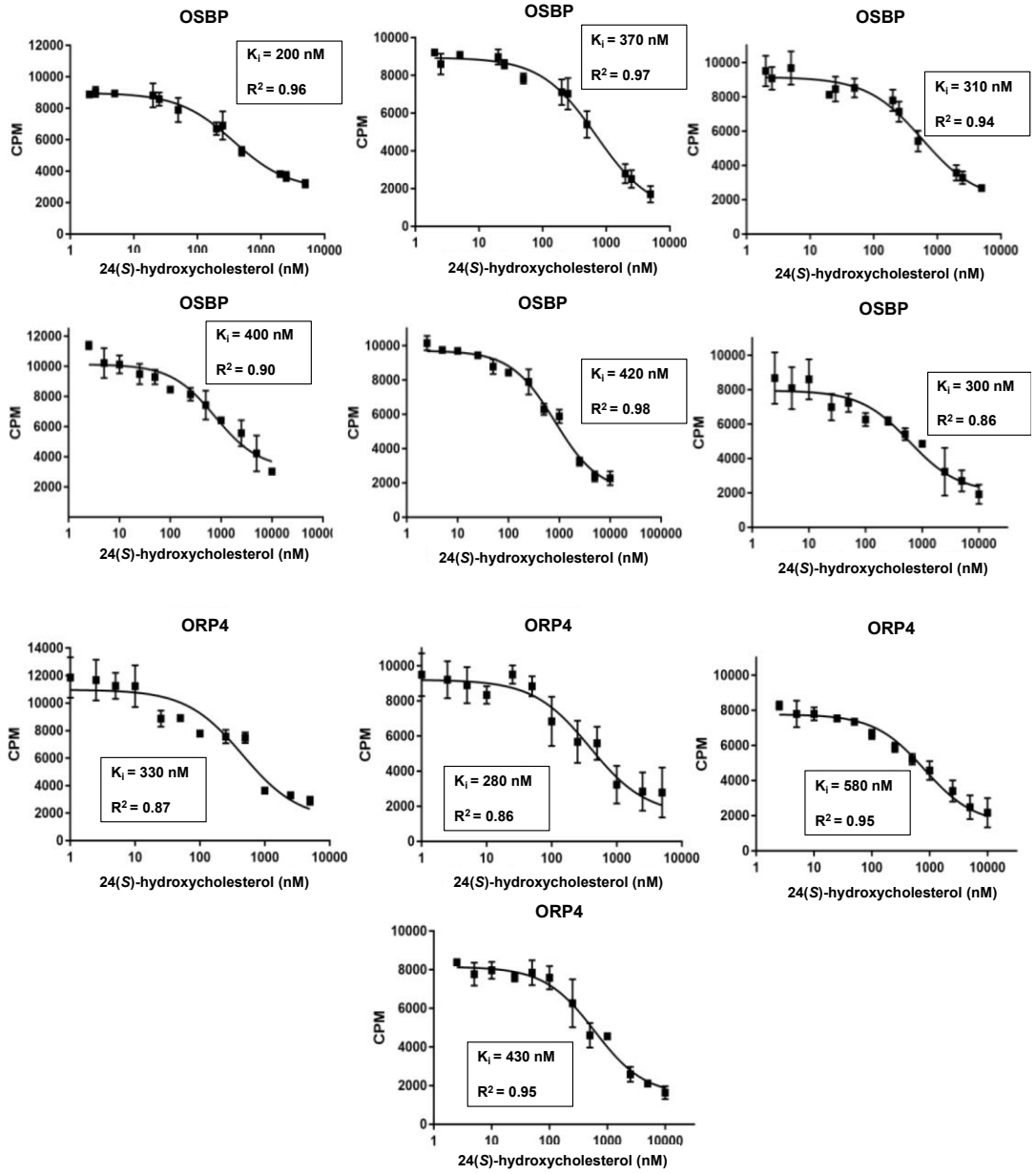

Figure 82: OSBP and ORP4 binding curves for 24(*S*)-OHC.

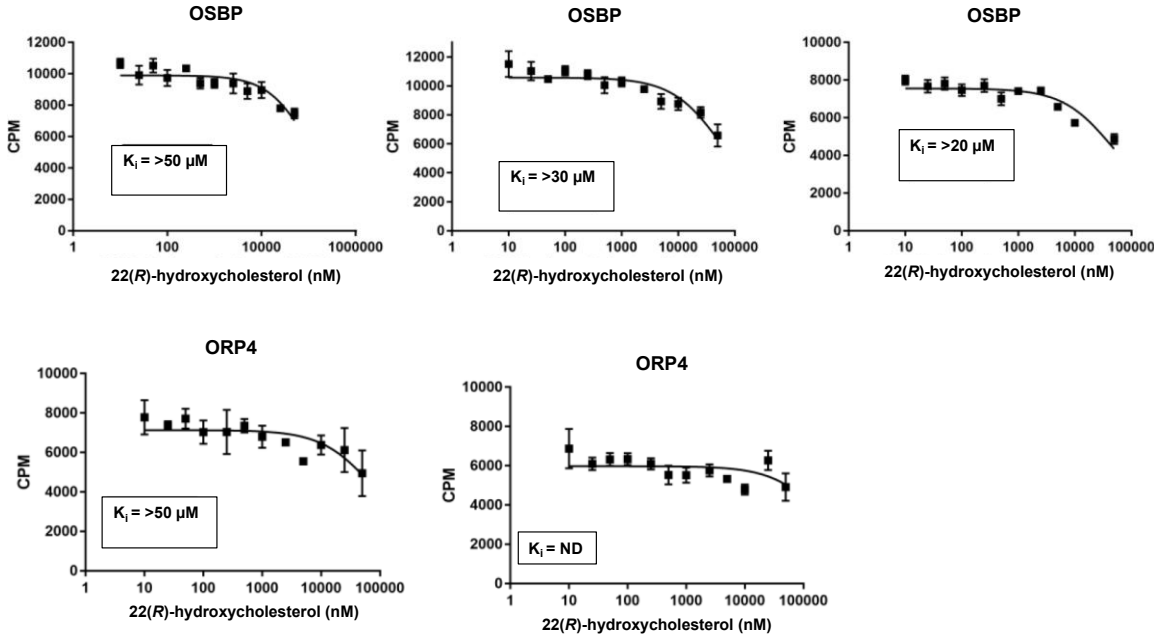

Figure 83: OSBP and ORP4 binding curves for 22(*R*)-OHC.

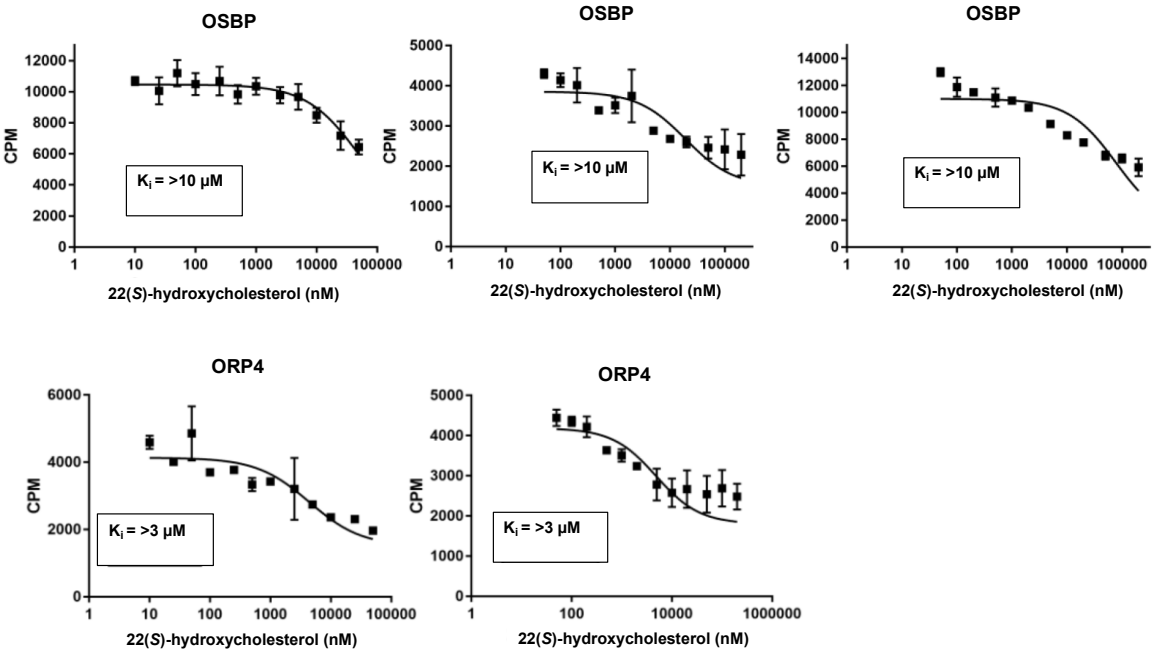

Figure 84: OSBP and ORP4 binding curves to 22(*S*)-OHC.

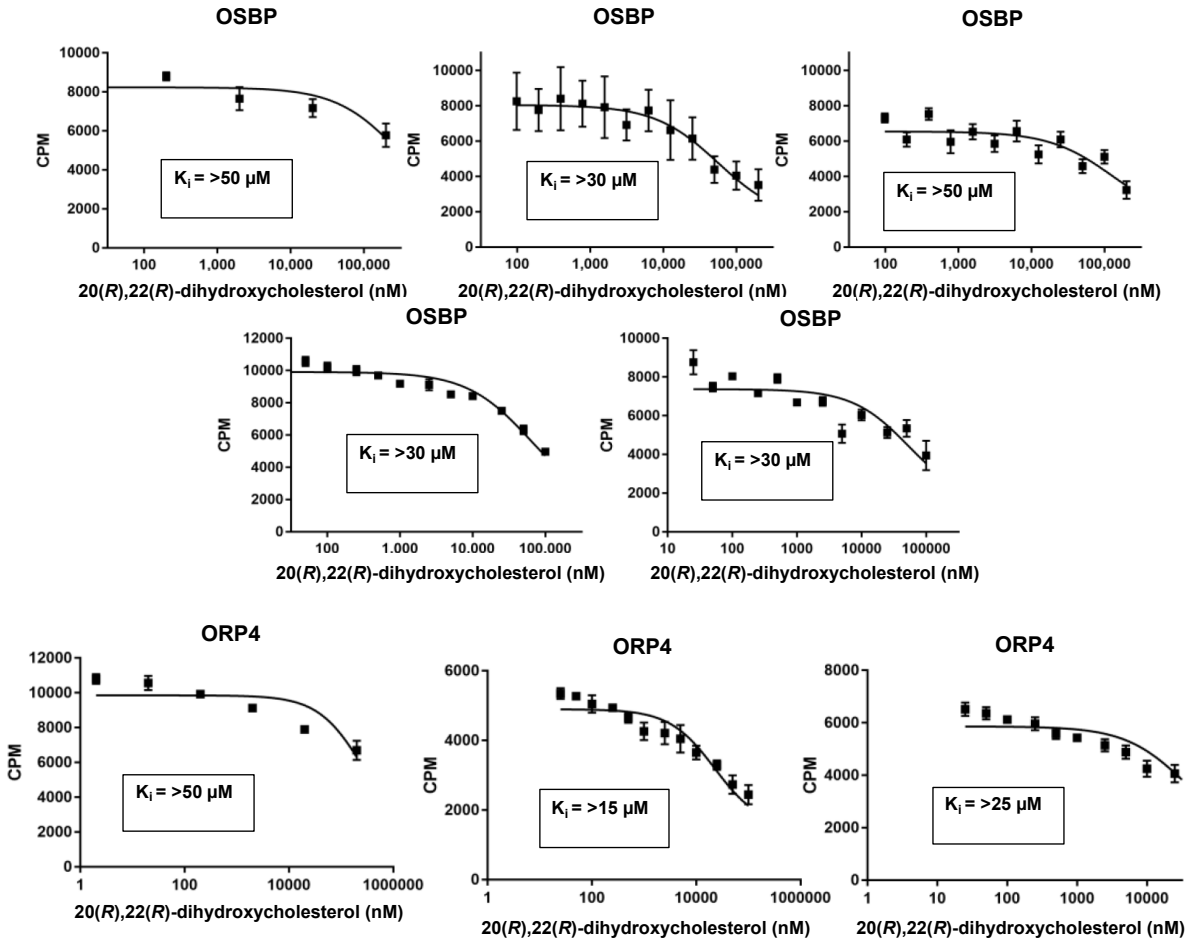

Figure 85: OSBP and ORP4 binding curves for 20(*R*), 22(*S*)-OHC.

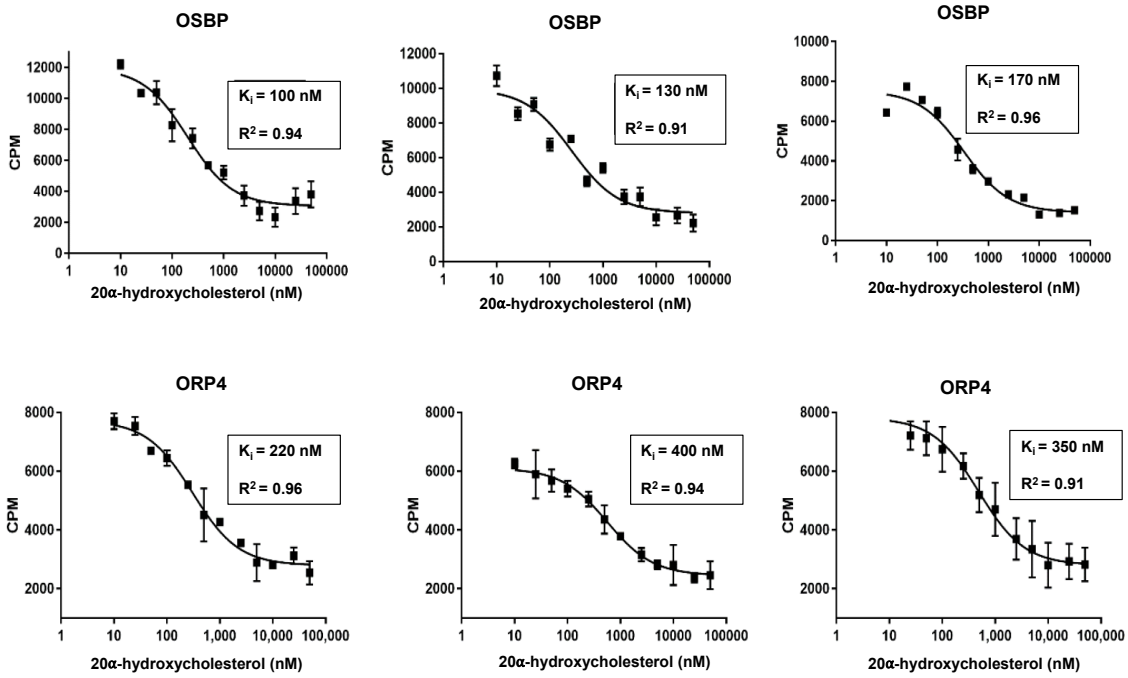

Figure 86: OSBP and ORP4 binding curves for 20-OHC.

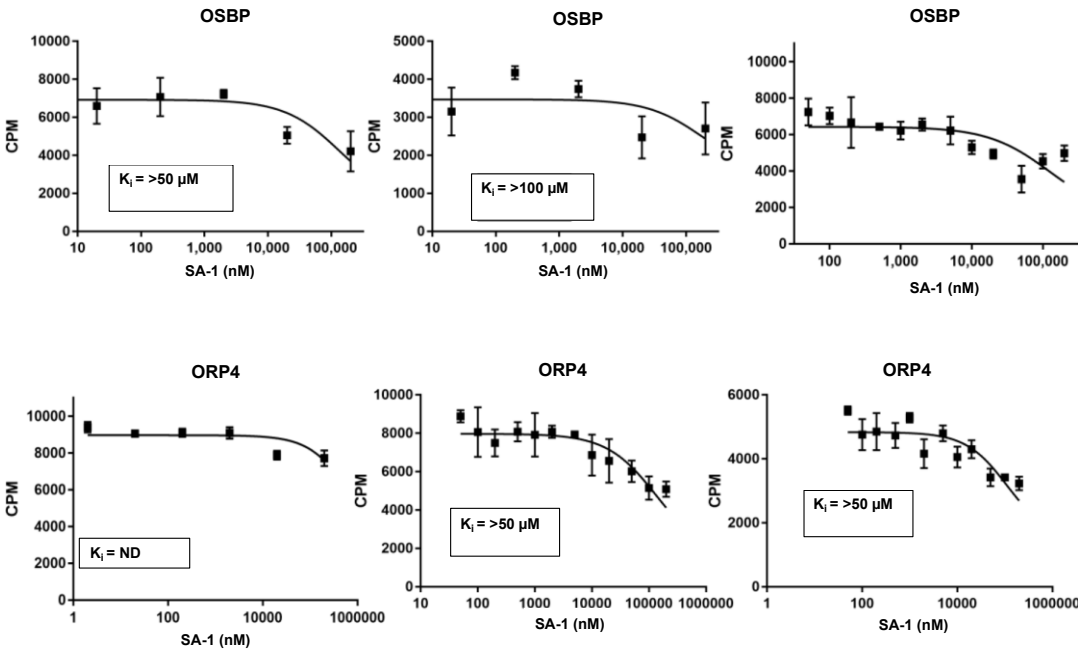

Figure 87: OSBP and ORP4 binding curves for SA-1.

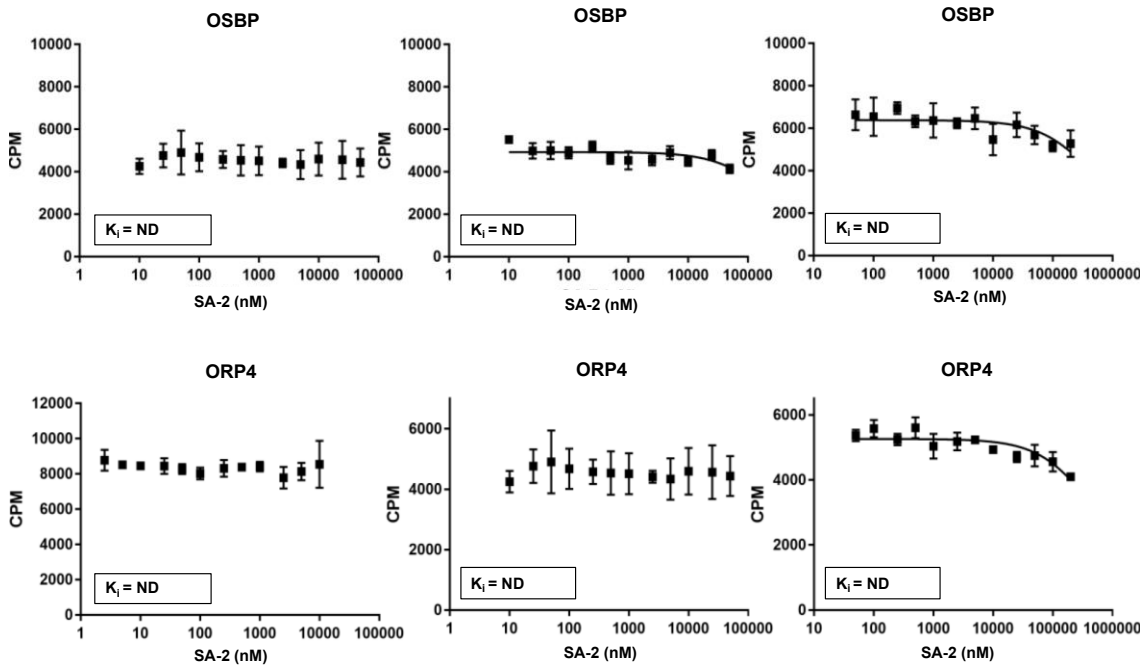

Figure 88: OSBP and ORP4 binding curves for SA-2.

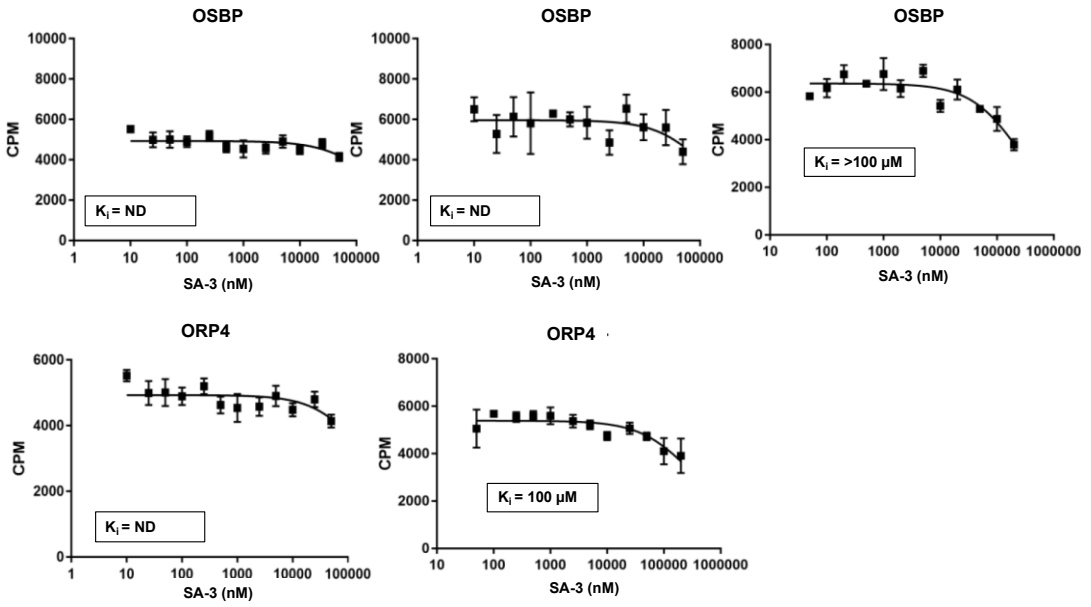

Figure 89: OSBP and ORP4 binding curves for SA-3.

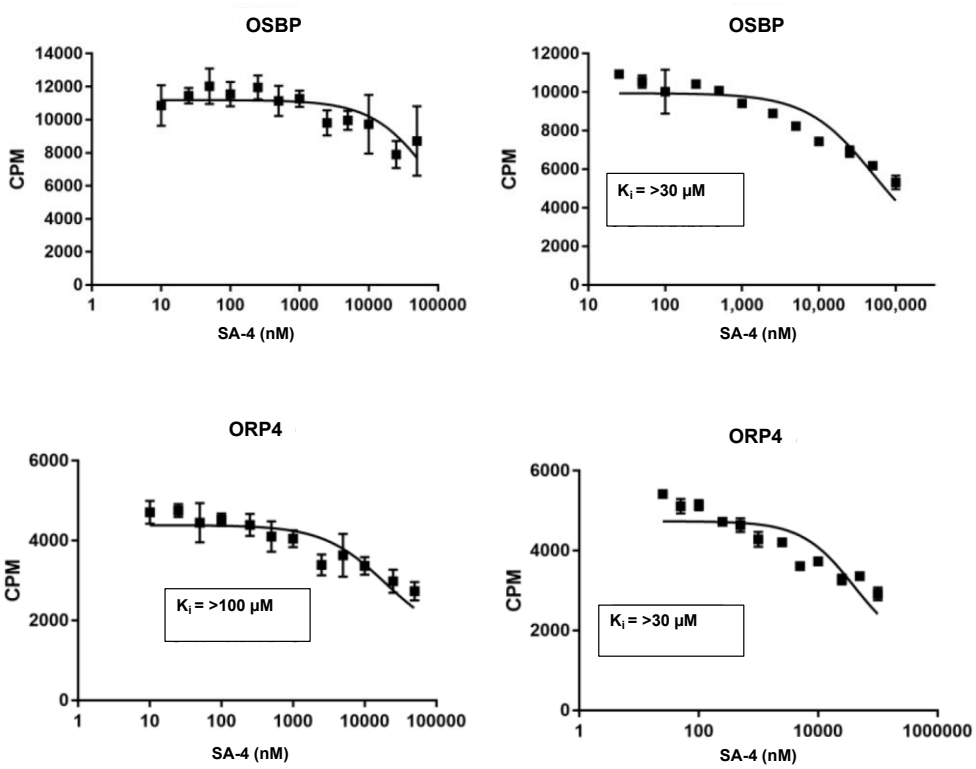

Figure 90: OSBP and ORP4 binding curves for SA-4.

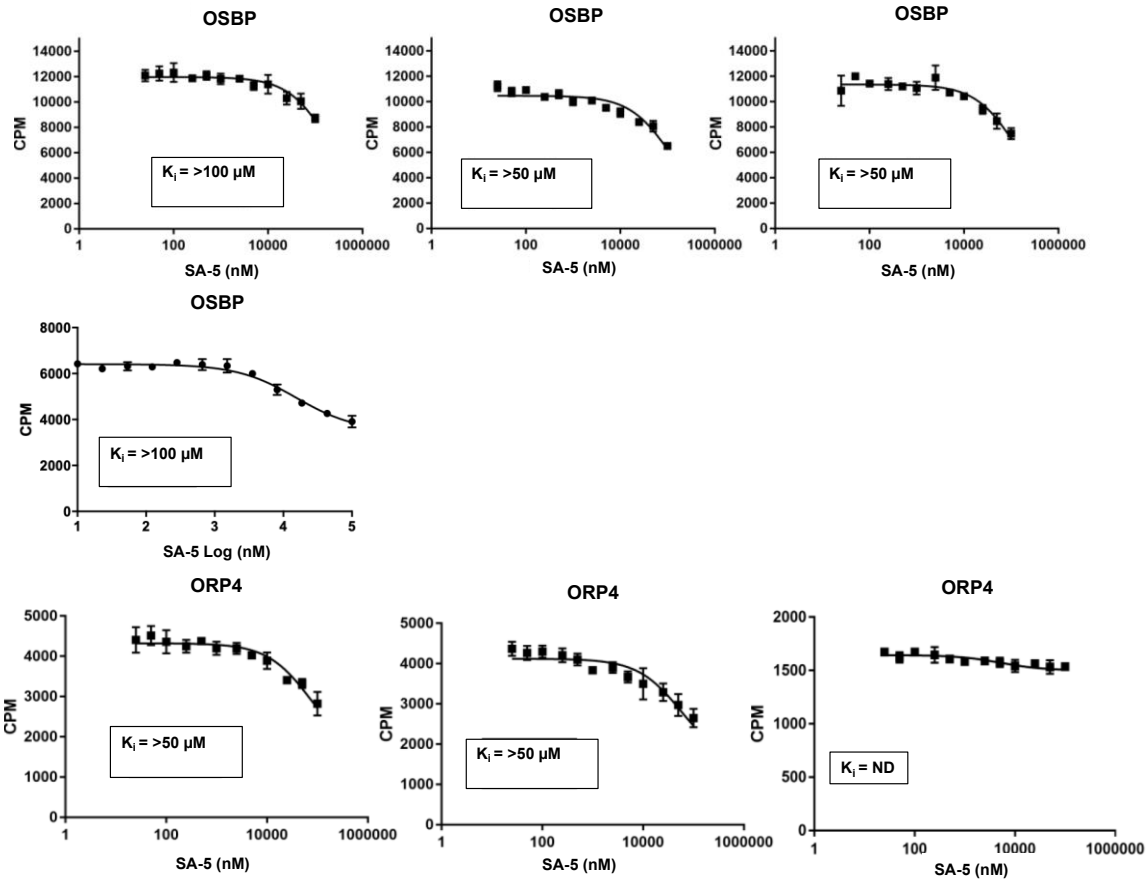

Figure 91: OSBP and ORP4 binding curves for SA-5.

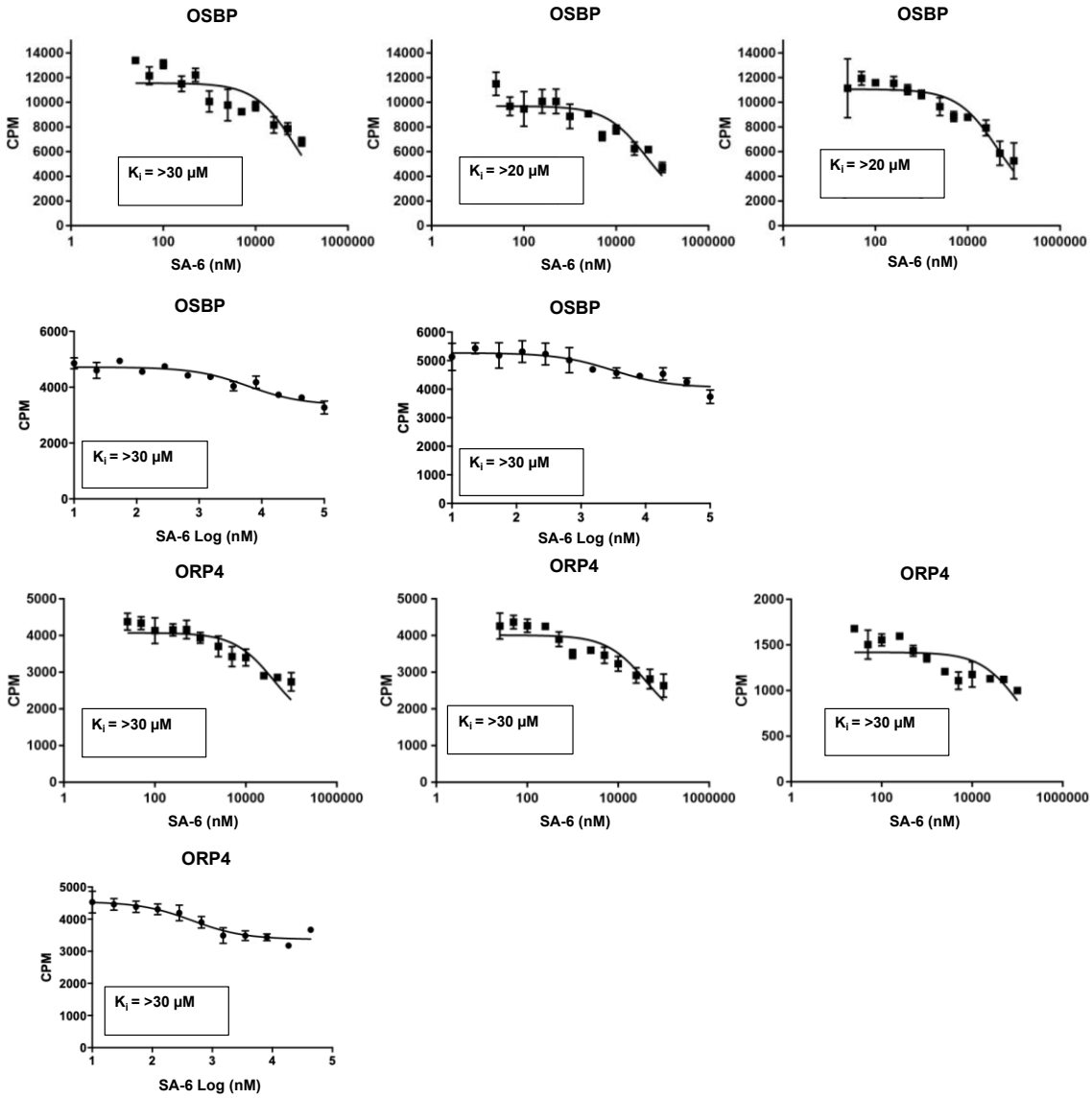

Figure 92: OSBP and ORP4 binding curves for SA-6.

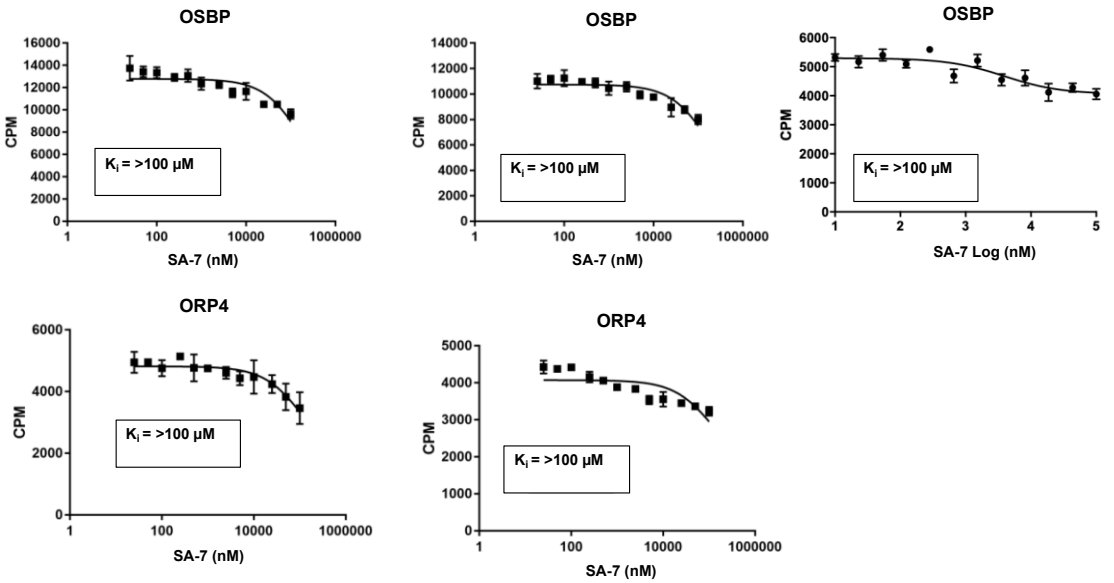

Figure 93: OSBP and ORP4 binding curves for SA-7.

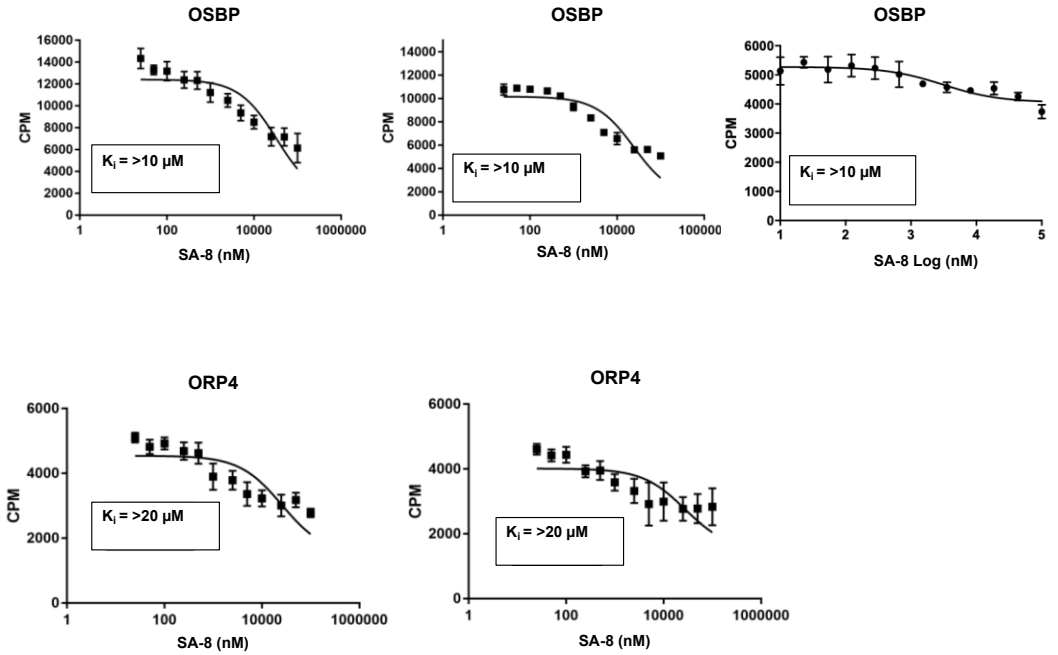

Figure 94: OSBP and ORP4 binding curves for SA-8.

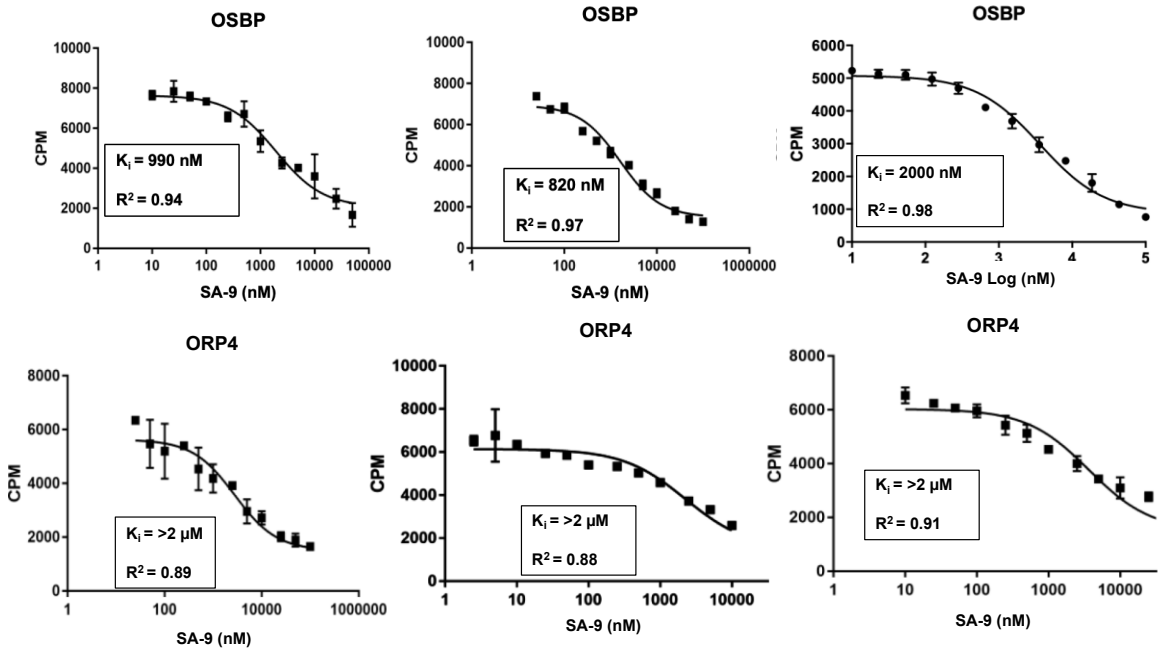

Figure 95: OSBP and ORP4 binding curves for SA-9.

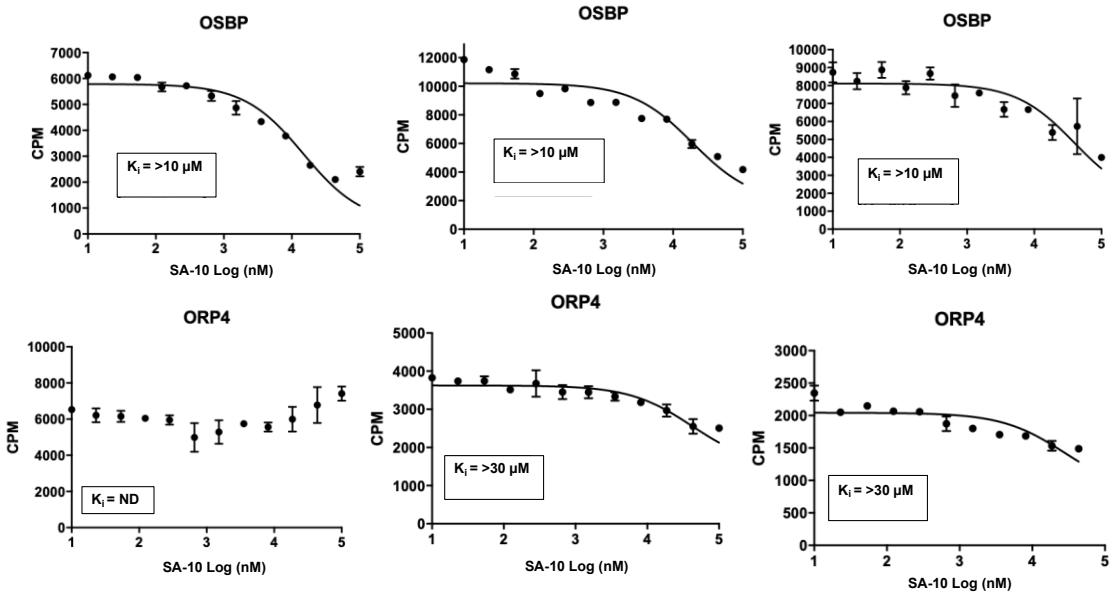

Figure 96: OSBP and ORP4 binding curves for SA-10.

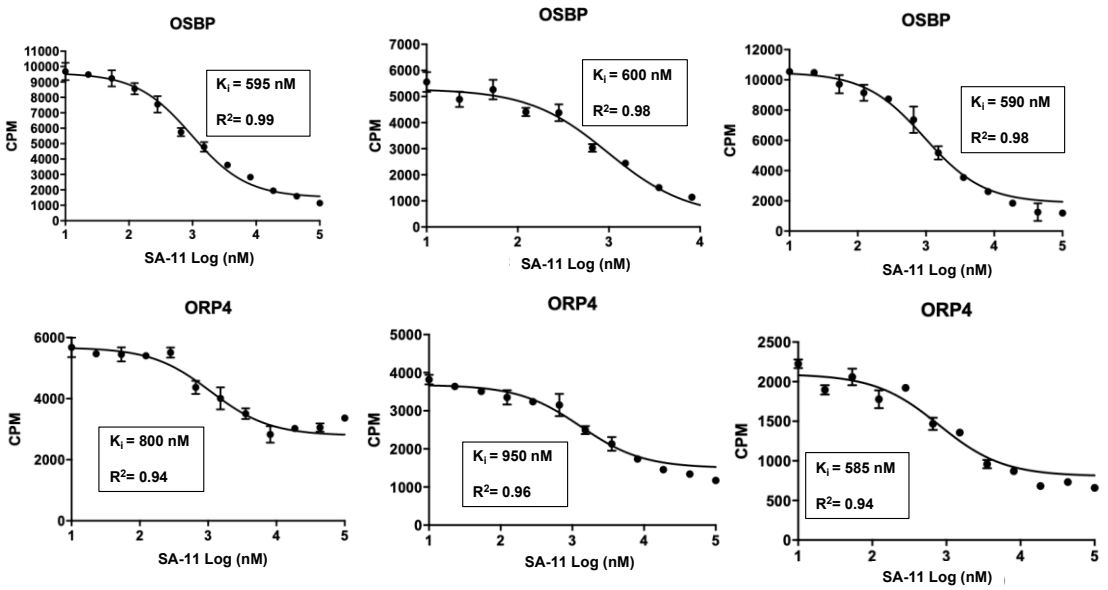

Figure 97: OSBP and ORP4 binding curves for SA-11.

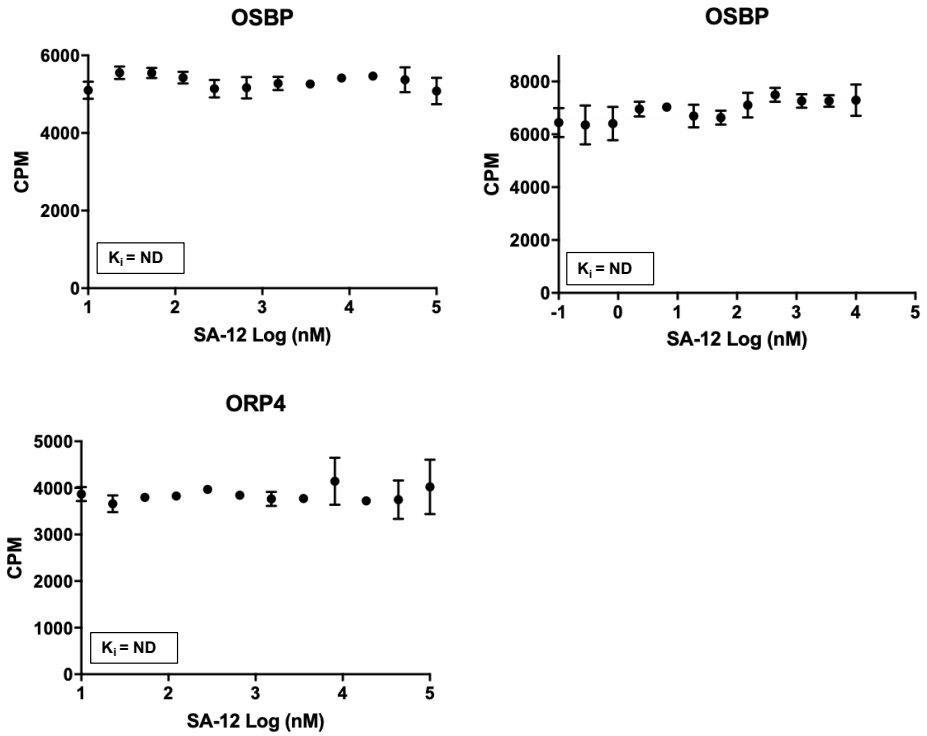

Figure 98: OSBP and ORP4 binding curves for SA-12